AD-A083 098 VIRGINIA UNIV CHARLOTTESVILLE DEPT OF MECHANICAL AND--ETC F/G 13/9
PROCEEDINGS OF THE CONFERENCE ON TIE STABILITY & DYNAMIC--ETC(U)
1979 DAAG29-79-M-0061

UNCLASSIFIED ARO-16660.1-E N/L

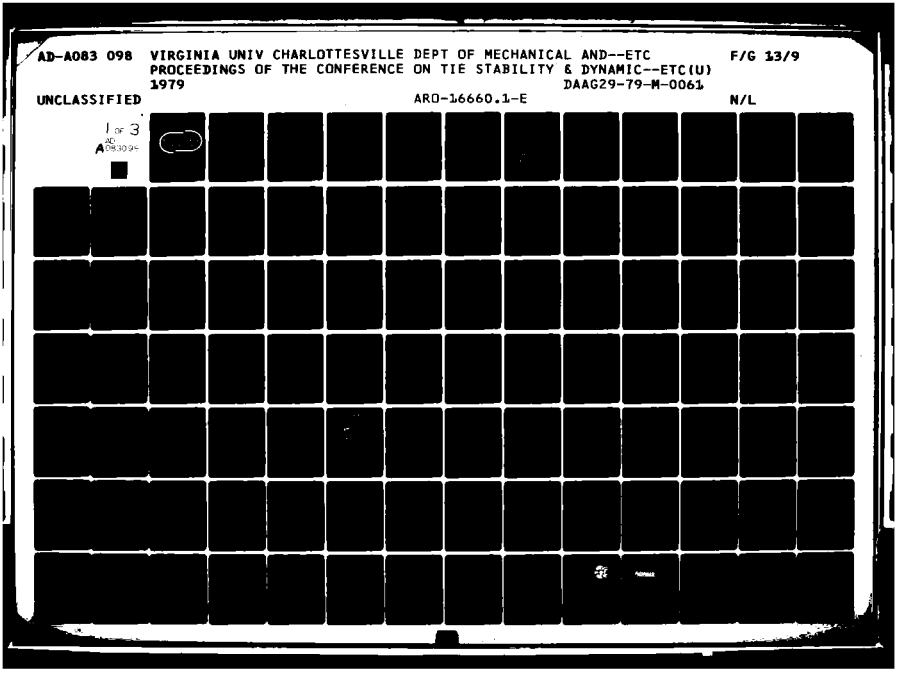

PROCEEDINGS

OF THE

CONFERENCE ON THE STABILITY AND DYNAMIC RESPONSE OF ROTORS WITH SQUEEZE FILM BEARINGS

8-10 MAY 1979

U. S. ARMY RESEARCH OFFICE
RESEARCH TRIANGLE PARK, NORTH CAROLINA

APPLIED TECHNOLOGY LABORATORY
U.S. ARMY RESEARCH AND TECHNOLOGY LABORATORIES (AVRADCOM)
FORT EUSTIS, VIRGINIA

DISCLAIMERS

The findings in this report are not to be construed as an official Department of the Army position unless so designated by other authorized documents.

When Government drawings, specifications, or other data are used for any purpose other than in connection with a definitely related Government procurement operation, the United States Government thereby incurs no responsibility nor any obligation whatsoever; and the fact that the Government may have formulated, furnished, or in any way supplied the said drawings, specifications, or other data is not to be regarded by implication or otherwise as in any manner licensing the holder or any other person or corporation, or conveying any rights or permission, to manufacture, use, or sell any patented invention that may in any way be related thereto.

Trade names cited in this report do not constitute an official endorsement or approval of the use of such commercial hardware or software.

DISPOSITION INSTRUCTIONS

Destroy this report when no longer needed. Do not return it to the originator.

Unclassified

SECURITY CLASSIFICATION OF THIS PAGE (When Data Entered)

REPORT DOCUMENTATION PAGE		READ INSTRUCTIONS BEFORE COMPLETING FORM
1. REPORT NUMBER	2. GOVT ACCESSION NO.	3. RECIPIENT'S CATALOG NUMBER
4. TITLE (and Subtitle) PROCEEDINGS OF THE CONFERENCE ON THE STABILITY AND DYNAMIC RESPONSE OF ROTORS WITH SQUEEZE FILM BEARINGS		5. TYPE OF REPORT & PERIOD COVERED FR 6. PERFORMING ORG. REPORT NUMBER
7. AUTHOR(s)		8. CONTRACT OR GRANT NUMBER(s)
9. PERFORMING ORGANIZATION NAME AND ADDRESS Department of Mechanical & Aerospace Engineering University of Virginia Charlottesville, Virginia 22901		10. PROGRAM ELEMENT, PROJECT, TASK AREA & WORK UNIT NUMBERS
11. CONTROLLING OFFICE NAME AND ADDRESS U.S. Army Research Office Post Office Box 12211 Research Triangle Park, NC 27709		12. REPORT DATE 13. NUMBER OF PAGES 267
14. MONITORING AGENCY NAME & ADDRESS(if different from Controlling Office) Applied Technology Laboratory U.S. Army Research & Technology Laboratories (AVRADCOM) Fort Eustis, Virginia 23604		15. SECURITY CLASS. (of this report) Unclassified 15a. DECLASSIFICATION/DOWNGRADING SCHEDULE

16. DISTRIBUTION STATEMENT (of this Report)

Approved for public release; distribution unlimited.

17. DISTRIBUTION STATEMENT (of the abstract entered in Block 20, if different from Report)

18. SUPPLEMENTARY NOTES

19. KEY WORDS (Continue on reverse side if necessary and identify by block number)

Rotordynamics
Stability
Dampers
Rotors
Flexible Shafts
Dynamics
Bearings

20. ABSTRACT (Continue on reverse side if necessary and identify by block number)

This document contains presentations made at the Conference on the Stability and Dynamic Response of Rotors with Squeeze Film Bearings. The conference, co-sponsored by the U.S. Army Research Office, the Applied Technology Laboratory, and the Rotor Dynamics Laboratory of the University of Virginia, Department of Mechanical and Aerospace Engineering, was held in Charlottesville, Virginia on May 8-10, 1979. The purpose of the conference was to assemble experts on squeeze film bearings to assess the current state of the art squeeze film bearing technology and to determine future research requirements.

DD FORM 1 JAN 73 1473 EDITION OF 1 NOV 65 IS OBSOLETE

Unclassified

SECURITY CLASSIFICATION OF THIS PAGE (When Data Entered)

PREFACE

This volume contains presentations made at the Conference on the Stability and Dynamic Response of Rotors with Squeeze Film Bearings. The conference, co-sponsored by the U.S. Army Research Office, the U.S. Army Applied Technology Laboratory and the Rotor Dynamics Laboratory of the University of Virginia, Department of Mechanical and Aerospace Engineering, was held in Charlottesville, Virginia on May 8-10, 1979.

The purpose of the conference was to assemble experts on squeeze film bearings to assess the current state of the art squeeze film bearing technology and to determine future research requirements. Over 50 participants attended the conference, representing industry, government and university interests in squeeze film bearing technology. They represented five countries, Australia, Canada, Denmark, England, and the United States.

Papers presented at the conference dealt with the basic hydrodynamic behavior of squeeze bearing oil films, the effects of squeeze film bearings on the dynamic response of rotor-bearing systems, design techniques and methods of analyzing complicated rotor-bearing systems including squeeze film bearings. The consensus of the participants was that further research is needed to more fully understand the behavior of lubricant films undergoing squeeze actions. This research involves both the experimental determination of squeeze flow effects with fluid cavitation and a more precise analytical description of the forces developed. The results of such future research would allow more confidence in squeeze film bearing design applications including the nonlinear aspects of such designs.

The editors wish to thank all those who participated in the conference. Special thanks go to Dr. Edward Saibel of the U.S. Army Research Office, Research Triangle Park, North Carolina and to Mr. Allen Royal of the U.S. Army Applied Technology Laboratory, Ft. Eustis, Virginia.

L. E. Barrett
P. E. Allaire
E. J. Gunter

TABLE OF CONTENTS

A Current Review of Rotordynamics Problems in High Speed Lightweight Turbomachinery and Power Shafting

by

Dr. John M. Vance, P.E.
Associate Director,
Gas Turbine Laboratories
Texas A&M University
College Station, Texas 77843

ABSTRACT

The special requirements and characteristics of turboshaft engines and power shafting for aircraft applications are reviewed, from the viewpoint of their impact on rotor dynamics and vibration problems.

Rotor dynamics and vibration problems are classified according to the type of excitation and useful diagnostic information. Suggestions are made to increase the use of vibration instrumentation and diagnostic electronics, following the lead of industrial compressor users.

The current role and future potential of squeeze film bearing dampers for solving the identified problems are discussed.

Recommendations for future research are given.

INTRODUCTION

As described in reference 1, there are a number of special requirements connected with rotor dynamics that are peculiar to the rotor-bearing systems in the class of small turboshaft engines and power drives being developed for U.S. Army aviation. They are:

1. Increasing power/weight ratios, now approaching about 4 HP/lb. This results in flexible engine rotors and structures.
2. Small physical size, especially in frontal area and wheel diameter.
3. Increasingly higher shaft speeds, to satisfy requirements 1. and 2.
4. Front drive, which usually has the power shaft passing through the compressor spool (Figures 1 and 2).
5. Maintainability, so that individual components making up the rotor-bearing assembly are easily replaceable.
6. Long life, to reduce frequency of downtime and overhauls.

AIRCRAFT ENGINE SCHEMATIC

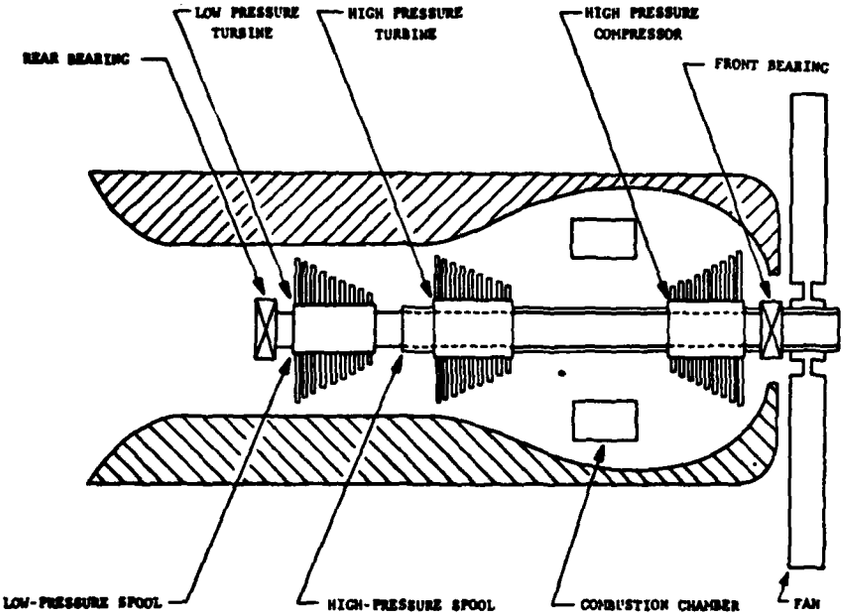

Fig. 1: Turboshaft Front Drive Schematic

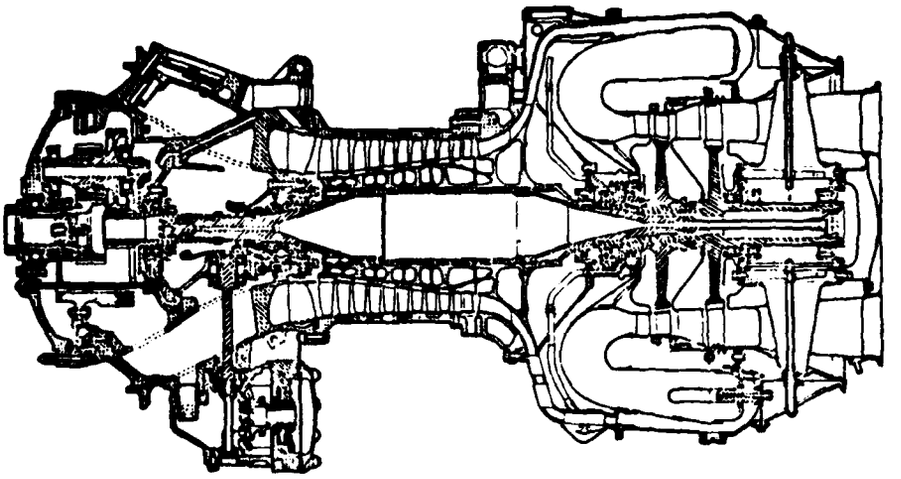

Fig. 2: Turbine Engine Cutaway

Taken together, these requirements are a severe challenge. For example, the combination of requirements for high power and small wheel diameter results in extremely small blade tip clearances. This limits the acceptable rotor disk excursions due to shaft whirl, and is therefore difficult to achieve with flexible lightweight rotors.

The higher output shaft speeds found in these new engines also presents a challenge to the power transmission shaft designer. For aircraft applications, a current goal is to develop a shaft/coupling system which can transmit 500-1500 HP at 20,000-30,000 rpm while tolerating large angles of misalignment. Figures 3, 4, and 5 show some of the whirling modes which must be considered.

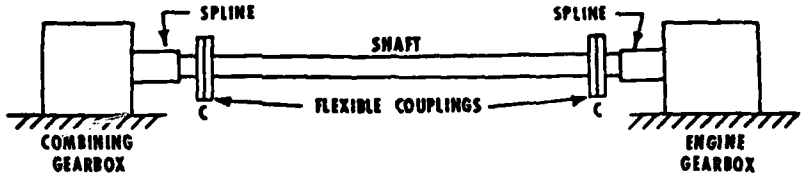

Fig. 3: **SCHEMATIC OF CHINOOK CROSS SHAFT ASSEMBLY**

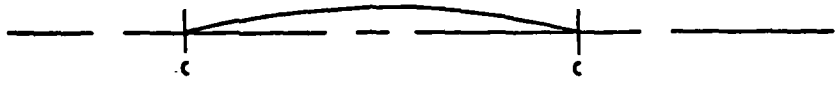

Fig. 3(a): **FIRST FLEXURAL MODE SHAPE FOR DRIVE SHAFT**

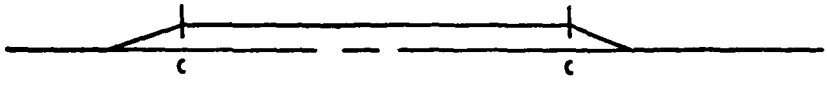

Fig. 3(b): **RIGID-BODY MODE SHAPE, CYLINDRICAL WHIRL**

Fig. 3(c): **RIGID-BODY MODE SHAPE, CONICAL WHIRL**

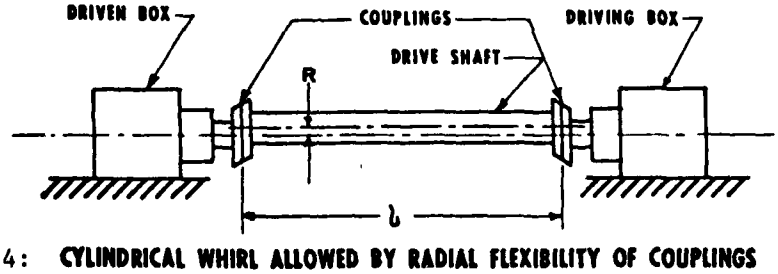

Fig. 4: **CYLINDRICAL WHIRL ALLOWED BY RADIAL FLEXIBILITY OF COUPLINGS**

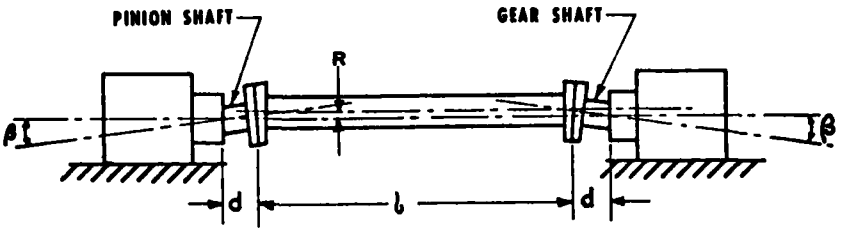

Fig. 5: **CYLINDRICAL WHIRL ALLOWED BY BEARING OR SPLINE CLEARANCE AND BENDING FLEXIBILITY OF COUPLINGS**

From the standpoint of U.S. Army needs, there are two incentives for developing improved technology for rotor-bearing systems design:

a. Optimization of design parameters to maximize the life, reliability and safety of engines and power shafting, and
b. Accurate prediction of dynamics so as to avoid costly problems and delays associated with new hardware development programs.

Squeeze Film Dampers

Rotor dynamics design is mostly involved with adjusting existing machine parameters (bearing stiffness and damping, unbalance, etc.) to achieve stable and smooth running of the rotors and shafts. The one machine component which is added solely for the purpose of improving the rotor dynamics is the squeeze film bearing damper (Figure 6). The fact that most new engines are now fitted with these dampers is testimony to their effectiveness.

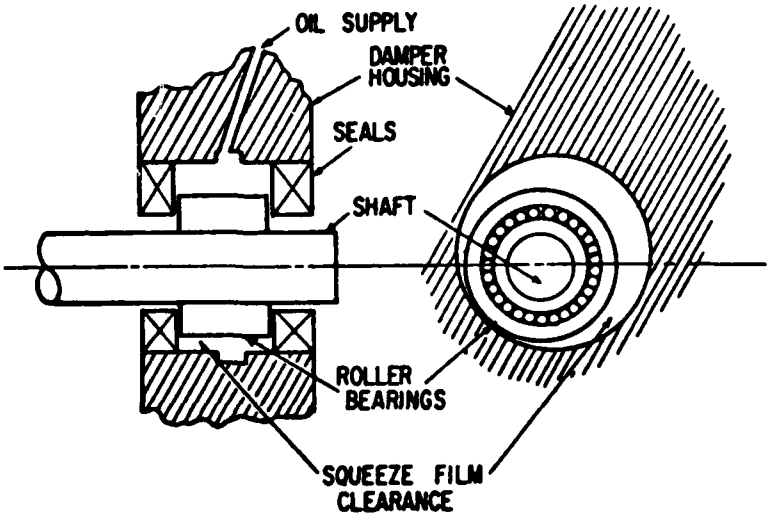

Fig. 6: Squeeze Film Bearing Damper

Many squeeze film dampers in use today were designed by "cut and try" methods. In spite of a considerable amount of research which has been done to develop an analytical capability for predicting their performance, it is still not clear that this can be done reliably and accurately for all cases and conditions of practical interest. Also, it is the opinion of the author that the available technology for design analysis has not been fully utilized by the engine and airframe contractors, due to the natural inertia of technology transfer.

It has been demonstrated, however, that well designed dampers can be effective for reducing both synchronous and nonsynchronous vibrations. The main purpose of this paper is to review the current state-of-the-art for rotor dynamics technology, in order to suggest both the potential and the limitations of these dampers for turbomachinery applications.

Since the proper design of a damper must be governed in part by the type of vibration it is meant to suppress, it is helpful to classify rotor dynamics problems accordingly. When problems occur in hardware development programs or in the field, a proper classification of the problem is an essential part of the troubleshooting procedure which leads to a solution. The petrochemical and chemical process industries have led the way in utilizing modern instrumentation and vibration analysis techniques for diagnosis of vibration problems in rotating machinery. As will be seen in the next section, frequency spectrum analysis has been found to play a useful and powerful diagnostic role. In the author's opinion, this is a technology which should be more fully utilized in developing turbomachinery for military applications.

Rotor Dynamics Problems Classified

In general, rotor dynamics problems can be classified as either forced vibration which mainly involves the shaft-whirling and vibration response to rotor unbalance, or as whirling instabilities, which are generated by self-excited forces arising from internal friction, gas pressure forces, etc., or by parametric excitations.

Table I shows the specific types of forced vibration, along with diagnostic information and solutions which have been found to be effective. Table II given the same kind of information for shaft whirling instabilities. These tables are modifications and extensions of Table 1 in reference 2.

Forced vibration is much more common than whirling instability, but the latter is usually more destructive, more difficult to predict, and more difficult to diagnose and control.

The two classes of problems are characterized by different vibration amplitude vs. rpm behavior. Forced vibration, especially synchronous response to unbalance, exhibits amplitude peaks at the critical speeds which fall off as the speed exceeds the critical speed. Whirling instabilities, on the other hand, show sharply rising amplitudes as a threshold of speed (and/or load) is reached. The threshold usually cannot be exceeded without damage to the machinery. Figure 7, taken from reference 3, shows the typical change in vibration spectrum and amplitude which occurs as a threshold of instability is reached. This type of plot, called a "raster" or "waterfall",

can be generated in real time and plotted automatically by electronic equipment which is now developed to a high state of refinement and efficiency. Figure 7 was taken from a centrifugal compressor used in the petroleum industry. It can be seen that the frequency spectrum analysis is an indispensable diagnostic tool. If only vibration amplitude measurements were made, it might simply be assumed that the rotor was out-of-balance, since this is the most common cause of machinery vibration.

TABLE I: Classification of Forced Vibration of Rotating Machinery

Diagnostic Information ↓ / Type of Vibration →	Synchronous Response to Unbalance (Shaft Whirling)		Intershaft Response	Externally Forced	Supersynchronous Response
	Rigid-Body Modes	Flexible Modes			
Source of Excitation	Rotor unbalance, static and dynamic	Rotor and shaft unbalance, distributed along shaft	Vibration of connected shafts (e.g., intershaft bearings)	Airframe or foundation vibration (e.g., air loads on helicopter rotary wing)	Coupling misalignment, shaft misalignment, shaft stiffness asymmetry, rolling element bearing imperfections
Vibration Frequency	Synchronous with shaft rotational speed $f_s = \frac{N\ rpm}{60}$ Hz	Synchronous with shaft rotational speed $f_s = \frac{N\ rpm}{60}$ Hz	Asynchronous, at rotational frequency of connected shafts	Asynchronous, frequency of external vibratory force, Natural frequencies of structure	Multiples of shaft rotational speed, $f_n = n\frac{N\ rpm}{60}$ Hz Typically, n = 2
Effective Solutions	Single-plane (static) or two-plane (dynamic) balancing, Squeeze-film bearing dampers, tuning of critical speeds to avoid resonance	Multi-plane or modal balancing, tuning of critical speeds to avoid resonance, bearing dampers may not be effective at supports or near nodes.	Balancing of other shafts in multi-spool rotors, tuning to avoid resonance with exciting frequencies, isolated mounting of intershaft bearings	Reduce amplitude of external vibratory forces, Isolate the rotating machinery with soft mounts and/or couplings Tune natural frequencies to avoid resonance	Align shafts and couplings, make shaft sections circular, tune critical speeds to avoid resonance with nN

There are a number of self-excitation mechanisms which can produce whirl instabilities. They are listed on Table II. Figures 8 and 9 show how two of them are generated. Figure 8 illustrates the forward tangential force component generated by the shaft whirl motion when there is a fluid trapped inside a hollow rotor. It can be seen that any small perturbation of shaft whirling will produce this tangential force, which will then increase in proportion to the whirl magnitude. Thus, the motion is "self-excited", and an unstable build-up will result unless there is sufficient external damping to oppose it.

Figure 9 illustrates "Alford's force", which is a similar type of destabilizing force induced by the circumferential variation of dynamic gas pressure forces on blading in axial-flow turbomachines. Alford hypothesized that the tangential forces on the blades should vary as a result of tip

clearance variations produced by the disk whirling displacement. This theoretical model is contained in most of the computerized stability analyses used by rotor dynamics consultants. It has never been experimentally verified, although a test rig to accomplish this has recently been built at the University of Florida (reference 4).

TABLE II: Classification of Shaft Whirling Instabilities in Rotating Machinery

Diagnostic Information ↓ / Type of Vibration →	Self-Excited Nonsynchronous Whirl	Parametrically Excited Whirl
Sources of Excitation	Oil film bearings ("oil whip"), internal friction in rotating parts, trapped fluid in rotor, tip clearance effects in axial flow bladed disks ("Alford's force"), labyrinth seals, ring seals, high gas pressure in centrifugal stages, rotor/stator rubbing friction (induces backward whirl), high torque loading on disks misaligned by the mode shape ("torquewhirl"), variable angle of attack on blades of axial stages ("propeller whirl flutter", can be forward or backward), dense or viscous fluid in impeller housings	Asymmetric shaft stiffness, asymmetric rotor inertia, pulsating torque.
Whirl Frequency Ratio $\frac{f}{fs}$	Almost always subsynchronous, typically 0.3 - 0.8	Usually supersynchronous, f/fs > 1.0
Shaft Speeds Where Encountered	Supercritical speeds, especially at $2w_{CR}$ and above	Subcritical speeds
Effective Solutions	Stiffen shafts or shorten bearing spans to raise bending critical speeds, Asymmetric bearing supports, Squeeze-film bearing dampers, Soften bearing supports to allow dampers to operate effectively	Squeeze-film bearing dampers, remove asymmetries, isolate pulsating torque with torsionally soft coupling

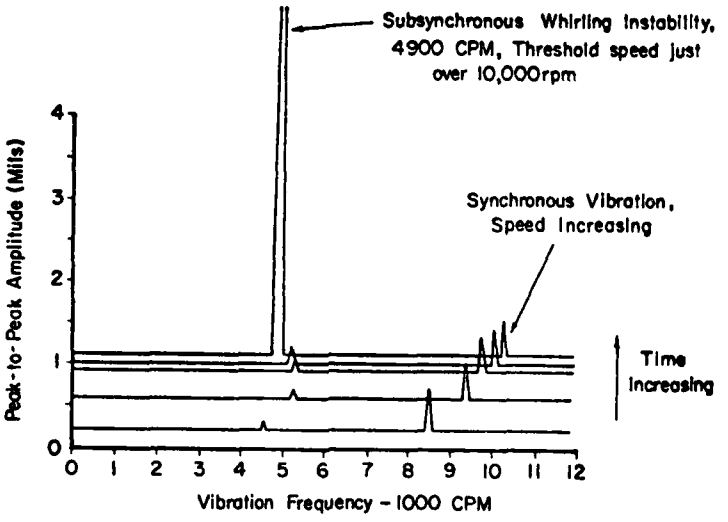

Fig. 7: "Waterfall" Plot of Vibration Specturm Showing Rotor Whirl Instability in Centrifugal Compressor Taken From Reference 3 (Poulie and Miles).

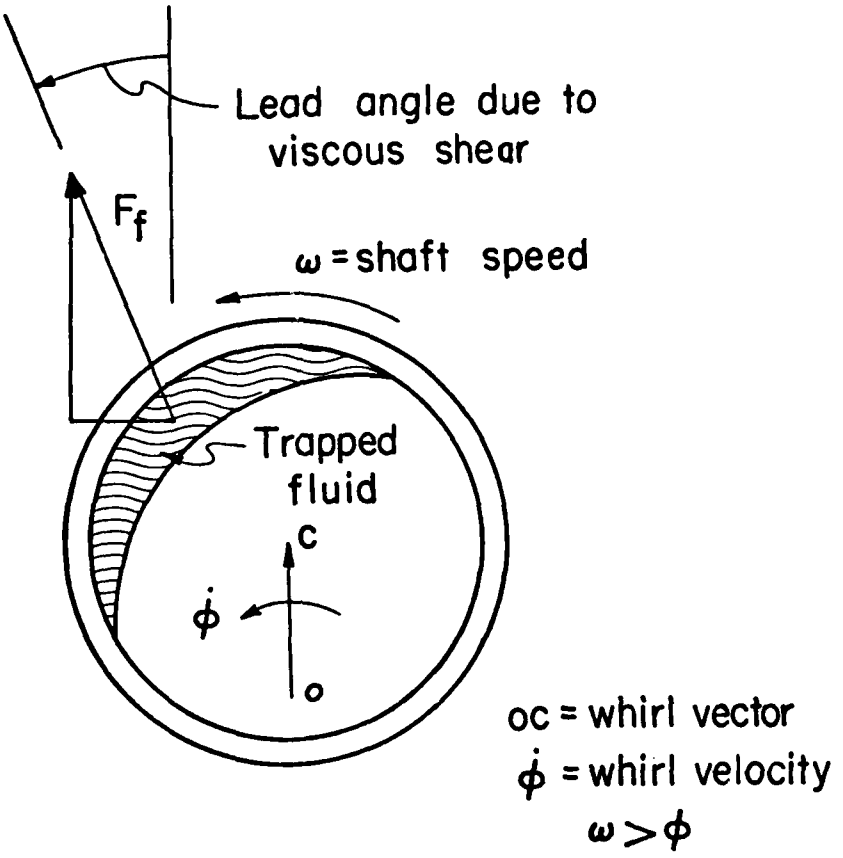

Figure 8: Whirl Induced by Trapped Fluid

In Table 1, synchronous response to unbalance is subclassified according to whether rigid-body or flexible (bending) modes are the dominant motion. The type of mode is determined by the speed and relative stiffness of bearing supports and shafts. Figure 10 shows the effect of bearing support stiffness on the whirling mode shapes. In high speed turbomachinery, the bearing supports are generally made soft to reduce dynamic bearing loads due to rotor unbalance. However, squeeze film dampers have stiffness properties which vary (typically increasing) with speed, so that the supports may become effectively hard under certain conditions. Therefore, a given engine or rotor-bearing system could display any of the different types of mode shapes shown on Figure 10, depending on the operating conditions.

In general, both the response to unbalance and whirling instabilities are more difficult to control when they involve shaft bending modes. When the shaft bends, the magnitude and distribution of unbalance changes, so that a

rigid-body approach to balancing is not adequate. Also, bending modes may not induce enough motion at the support locations to make dampers effective.

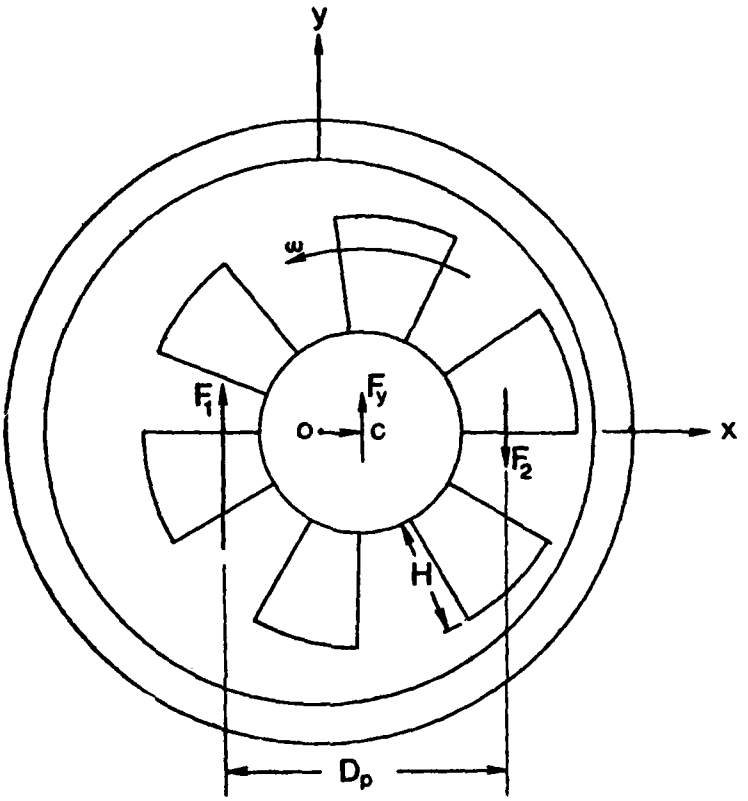

$$F_y = F_1 - F_2 = -K_{yx} X = -K_{yx} \overline{OC}$$

$$K_{xy} = -K_{yx} = \frac{\eta T_s}{D_p H}$$

Fig. 9: Alford's Force

State-of-the-Art and Squeeze Film Damper Technology

Until a few years ago, most aircraft gas turbine rotors were normally designed to operate below the third critical speed (the first "bender", with very soft supports). Figure 11 shows the traditional "safe" region of operation on a critical speed map. The newest operational U.S. Army turboshaft helicopter engine runs at super critical speeds, relative to the third critical speed of the power shaft. A squeeze film damper is used to minimize balancing requirements and suppress any potential whirling instabilities.

This application exemplifies why the squeeze film hearing damper has become one of the most utilized solutions to many of the rotor dynamics problems classified in the previous section. It is, however, extremely difficult to

design a damper which is effective under all conditions for all types of problems. It has been shown, for example, that a damper designed to suppress synchronous response to unbalance, for normally expected levels of unbalance, can actually increase shaft whirling under increased levels of unbalance (see reference 5). Conversely, a damper optimized to guarantee rotor-bearing system survival under conditions of a lost turbine blade might not work well with nominal levels (design tolerances) of unbalance.

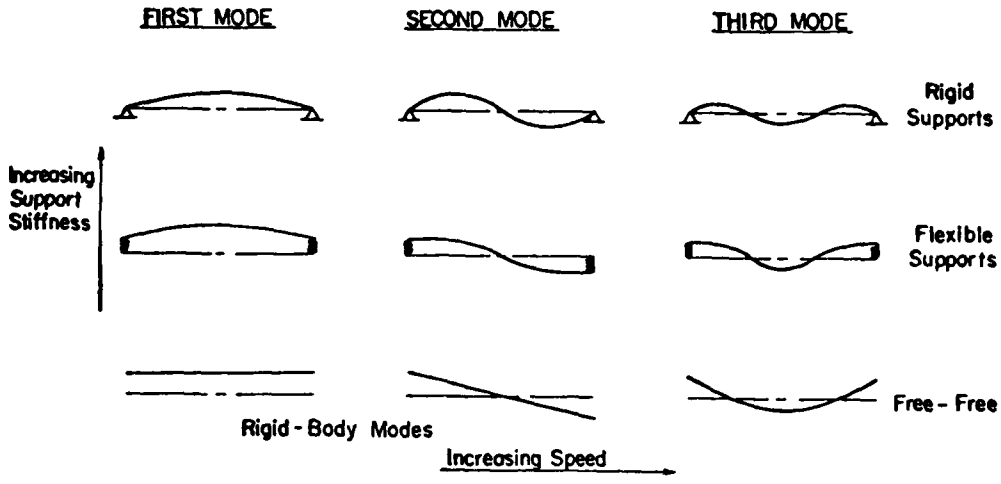

Fig. 10: Effect of Bearing Support Stiffness on Undamped Shaft Whirling Mode Shapes

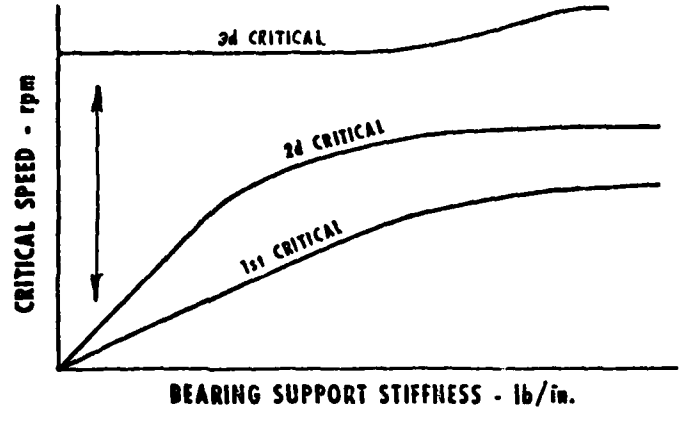

Fig. 11: Typical Critical Speed Map

At present, the analytical techniques that have been developed for squeeze film damper design are all based on solutions to Reynold's equation, which predict the viscosity-generated oil film pressures around the damper. References 6 and 7 exemplify the state-of-the-art. It has been shown experimentally that, at least under some conditions, such an analysis is adequate (references 8 and 9).

However, although blade loss experiments are reported in reference 9 to be good agreement with numerical predictions, the damper design parameters were not varied at all, and the nonlinear "jump" phenomenon reported in references 5 and 10 was therefore not investigated.

It is also becoming apparent that a Reynold's analysis does not apply in certain cases of practical interest. The pertinent and critical assumptions implicit in Reynolds equation are:

1. Fluid mass inertia effects are neglected,
2. The fluid is assumed to be single-phase (i.e., no gas bubbles),
3. Fluid viscosity is assumed to be constant in time and space.

In cases where Reynold's equation does apply, the equations are highly nonlinear, and the linear model used in some computer programs is adequate only under special conditions.

To the author's knowledge, all dampers currently used in aircraft gas turbine engines were designed primarily to suppress synchronous response to unbalance for passage through the critical speeds, assuming nominal design levels of unbalance. As engine designs progress to supercritical speeds, higher pressure ratios, and higher specific horsepower, an increasing number of whirling instability problems can be expected. Reference 11 recounts the experience of one turboshaft engine manufacturer with a problem of this type.

Rotor whirl stability is a problem which is now costing the petroleum industry and industrial compressor manufacturers hundreds of millions of dollars in lost production and expensive redesigns. Avoidance of these problems in the aircraft turbine industry through a program of farsighted research would appear to be cost effective.

For aircraft applications, the use of oil film dampers to suppress whirl instabilities is questionable from the standpoint of flight safety. In fact, although it is known that longer bearing life could be obtained with oil film bearings for rotor support, they are currently not used because of their catastrophic mode of failure in the event of lubricant supply interruption. It can be argued that dampers should not be used to suppress whirl instability, for the same reason, unless special provisions are made for redundancy, etc.

Power transmission shafts for modern helicopter propulsion systems are also now entering the regime of supercritical operation, and so are subject to whirling instability problems. The use of squeeze film dampers for suppression is especially difficult in this application, because of the high stiffness requirement on shaft support bearings, particularly when gear loads must be reacted in close proximity. The comments above on flight safety apply here also.

Thus, although the squeeze film bearing damper is now an effective device

for reducing vibracion, the following four limitations have been identified:

a. There are apparently certain cases of practical interest where a Reynold's equation analysis is not accurate or sufficient to predict damper performance,
b. Analytical design techniques are not yet verified to adequately treat the nonlinear effects associated with sudden large unbalance due to blade loss in a flexible-shaft turborotor system with squeeze-film dampers,
c. Analytical design techniques are not yet developed to optimize dampers for suppression of self-excited or parametrically excited whirl instabilities. The question of flight safety must be carefully considered if dampers are to be used for suppression of instabilities.
d. Design of squeeze film dampers for power transmission shafting is especially difficult, due to the usual requirement of high stiffness at the shaft bearing supports.

Suggestions for Future Research

It is the opinion of this author that the analytical tools (computer programs, etc.) in this field have been refined to a point (see, for example, reference 12) where any further progress must be guided by new experimental research designed to identify appropriate new directions for development.

Each of the four limitations identified in the previous section suggests a need for new experimental research. Taking each of them in order, the following experimental programs are suggested:

a. Full scale, full speed, testing of actual engine damper hardware with sufficient instrumentation to identify two-phase liquid-gas formation, variation of temperature, fluid velocities, seal leakage, etc.
b. An extension of the experimental studies of reference 9 to cover a wide range of damper design parameters and rotor dynamic parameters. Predicted conditions for bistable orbits should be verified or modified.
c. The sources of excitation of rotor whirl stabilities should be studied experimentally, using test rigs designed to exhibit the various types of known instabilities. Existing theories should be verified (or modified) by experimental measurements, and the excitations should be quantified in terms of measurable parameters wherever possible. The sensitivity to bearing support damping should be determined for each type of excitation.
d. A test program should be designed and carried out to investigate the use of elastomeric dampers for suppression of vibration and whirl in high speed (supercritical) power transmission shafts. Recent developments and improved data on elastomeric properties (see reference 13) should make it possible to improve the results of some years ago reported in reference 14.

REFERENCES

1 Vance, J. M., "High-Speed Rotor Dynamics--An Assessment of Current Technology for Small Turboshaft Engines," USAAMRDL-TR-74-66, July 1974, Eustis Directorate, U.S. Army Air Mobility Research and Development Laboratory (Now Applied Technology Laboratory, USARTL(, Ft. Eustis, VA.).

2 Ehrich, F. F., "Identification and Avoidance of Instabilities and Self-Excited Vibrations in Rotating Machinery," ASME Paper No. 72-DE-21, Design Engineering Conference, Chicago, IL, May 8-11, 1972.

3 Fowlie, D. W., and Miles, D. D., "Vibration Problems with High Pressure Centrifugal Compressors," ASME Paper No. 75-PeT-28, Petroleum Mechanical Engineering Conference, Tulsa, OK, Sept. 21-25, 1975.

4 Vance, J. M., and Sandor, G. N., "Investigation of Load-Induced Nonsynchronous Whirl Instabilities in Rotating Machinery," Final Report, ARO Grant No. DAAG29-77-G-0217, April 1979, U.S. Army Research Office, Durham, NC.

5 White, D. C., "The Dynamics of a Rigid Rotor Supported on Squeeze Film Bearings," Conference on Vibrations in Rotating Systems, London, Proceedings, Institution of Mechanical Engineers, Feb. 14-15, 1972.

6 Cunningham, R. E., Gunter, E. J., and Fleming, D. P., "Design of an Oil Squeeze Film Damper Bearing for a Multimass Flexible-Rotor Bearing System," NASA-TN-D-7892, Feb. 1975, Lewis Research Center, Cleveland, OH.

7 Holmes, R., "The Damping Characteristics of Vibration Isolators Used In Gas Turbines," Journal Mechanical Engineering Science, I. Mech. E., Vol. 19, No. 6, 1977.

8 Vance, J. M., and Kirton, A. J., "Experimental Measurement of the Dynamic Force Response of a Squeeze-Film Bearing Damper," ASME Journal of Engineering for Industry, pp. 1282-1290, November 1975.

9 Buono, D. F., Schlitzer, L. D., Hall R. G. III, and Hibner, D. H., "Transient Dynamics of a Flexible Rotor with Squeeze Film Dampers," NASA-CR-3050, Contract NAS3-18523 Final Report, September 1978, Lewis Research Center.

10 Mohan, S., and Hahn, E. J., "Design of Squeeze Film Damper Supports for Rigid Rotors," ASME Journal of Engineering for Industry, Vol. 96, No. 3, 1974, pp. 976-982.

11 Williams, R., Jr., and Trent, R., "The Effects of Nonlinear Asymmetric Supports on Turbine Engine Rotor Stability," SAE Paper No. 700320, National Air Transportation Meeting, New York, NY, April 20-23, 1970.

12 Marmol, R. A., and Vance, J. M., "Squeeze Film Damper Characteristics for Gas Turbine Engines," ASME Journal of Mechanical Design, January 1978, pp. 139-146.

13 Smalley, A. J., Darlow, M. S., and Mehta, R. K., "The Dynamic Characteristics of O-Rings," ASME Journal of Mechanical Design, January 1978, pp. 132-138.

14 Prause, R. H., Meachem, H. C., and Voorhees, J. E., "The Design and Evaluation of a Supercritical Speed Helicopter Power-Transmission Shaft," ASME Journal of Engineering for Industry, November 1967, pp. 719-727.

REVIEW OF TESTS ON THE HIGH-SPEED OIL-FILM DAMPER RIG

by

M. Botman

PRATT & WHITNEY AIRCRAFT OF CANADA LTD.

LONGUEUIL, QUEBEC, CANADA

ABSTRACT

The High-Speed Oil-Film Damper Rig at P&WC has been used for experiments on a number of oil-film dampers of various designs. The experiments included steady state as well as transient unbalance responses. From the viewpoint of the designer of aero turbo engines the characteristics of dampers of most interest are those that extend the capability of his design, e.g. the speed range of a rotor, or those that improve the acceptance by the customer, e.g. longer life of components or lower vibration levels. Since dampers operate practically always at relatively small eccentricities it is possible to generate useful design information on the basis of a simplified theory in which damper forces are assumed to be linear with deflection. The experimental and theoretical results have been obtained primarily for this purpose.

INTRODUCTION

Oil-film dampers are well established as components of rotor systems that provide damping and thereby suppress undesirable rotor dynamic responses. An extensive literature exists on the theoretical analysis of damper behavior. This behavior is characterized by strong nonlinearity at large eccentricities. Cavitation of the oil-film and instability of the rotor system are important effects at these eccentricities. Theoretical methods for the calculation of damper orbits under given support-, loading-, and boundary conditions are now generally available. These methods have limitations which make them unsuitable for design purposes. Their accuracy in the nonlinear range has not been established and is debatable. Also, they are very demanding in computer time and, therefore, not attractive for parameter studies.

The desirability of the presence of dampers at certain bearing locations can be determined quite early in the design phase of an engine on the basis of critical speed and unbalance response analyses. Specific damper designs evolve in the development phase as a result of experiments. However, increased sophistication of rotor designs, and the necessity to minimize design changes during the development phase, may force the designer to depend more critically on dampers to provide acceptable rotor dynamics behavior. Hence, there is a need for reliable design information on dampers that will be useful in preliminary and advanced design efforts.

This paper summarizes the experimental work on dampers that has been performed at P&WC, and it presents some conclusions that can be drawn from a simplified linearized theory (Refs. 1-3).

EXPERIMENTAL WORK

The test rig that has been used for damper investigations has a vertical rotor as shown in Fig. 1. The tests were aimed at the high speed range up to 60,000 RPM. The configuration chosen runs in vacuum and is driven by a simple air turbine. Measurements can be taken of all quantities of interest: damper deflections and loads in two directions, oil pressures, - flow and - temperatures, and rotor speed and phase with respect to a reference fixed on the rotor. Numerous steady-state unbalance response runs and transient tests have been performed. In the latter a small mass is released at a preselected speed simulating blade loss conditions.

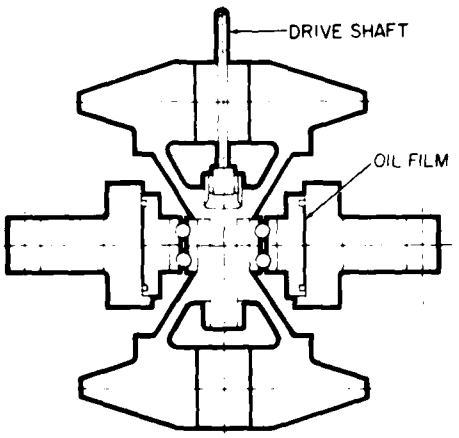

Fig. 1

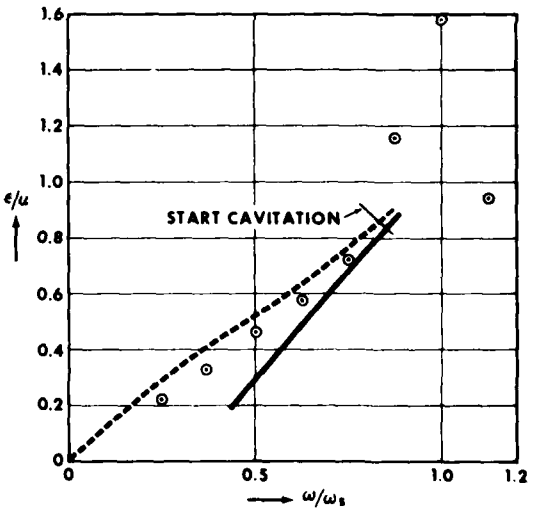

Fig. 2

Some steady-state deflection measurements are illustrated in Fig. 2 as a function of speed. The nondimensional quantities are defined as follows:

eccentricity $\varepsilon = e/C$
unbalance $u = am/CM$
speed of rotation ω/ω_s

where:

e = damper radial deflection

C = damper radial clearance

m = unbalance mass

M = rotating mass

a = radial location of m

ω_s = support natural frequency

It should be noted that $\epsilon / u = 1$ represents the condition where the rotor orbits around its unbalanced c.g. as it would if it was unsupported.

An example of a typical transient test is shown in Fig. 3 for the deflection in one direction and in Fig. 4 for the corresponding orbit. The transient mass release results in an eccentric orbit which is centered within about 10 revolutions.

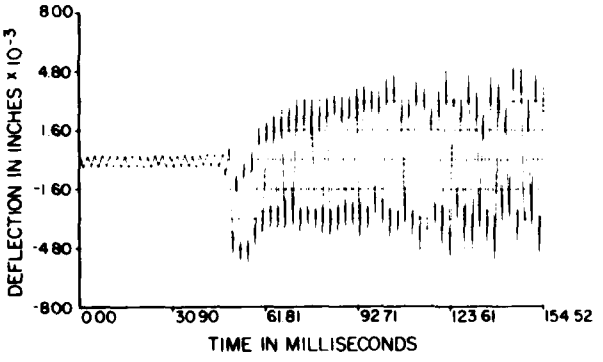

Fig. 3

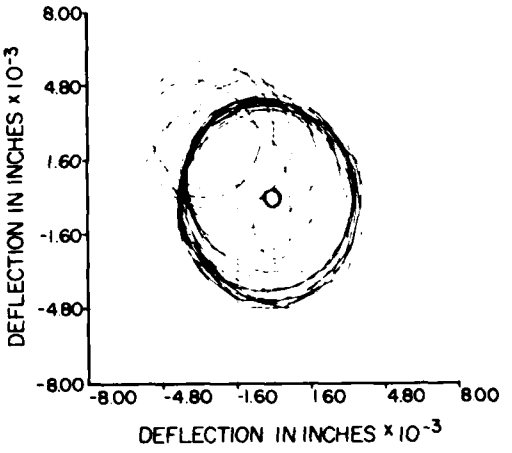

Fig. 4

THEORETICAL WORK

A linearization of the damper characteristics has been developed in Refs. 1 & 2 which is considered valid for small eccentricities ($\epsilon < .5$). This approximation gives reasonable agreement with the measured results as shown in Fig. 2 by the drawn line. The results are very sensitive to the actual values of the oil viscosity. For example, in Fig. 2 the drawn line has been calculated for viscosities corresponding to the measured temperatures at the various speeds. The dotted line has been calculated for the viscosity at the temperature measured at one speed.

On the basis of the simplified linear theory some damper characteristics of direct interest to the designer can be calculated. The more important are the transmissibility, the effective damping and the effective stiffness. The definitions and formulas are given in the references. Examples of the effective damping and stiffness as a function of speed are given in Figs. 5 & 6. The damping appears again to be sensitive to the viscosity of the oil. Both figures have limited validity at higher speeds because of the linearization.

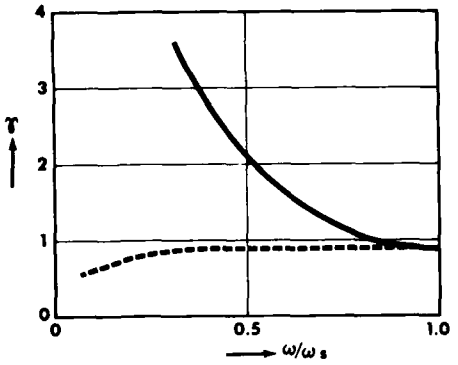

Fig. 5

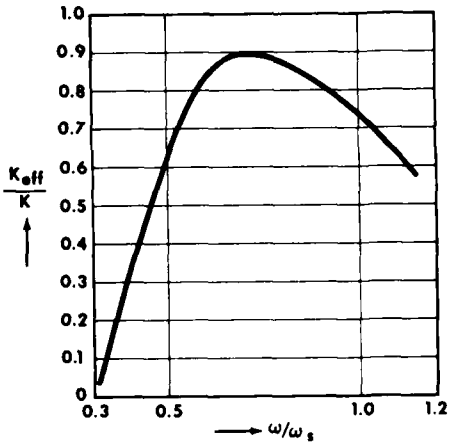

Fig. 6

CONCLUSION

The rig has performed satisfactorily allowing the measurement of all oil-film parameters over a wide speed range. The rig is especially useful for investigations of transient response phenomena.

The linearized theory appears adequate for the range of small eccentricities at which dampers operate in practice.

REFERENCES

1. Botman, M., "Experiments on Oil-Film Dampers for Turbomachinery", ASME Journal of Engineering for Power, Vol. 98, No. 3, July 1976, pp. 393-400.

2. Botman, M. and Sharma, R.K., "Experiments on the Transient Response of Oil-Film Dampers", ASME Journal of Engineering for Power, Vol. 100, No.1, Jan. 1978, pp. 30-35.

3. Sharma, R.K. and Botman, M., "An Experimental Study of the Steady-State Response of Oil-Film Dampers", ASME Journal of Mechanical Design, Vol. 100, No. 2, April 1978, pp. 216-221.

DYNAMIC CHARACTERISTICS OF A TWO-SPOOL GAS TURBINE HELICOPTER ENGINE

By

E. J. Gunter, Professor*
D. F. Li, Associate Senior Research Engineer**
L. E. Barrett, Research Assistant Professor*

*Department of Mechanical and Aerospace Engineering
University of Virginia
Charlottesville, Virginia

**General Motors Research Laboratories
Warren, Michigan

ABSTRACT

This paper presents a dynamic analysis of a two-spool gas turbine helicopter engine incorporating intershaft rolling element bearings between the gas generator and power turbine rotors. The analysis includes the nonlinear effects of a squeeze film bearing incorporated on the gas generator rotor. The analysis includes critical speeds and forced response of the system and indicates that substantial dynamic loads may be imposed on the intershaft bearings and main bearing supports with an improperly designed squeeze film bearing. A comparison of theoretical and experimental gas generator rotor response is presented illustrating the nonlinear characteristics of the squeeze film bearing. It was found that large intershaft bearing forces may occur even though the engine is not operating at a resonant condition.

INTRODUCTION

The requirement of high specific power output for gas turbine aircraft engines has resulted in highly flexible rotor designs. These rotors typically operate above several critical speeds. The use of rolling element bearings, with low inherent damping, makes it difficult to reduce vibrational amplitudes and dynamic loads transmitted to the rotor supporting structure. Operation over a wide range of speed and power levels aggravates the dynamic problems, and under some conditions, i.e. locked rotor starts, a bowed rotor may result due to nonuniform thermal distributions.

The low levels of rolling element bearing damping and large strain energy levels in modern designs necessitate the use of squeeze film bearings to provide adequate damping to maintain low amplitude vibration levels and to reduce the dynamic loads exerted upon the bearings and rotor support structures. The number and location of squeeze film bearings is dictated by

the engine configuration and dynamic characteristics (1). In addition, engines may utilize intershaft differential bearings, especially with very flexible rotor designs. The design of squeeze film bearings requires careful attention since an improper design may, in fact, worsen the dynamic response of the system (2).

A schematic of a typical two-spool gas turbine engine used for helicopter application is shown in Fig. 1. The engine consists of an inner core rotor (power turbine), which is supported by main bearings No. 0 and No. 4, located at the shaft extremities. There are two intershaft differential bearings connecting the power turbine to the gas generator rotor. The gas generator rotor consists of a two-stage turbine which drives an axial compressor. The gas generator rotor is supported principally by the Nos. 1, 2, and 3 bearings.

The No. 1 bearing is an elliptical roller bearing mounted in a thermal gradient housing. The No. 2 bearing is a thrust ball bearing mounted in the compressor rear frame, and the No. 3 or aft bearing is a close clearance roller bearing mounted in an oil film damper support near the gas generator turbine. The No. 0 roller bearing is mounted in the power turbine take off and supports the output turbine spline shaft. The No. 4 bearing is located in the exhaust frame and is a thrust ball bearing that carries the weight of the power turbine. The first or forward intershaft bearing is an elliptic differential bearing mounted between the power turbine shaft and the compressor No. 1 bearing. The second or aft intershaft bearing is mounted forward of the No. 3 bearing.

The gas generator rotor speed range is from 10,500 RPM to 18,230 RPM, and the power turbine speed is from 0 to 17,000 RPM. Typical continuous power turbine operating speed is 14,000 RPM.

The analysis presented herein includes both flexible rotors, the effects of the intershaft bearings, and the bearings connecting the rotors to the engine case. The case is considered rigid, although casing flexibility may be an important effect in certain applications.

CRITICAL SPEED ANALYSIS

The preliminary analysis of any rotor-bearing system usually includes the determination of the undamped critical speeds and associated mode shapes of the system. These results provide the basis for refining the system model and anticipating locations where squeeze film bearings may be potentially applied, i.e., locations where significant motion of the squeeze film bearing journal will occur to produce the required damping forces. The critical speed analysis utilized the transfer matrix method (3), (4).

Critical Speeds with Intershaft Bearings

Figures 2-4 illustrate the first three critical speed mode shapes of the two-spool engine of Fig. 1, including the stiffness of the intershaft bearings. For this analysis the gas generator rotor was assumed to be operating at 15,000 RPM and the critical speeds were calculated assuming synchronous motion of the power turbine.

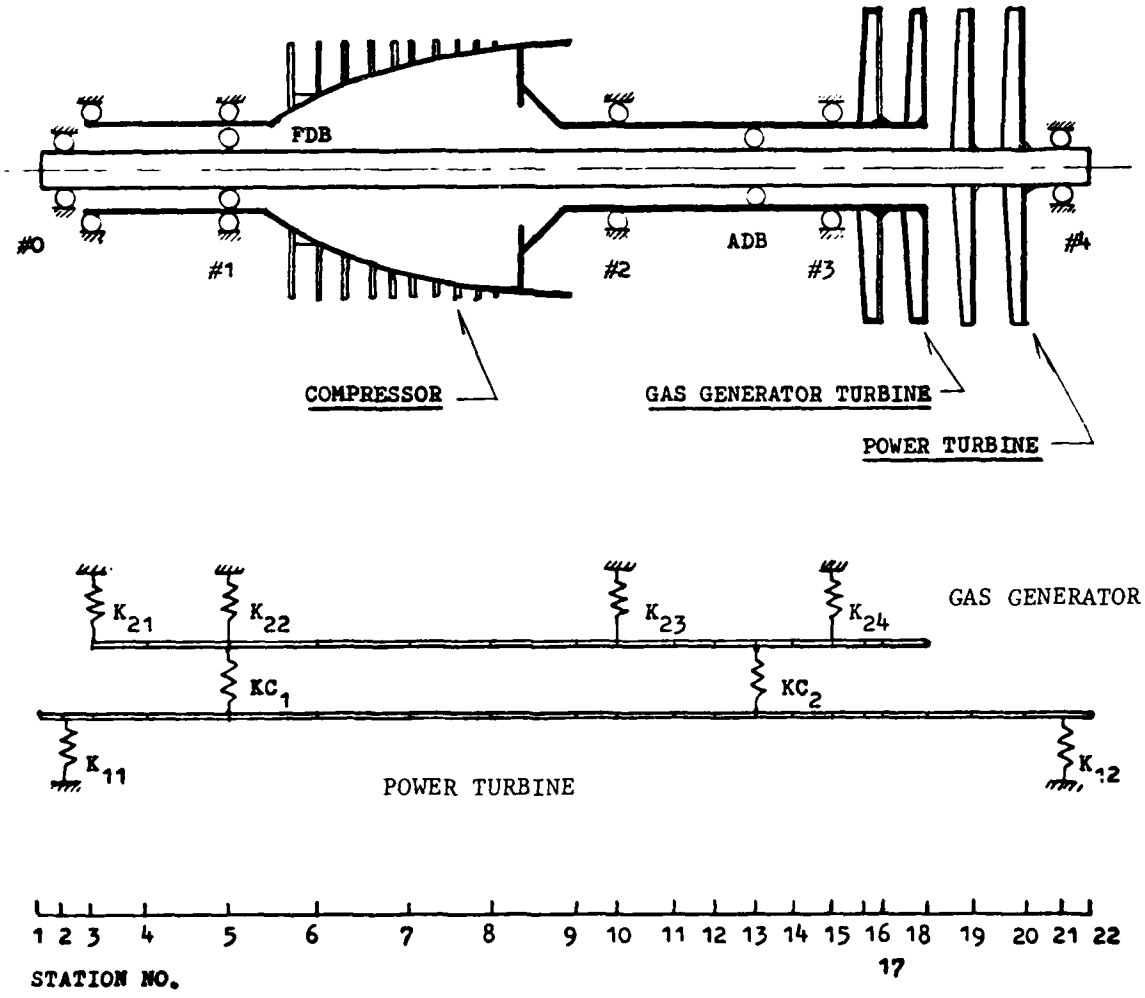

Fig. 1 Schematic of Two-Spool Gas Turbine Helicopter Engine with Computer Model.

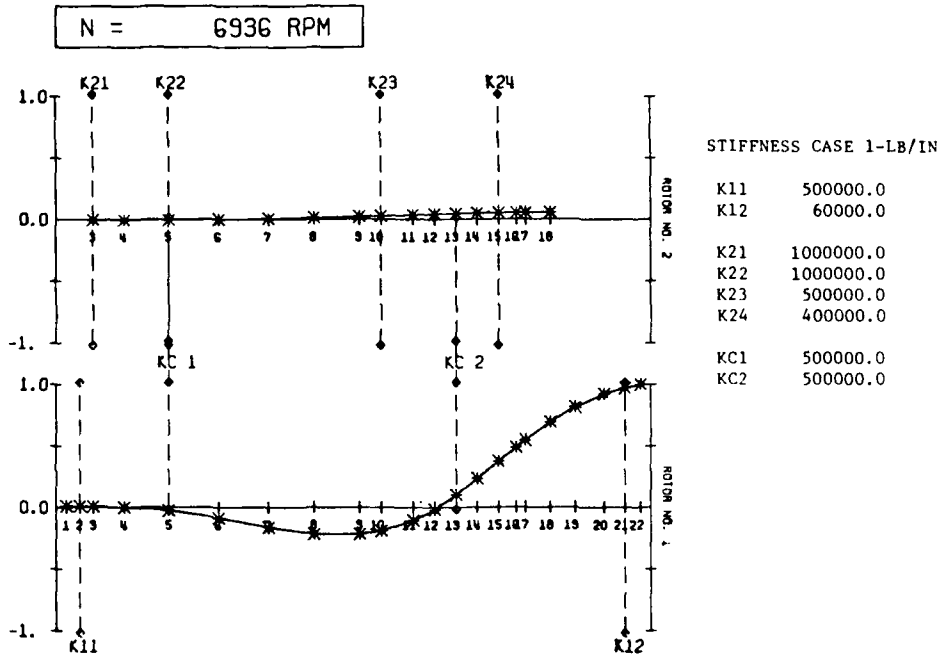

Fig. 2 First Engine Undamped Critical Speed with Aft Intershaft Differential Bearing

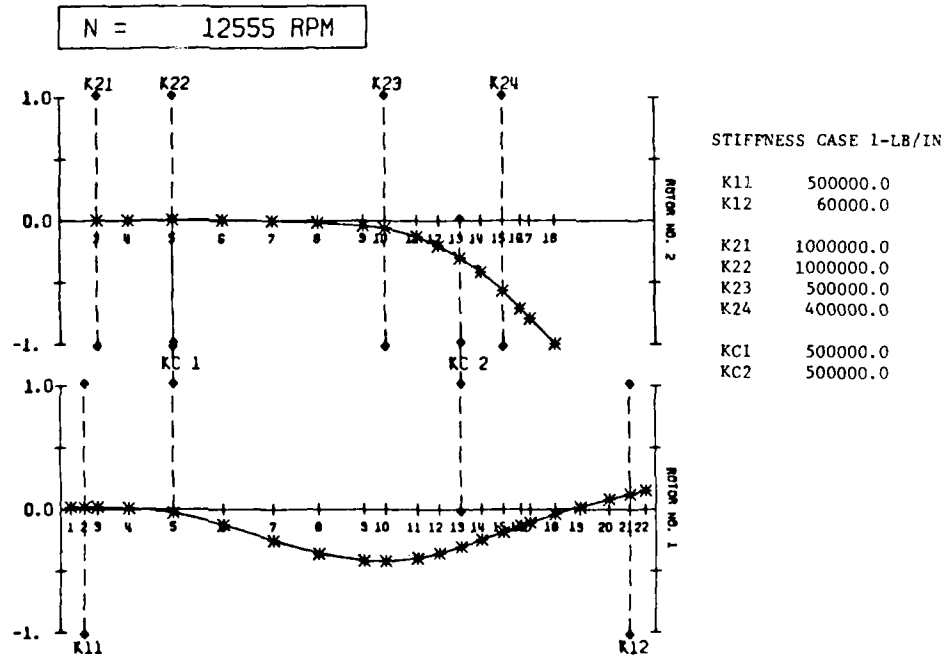

Fig. 3 Second Engine Undamped Critical Speed with Aft Intershaft Differential Bearing

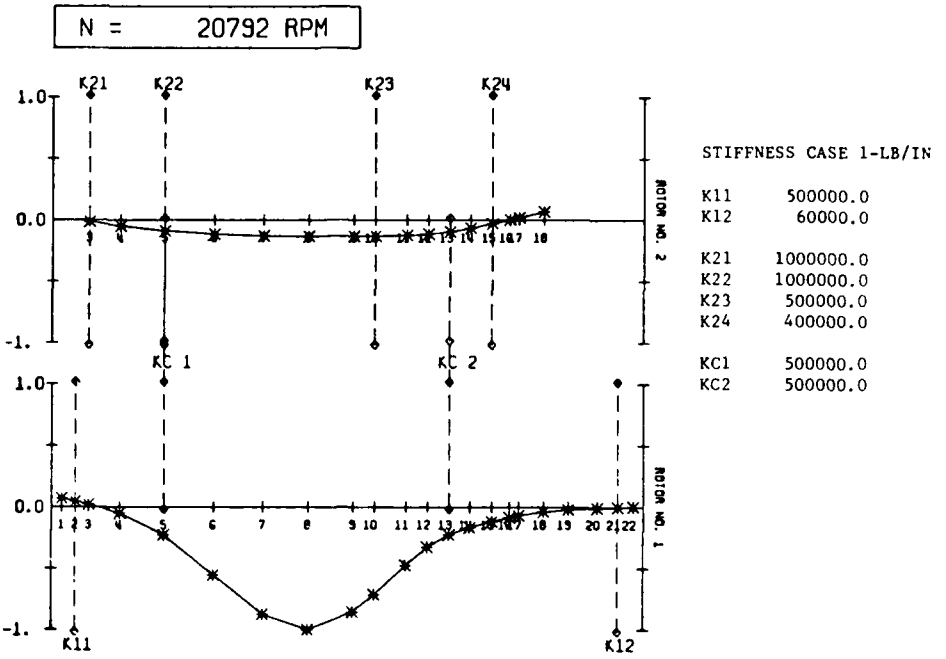

Fig. 4 Third Engine Undamped Critical Speed with Aft Intershaft Differential Bearing

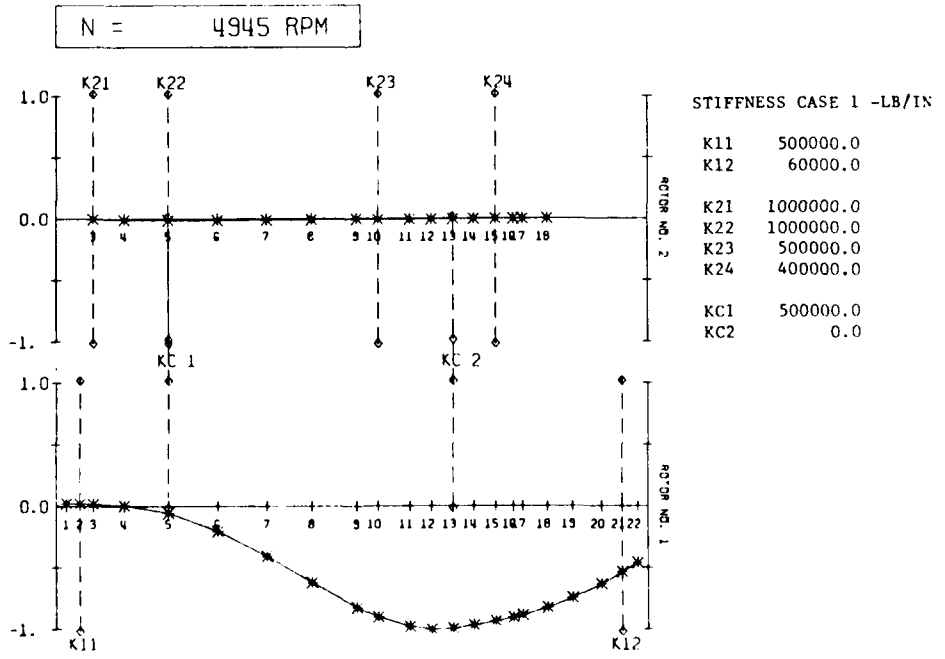

Fig. 5 First Engine Undamped Critical Speed without Aft Intershaft Differential Bearing

Figure 2 shows that the first critical speed at 6,936 RPM is predominantly a bending mode of the power turbine. The largest amplitude occurs at the power turbine location. It can be observed that a squeeze film bearing located at the No. 4 bearing (K12) would be extremely effective in damping out this particular mode.

A slight deflection of the gas generator rotor is observed for this mode due to the forces transmitted through the aft intershaft differential bearing (KC2). A squeeze film bearing employed at the gas generator No. 3 bearing support (K24) will not effectively suppress this mode. Since there is little motion at the aft intershaft differential bearing (KC2) at this mode, unbalance at the gas generator location should cause relatively little excitation of the power turbine first mode. This mode will be primarily influenced by unbalance at the power turbine stages. If the power turbine unbalance is excessive, then tip rubs of the power turbine blades could occur.

Figure 3 illustrates the second system critical speed mode shape. This mode at 12,555 RPM represents the first gas generator mode with the motion primarily occurring in the gas generator rotor turbine section. The aft intershaft differential bearing (KC2) connecting the gas generator and the power turbine causes a considerable deflection of the power turbine shaft. It appears possible that should the power turbine shaft become thermally bowed, it may excite this mode. Substantial loads would be transmitted through the aft intershaft differential bearing. Since the motion at the No. 4 bearing (K12) is small, a squeeze film bearing at this location would be relatively ineffective in suppressing the power turbine motion due to excitation from the gas generator. A squeeze film bearing located behind the No. 3 bearing (K24) should be quite effective in suppressing this mode if properly designed. The actual bearing loads transmitted through the various bearings will be examined in a subsequent section.

The third system critical speed of the gas turbine is predicted to be 20,792 RPM. The mode shape is shown in Fig. 4. This critical is above the operating speed range of both the gas generator rotor or the turbine. One interesting observation from this mode is that the aft intershaft differential bearing causes considerable deflection of the power turbine shaft. This mode would be particularly excited if there were a residual bow in the power turbine shaft. Such a bow might be produced by thermal gradients. Although this critical speed is predicted to be over 20,000 RPM, large differential bearing forces may be developed at speeds below this critical speed due to the shaft deflection caused by the intershaft differential bearing. The relatively small motion that occurs at the gas generator No. 3 bearing suggests that a squeeze film bearing there would be relatively ineffective.

Critical Speeds without Aft Intershaft Differential Bearing

Under certain operating conditions, such as a locked power turbine rotor start, excessive wear and degradation have occurred in the aft intershaft differential bearing. The critical speeds and mode shapes for the system were also calculated assuming negligible aft intershaft differential bearing stiffness. The first critical speed of the system without the aft

intershaft is approximately 4,945 RPM, a reduction of nearly 2,000 RPM. Figure 5 shows that this mode shape has changed considerably from the original first critical speed as shown in Fig. 2. The highest amplitude of motion with this mode does not occur at the power turbine but near the aft intershaft differential bearing and the internal seals. It appears likely that this mode could be excited by a bow in the power turbine rotor. The relative motion at the forward intershaft differential bearing is small and there is little motion of gas generator rotor as this is primarily a power turbine rotor mode.

The second mode without the aft intershaft differential bearing is shown in Fig. 6. The critical speed for this mode is approximately 11,500 RPM. This mode is also primarily a power turbine rotor mode and is well within the normal operating speed range of the power turbine rotor and would be easily excited by power turbine unbalance or bow of the power turbine rotor. Sustained operation at this mode could result in the power turbine rubbing on the gas generator rotor. Experimental testing of this engine configuration without the aft intershaft differential bearing showed evidence of rubbing at the center of the power turbine rotor. It is evident from Figs. 5 and 6 that a squeeze film bearing mounted at the gas generator rotor No. 3 bearing support would be ineffective in suppressing either of the first two engine modes with a failed or eliminated aft intershaft differential bearing.

The third engine critical speed is approximately 12,500 RPM, and the mode shape is shown in Fig. 7. This mode is essentially the same as the second mode with full aft intershaft differential bearing stiffness and is primarily a gas generator rotor mode. The relatively large motion that occurs at the gas generator No. 3 bearing implies that a squeeze film bearing at this location would be effective in suppressing this mode.

Because the rotors in this engine are quite flexible, the intershaft differential bearings are essential components to ensure that rubbing between the two rotors does not occur. The aft intershaft differential bearing plays an important role in determining the second power turbine rotor critical speed. Loss of stiffness in this bearing results in a reduction of the power turbine rotor second critical speed which then occurs within the normal engine operating speed range. It is also apparent from the critical speed mode shapes that a single squeeze film bearing may not provide adequate damping capability for all engine modes within the engine operating speed range.

GAS TURBINE ENGINE UNBALANCE RESPONSE

Although the undamped critical speeds and mode shapes presented in the previous secion provide useful design information, they do not provide quantitative information on the vibration amplitudes, bearing forces and effects of damping with unbalance forces acting on the system. This section describes the results of an unbalance response analysis of the engine, including both linear and nonlinear squeeze film bearing forces. The transfer matrix method was also used to generate the results (4), (5).

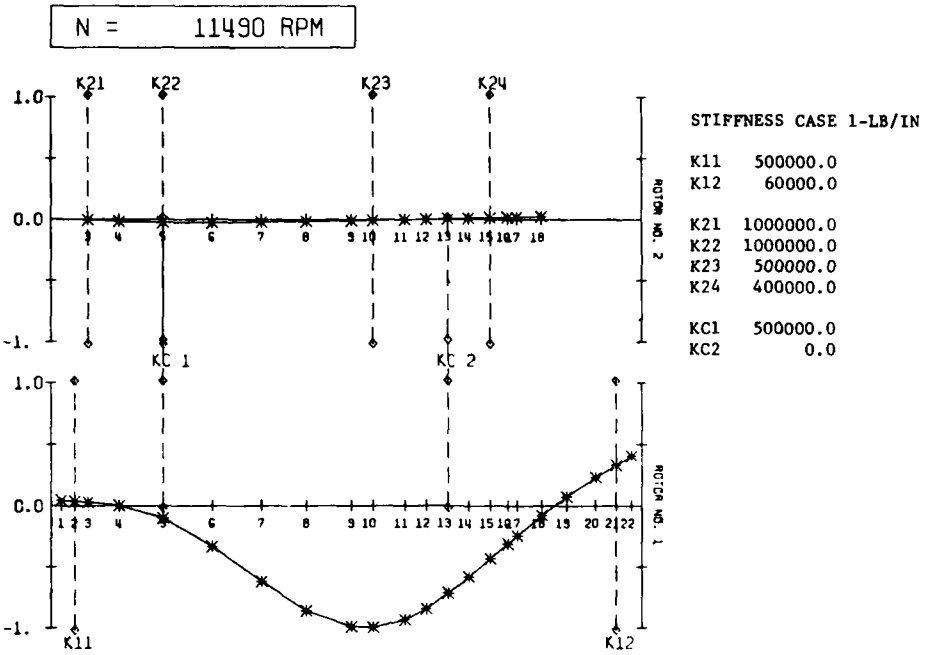

Fig. 6 Second Engine Undamped Critical Speed without Aft Intershaft Differential Bearing

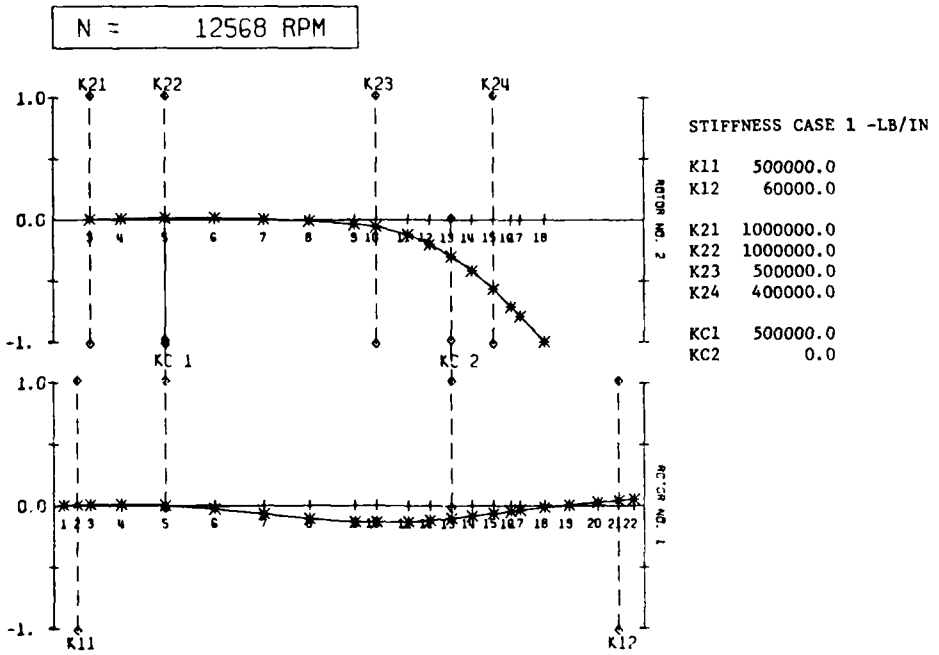

Fig. 7 Third Engine Undamped Critical Speed without Aft Intershaft Differential Bearing

Response with Power Turbine Unbalance

For this portion of the analysis, the gas generator rotor was considered balanced and operating at 15,000 RPM (N_g). Out of phase unbalances of 10 gm-in. were assumed at the first stage power turbine and center of the power turbine rotor. This unbalance distribution was assumed to be representative of a small bow in the power turbine rotor.

A squeeze film bearing was assumed to be located at the gas generator rotor No. 3 bearing location. Linear squeeze film damping and support diaphram stiffness coefficients were assumed. The forces applied to the No. 3 bearing support are shown in Fig. 8 as a function of power turbine rotor speed. With the gas generator rotor speed constant, this response is representative of a locked-rotor start. Full aft intershaft differential bearing stiffness was included.

In the first case, a diaphram stiffness of K_g = 400,000 lb/in. and squeeze film damping of C_g = 2 lb-sec/in. was assumed. This value of diaphram stiffness corresponds to the original design value for the engine. Figure 8 shows that the unbalance in the power turbine causes an excitation of the first power turbine critical speed at 7,000 RPM which generates a force at the No. 3 bearing of approximately 300 lb. As the power turbine speed is increased, a very large resonance peak occurs at 12,000 RPM, resulting in a peak force of 2,650 lb. In the actual testing of this engine, cracking of the gas generator diaphram has occurred along with seal rubs on the gas generator turbine. Both of these effects could be initiated by a bowed power turbine shaft during a locked rotor start since the analysis also revealed that an amplitude of 12 mils at the gas generator rotor turbine section would occur.

If the squeeze film bearing is assumed to develop a damping coefficient of C_g = 20 lb-sec/in., the peak bearing force is only reduced from 2,650 lb to 1,000 lb. Because of the high stiffness of the diaphram support, the squeeze film damper is not at optimum effectiveness.

If the effective diaphram stiffness is reduced from K_g = 400,000 lb/in. to K_g = 123,000 lb/in., Fig. 8 shows that the gas generator rotor resonance is reduced to 8,800 RPM and that the force in the No. 3 bearing is also reduced to less than 400 lb with a squeeze film bearing damping of 20 lb-sec/in. To avoid cracking of the No. 3 bearing support, the effective diaphram stiffness should be reduced. Intuitively, support stiffening might be considered a remedy for diaphram failure. However, this would result in even larger forces being transmitted.

Regardless of the diaphram support stiffness, it is seen that as the power turbine rotor speed approaches the second power turbine rotor critical speed of 20,000 RPM, extremely high bearing loads are predicted. The maximum power turbine speed is not intended to exceed 18,000 RPM. Another interesting effect that is observed on the gas generator rotor is that at 17,400 RPM the system is tuned such that practically no bearing forces are transmitted. Hence, at this speed, even with large power turbine unbalance values, little motion would be observed on the gas generator.

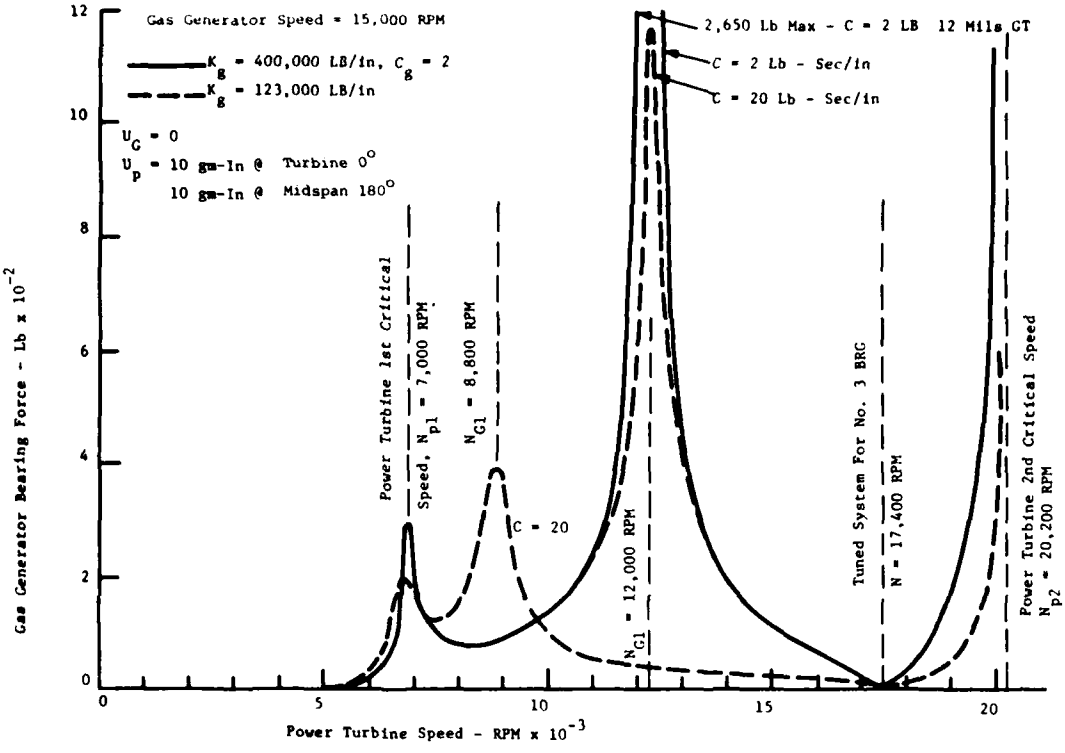

Fig. 8 Forces in No. 3 Bearing Due to Power Turbine Unbalance

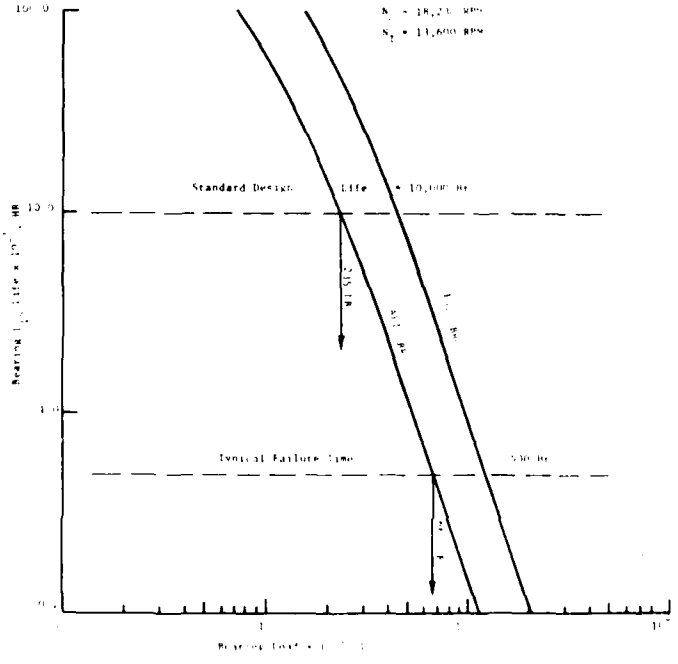

Fig. 9 Intershaft Differential Bearing Life as a Function of Bearing Load

An additional problem encountered with this engine is failure of the aft intershaft differential bearing. Failure rates of this bearing are functions of the type of engine service and appear to be related to the number and severity of locked-rotor starts.

Figure 9 represents the life of the differential bearings as a function of bearing loading. For example, with a loading of 235 lb on the aft intershaft differential bearing, the design L10 life is 10,000 hours. If the loading should increase to 660 lb, there is a dramatic drop in the predicted life from 10,000 hours to only 500 hours, using the relationship that predicted bearing life is inversely proportional to the cube of the load.

Figure 10 represents the forces transmitted to the aft intershaft bearing and the No. 4 bearing supporting the turbine stages as a function of power turbine speed. As expected, large bearing forces are transmitted at the first power turbine rotor critical speed of 7,000 RPM. The No. 4 bearing carries the largest load (over 700 lb) and almost 400 lb is transmitted through the aft differential bearing. If the transition through this speed is rapid, the life of the bearings should not be greatly reduced since this speed is well below the idle speed of the engine. However, it is observed that above 10,000 RPM the loading on the No. 4 bearing decreases, while the loading on the aft intershaft differential bearing increases.

Superimposed in Fig. 10 are the load lines representing the aft intershaft differential bearing life of 10,000 hours and 500 hours. Continuous operation below 14,000 RPM would not reduce the life of the aft intershaft differential bearing, whereas a severe reduction in life would occur with continuous operation near the maximum power turbine rotor speed of 17,400 RPM. The aft intershaft differential bearing carries more load than the main No. 4 bearing for power turbine rotor speeds above 8,000 RPM. Furthermore, substantial loads can be imposed upon the aft intershaft differential bearing at speeds well below the second power turbine rotor critical speed. Although skidding damage was observed on many aft intershaft differential bearings, it is apparent that anti-skid designs, such as elliptical bearings, will not reduce the large bearing forces. These forces are an inherent dynamics problem.

Figure 11 illustrates the amplitude of the power turbine as a function of power turbine rotor speed for various values of the gas generator rotor No. 3 bearing stiffness and damping coefficients. With the stiffness of the No. 3 bearing support diaphram K_g = 400,000 lb/in., the peak amplitude of the first power turbine stage is approximately 10 mils at 7,000 RPM. Very little amplitude change occurs with No. 3 squeeze film bearing damping coefficients of 2-20 lb-sec/in. If the diaphram stiffness is reduced to K_g = 123,000 lb/in., the peak first power turbine stage response is 7 mils at approximately 6,700 RPM. Both peak responses are well below the normal power turbine rotor operating speed range. For power turbine rotor speeds between 8,000 and 20,000 RPM, the first stage power turbine response is low, independent of the gas generator rotor No. 3 bearing stiffness and damping coefficients. A large response also occurs at the second power turbine rotor critical speed (20,200 RPM) and is relatively unaffected by the No. 3 bearing characteristics, as predicted by the critical speed

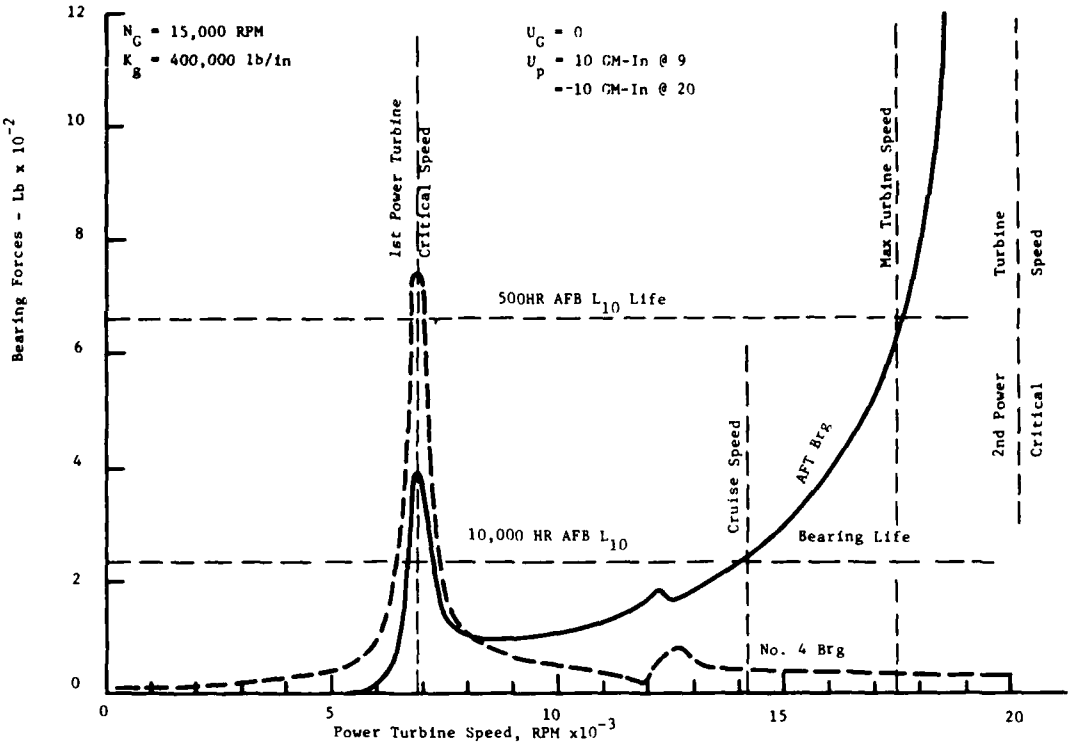

Fig. 10 Aft Intershaft Differential Bearing Load Due to Power Turbine Unbalance

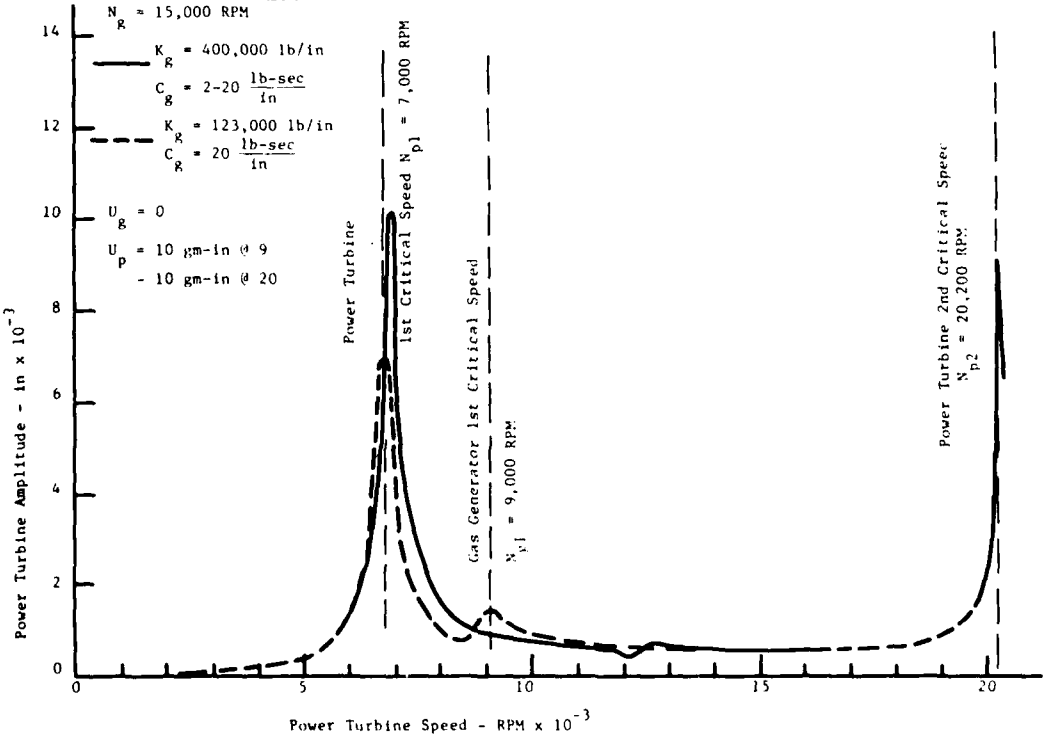

Fig. 11 Power Turbine Amplitude Due to Power Turbine Unbalance

analysis of Fig. 4. The relative amplitude between the power turbine and gas generator rotors near the power turbine rotor midspan is shown in Fig. 12. A peak relative motion occurs when the speed of the power turbine coincides with the gas generator rotor first critical speed as well as the first power turbine rotor critical speed. These peak relative responses are substantially lower with reduced No. 3 bearing diaphram stiffness.

At power turbine rotor speeds above 14,000 RPM the relative amplitude increases reaching a very large value at the second power turbine rotor critical speed. This could result in wear to the hot gas seal between the power turbine and gas generator rotors allowing hot gas leakage into the aft intershaft differential bearing which could further reduce the life of this bearing. Uneven hot gas leakage could also induce a thermal bow of the power turbine rotor.

Gas Generator Rotor Unbalance

Figures 13-15 illustrate the effects of unbalance at the gas generator rotor turbine section. The power turbine rotor is assumed balanced and operating at 15,000 RPM. The forces transmitted to the gas generator rotor No. 3 bearing are shown in Fig. 13. With high No. 3 bearing diaphram stiffness, large forces are transmitted at the gas generator rotor critical speed at 12,200 RPM, even with a damping coefficient of 21 lb-sec/in. at the No. 3 bearing. With the diaphram stiffness reduced to 123,000 lb/in., the No. 3 bearing forces are reduced by approximately 60% at the gas generator rotor resonant speed of 8,600 RPM. Very little excitation of the power turbine rotor occurs with gas generator rotor unbalance. The vibration amplitudes at the gas generator rotor turbine section are shown in Fig. 14. These amplitudes are also lowered when the No. 3 bearing diaphram stiffness is reduced from 400,000 to 123,000 lb/in.

The forces on the aft intershaft differential bearing for these conditions are shown in Fig. 15. These forces are somewhat increased at gas generator rotor speeds below 11,000 RPM when the No. 3 bearing diaphram stiffness is reduced to 123,000 lb/in. However the overall force levels are below 100 lb in this speed range. When the diaphram stiffness is 400,000 lb/in., a greater force on the aft intershaft differential bearing occurs at the power turbine rotor first critical speed rather than at the gas generator rotor resonance. This effect is reversed when the diaphram stiffness is reduced to 123,000 lb/in.

Regardless of the stiffness and damping at the No. 3 bearing, large forces will occur in the aft intershaft differential bearing when the second power turbine rotor resonance at 20,200 RPM is excited. However, for gas generator rotor speeds below 19,000 RPM, the force will not exceed 100 lb.

Additional forces will also be transmitted to the engine bearings and seals due to gyroscopic effects of aircraft maneuvers. To determine these loads, unbalance couples were placed at both the turbine sections of both the gas generator and power turbine rotors. These unbalances were selected to simulate the gyroscopic moments that would be created by a yaw maneuver of 0.2 RPS. The results are summarized in Table 1. The largest forces

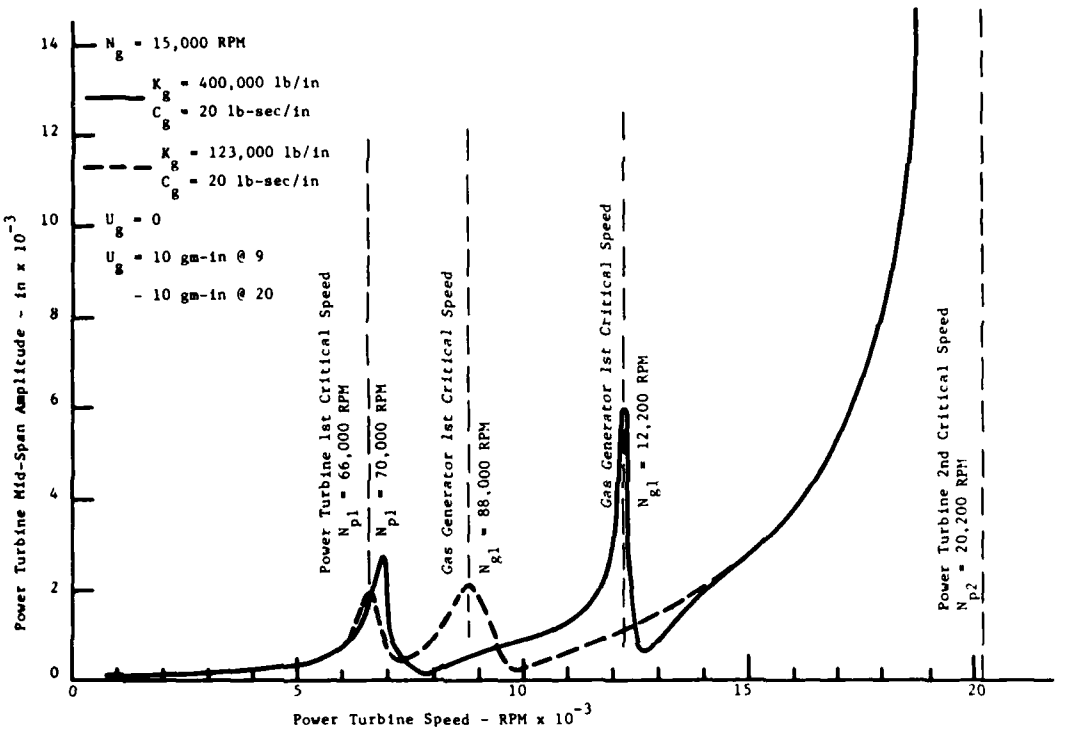

Fig. 12 Power Turbine Midspan Amplitude Due to Power Turbine Unbalance

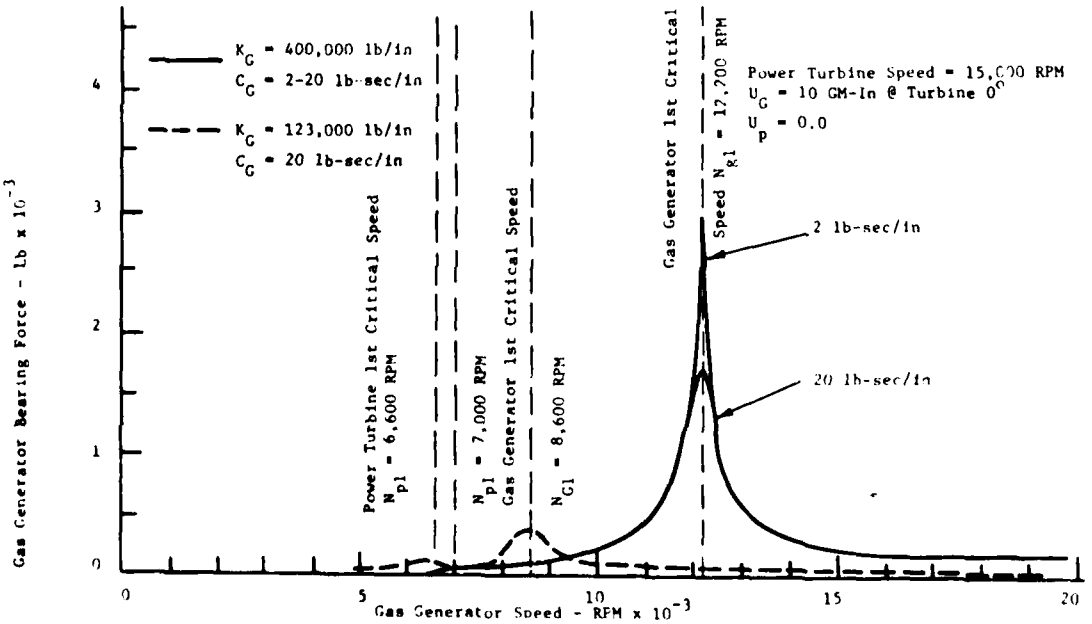

Fig. 13 No. 3 Bearing Forces Due to Gas Generator Turbine Unbalance

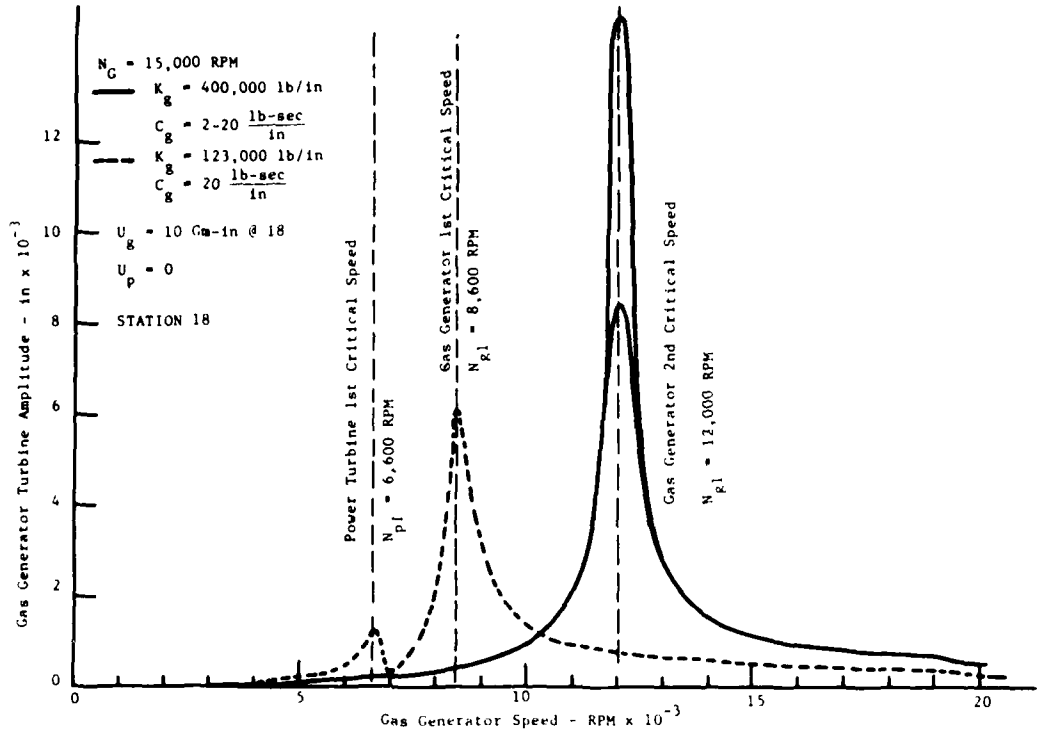

Fig. 14 Gas Generator Turbine Amplitude Due to Gas Generator Turbine Unbalance

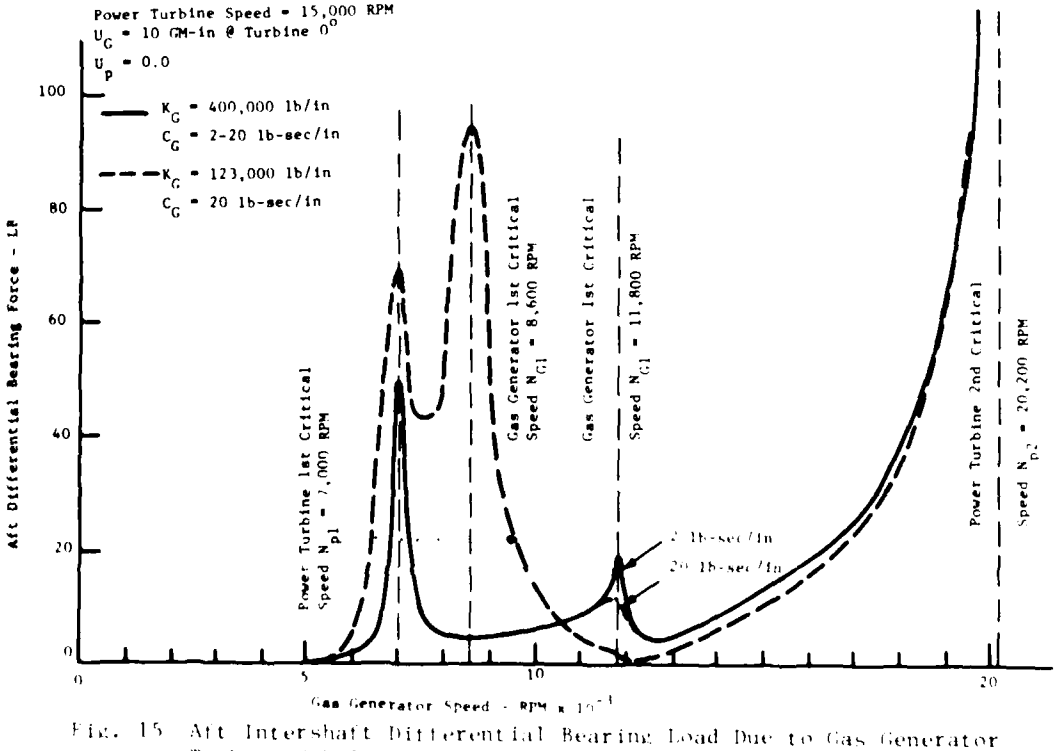

Fig. 15 Aft Intershaft Differential Bearing Load Due to Gas Generator Turbine Unbalance

TABLE 1

Bearing Loads Due to Gyroscopic Moments
Induced by Helicopter Yaw Motion

STATION NUMBER	DESCRIPTION	EFFECTS DUE TO GAS GENERATOR GYROSCOPIC FORCES		EFFECTS DUE TO POWER TURBINE GYROSCOPIC FORCES	
		AMPLITUDE in x 10^{-3}	FORCE lb.	AMPLITUDE in x 10^{-3}	FORCE lb.
5	Fwd Bearing	_____	404	_____	16
13	Aft Bearing	_____	347	_____	669
15	G. G. #3 Brg.	_____	1163	_____	66
21	P. T. #4 Brg.	_____	40	_____	138
18	Gas Generator Turbine	2.38	_____	1.24	_____
19	Power Turbine	0.16	_____	2.19	_____
18	Turbine Seal	1.69	_____	4.4	_____

Yaw Rate = 0.0033 RPM, N_g = 17,400 RPM, N_p = 17,400 RPM

occur at the No. 3 and aft intershaft bearing locations. The load on the aft intershaft differential bearing of 669 lb due to power turbine rotor gyroscopics is very close to the load for an L10 life of 500 hours for that bearing. The amplitudes of vibration at the turbine sections are relatively small.

The unbalance response studies indicate that the design of the No. 3 bearing on the gas generator rotor strongly affects the engine response and aft intershaft differential bearing forces. A squeeze film bearing applied at that location must be carefully designed to insure adequate engine performance.

NONLINEAR RESPONSE WITH SQUEEZE FILM BEARING

Because of the high bearing loads that can be transmitted through the No. 3 bearing and the supporting structure due to gas generator turbine unbalance, a squeeze film damper was incorporated behind the No. 3 bearing. The squeeze film damper consists of an 0.004 in. radial clearance space around the outer race of the No. 3 bearing with oil supplied to the annular region. In the original design, a retainer spring connecting the outer race of the bearing to the supporting diaphram structure was not used. Unbalance in the gas generator turbine will cause a precessive journal motion in the oil film which will in turn generate a hydrodynamic force in the oil film, producing an equivalent stiffness and damping effect. The forces and motion of the system are highly complex and are functions of both the static and dynamic journal loading. The oil film was modeled using the short bearing approximation to Reynolds equation (6) and was considered incompressible and isoviscous.

In its original configuration, the squeeze film bearing was 0.45 in. in length, with journal radius of 2.55 in. The oil viscosity was assumed to be 3.82×10^{-6} lb-s/in.^{2} Figure 16 illustrates the nonlinear limit cycles for the original bearing with the radial clearance ranging from 0.004 to 0.006 in. The dynamic unbalance loading is 66 gm-in. The unbalance parameter EMU is defined as e_u/c, where e_u is the equivalent mass eccentricity required to produce a given unbalance magnitude. The gas generator rotor speed was taken to be 16,800 RPM.

In Figs. 16a and 16b the effect of removing the journal preload centering or retainer spring is shown. In both cases the bearing is dynamically overloaded and the journal orbit nearly fills the available clearance. The dynamic force transmitted to the bearing and support structure is approximately 6.2 times the dynamic unbalance force in each case (TRD = 6.2). In Fig. 16c, the radial clearance has been increased to 0.006 in., thus reducing EMU. The dynamic force transmissibility increased to TRD = 7.14. Thus, a dynamic load of 8,433 lb is transmitted to the bearing housing. In Fig. 16d, the oil supply pressure was increased to 400 psi above the assumed fluid cavitation pressure to reduce the radial hydrodynamic forces on the squeeze bearing journal. The effects are similar to the previous cases. The large amplitude limit cycle orbits of Fig. 16 are indicative of a dynamically overloaded system.

To increase the dynamic load capacity of the squeeze film bearing,

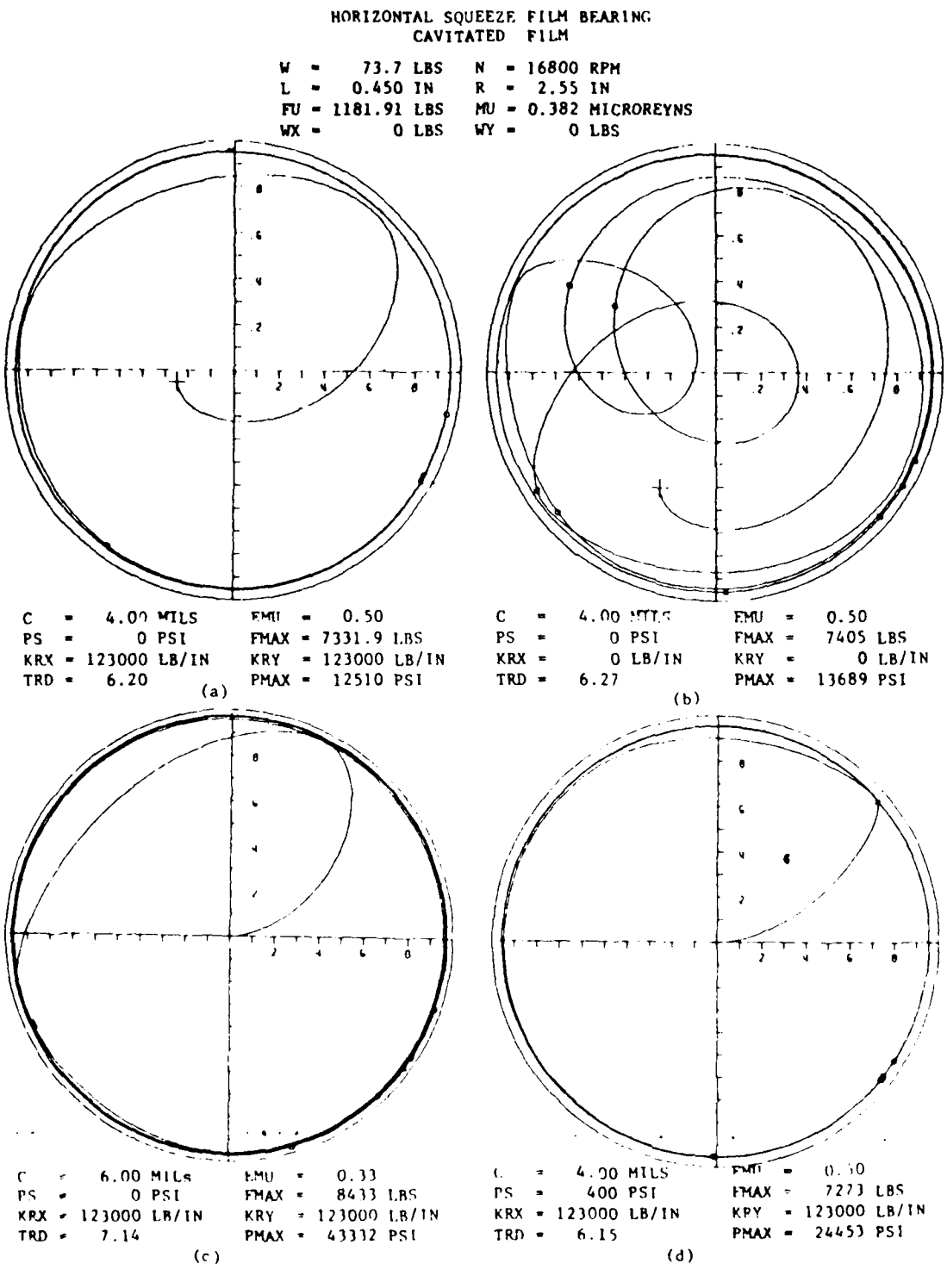

Fig. 16 Transient Motion of No. 3 Bearing Squeeze Film Bearing, L = 0.45 in.

the bearing length was assumed doubled to 0.90 in. The resulting limit cycle orbits are shown in Fig. 17. In each case, the clearance was taken as 0.004 in. and the effect of removing the preload or retainer spring was examined. For a dynamic unbalance of 33 gm-in (EMU = 0.25) the limit cycles shown in Figs. 17a and 17b are of relatively small amplitude. The oil film both with and without the retainer spring attenuates the dynamic loading producing TRD < 1.0. With the retainer spring removed, the resulting orbit is further offset from the bearing center, and a slight increase in force transmissibility occurs. With the unbalance doubled to 66 gm-in., the orbits in Figs. 17c and 17d result. The limit cycle orbits are again of large amplitude and the force transmissibility again exceeds unity.

Figures 18 and 19 illustrate the variance in squeeze film bearing equivalent stiffness and damping coefficients for centered circular journal orbits for the bearing geometries previously considered. A cavitated film is assumed to occur. These illustrate the nonlinear effects of increasing orbit amplitude for various bearing clearances. Both stiffness and damping coefficients exhibit nonlinear hardening with increasing orbit amplitude. Such systems possess multiple forced steady state response amplitudes, and if the forcing function is sufficiently large, extreme nonlinear dynamic response may occur.

Figure 20 represents experimental gas turbine engine response with the short (L = 0.45 in.) squeeze film bearing. The response, obtained on the engine casing, illustrates this nonlinear phenomenon. As engine speed increases the amplitude increases nonlinearly and, because of flexibility of the support, undergoes a nonlinear jump to a lower amplitude.

This response was simulated using the nonlinear squeeze film bearing coefficients shown in Fig. 18. The results, shown in Fig. 21, reasonably duplicate the experimental observations. The various curves represent different gas generator rotor turbine unbalances. The nonlinear region in the vicinity of the gas generator rotor resonance is strongly affected by the unbalance magnitude which, for a specified support stiffness, controls the speed at which the amplitude jumps to a lower value. In general, large nonlinear ranges are indicative of a dynamically overloaded system.

CONCLUSIONS

The dynamic response of multi-spool gas turbine aircraft engines is strongly affected by the intershaft differential bearings separating the spools. The engine resonant speeds may be drastically altered by changes in the stiffness of these bearings. Since rolling element bearing life is strongly controlled by the bearing loads, consideration of the dynamic forces transmitted to these bearings must be made. Loss of intershaft bearing stiffness due to centrifugal loading or bearing degradation can cause resonant speeds to occur within the normal engine operating speed range. This could result in substantial increases in bearing dynamic loading and further reduction in engine performance and operational safety.

The forced response analysis indicates that large intershaft differential bearing dynamic loading can occur even when operational speeds are not coincident with engine resonant speeds. Furthermore, these forces are

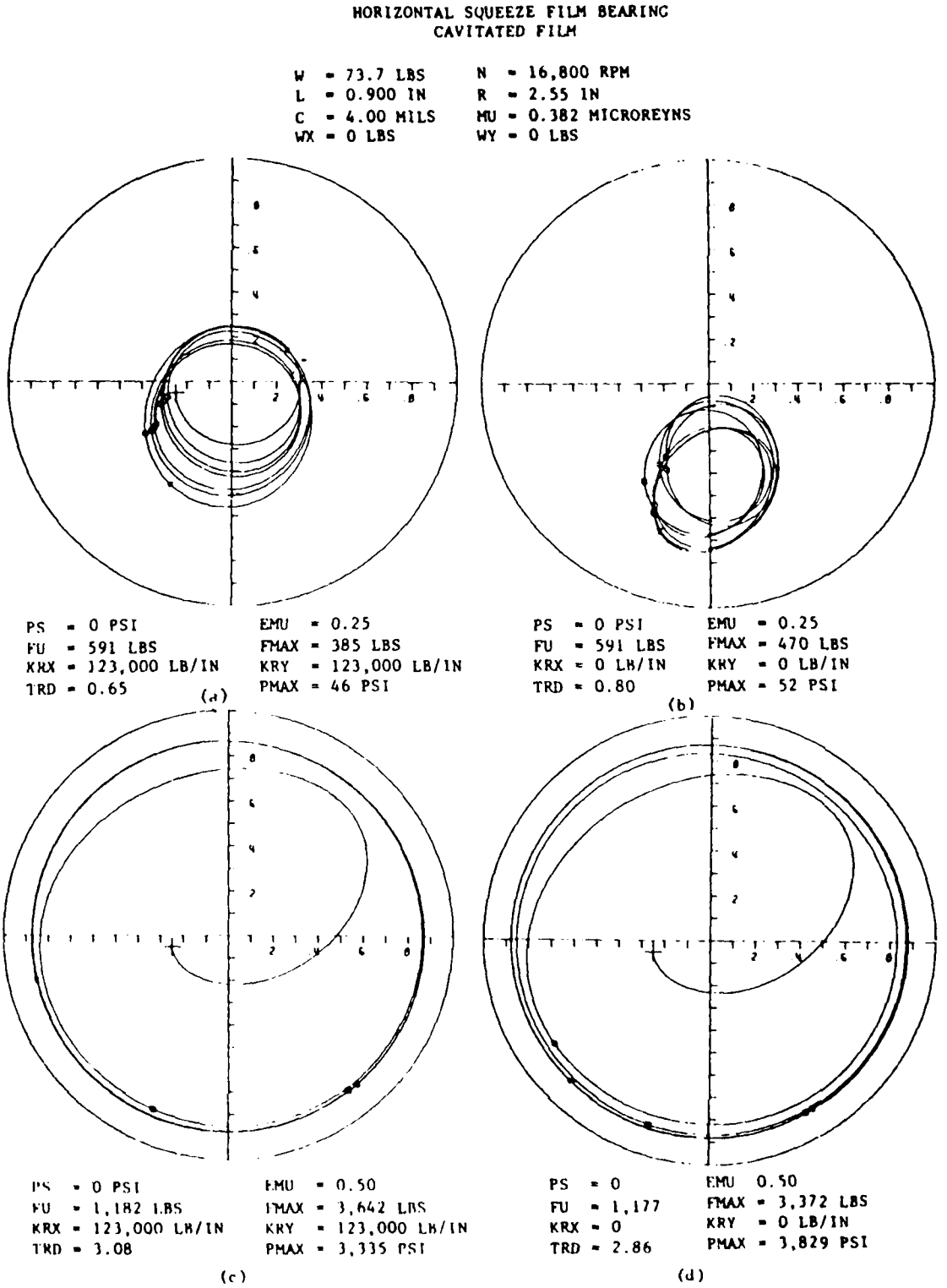

Fig. 17 Transient Motion of No. 3 Bearing Squeeze Film Bearing, L = 0.90 in.

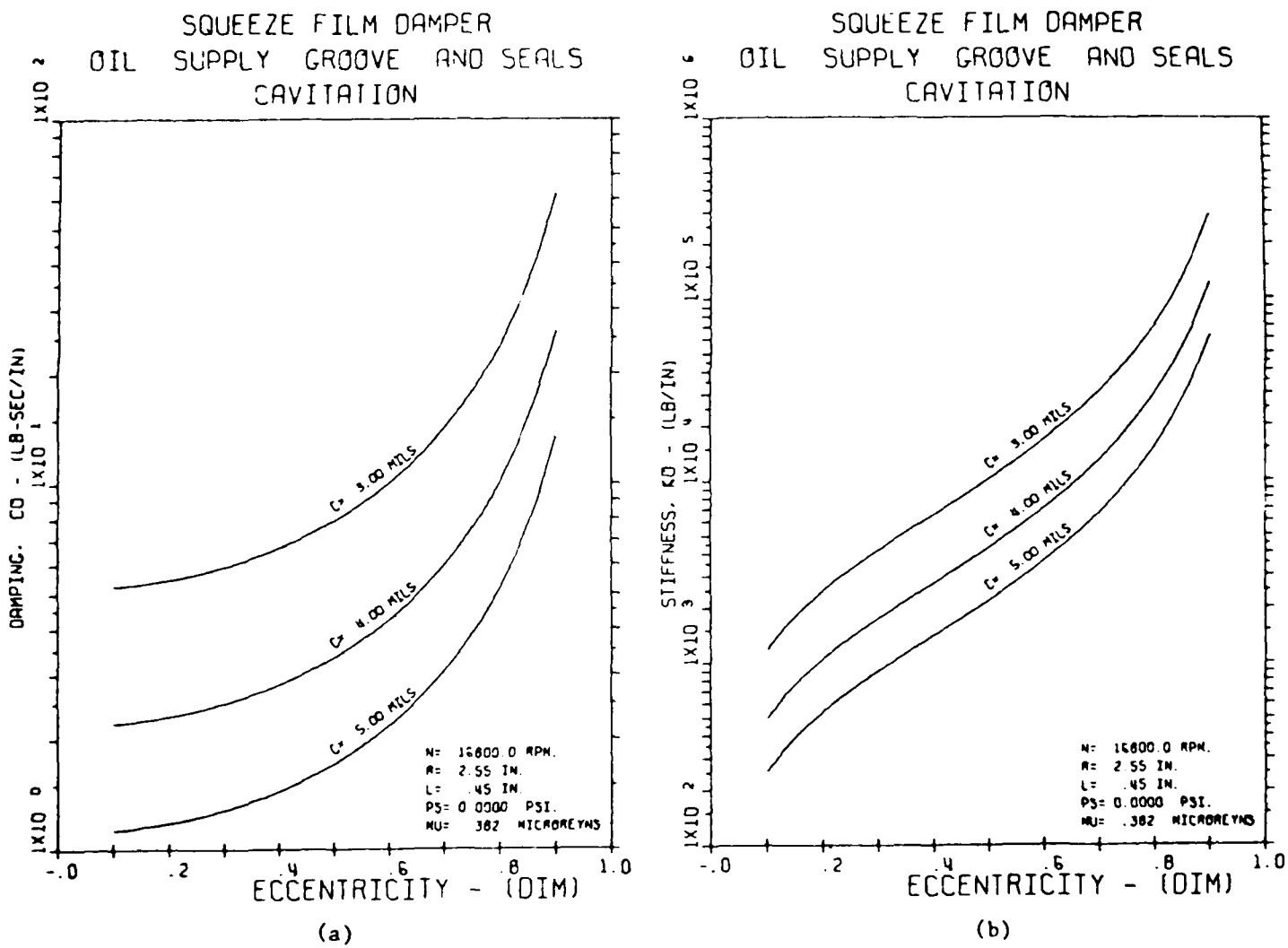

Fig. 18 Synchronous Squeeze Film Bearing Stiffness and Damping Coefficients, L = 0.45 in.

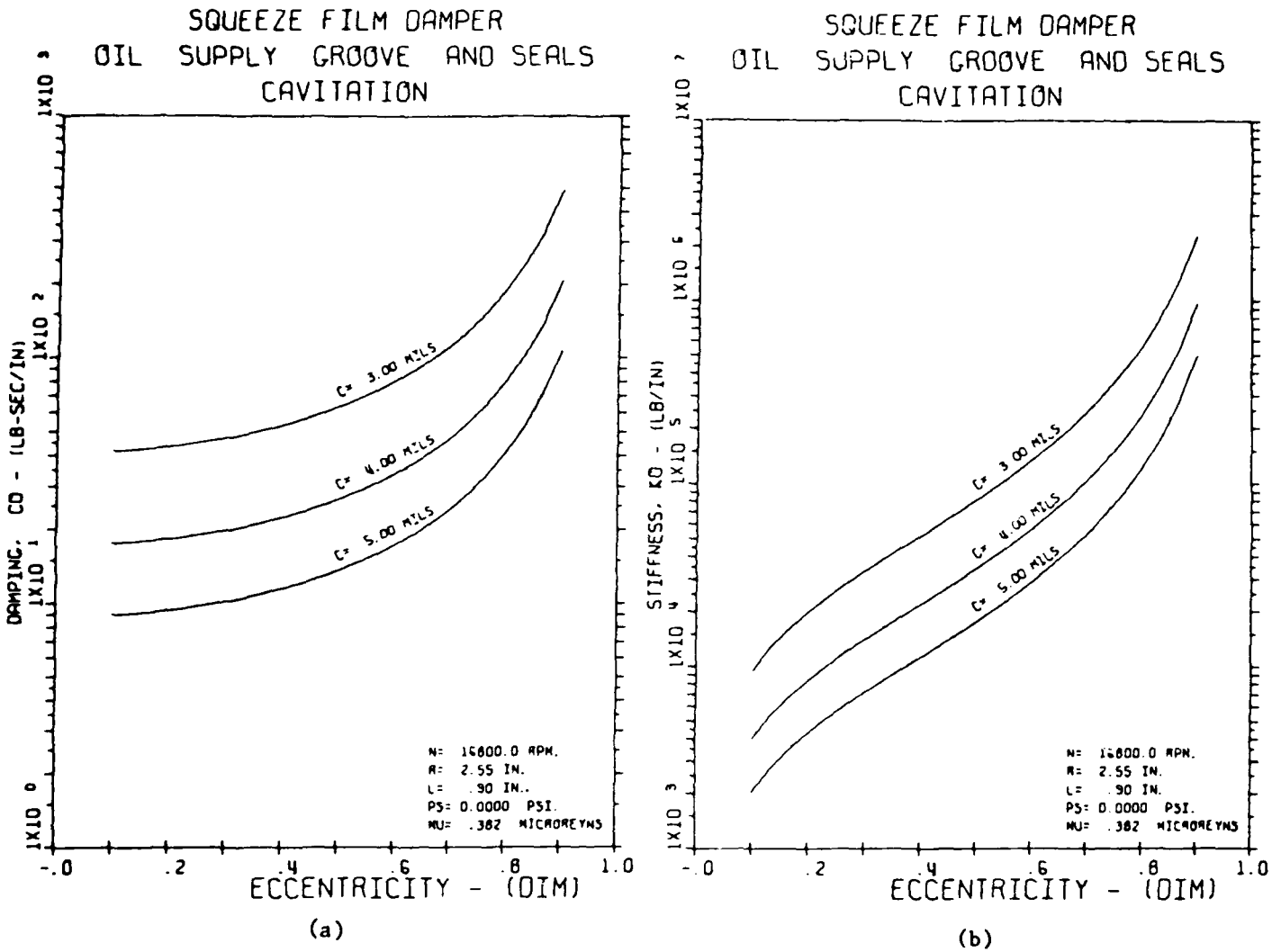

Fig. 19 Synchronous Squeeze Film Bearing Stiffness and Damping Coefficients, L = 0.90 in.

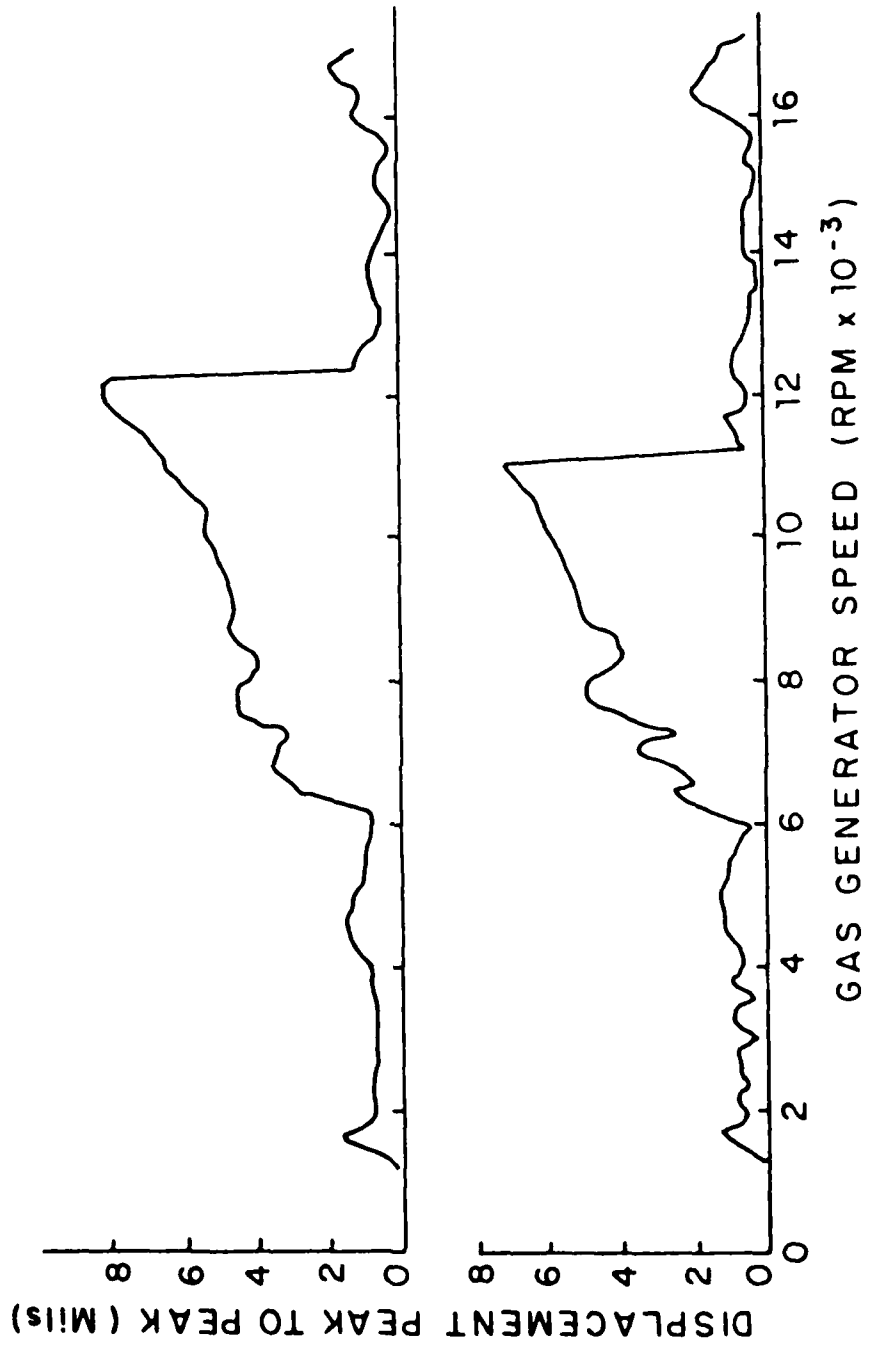

Fig. 20 Engine Test Data from Engine Casing Showing Nonlinear Jump

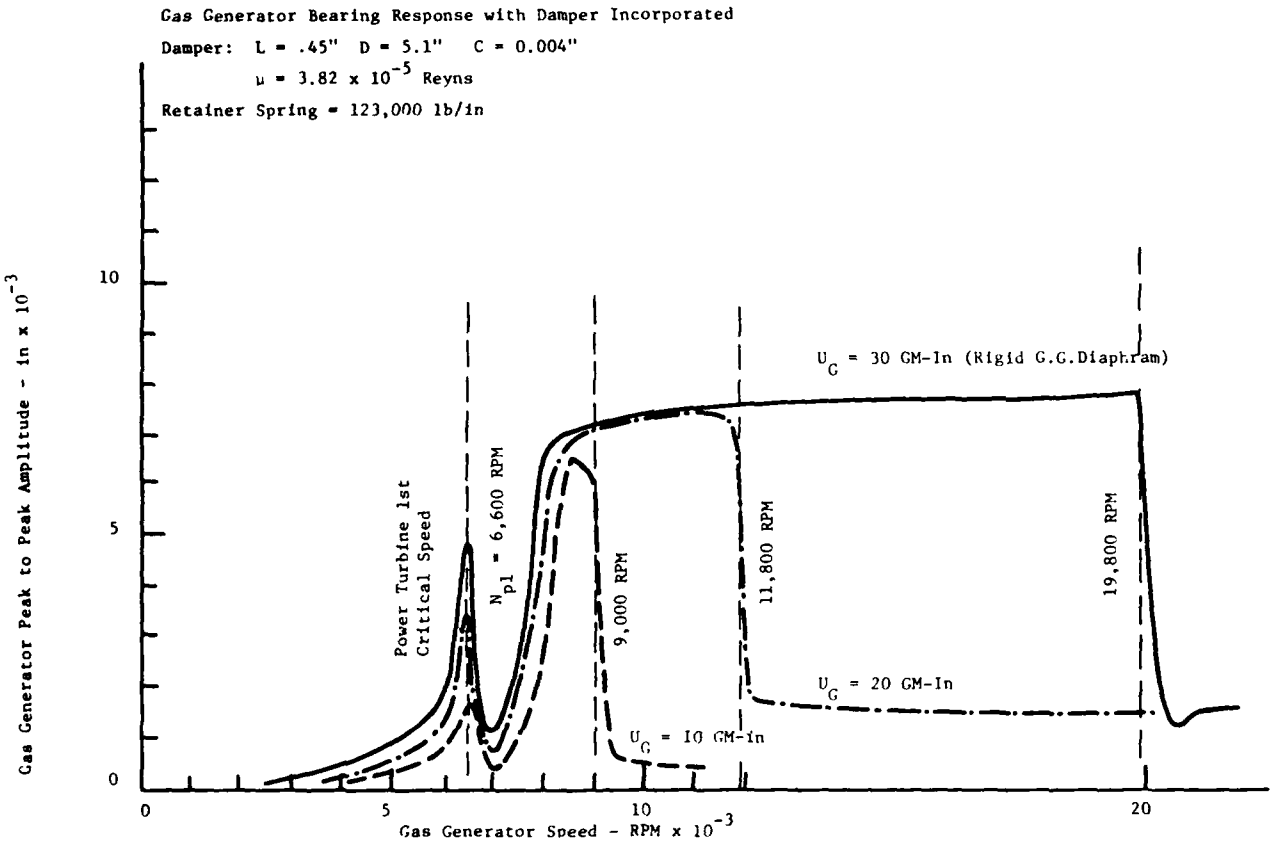

Fig. 21 Gas Generator Rotor Bearing Amplitudes with Nonlinear Squeeze Film Bearing Simulation Showing Nonlinear Amplitude Jump

strongly affected by the location and magnitude of viscous damping mechanisms in the system. It is apparent that with highly flexible rotor systems, viscous damping at a single location will not necessarily suppress resonant response at all resonant speeds.

The use of linear force coefficients to model squeeze film bearing effects provides quantitative information for the preliminary design of squeeze film bearings. The combination of stiffness and damping values which will effectively attenuate engine response can be readily identified. However, because of the nonlinear nature of squeeze film bearing forces, a nonlinear response analysis is valuable in determining whether the required forces will be generated. If the squeeze film bearing is undersized or if the dynamic unbalance forces become excessive, large orbiting of the journal will result, causing extremely large forces to be transmitted through the bearing and support structure. Because of the nonlinear effects, this may occur over a very large speed range. When properly designed for the dynamic conditions which are likely to occur, the squeeze film bearing is capable of substantially reducing the dynamic loads.

ACKNOWLEDGMENTS

This work was supported by the U.S. Army Research Office, Contract No. DAG 29-77C-0009, the Department of Energy, Contract No. EF-76-5-2479, and NASA Research Center, Contract No. NSG-3105

REFERENCES

1. Hibner, D. H., Bansal, P. N. and Buono, D. F., "Analytical and Experimental Investigation of the Stability of Intershaft Squeeze Film Bearings - Part 2: Control of Instability, Journal of Mechanical Design, July 1978, pp. 558-562.

2. Gunter, E. J., Barrett, L. E., and Allaire, P. E., "Design of Nonlinear Squeeze-Film Dampers for Aircraft Engines," Journal of Lubrication Technology, Vol. 99, No. 1, January 1977, pp. 57-64.

3. Lund, J. W., "Stability and Damped Critical Speeds of a Flexible Rotor in Fluid-Film Bearings," Journal of Engineering for Industry, May 1974, pp. 509-517.

4. Li, D. F., Dynamic Analysis of Complex Multi-Level Flexible Rotor Systems, Ph.D. Dissertation, University of Virginia, August 1978.

5. Lund, J. W. and Orcutt, F. K., "Calculations and Experiments on the Unbalance Response of a Flexible Rotor," Journal of Engineering for Industry, November 1967, pp. 785-796.

6. Barrett, L. E. and Gunter, E. J., "Steady State and Transient Analysis of a Squeeze Film Bearing for Rotor Stability," NASA CR-2548, May 1975.

DISCUSSION

D. L. Taylor, Assistant Professor, Sibley School of Mechanical & Aerospace Engineering, Cornell University.

Since many of the questions and comments during the workshop dealt with the phenomenon of bistable operation, it is worthwhile pointing out some interesting aspects of this type of response. These comments are particularly relevant to the presentation of the work by Professor Gunter because they deal with a similar rotor system. When using numerical integration to analyze the transient response of squeeze film damper systems, a primary question which must be addressed is how long to integrate the solution in time. Many presentors at the workshop have shown computer generated orbits that appear to involve only three or four orbits, which is quite understandable in terms of computer expense. However, the discussor has found that some solutions which appear to be steady state are deceptive.

Consider a planar rigid rotor carried in a squeeze film isolator (damper and centering spring in parallel). The values of the parameters given in the following table are taken from Professor Gunter's paper (which it will be noted is not a single planar rotor). An Ocvirk short bearing film is used for bearing forces. The differential equations can be obtained and integrated numerically. The planar model is found to display bistable operation over a speed range of approximately 10,000 rpm to 14,000 rpm. Several questions during the discussion dealt with methods of numerical integration. The results which follow are based on a variable time step Kutta-Merson algorithm. This type of program will constantly adjust the effective time step of the integrator to maintain a requested degree of accuracy. The discussor has found this type of algorithm to be very effective. It can handle quite rapid transients such as blade loss but tracks an almost circular orbit with approximately six to ten time steps per revolution. This is quite efficient with regards to computer time. The orbits which follow were generated by such an algorithm using a requested time step of .00032 sec. The plots appear to be crude simply because of the large time steps involved. The sharp corners result from the plotting program which connects the calculated points with straight lines. Much smaller time steps (100 or 1,000 times smaller) lead to orbits which still pass through the points which are plotted (the corners).

Any transient solution must begin from specific initial conditions. The orbit in Figure 1 shows the orbit calculated for initial conditions of initial eccentricity of 1. mil, initial eccentric velocity of 0., initial whirl velocity of 12,000 rpm (synchronous) and initial phase relationship between shaft center displacement and mass center displacement of .7 radians. The orbit starts from the circled point, settles into a radius of 3.09 mils, but later diverges from this orbit and finally settles into a whirl orbit of about 1.8 mils. The true nature of the response is better understood from Figure 2 which shows the eccentricity plotted versus time.

The pitfall to beware in numerical integration can be seen from Figure 2 where it is very tempting to stop the integration at about t = .05 sec. This phenomenon has not been completely understood by the discussor but has been observed many times. The major pattern is that it always involved initial convergence to the higher of the two possible orbits. Also, even though the eccentricity appears to be relatively constant for a long period in Figure 2, the phase angle between the shaft center and the mass center is steadily shifting. The question raised concerns its observance by other investigators (experimentally or computationally).

Table 1

m	= 73.8 lb	Ω	= 12,000 rpm
k	= 1.23×10^6 lb/in	R	= 2.55 in
μ	= .0266 poise	L	= .9 in
d	= 1 mil (c.g. offset)	C	= 4 mil

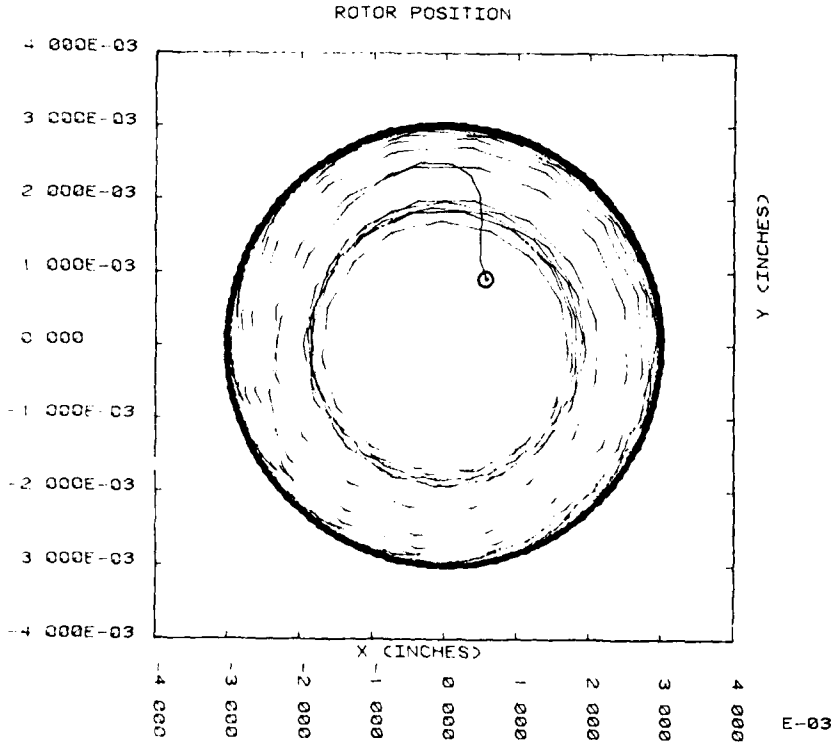

Fig. 1 Transient whirl orbit, x-y location of shaft center

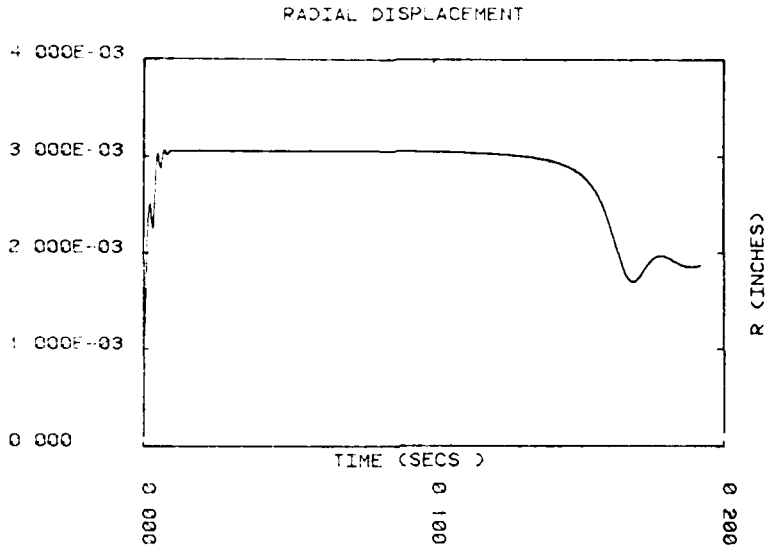

Fig. 2 Transient eccentricity versus time

AUTHORS' CLOSURE

Professor Taylor has raised two very interesting points in his discussion. First, the possibility of bi-stable operation for jumps occurring in a non-linear system, and second, the type of numerical integration procedure used and the associated time step.

In the operation of a squeeze film bearing, a jump phenomena may occur over parts of the operating range. This is caused by the non-linear characteristics of the squeeze film bearing oil film and the associated elasticity of the rotor and bearing support. Professor Taylor presents a numerical transient analysis of a squeeze film bearing operating at 12,000 rpm, including a retainer spring of 1.23×10^5 lb/in. In Fig. 1, the orbit shows an initial transient orbit of 3.09 mils, which decreases to 1.8 mils after .15 sec. of running time. When dealing with non-linear systems, one must evaluate the numerical integration procedure. What may appear to be a jump due to the non-linear characteristics of the system may in fact be caused by numerical error in the integration scheme. For example, in the procedure used by Professor Taylor, a time step of .00032 sec. was used. At an operating speed of 12,000 rpm, this is equivalent to only 15.6 steps per cycle. To accurately determine whether this non-linear jump is truly occurring, the integrated solution should be run with a much finer time step. Professor Taylor mentioned that although the eccentricity appears to be relatively constant for a long period, as shown in Fig. 2, the phase angle between the shaft center and the mass center is steadily shifting. This has been observed in a number of instances and has been associated with the numerical propagation of error in the solution.

THE CONTROL OF ROTOR VIBRATION USING SQUEEZE-FILM DAMPERS

by R. Holmes

University of Sussex
U.K.

ABSTRACT

This paper describes the roles of the squeeze-film damper when used in parallel with a flexible element in a vibration isolator and when used alone. The effects of cavitation on performance are elucidated and the dangers of jump phenomena and subharmonic resonance are discussed.

Experimental work is described which investigates both roles of the squeeze-film damper and the results are compared with theoretical predictions with the object of defining some design philosophy.

Finally areas of inadequate knowledge are highlighted, together with possible means of reducing them, especially with a view to incorporating squeeze-film characteristics in programs for the solution of linear multi-degree of freedom rotor-bearing systems.

NOMENCLATURE

A	$\pi R(l/c)^3/\sqrt{km}$	Q_c	$P_c/mc\omega^2 = u/c$
b	Negative pressure factor	R	Journal radius
c	Radial clearance of squeeze-film	T	Transmissibility
e	Eccentricity of journal in bearing	t	Time
k	Stiffness of retainer spring per land	u	Displacement of rotor centre of mass from geometric centre due to addition of unbalance mass or loss of mass
l	Squeeze-film land length		$\pi Rl^3/mc^3\omega$
m	Rotor mass per land		Dynamic eccentricity ratio (= e/c)
p	Local film pressure		Oil viscosity
P_{st}	P/2Rl		Frequency of dynamic load
P	Static load per land	ω_n	$\sqrt{k/m}$
P_c	Rotating force vector per land		
Q	$P/mc\omega^2$		

INTRODUCTION

An annulus of oil provided between the outer race of a rolling-element bearing and its housing is often used as a multi-directional damping element for the control of shaft and rotor vibrations in many designs of turbomachinery. This damping element, known as a squeeze-film, may be accompanied by a flexible element in a series combination constituting a vibration isolator. This flexible element is often in the form of a set of bars cantilevered from the machine frame. Its purpose is to artificially reduce the natural frequencies of the rotating system so that the speed range of high vibration amplitudes and transmitted forces may be traversed well before the normal operating speed range is reached. The squeeze-film damper then acts simply as a device to reduce to acceptable limits such amplitudes and transmitted forces.

Alternatively squeeze-film dampers are often used without flexible elements, in which case their role is solely one of damping with no measurable effects on the natural frequencies of the rotating system. Such effects are here forfeited in favour of a simpler mechanical design, which avoids problems of fatigue in any flexible element. Because of this and due to the fact that many turbines run above the rigid rotor (bounce) modes anyway, flexible elements are dispensed with for the most part in such applications as aeroengines. Rotation of the outer race of the rolling-element bearing is then prevented by anti-rotation pins or 'dogs'. However there are some aeroengine bearings which support fairly heavy loads such as large fans. For these applications flexible elements in the form of stacked Belville washers are often used to help carry the gravity load, rather than to effect any softening of the system.

This paper describes investigations into the performance of squeeze-film dampers when used with and without a parallel flexible element in turbomachinery applications.

THE SQUEEZE-FILM DAMPER AS AN ELEMENT OF A VIBRATION ISOLATOR

The purpose of the squeeze-film damper in this application is to reduce the amplitude of vibration and transmitted force as the rotor is run up through the artificially low natural frequencies of the system (ensured by the soft spring element) towards the normal operating speed. Most analyses, e.g. [1], assume that concentric vibration orbits exist when the rotor is running, either due to preloading in the spring element or because the dynamic loading is large compared to the static loading, as it may well be the case in the vicinity of a system natural frequency.

The squeeze-film is, however, a non-linear damper and, if its contribution to the system is fairly light the designer must guard against two classical disadvantages of light non-linear damping, namely jump phenomena and subharmonic resonance.

The former can arise in situations where cavitation occurs in the squeeze-film [1]. Owing to the non-linearity of the squeeze-film, the forced response curve can be distorted to such an extent that large vibrations (and hence transmitted forces) can be maintained for an extended speed range during run-up before jumping down to an acceptably low level.

Subharmonic resonance has also been recorded in systems employing squeeze-film isolators [2] and may be predicted whether or not cavitation is assumed to occur in the squeeze-film. Fig. 1 shows numerically-predicted orbits for a rigid rotor in uncavitated squeeze-film isolators which are centrally preloaded and in which the damping is fairly light. In this figure A is a measure of the damping in the system, u/c is the ratio of unbalance eccentricity to squeeze-film radial clearance and ω/ω_n is the frequency ratio. Strong subharmonic resonances are noted at running speeds of twice, three times and four times the lowest (bounce) natural frequency.

A design of squeeze-film isolator used in some experiments at Sussex University is illustrated in cross section in Fig.2a. It consists of a mild steel bearing housing A and a 1.75 kg cast iron damper bush B surrounding the silver steel journal C on which a rotor runs rather than in a rolling-element bearing. The bush is suspended concentrically in the squeeze-film clearance D by means of two horizontal and one vertical spring E made up of Watveare Belleville washers stacked in series along silver steel guide rods and preloaded for compression. The rods are connected to the bush via loose joints. The lubricating oil enters the circumferential groove F at point G. Some of the oil continues through the oil hole in the damper bush to the circumferential oil groove H of the journal bearing. A grub screw with a central hole can be inserted in this oil hole to restrict the oil flow and thus ensure that the journal bearing oil film clearance J is incomplete whatever the supply pressure. The outlet oil is collected in trays and pumped back to the reservoir, fitted with a heater to facilitate viscosity variations.

When the oil supply is turned on, both the circumferential oil grooves and the spaces between the Belleville washers are filled with oil. In order to prevent damping due to the dynamic compression of the oil-filled Belleville washers a pressure relieving groove is provided along each guide rod.

The isolator stiffness can be varied by changing the number of Belleville washers on each guide rod. Two hollow cylinders K are fitted to each guide rod as a substitute for Belleville washers so that any number of washers between zero and about 70 can be employed, thus giving a stiffness variation from 5.10^7 N/m with no washers to about 8.10^4 N/m with all washers in position.

The length and diameter of each squeeze-film land were 1.27 cm and 10.16 cm respectively and four radial clearances of $7.66.10^{-4}$ m, $3.74.10^{-4}$m, $1.39.10^{-4}$m and $0.9.10^{-4}$ m, were used. Together with the available viscosity range, variation of the squeeze-film damping from about 100 Ns/m to about 100,000 Ns/m could be obtained.

For experimental purposes, this isolator design has some obvious advantages over the 'squirrel-cage' configuration. The isolator stiffness can be easily varied by altering the suspension springing, the horizontal and vertical bush vibrations may be easily monitored by position transducers L facing the free ends of the two guide rods and centering of the damper bushes in the squeeze-film clearance is easily carried out by means of the spring preloading nuts M compressing the Belleville washer stacks.

Agreement between theoretical predictions and experimental findings is fairly good for such uncavitated squeeze-film isolators as Fig.2b shows. This figure relates to a rigid rotor centred in each squeeze-film annulus by pre-

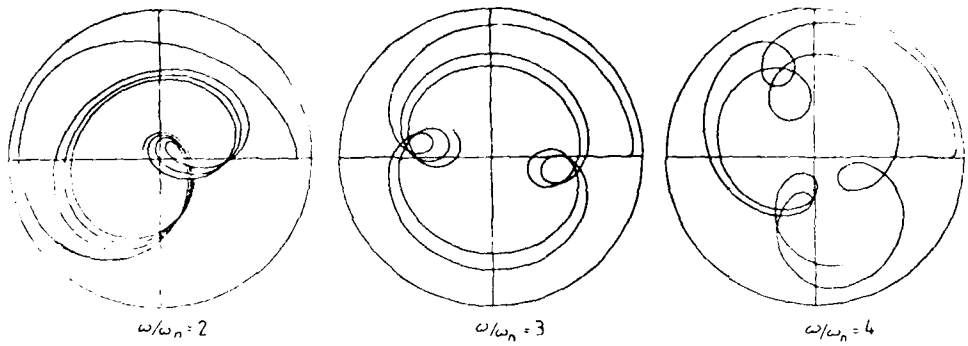

Fig 1

Sub-harmonic Resonance Short Squeeze Film
$A = \pi\eta R(\ell/c)^3/\sqrt{km} = 0.0284$
$\ell/c = 0.25$

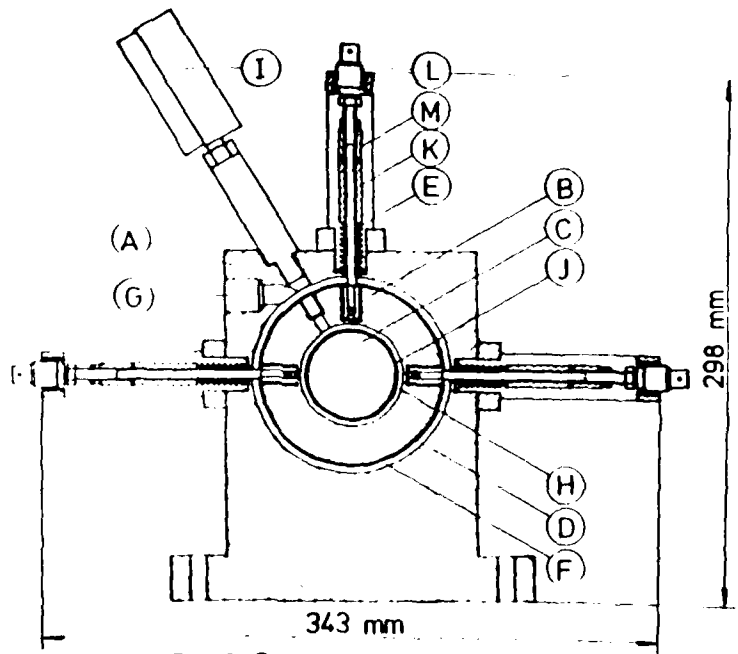

Fig 2a. Squeeze - film isolator

loading the flexible elements. Such agreement enables numerical results for uncavitated squeeze-films [1] to be accepted with a certain amount of confidence. If cavitation can take place however, uncertainties as to its likely extent for a given dynamic loading and supply pressure make predictions difficult [3]. Fig.3 shows the adverse effect on concentric vibration amplitude ε and on transmissibility T of cavitation which extends over half the annulus of the squeeze film. Thus if there is any likelihood of cavitation existing extra caution will be required in rotor balancing and the oil-supply pressure should be made as high as possible to reduce the amount of cavitation.

In spite of these reservations the use of squeeze-film isolators in practical installations [1], [2], [4], [5] has usually resulted in smoother running of the equipment concerned.

Fig. 2c shows a flexible rotor-bearing system used in ref [2] to further assess the performance of the isolators shown in Fig.2a.The flexible symmetrical rotor was supported by two identical plain fluid-film bearings surrounded by the squeeze-film isolators. The fluid-film bearings were each supplied with oil to a central circumferential groove and their dimensions were land length 1.69 cm, diameter 5.08 cm and radial clearance 0.116 mm. The 8.2 kg discs D1, D2 and D3 were positioned so as to allow easy unbalance excitation of the two lowest shaft bending modes by the attachment of unbalance masses at their peripheries. Journals J1 and J2, made of silver steel and of mass 2.52 kg were fixed at each end of the 5.14 kg stainless steel shaft and were supported by the squeeze-film isolators S1 and S2. The discs and journals were balanced to within 0.002 ounce-inches ($1.44.10^{-6}$ kgm) and the total rotor mass of 35 kg was chosen so as to provide sufficient plain-bearing load to ensure fluid-film cavitation. The central deflection due to gravity was about fifteen times the radial clearance in the journal bearings and in view of this, the bearing housings had to be tilted to about 0.25^{o} in order to obtain alignment between journals and bearings. The alignment process resulted in a relative slope between each journal and its bearing of less than 0.001 inch in 2 inches.

Both the experimental results and the numerical predictions showed a continuous reduction of the maximum shaft displacement amplitude at both the first and second critical speeds for increasing support damping up to about 10^4 Ns/m, with an increase in displacement for further increase in damping.

Well defined instability threshold speeds, as predicted by linear theory were observed for large values of squeeze-film damping, while for low squeeze-film damping (below 5×10^3 Ns/m) the system was stable and well damped in the entire operating speed range 0 - 4000 rev/min. However, in the damping range 6.10^3 - 3.10^4 Ns/m steady nonsynchronous whirling commenced at a rotational speed in the region of 1740 - 2250 rev/min, that is between twice and three times the first critical speed, with the exact onset speed depending on the damping value. The nonsynchronous whirl amplitude would increase with speed up to about 2400 rev/min, that is to about three times the first critical speed, whereafter the nonsynchronous whirl component amplitude would decrease rapidly and vanish at about 2400 - 2740 rev/min, marking the termination of the first whirl region. The response would then remain synchronous up to about 2870 - 3230 rev/min, still depending on the particular squeeze-film damping value, where nonsynchronous whirling would reappear. In some instances, again depending on the damping, the whirl amplitudes at this speed would continue to grow, indicating conventional system instability, while in other cases

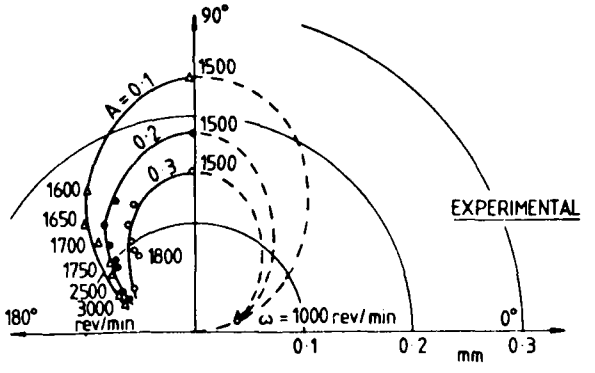

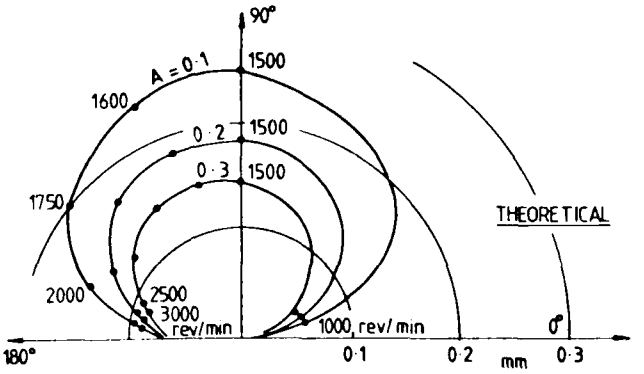

Fig 2b Response of rigid rotor in squeeze-film isolators
$u = 0{\cdot}068$, $c = 0{\cdot}384$mm, $\omega_n = 1500$ c/m

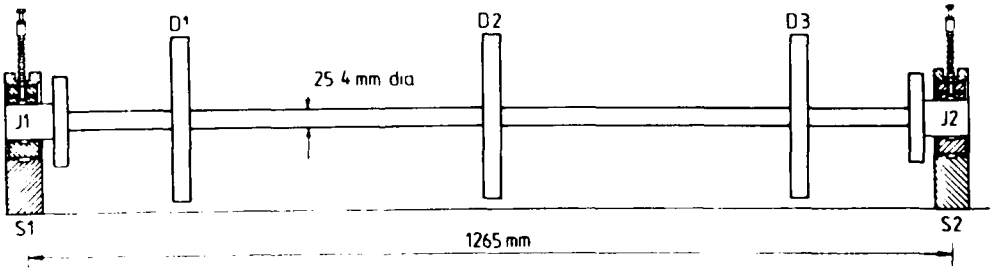

Fig 2c Flexible rotor - bearing system

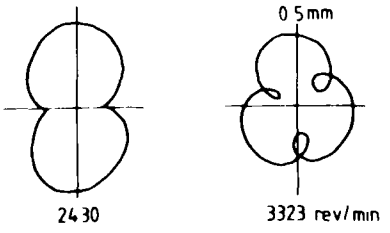

Fig 2d Nonsynchronous whirl orbits

the amplitude grew to a maximum with increasing speed and disappeared at about 3690 - 3800 rev/min, marking the termination of the second whirl region. Thereafter, the system would remain stable up to and including the maximum operating speed of 4000 rev/min. The repeatibility of the instability threshold speeds and of the onset speeds of nonsynchronous whirling was found to be fair. On average, both could be reproduced to within about $\pm$ 100 rev/min.

With an increase in oil temperature it was possible to eliminate the second nonsynchronous whirl region and a further temperature increase would result in the disappearance of the first whirl region also, making the system inherently stable by not allowing the journal bearing oil films to exert their full influence. However, the system remained very sensitive to random transient excitation, such as tapping of the foundation with a rubber hammer, particularly near the first whirl region, and generally appeared to be very lightly damped at all speeds above twice the first critical speed. Variations in oil supply pressure had relatively little effect and the nonsynchronous whirling exhibited the well-known hysteresis effect of persisting over a wider speed range once initiated.

Fig.2d shows examples of the nonsynchronous whirl orbits in the two whirl regions. The steady state double and triple loops indicate whirl speeds of exactly 1/3 and 1/4 of the respective rotational speeds. Only at speeds of 2430 and 3323 rev/min (corresponding to roughly three times and four times the first critical speed) were the orbits stationary. Nonsynchronous whirling was never found to reappear as a result of reduction in the bearing support damping from about 1×10^4 Ns/m down to the minimum value of about 200 Ns/m. Both the experimental and the predicted effect of bearing support stiffness was almost negligible within the covered stiffness range of 7×10^5 down to 8.85×10^4 N/m.

The observed pattern of nonsynchronous steady-state whirling is probably indicative of the inherent nonlinearity of the experimental rotor-bearing system which is mainly due to the bearing and damper fluid-films. In the terminology of nonlinear vibration theory, the observed nonsynchronous vibrations would be subharmonic vibrations of the third and fourth order. The occurrence of these subharmonics of order higher than two in the present system was facilitated by the introduction of the bearing support damping which, within a certain range of values, stabilized the system sufficiently to permit the required speeds of three and four times the first critical speed but was still not adequate for preventing a subharmonic response. It would thus seem reasonable to interprete the observed nonsynchronous whirling patterns of the experimental rotor-bearing system as being manifestations of subharmonic resonance of the poorly damped first bending mode of the shaft rather than being due to system instability in the linear sense.

In reference [4] other types of element were considered such as the laminated sheet damper, the metal braid damper and the disk damper. They all resulted in improved system performance.

Since the flexible element of a squeeze-film isolator is usually quite soft it may not always be possible to assume circular concentric orbits of vibration of the rotor centre when subjected to unbalance forces. If,however, any vibrations may be assumed to have amplitudes less than about one third of the radial clearance (a reasonable assumption in many practical situations)

then linear damping coefficients [6], [7] may be assigned to the squeeze-film and used in the linear analysis of rotor-bearing systems. For any larger vibrations quasi-linear (amplitude dependent) coefficients may be specified [6] and again used in linear analyses, albeit in an iterative fashion.

Darlow and Smalley [8] report a program of research on a supercritical transmission shaft using a squeeze-film damper in which 'O'-rings played the role of a flexible element. Here, however, the arrangement constituted a damper rather than an isolator, being mounted at a point in the shaft span and not in series with the main support bearings. Other attractive damping elements for use in such inter-span positions appear to be elastomers [8] and electro-magnetic dampers [9] .

THE SQUEEZE-FILM UNASSISTED BY A FLEXIBLE ELEMENT

Owing to the fact that mechanical elements such as springs are prone to fatigue failure, squeeze-film dampers on their own have been used by aeroengine designers for the last twenty years. When designed in this way there is no attempt to reduce the natural frequencies of the overall system as the rotor usually runs supercritically anyway, that is well above its two rigid-body bounce modes. The purpose of the squeeze-film is simply to introduce damping into the system so that the rotor can safely negotiate those bounce modes and operate smoothly at a speed perhaps not far short of the first flexural mode.

Since an unassisted squeeze-film damper is in effect a journal bearing in which the inner member does not rotate, it is not possible to assign to it any linear stiffness coefficients which might allow the oil film to take any gravity or other static load. Any lift produced emanates from non-linear effects and this makes the analysis of an unassisted squeeze-film damper somewhat more cumbersome to undertake.For certain operating conditions, such as in the regions of critical speeds where any static load is small compared to the dynamic load, circular concentric orbits can again be assumed [10] , with the result that quasi-linear amplitude-dependent coefficients can again be used. Linear analyses can thus be carried out to obtain the vibration orbits in an iterative fashion. Transmitted forces can then be computed.

For cases where the static load is not small a nonlinear analysis is called for and has been used by some investigators [1], [3] . Such an analysis requires a specification of the extent of cavitation which has a profound effect on both the static and the dynamic load-carrying capacity. For example it may be shown [3] that the assumption of an uncavitated film leads to the complete elimination of load-carrying capacity. Using the short-bearing approximation the effect of assuming that the oil can support differing amounts of subatmospheric pressure before cavitating is shown in Fig.4 which is taken from ref. [3] . In this figure Q is a non-dimensional static load, Q_c a non-dimensional dynamic load due to unbalance and β a non-dimensional viscosity. The b factor is the ratio by which the negative hydrodynamically-generated pressures in the squeeze-film have been reduced and in a practical situation will depend upon the average static-load pressure and on the oil-supply pressure. Experimental tests were carried out [3] on a rigid rotor (Fig. 5a) supported in squeeze-film dampers each having two lands supplied from a central, circumferential oil groove (Fig. 5c). Using the values of the non-dimensional groups shown in Fig. 4, together with a static load pressure p_{st} of 10 lbf/in^2

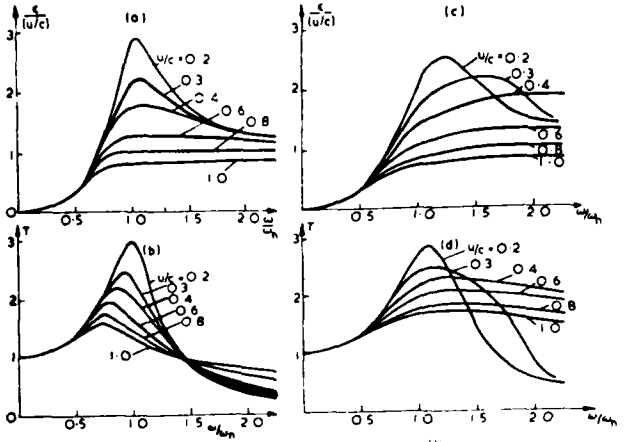

Fig 3 ε/(u/c) and Transmissibility v ω/ωn
a and b Full film
c and d Half-cavitated film
A = 0·2

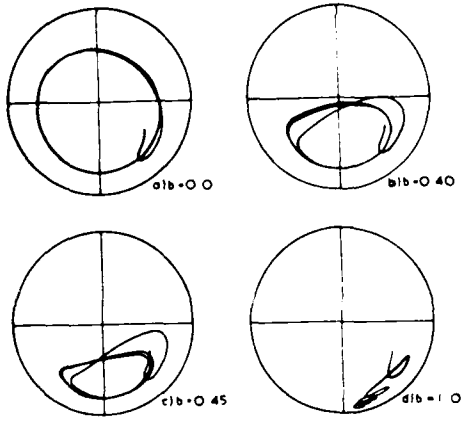

Q = 0·90 Q_c = 2·26 β = 0·61

Fig 4 Theoretical vibration orbits for four values of factor b

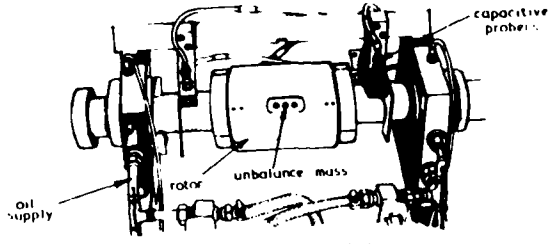

a) General view of test rig

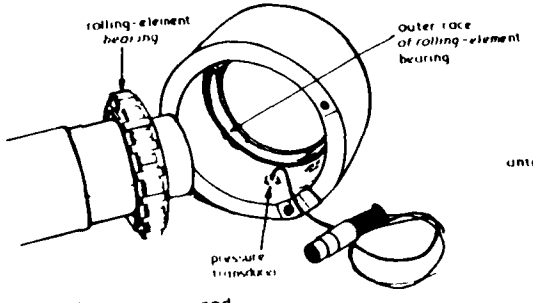

b) Squeeze ring and pressure transducer

Fig 5

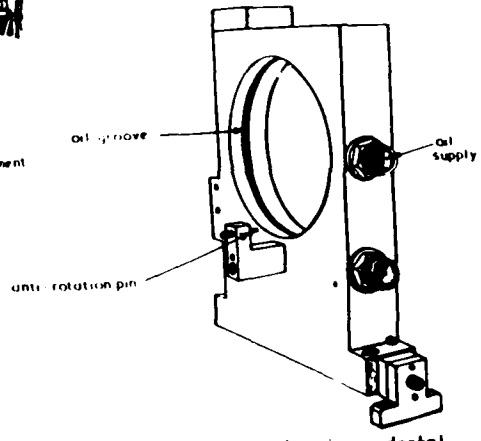

c) Squeeze bearing pedestal

(69 kN/m^2) and a supply pressure of 2 lbf/in^2 (13.8 kN/m^2) gave an orbit (Fig.6) similar to that of Fig.4c, for which b = 0.45.

Fig. 7a shows the computed hydrodynamic pressure generated in the squeeze-film at a mid-land position at the base of the clearance circle as a function of non-dimensional time ωt and for b = 0.45. A maximum negative pressure of about-540 kN/m^2 is indicated, suggesting the presence of tensile stress in the oil film. Although large this value is not unlike negative pressures observed in journal bearings [11],[12] and squeeze bearings [13] by other workers. A pressure transducer mounted at the squeeze-film (Fig. 5b) indicated a similar pattern of pressure at the base of the clearance circle, Fig. 7b. The secondary pressure peak was due to the rotor centre moving round the tail T of the orbits indicated in Figs. 6 and 7a, A pronounced negative-pressure region can also be observed amounting to about -40 lbf/in^2(-276 kN/m^2). This confirms that not only can the oil in the squeeze-film support subatmospheric pressures but suggests that tension forces may also exist. The heights of the main pressure peaks are considerably less than predicted in Fig.7a. The implication of this is that the shaft is subjected to much smaller squeeze-film forces than the theoretical analysis would suggest, a feature also noted by White [10]. A modification of the theoretical model to allow for experimentally observed limitations to the maximum and minimum pressures resulted in a general lowering of the vibration orbit in the clearance circle. This agreed with experimental findings as a comparison of the orbits of Figs. 6 and 7a will show. As to the reason for the observed low positive-pressure peaks, the indications are that cavitation bubbles trapped in the squeeze-film are responsible, a reason also suggested by White [10]. Unlike a normal turbine bearing in which the journal rotates, there is no effective inducement for such bubbles to remove themselves except by the presence of a sufficient supply pressure to flush them away.

Further experimental and computed orbits are shown in Fig.8. Sets A show the computed orbits for the case of a short film, that is b = 0, while sets B show the predicted orbits obtained by allowing the negative pressure to be defined by the factor b = 0.45. The corresponding experimental orbits are shown in sets C and are accurate reconstructions of oscilloscope traces. For all the comparisons made, of which Fig.8 is typical, sets B showed much better agreement with the experimental sets C than did sets A.

A further item of interest is the way in which the force transmitted to the engine frame varies throughout one rotor revolution. The transmitted force is the resultant of the film forces, and may be easily computed. Large vibration orbits and orbits which feature a pronounced tail should be avoided in practice. In the former, the centrifugal force, and hence the transmitted force, become appreciable, while in the latter the rapid decelerations and accelerations in the vicinity of the tail lead to sudden large changes in the force transmitted to the engine frame.

The evolution of aeroengine squeeze-film dampers has taken somewhat different courses in different companies. In the United Kingdom a simple type of squeeze-film geometry has evolved which features a central circumferential groove at the oil inlet and end seals at the outlet. These impose quite simple boundary conditions on the dynamic pressure distributions occurring in the squeeze-films and make computation relatively easy to carry out. On the other hand in the U.S.A. at least one large engine manufacturer uses

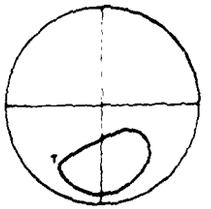

Fig 6 Experimental vibration orbit
$\beta = 0.61$, $Q = 0.90$ $Q_c = 2.26$

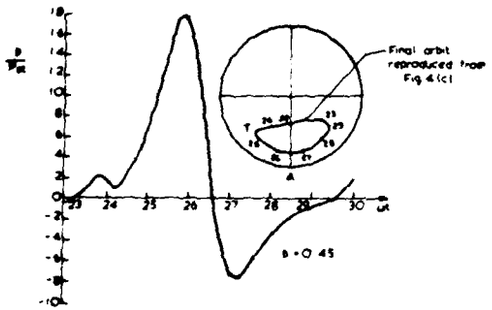

Fig 7a Dynamic squeeze film pressure at Base A of clearance circle

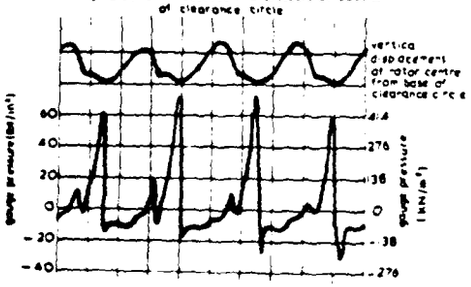

Fig 7b Experimental pressure at base of clearance circle

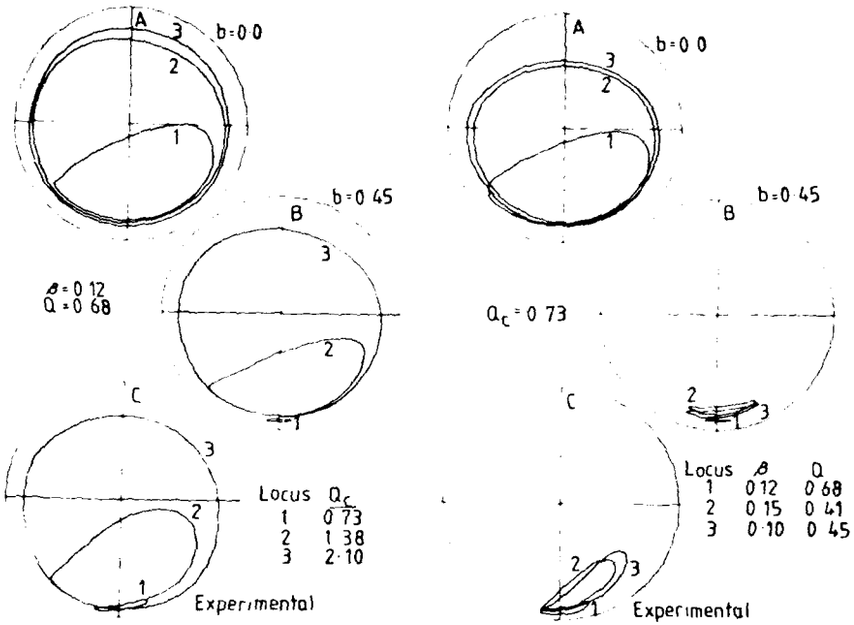

Fig 8 Theoretical and experimental orbits

squeeze-film dampers supplied from one or more oil holes in a central axial plane, with one of various types of seal at the outlet. This makes an effective mathematical model difficult to realise but has been attempted with some success by Marmol and Vance [14] and by Bansal and Hibner [15].

As the damping endowed to the system by these unassisted squeeze-films is invariably fairly light, non-linear effects such as the jump phenomenon and subharmonic resonance must again be anticipated. White [10] presents a well documented account of the jump phenomenon from an unassisted squeeze-film damper.

RECOMMENDATIONS FOR FUTURE RESEARCH

There is a strong need to represent the parameters of a general non-linear squeeze-film in some sort of quasi-linear fashion for inclusion in programs for the solution of linear multi-degree of freedom rotor-bearing systems.

One method of attack might be as follows. Assume that, for whatever reason, vibration takes place in the clearance circle of a squeeze-film damper about some mean eccentricity ratio ε_0. Then experience of journal-bearing operation indicates that four damping coefficients can be assigned to the squeeze-film provided that vibration amplitudes are not more than about one third of the radial clearance. Since the mean eccentricity ratio depends on the value of the non-dimensional dynamic force Q_c these damping coefficients would also be dependent on dynamic force. Then, following the analogy of a conventional journal bearing, the specification of four local stiffness coefficients is called for. Such stiffness coefficients would account for the lift generated by a squeeze-film and, being non-linear, would again depend on the value of the dynamic load causing the vibration. They could perhaps be found from measurements of amplitude and average phase relative to unbalance along mutually perpendicular axes. For given values of β and Q a tabulation could thus be made of all eight coefficients against dynamic force for use in linear multi-degree of freedom programs. Such an empirical procedure might offer a means of assessing the performance of complex machinery employing squeeze-film dampers and is at present being attempted by the author.

CONCLUSIONS

The purpose of this paper has been to elucidate the roles of the squeeze-film damper when used with and without a parallel flexible element in turbomachinery applications.

Since the amount of damping endowed to the system by this means is almost invariably light and since this damping is strongly non-linear, such effects as the jump phenomenon and subharmonic resonance should be guarded against.

The role of cavitation bubbles and of subatmospheric and negative squeeze-film pressures on the performance of such dampers is very important and should be appreciated at the design stage.

Finally there is a need to be able to represent a squeeze-film in terms of quasi-linear stiffness and damping coefficients so that standard linear programs can be used to analyse the performance of multi-degree of freedom rotor-bearing systems.

In the regions of the system criticals, where vibration orbits are likely to be large and fairly concentric, the task is not too difficult. For other regions a possible method of attack has been suggested.

ACKNOWLEDGEMENTS

The author acknowledges with thanks financial support given for the work described in this paper by the Science Research Council, London, and by the Ministry of Defence, London.

Thanks are also due to the Chairman of the Propulsion and Energetics Panel of AGARD for permission to publish Figs. 3 - 7 inclusive.

REFERENCES

1 Gunter,E.J., Barrett,L.E. and Allaire,P.E. 'Design of non-linear squeeze-film dampers for aircraft engines', A.S.M.E. Jnl.Lub.Tech. Vol.99, No.1 Jan. 1977, pp.57.

2 Nikolajsen, J.L. and Holmes, R. 'Investigation of squeeze-film isolators for the vibration control of a flexible rotor'. Jnl. Mech.Eng.Sci. 1979.

3 Holmes,R. and Humes,B. 'An investigation of vibration dampers in gas-turbine engines'. Proceedings of the 52nd AGARD Symposium, Cleveland, U.S.A. Oct.1979.

4 Glienicke,J. and Stansi,U. 'External bearing damping - a means of preventing dangerous shaft vibrations in gas turbines and exhaust turbo-chargers', C.I.M.A.C. Conference, Barcelona, 1975, pp.287-311.

5 Gunter, E.J., Barrett,I.E. and Allaire,P.E. 'Stabilization of Turbomachinery with squeeze-film dampers - Theory and Applications' Paper No. C233/76, Proceedings of Inst.Mech.Engrs.Conference on Vibrations in Rotating Machinery, Cambridge, 1976.

6 Holmes, R. 'The damping characteristics of vibration isolators used in gas turbines', Jnl. Mech.Eng.Sci. Vol.19, No.6, 1977, pp.271-277.

7 Tønnesen,J. 'Experimental parametric study of a squeeze-film bearing', A.S.M.E. Jnl. of Lubrication Technology, April 1976, pp.206-213.

8 Darlow,M.S. and Smalley, A.J. 'Design and test of a squeeze-film damper for a flexible power transmission shaft'. The Design Engineering Conference, Chicago, Illinois, April 1978.

9 Nikolajsen, J.L., Goldhalekar,V. and Holmes, R. 'Investigation of an electromagnetic damper for the vibration control of a transmission shaft'. Proc. Instn. Mech.Engrs, London 1979.

10 White, D.C. 'Squeeze-film journal bearings'. Ph.D. Thesis, Cambridge,1970.

11 Dyer,D. and Reason,B.R. 'A study of tensile stresses in a journal-bearing oil film', Jnl. Mech.Eng.Sci. 18, 1, Feb.1976, pp.46-52.

12 Patrick,J.K. 'Detection of tensile stresses in an oil film by means of a balanced pressure piston', Proc.Inst.Mech.Engrs., 1968, 182 (3G), 73-74.

13 Feder,E., Bansal, P.N. and Blanco,A. 'Investigation of squeeze-film damper forces produced by circular centered orbits', A.S.M.E. Paper No. 77-GT-30.

14 Marmol, R.A. and Vance, J.M. 'Squeeze-film damper characteristics for gas turbine engines', A.S.M.E. Paper No. 77-DET-18.

15 Bansal,P.N. and Hibner, D.H. 'Experimental and Analytical investigation of squeeze-film bearing damper forces induced by offset circular whirl orbits'. A.S.M.E. Journal of Mechanical Design, Vol.100, July 1978.

DISCUSSION

D. L. Taylor, Assistant Professor, Sibley School of Mechanical & Aerospace Engineering, Cornell University.

Several questions raised during Professor Holmes' presentation dealt with the small inner loops which were observed in certain orbits determined by numerical integration. The experience of the discussor has been that these loops may sometimes be a stable phenomenon and other times may be unstable and die out. The orbits which follow were determined for a rotor model similar to that discussed by Professor Holmes. A planar rigid rotor is carried in a squeeze film isolator (damper and centering spring in parallel). Fluid film forces are based on an Ocvirk short bearing film. Rotor parameters are given in Table I. At 23,000 rpm, the whirl path in Figure 1 shows the inner loops discussed. The orbit starts from the circled point. However, if the integration program is run longer, as in Figure 2, the single inner loop is seen to die out. At a higher speed (32,000), the orbit shown in Figure 3 is obtained. This time a two loop pattern occurs, and if the integration is continued, the orbit shown in Figure 4 results. The inner loop structure is decaying, but more slowly than in Figure 2. Finally, at a speed of 42,000 rpm, the orbit in Figure 5 is obtained. The final disposition is hard to determine without continuing the integration. The extended orbit is shown in Figure 6. The two loop structure is now seen to be stable, slightly precessing.

Several questions during the discussion dealt with methods of numerical integration. The results which have been presented were obtained by a variable time step Kutta-Merson algorithm. This type of program will constantly adjust the effective time step of the integrator to maintain a requested degree of accuracy. The discussor has found this type of algorithm to be very effective. It can handle quite rapid transients, such as blade loss, but tracks an almost circular orbit with approximately six to ten time steps per revolution. This is quite efficient with regards to computer time. The orbits which follow were generated by such an algorithm using a requested time step of .00005 sec.

In conclusion, the discussor has observed a critical speed below which the inner loop structure is unstable. The decay rate decreases with increasing speed and, above the critical speed, there is a stable noncircular structure which then evolves with further increases in speed.

Table I

m = 73.8 lb	Ω = 12,000 rpm
k = 1.23 x 10^6 lb/in.	R = 2.55 in.
μ = .0266 poise	L = .9 in.
d = 1 mil (c.g. offset)	C = 4 mils

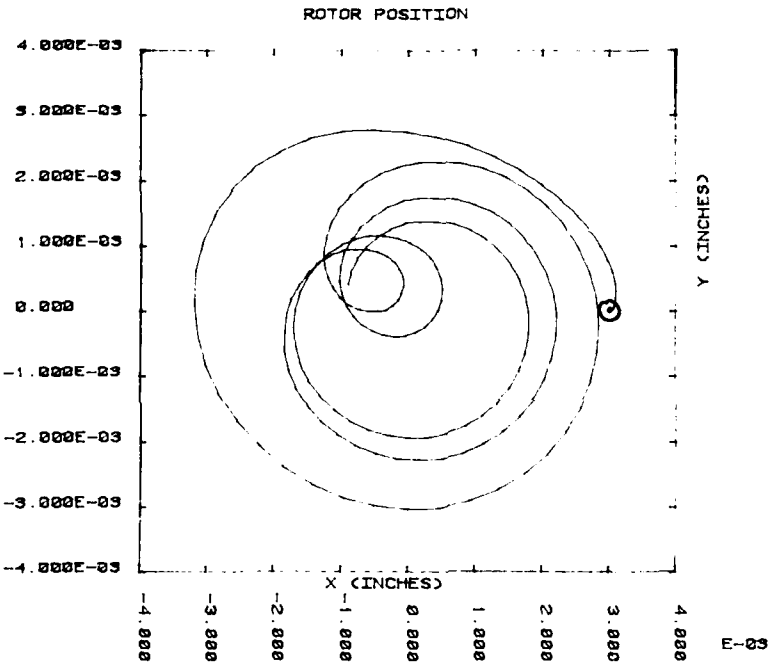

Fig. 1 x-y response of rotor shaft center, 23,000 rpm, 100 time steps

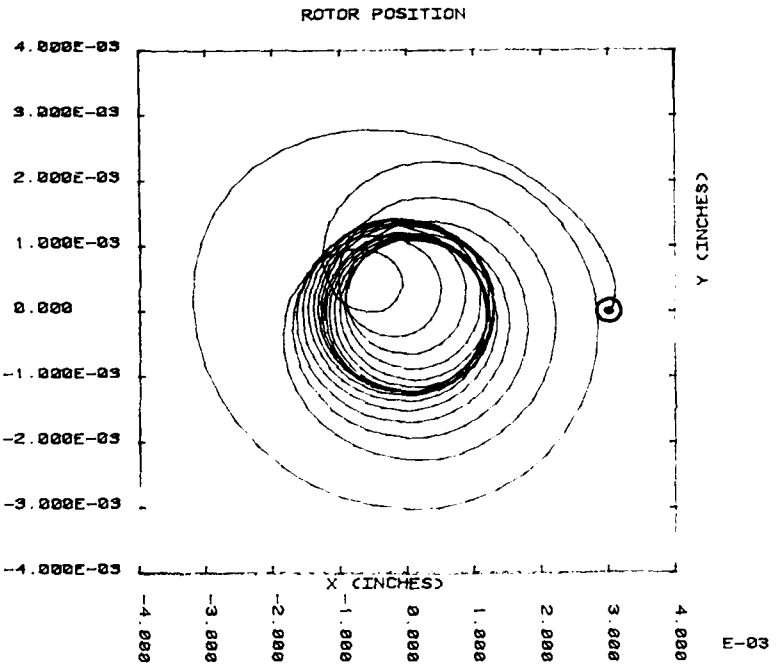

Fig. 2 x-y response, 23,000 rpm, 400 time steps

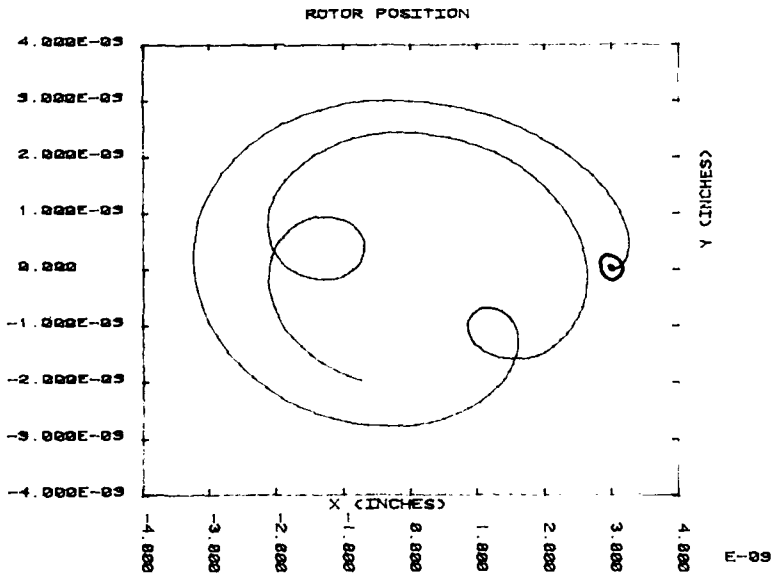

Fig. 3 x-y response, 32,000 rpm, 100 time steps

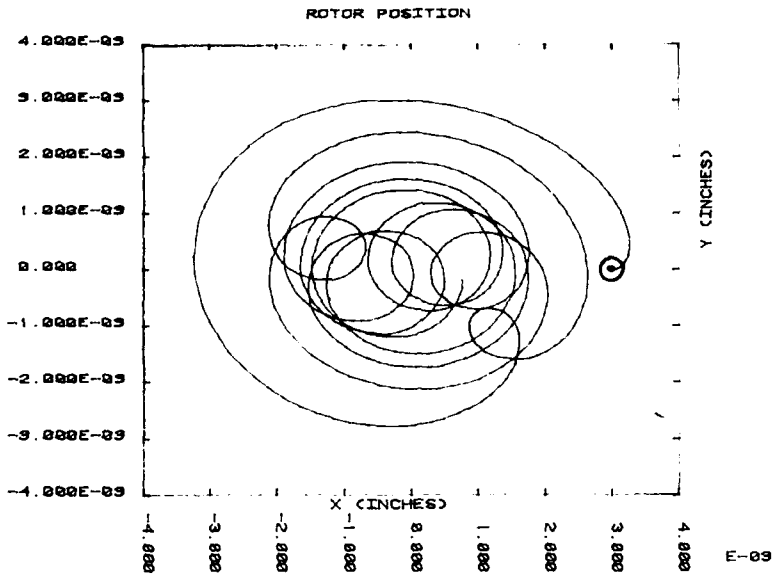

Fig. 4 x-y response, 32,000 rpm, 400 time steps

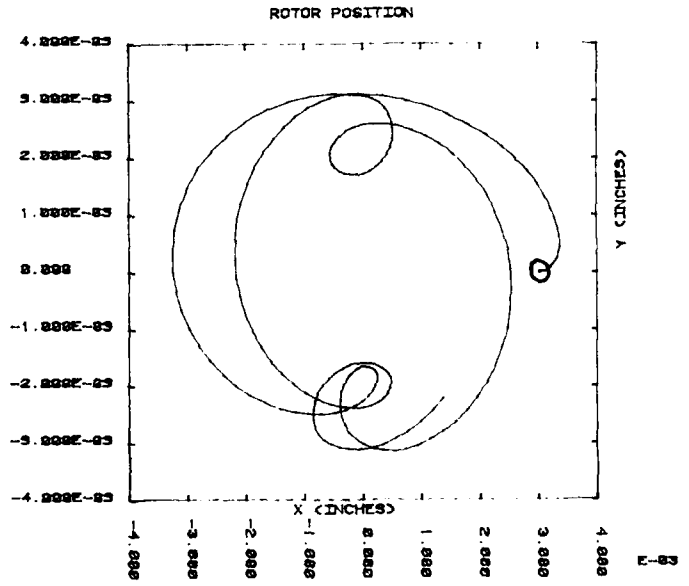

Fig. 5 x-y response, 42,000 rpm, 100 time steps

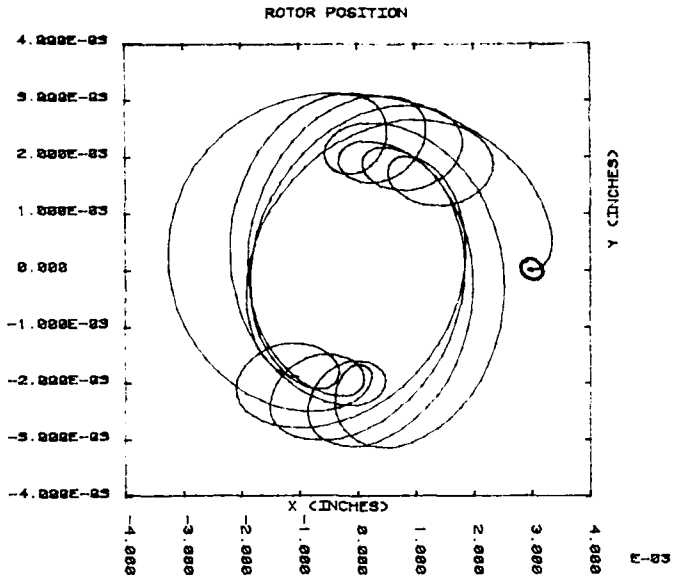

Fig. 6 x-y response, 42,000 rpm, 400 time steps

E. J. Hahn, Senior Lecturer, University of New South Wales, Kensington, New South Wales, Australia.

The author has presented a very interesting and informative paper. There are however a few points which appear to need qualification and further comments would be appreciated.

The author is quite correct in noting that jump phenomena may be associated with cavitated squeeze film dampers. However, should the unbalance behaviour of squeeze film damper supported rotors be simply of the type described in the paper, viz: that large vibrations are maintained for an extended speed range during run up before jumping down to an acceptable level, one could be excused for being thankful that jump phenomena exist. After all, such a jump down is preferable to its absence, as pertains, for instance, to the operating condition illustrated in Fig. 2 of Ref. [1]. Rather, one needs to guard against jump phenomena to avoid the possibility of jump up. The author appears to imply that the jump phenomena is restricted to light (non-linear) damping. As shown in Fig. 2 of Ref. [1], for a given unbalance, although the higher the system damping, as measured by B, the less likelihood of entering the bistable region, the system unbalance is an equally if not more important parameter in determining jump behaviour. Thus, regardless of the extent of the system damping, should the unbalance parameter u/c (= U in Ref. [1]) be less than unity, bistable operation is possible, if the operational speed is high enough. Also, bistable operation is not possible if the unbalance parameter is greater than one.

In Fig. 1, the author suggests that sub-harmonic resonance is present in a centrally preloaded squeeze film damper supported rigid rotor. In the case cited by the author, the value of $A = 0.0284$ is equivalent to $B = 0.009$ in Ref. [2] and from Fig. 8 of Ref. [2], corresponds approximately to a damping ratio of the order 0.01. The system here could, therefore, be termed very lightly damped. Hence, it would be instructive for the author to continue his numerical solution for a sufficient number of cycles to ensure that steady state conditions have indeed been reached. The writer suspects that if this were done, only a synchronous circular orbit would remain.

It is not totally surprising that non-synchronous operation has been observed experimentally by the author, and in this regard, it is informative to note the special need for accuracy in numerical solutions of very lightly damped systems. (In no way is it here suggested that the numerical solutions of the author were insufficiently accurate.) For example, it has been possible to reproduce exactly the so-called non-synchronous stable operating mode reported in [3], only to find that further improvement in accuracy (in this case by further increase in sampling rate) resulted in the eventual disappearance of the non-synchronous component [4]. Just as truncation and round off errors in numerical procedures may in a sense be regarded as continuous, albeit very small, external force excitations to a system which, if sufficiently underdamped, will either not reach steady state conditions, or will reach a steady state condition dependent on the periodicity of the overall force excitation, so also very lightly damped rotor bearing systems in practice or in experimental rigs will be significantly influenced not only by unbalance excitation but by other unwanted but nevertheless unavoidable external force excitations. This is not to say that such very lightly damped systems are acceptable. On the contrary, they tend to be associated with high vibration amplitudes and high transmissibilities. As noted by the author, they should be guarded against, and highlight the need for design information on the damping reserve of stable (in the linear sense) systems.

1. Hahn, E.J., "Unbalance Behaviour of Squeeze Film Supported Rigid Rotors". Paper presented at Workshop on Stability and Dynamic Response of Rotors with Squeeze Film Bearings, Charlottesville, Va., May, 1979, 13 pp.

2. Simandiri, S. and Hahn, E.J., "Effect of Pressurization on the Vibration Isolation Capability of Squeeze Film Bearings", Journal of Engineering for Industry, Trans. ASME, Vol. 98, No. 1, February, 1976, pp. 109-117.

3. Mohan, S. and Hahn, E.J., "Design of Squeeze Film Damper Supports for Rigid Rotors", Journal of Engineering for Industry, Trans. ASME, Vol. 96, No. 3, 1974, pp. 976-982.

4. McLean, L.J., "Hybrid Computer Analysis of Rotor Bearing Systems", M.Eng.Sc. Thesis, UNSW, Kensington, Australia, 1977.

AUTHOR'S CLOSURE

I would like to thank Professor Taylor for his interesting comments and to add that on returning from the Conference I, too, endeavoured to obtain more definite conclusions on these subsynchronous orbits. Inasmuch as any conclusions could be drawn, the indications were that, as in Professor Taylor's Fig. 6, the multiloop orbits appeared to be stable and slightly precessing. This may well be due to the fact that I was concerned with speeds that were always an integer multiple of the undamped natural frequency $\sqrt{k/m}$, which in Professor Taylor's case would have been $2\sqrt{k/m}$ = 48,440 rev/min.

I should like to thank Dr. Hahn for further elucidating the subharmonic and jump phenomena, in particular drawing attention to jump-up rather than jump-down. I think this is a very valid point. With regard to the numerical prediction of non-synchronous operation, I can but say that after a costly amount of computing time using my Runge-Kutta-Merson program, the internal loops of Fig. 1 of my paper could not be made to disappear. Instead, an ultimate orbit was found, which precessed slowly, rather as did the orbits calculated by Dr. Taylor in his contribution to this discussion. But, as both Dr. Hahn and I have found, such orbits certainly occur in practice, perhaps due to influences akin in their effect to numerical inexactitudes.

SQUEEZING FLOW OF VISCOELASTIC FLUIDS INCLUDING THE EFFECT OF FLUID INERTIA

By

John A. Tichy
Assistant Professor
of Mechanical Engineering
Rensselaer Polytechnic Institute
Troy, New York 12181

ABSTRACT

The Reynolds equation of hydrodynamic lubrication is used to predict stiffness and damping coefficients for the analysis of rotor dynamic systems using squeeze film dampers. Due to the effects of fluid inertia and viscoelasticity, separately or in combination, the Reynolds equation of hydrodynamic lubrication can be significantly and qualitatively in error. For the case where one of the bearing surfaces performs small sinusoidal oscillations, the deviations from lubrication theory can be readily predicted in terms of a Reynolds number and the so-called Deborah number. Unusual resonance-like effects in the behavior of the lubricant film itself are exhibited, which may be a cause of reported discrepancies between theory and experiment in rotor dynamic studies.

NOMENCLATURE

c	=	radial clearance, see Fig. 7
G	=	complex viscosity component, shear modulus
h	=	film thickness
h_0	=	reference film thickness
i	=	$(-1)^{\frac{1}{2}}$
L	=	characteristic length
p	=	pressure
Re	=	Reynolds number = $\omega h_0^2/\mu$
t	=	time
u,v	=	velocity in the x and y directions
V	=	bearing surface velocity
x,y	=	coordinate directions
W^*	=	dimensionless load amplitude

$\gamma, \dot{\gamma}$ = shear strain, shear strain rate
δ = amplitude of top surface oscillation
ε = eccentricity ratio
θ = Deborah number = $G/\mu\omega$
μ = dynamic viscosity
μ^* = complex viscosity = $\mu - iG/\omega$
ρ = density
ϕ = phase angle
τ = shear stress
ω = frequency of top plate oscillation

Subscripts

1,2 = surface 1 or 2
$_0$ = reference
$_\ell$ = lubrication theory

INTRODUCTION

In the modeling and analysis of rotor dynamic systems using squeeze film damper bearings, the stiffness and damping coefficients for the lubricant film are nearly always obtained from the Reynolds equation of hydrodynamic lubrication. The damper itself consists of an inner non-rotating journal and a fixed outer bearing. The linear stiffness and damping coefficients are obtained, in principle, by subjecting the journal to very small perturbations in displacement and velocity, respectively; and calculating the resulting forces on the journal from lubrication theory.

Squeeze film damper bearings are often constructed with very large radial clearances relative to plain journal bearings, e.g. c = 0.025 cm vs. 0.0025 cm (~ 10 mils vs. 1 mil). They also tend to be used in very high oscillatory speed applications, e.g. ω = 3000 rad/sec (~ 30,000 rpm) where rotor dynamics problems are most prevalent. These conditions - large gaps and high speeds - conspire to create conditions where fluid inertia effects may become significant in the lubricant film, violating the conditions under which the Reynolds equation can be applied.

It is well known that modern lubricants are significantly viscoelastic due to the addition of high molecular weight polymer additives. It can be said that viscoelastic fluids possess a characteristic material property time parameter which roughly corresponds to the time it takes for a fluid flow to adjust to a suddenly imposed stress. For the Newtonian fluid model, which is used in the derivation of the Reynolds equation, this time parameter is zero. An unsteady process, such as an oscillatory flow, will have an associated characteristic process time parameter, roughly $1/\omega$. When the ratio of the fluid property time parameter to this process time parameter becomes non-negligible, viscoelastic effects are expected to be significant and the Newtonian fluid model may no longer be applicable. This may be the case in high speed squeeze film damper bearings when a lubricant with high molecular weight additives is used.

It can be shown that fluid inertia effects, perhaps in combination with viscoelastic effects, under certain conditions introduce significant errors into the Reynolds equation. It will be seen that the behavior of the lubricant film can be qualitatively quite different than that predicted by lubrication theory. The values of the stiffness and damping coefficients will surely be affected as may the predicted behavior of the entire rotor dynamic system.

These concepts have been developed in a series of papers by this author and co-workers (1-4), to which the interested reader is referred for mathematical details. Basic background concepts and results will be presented here, as well as future research which may be of more direct benefit to those working in the analysis of squeeze film dampers.

BACKGROUND

Consider the flow behavior in an arbitrary squeeze film geometry, as shown in Fig. 1. For convenience, the film is shown "unwrapped" and the infinitely long bearing (one-dimensional) assumptions are used. The lower surface is stationary while the upper surface can move in the direction across the film. The velocities in the x and y directions, along and across the film, are u and v respectively, and t denotes time.

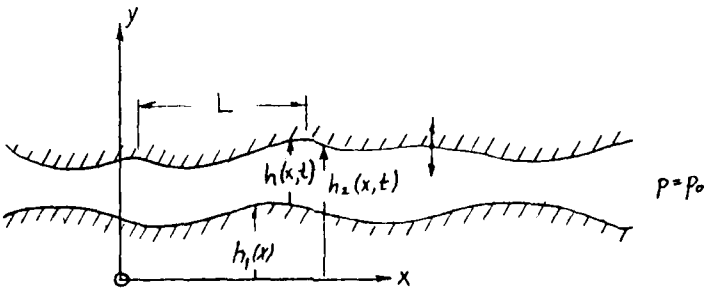

Figure 1. Arbitrary Squeeze Film Geometry

Recall the basic development of the Reynolds equation, using the continuity, x, and y momentum equations:

$$\frac{\partial u}{\partial x} + \frac{\partial v}{\partial y} = 0 \ , \tag{1a}$$

$$\frac{\partial p}{\partial x} = \mu \frac{\partial^2 u}{\partial y^2} \ , \tag{1b}$$

$$\frac{\partial p}{\partial y} = 0 \ . \tag{1c}$$

Typical boundary conditions for squeezing flow are

$$\begin{aligned} &y = 0: && u = v = 0, \\ &y = h(x,t): && u = 0 \qquad v = \frac{\partial h_2}{\partial t} = h_2(x) + V(t) \\ &x = 0: && \frac{\partial p}{\partial x} = 0 \\ &x = x_0: && p = p_0 \end{aligned} \tag{2}$$

where p is pressure, μ is viscosity, and V(t) is the bearing upper surface velocity. The basic momentum balance on a fluid element in eq (1b) can be expressed as:

$$\text{net pressure force} = \text{net viscous shear force.} \tag{3}$$

Note that time effects enter the problem only through the boundary conditions. This means that the problem is fluid mechanically steady. When eqs (1) and (2) are combined, a form of the Reynolds equation results:

$$\frac{\partial}{\partial y}\left(h^3 \frac{\partial p}{\partial x}\right) = 12\mu \frac{\partial h}{\partial t} \tag{4}$$

with time now appearing explicitly, although this does not change the basic quasi-steady nature of the problem.

The resulting velocities become

$$u(x,y,t) = 3V(t)x \left\{\left[\frac{y}{h(x,t)}\right]^2 - \left[\frac{y}{h(x,t)}\right]\right\} ,$$

and (5)

$$v(x,y,t) = V(t) \left\{3\left[\frac{y}{h(x,t)}\right]^3 - 2\left[\frac{y}{(h(x,t)}\right]^2\right\} .$$

Note that the velocity profile u(y) is always parabolic and that the fluid velocity is precisely in phase with the bearing surface velocity V(t). This means that according to lubrication theory, the fluid must respond instantaneously to the surface velocity.

In reality, for a fluid possessing inertia a finite time lag must be associated with the fluid response. Similarly, in a viscoelastic fluid (even in the absence of inertia) a finite time lag is associated with a fluids' response to an applied stress as mentioned above. If a constant force F ($\sim$ stress τ) is suddenly applied to an idealized dashpot of constant μ ($\sim$ viscosity) an instantaneous velocity response $\dot{x}$($\sim$ shear rate $\dot{\gamma}$) is evoked, see Fig. 2. This is analogous to the viscous Newtonian fluid model. If a sudden force is applied to a spring and a dashpot in series, however, a time delay is associated with the fluid response. This example is analogous to the case of a viscoelastic fluid. Thus both fluid inertia and viscoelastic properties introduce phase shifting effects into the behavior of a lubricant film, whereas such behavior is absolutely ruled out by the Reynolds equation theory.

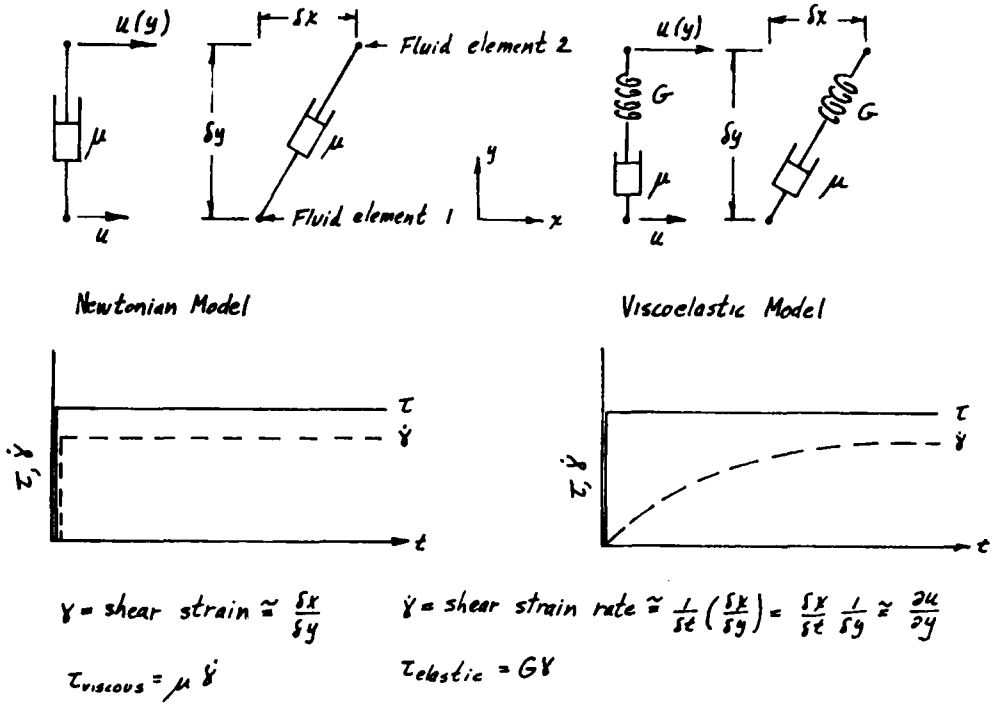

Figure 2- Viscoelasticity Concepts

THE OSCILLATORY SQUEEZING PROBLEM

Theory

Solution of the general problem of the squeezing flow of a viscoelastic fluid subject to inertia effects is complicated by two factors: (1) the nonlinear convective inertia terms in the momentum equation; and (2) lack of agreement on a suitable viscoelastic fluid model. In addition, most of the likely candidates for viscoelastic fluid models are nonlinear.

In squeeze film damper bearings, the inner journal performs an oscillatory squeezing motion of the lubricant film as it moves around its orbit. This case does not correspond to the more convenient geometry of Fig. 1 but can be easily handled along the lines of Ref (3). If the oscillatory squeezing problem is now considered, a restrictive assumption is made which is very convenient in that no further assumptions or limitations at all are required. Referring to Fig. 1, the sinusoidal oscillations are described by

$$h_2(x,t) = h_2(x) - \delta \cos \omega t \ . \tag{6}$$

The assumption is that

$$\delta << h_{min} << L \tag{7}$$

i.e. the oscillation amplitude δ is "small."

In this case, by simple order-of-magnitude considerations convective inertia terms like $u\,\partial u/\partial x$ are small relative to the unsteady inertia term $\partial u/\partial t$. This point is discussed in detail in Ref (2) and in the hydrodynamics text of Happel and Brenner (5). Note from Eqs (2) and (6) that the magnitude of the upper surface velocity $V(t)$ is $\delta\omega$. Thus for sufficiently small δ, the flow is always "slow" (small u), but may be highly unsteady (large $\partial u/\partial t$). Therefore the process could be performed at an arbitrarily high ω and in principle the flow would never become turbulent.

For the case of small sinusoidal displacements, all viscoelastic models reduce to the complex linear form

$$\tau = \mu^* \dot{\gamma} \tag{8}$$

where τ and $\dot{\gamma}$ are shear stress and shear rate, respectively. The symbol μ^* denotes the complex viscosity

$$\mu^* = \mu - i\,\frac{G}{\omega} \quad . \tag{9}$$

in which G is the elastic shear modulus of the viscoelastic fluid, see Fig. 2. For simple shearing flows, the shear rate $\dot{\gamma}$ is the velocity gradient $\partial u/\partial y$. The material properties μ and G are in general functions of frequency ω, which can be measured on standard rheological instruments. The velocities and pressures are all now expressed in the complex form $u = u(x,y)\exp(i\omega t)$.

The x-momentum balance is now

$$\underset{\text{inertia force}}{\rho\,\frac{\partial u}{\partial t}} = \underset{\text{pressure force}}{-\frac{\partial p}{\partial x}} + \underset{\text{viscous force}}{\mu\,\frac{\partial^2 u}{\partial y^2}} \underset{\text{elastic force}}{- i\,\frac{G}{\omega}\,\frac{\partial^2 u}{\partial y^2}} \tag{10}$$

The problem is now governed by two simple dimensionless groups:

$$\begin{aligned} \text{Reynolds Number} = \text{Re} &= \rho\,\frac{\omega h_0^2}{\mu} \\ &= \frac{\text{inertia force}}{\text{viscous force}} \\ \text{Deborah Number} &= \frac{G}{\mu\omega} \\ &= \frac{\text{elastic force}}{\text{viscous force}} \end{aligned} \tag{11}$$

The parameter h_0 is some reference or characteristic film thickness (such as the radial clearance, minimum clearance, etc.) depending on the particular problem..

Results

Very unusual lubricant velocity fields are exhibited as shown in Figs. 3-5. Equations of the form (10) are solved for various sets of boundary conditions in Refs (1-4) by standard methods. Subject to the assumption (7) above, the solutions are "exact." In each case, the figures on the left-hand side (a) correspond to the instant of time when the bearing surface is at the maximum velocity downstroke, while the right-hand side (b) corresponds to the time when the bearing surface is instantaneously motionless, about to reverse directions. The flow profile is only parabolic for the lubrication theory case ($Re \to 0$, $\theta \to 0$). Peculiar flow reversals and a circulating flow are exhibited. Lubrication theory requires that if the bearing surfaces are motionless at any instant of time, the lubricant is also. This is clearly not the case here, as fluid motion continues to inertia and elasticity in Figs. 3b, 4b, and 5b.

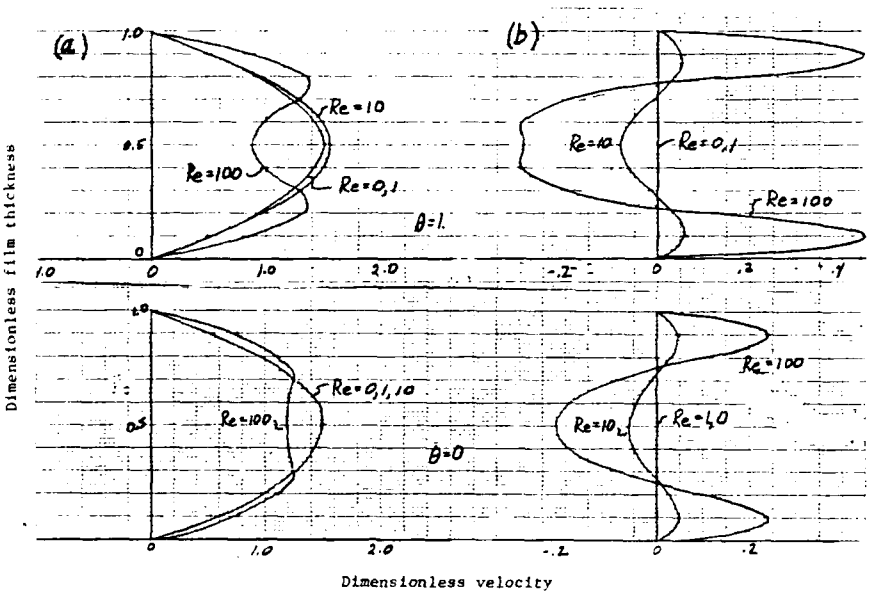

(a) V(t) = max (b) V(t) = 0

Figure 3. Typical Velocity Profiles - Parallel Circular Disks, separation h_o, $Re = \rho\omega h_o^2/\mu$

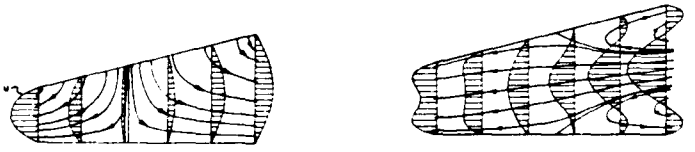

(a) V(t) = max (b) V(t) = 0

Figure 4. Typical Velocity Profiles and Streamlines - Simple Tapered Thrust Bearing (2)

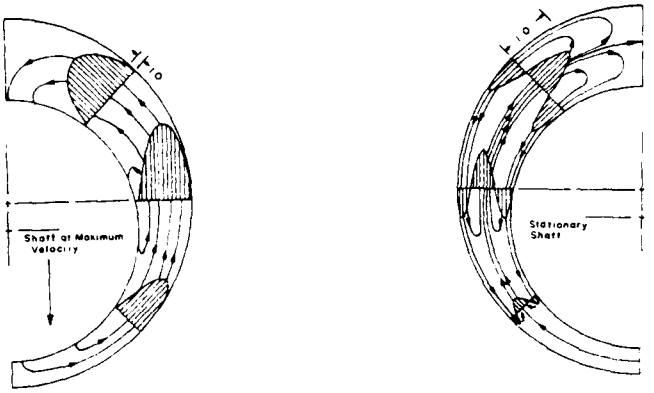

(a) V(t) = max (b) V(t) = 0

Figure 5. Typical Velocity Profiles and Streamlines Journal Bearing (3)

Loads are also profoundly affected by inertia and viscoelastic effects. For sinusoidal motion, loads can be expressed in terms of a dimensionless load amplitude and a phase angle, as is common for oscillatory behavior. The dimensionless load $\mathcal{W}$ is the ratio of the load amplitude predicted by the improved theory W* to the load amplitude predicted by lubrication theory W_c^*. The phase angle ϕ is the angle between the load and the oscillating surface velocity. This angle must be zero for lubrication theory. Figures 6 and 7 show the load amplitude and phase angle behavior for a variety of bearing geometry conditions. More detailed explanations, and additional results appear in Refs (1-4). Note, however, that virtually any sort of behavior can result relative to that predicted by lubrication theory: i.e. the load amplitudes may be increased or decreased ($W^* \lesssim W_c^*$), and the load may be in or out of phase with respect to the surfaces velocity ($0 < \phi < 180°$; $\phi_c \equiv 0$). Note also that a continuous increase in Reynolds or Deborah number does not mean a continuous increase (or decrease) in the load variables.

Range of Variables

It appears that squeeze film damper bearings may very well operate in the range of variables for which inertia and viscoelastic effects are significant. Consider the following set of variables:

Density	ρ = 0.8 gr/cm^3
Oscillatory speed	ω = 3000 sec^{-1} (≈ 28000 rpm)
Viscosity	μ = 0.1 gr/sec-cm = 10 cp (≈ 1.45 μ reyn)
Radial clearance	c = 0.025 cm(≈ 0.010 in)
Shear modulus	G = 300 dyne/cm^2 (≈ 0.003 psi)

From these values the following values for Reynolds and Deborah number obtained:

Reynolds number, $Re = \frac{\rho\omega c^2}{\mu} = 15.$ Deborah number, $ = \frac{G}{\mu\omega} = 1.$

For these sets of dimensionless parameters, viscoelastic and inertia effects would be expected to become significant, from Fig. 6.

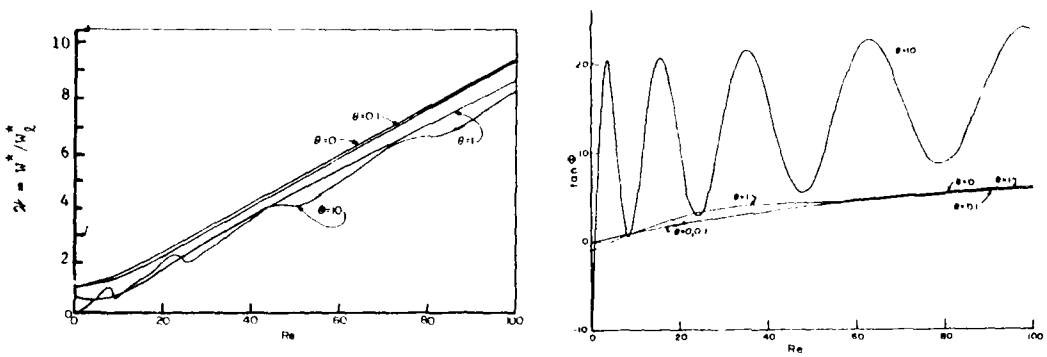

Figure 6. Typical Load Behavior, Amplitude and Phase Angle
Parallel Circular Disks, separation h_o, $Re = \rho\omega h_o^2/\mu$ (1)

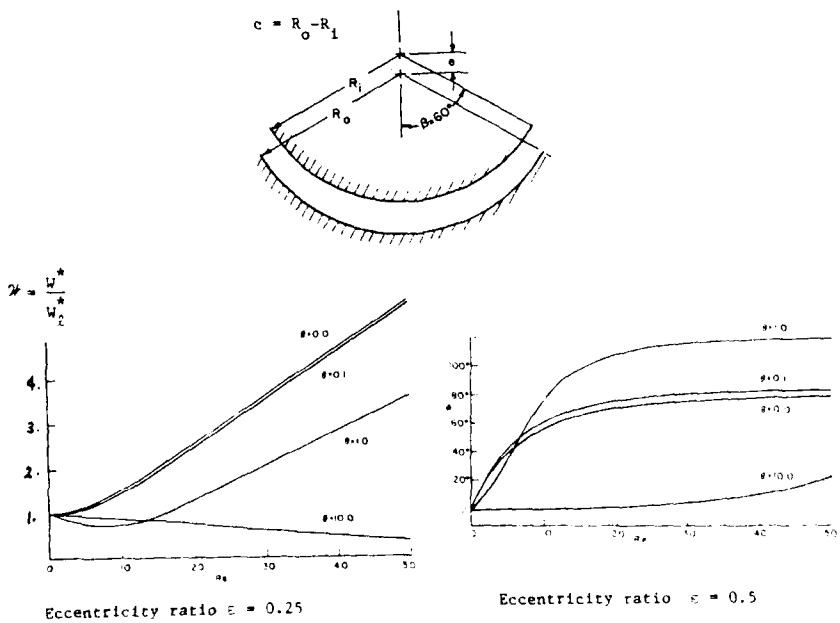

Eccentricity ratio $\varepsilon = 0.25$ Eccentricity ratio $\varepsilon = 0.5$

Figure 7. Typical Load Behavior, Amplitude and Phase Angle
Partial Journal Bearing, $Re = \rho\omega c^2/\mu$ (4)

CONCLUSIONS

Analytic solutions have been developed for the flow of a viscoelastic fluid between arbitrary two-dimensional surfaces, one of which is subject to small high-frequency oscillations. Fluid inertia effects are included and the results are valid for any simple viscoelastic fluid provided the oscillation amplitude is sufficiently small. Solutions are available in terms of a Reynolds and Deborah number, and unusual resonance effects in velocity field and load are exhibited as the oscillation frequency (or Reynolds number) is increased for a particular fluid. Lubrication theory may be significantly in error for fairly low combinations of Reynolds and Deborah number.

The very restrictive assumption that the oscillation amplitude is small renders the problem linear with respect to both inertia and viscoelastic effects. What then are the effects of viscoelasticity and inertia if δ/h is no longer $<< 1$? One can only speculate, but it is this author's opinion that these sort of phenomena will still prevail at higher values of δ/h. It hardly seems likely that non-linear effects tend to produce the more orderly behavior required by lubrication theory. Controlled experimental studies and perhaps more involved analytical techniques may ultimately provide the answer, although in the latter case the whole range of issues regarding an appropriate viscoelastic model must be addressed.

Results have only been developed, to date, for the infinitely long, one-dimensional bearing; and in the case of full journal bearings (with their more complex boundary conditions), for inertia effects only. The case most commonly used in anslysis of rotor dynamic systems is the short bearing hypothesis. This case is a straightforward extension of existing solutions, and work is in progress to derive stiffness and damping coefficients, based on the improved theory. When completed, a full analysis can be performed, examining the influence of fluid inertia and viscoelastic effects on rotor dynamic behavior.

REFERENCES

1. Tichy, J. A., "The Behavior of Viscoelastic Squeeze Films Subject to Normal Oscillations, Including the Effect of Fluid Inertia," *Applied Scientific Research*, Vol. 33, Jan. 1978, pp. 501-517.
2. Tichy, J. A., and M. F. Modest, "Squeeze Film Flow in Arbitrarily Shaped Journal Bearings Subject to Oscillations," ASME Journal of Lubrication Technology, Vol. 100, No. 3, July 1978, pp. 323-329.
3. Tichy, J. A., and M. F. Modest, "Squeeze Film Flow Between Arbitrary Two-Dimensional Surfaces Subject to Normal Oscillations," ASME Journal of Lubrication Technology, Vol. 100, No. 3, July 1978, pp. 316-322.
4. Tichy, J. A., and M. E. Skinkle, "An Analysis of the Flow of a Viscoelastic Fluid between Arbitrary Two-Dimensional Surfaces Subject to High Frequency Normal Oscillations," ASME Journal of Lubrication Technology, Vol. 101, No. 2, April 1979, pp. 145-153.
5. Happel, J., and H. Brenner, *Low Reynolds Number Hydrodynamics*, Prentice-Hall, Englewood Cliffs, N.J., 1965, pp. 52-55.

Experimental Squeeze Bearing Orbit Studies

by

Jørgen Tønnesen
Associate Professor
Dept. of Machine Elements
Technical University of Denmark
DK-2800 Lyngby, Denmark

ABSTRACT

The paper presents the results of experimental investigations in which the damping coefficients of a squeeze-film bearing are obtained from impedance measurements. Good correlation is found with a simplified linearized theory for moderate force levels when referred to the concentric case. Only fair correlation is found in the eccentric case, however the oil supply pressure has a strong influence. The oil film extent is found to vary between 180 and 360 degrees and the extent is influenced by bearing length, radial clearance and oil viscosity. Examples are shown of present laboratory type test rigs using damper bearings and a general outline is given for designing and optimizing a squeeze film bearing.

EXPERIMENTAL APPARATUS

Typical laboratory test rigs are shown in Fig. 1 [1-4]. The test rig in Fig. 1a has a damper bearing with an outside diameter of 7 mm (.28 in.) and the L/D is .3⅜. The clearance ratio is typically from 1 to 7x10^{-3} and the clearance space is filled with the damping fluid which is pressure fed into a circumferential groove. The end flow is restricted by some kind of sealing arrangement like diaphragm-lip-type, piston rings or o-rings (in rubber). Load is applied to the damper bearing from a ball bearing supported by weights and variable weights are attached. The arrangement is a reasonable approximation for producing a purely periodic force and at the same time keeping the influence of rotor dynamics to a minimum. The motor is driven by a speed controlled D-motor with a maximum speed of 3 Hz.

The second test rig in Fig. 1a has a damper bearing with an outside diameter of 4 mm (.16 in.) and two lands with an L/D = .1 and with a similar clearance and sealing arrangement. A unidirectional load is applied to the bearing housing from an electro dynamic shaker which is rotated at

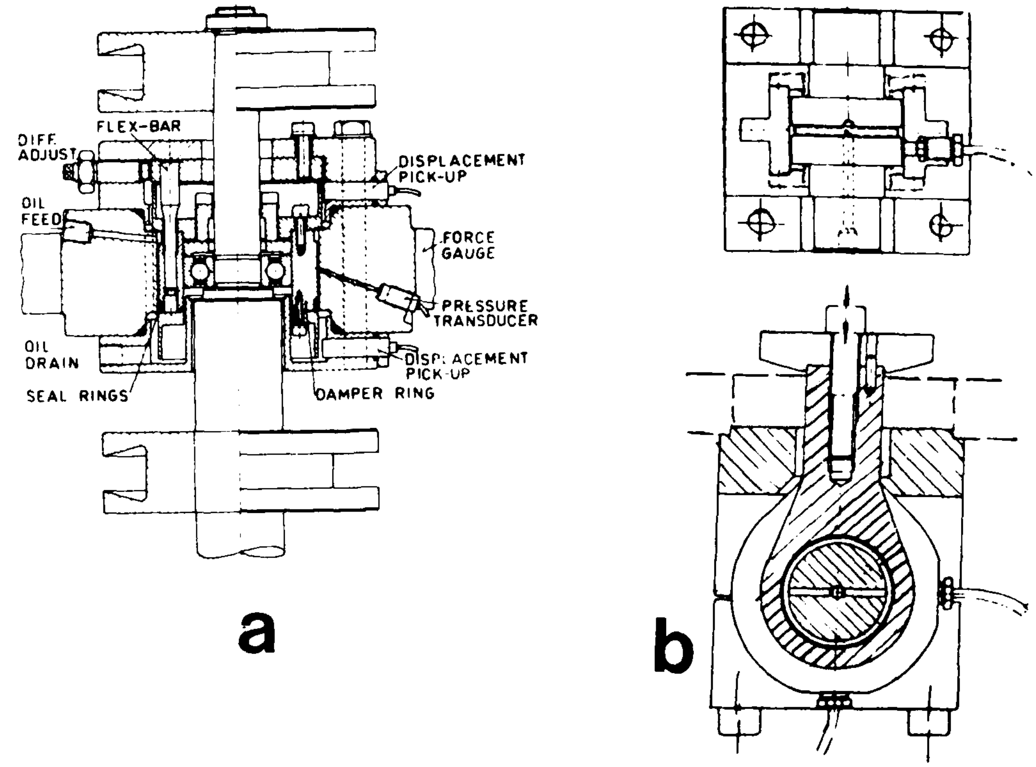

Fig.1 Cross sectional view of experimental apparatus

1150N (~250lbs force) with a practical maximum excitation frequency of [illegible] Hz. With a unidirectional force arrangement it is assumed that the damper bearing behaves isentropic and orthogonal.

Both test rigs are instrumented with probes for joint measurements of forces, displacements, phase angles and frequencies. In addition, it is possible to determine the extent of the oil film in the midplane by 1) measuring the instantaneous fluid-film pressure distribution as in the test rig Fig.1a and by 2) observing the change in the dielectric properties when using capacitance probes as in the test rig Fig.1b. The damper bearing orbits are typically displayed on an X-Y oscilloscope.

TEST RESULTS

Concentric case

The damping coefficients of a squeeze damper may be expressed as [[illegible]]:

$$C_{xx} = C_{yy} = \frac{\pi}{2}\cdot\mu\cdot R\cdot\left(\frac{L}{c}\right)^3 \quad (1)$$

where μ is the fluid viscosity, R and L the bearing radius and length and c is the radial clearance. The expression is for a 180 deg film extent and [illegible] for [illegible] and furthermore it is assumed that [illegible] < [illegible].

and that we have small circular orbits where small is <0.1. In other words, from a practical viewpoint, we may treat the damper bearings as a linear element.

The purpose of the experiments is to establish the correlation with the above equation (1) and from an operating viewpoint is the following four parameters of particular importance: 1) independence of frequency, 2) viscosity 3) radial clearance and 4) orbit size. Typical test results, from the test rig in Fig.1a, are shown in Fig.2 [3], from which it is seen that for a constant viscosity and clearance is the damping coefficient independent of the frequency until the transmitted force and hence the orbit exceeds a certain value. The damping coefficient is found to be between the 180° and 360° deg film extent. The above tests are easily performed as the damper bearing itself generates very little heat and thus is it possible maintaining a constant viscosity and clearance for test purposes.

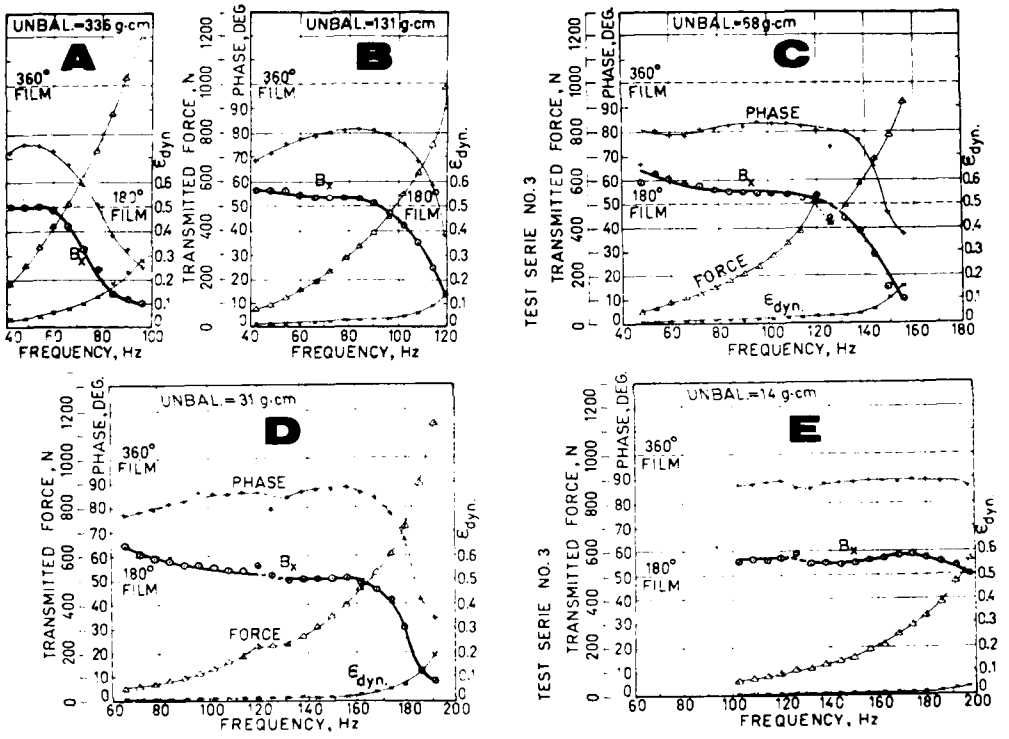

Fig. 2 Influence of force on the damping coefficient

Typical test results from the test rig in Fig.1a are shown in Fig. 2 [3] from which it is seen that varying the viscosity, Fig.2a, the radial clearance, Fig.2b and the unbalance Fig.2c gives a linear relationship with the force. Fig.3 shows the comparison with theory and shows the damping coefficient to be independent of frequency for small amplitudes, and the order of magnitude is confirmed.

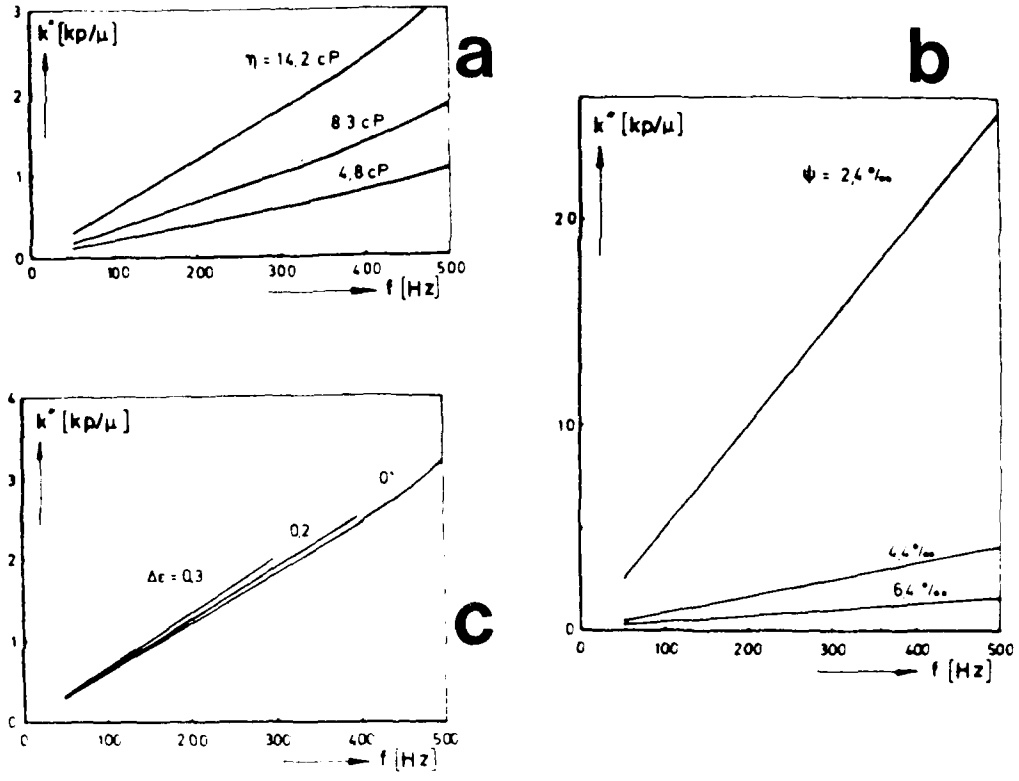

Fig. 5 Influence of viscosity, radial clearance and orbit amplitude on the damper coefficient.

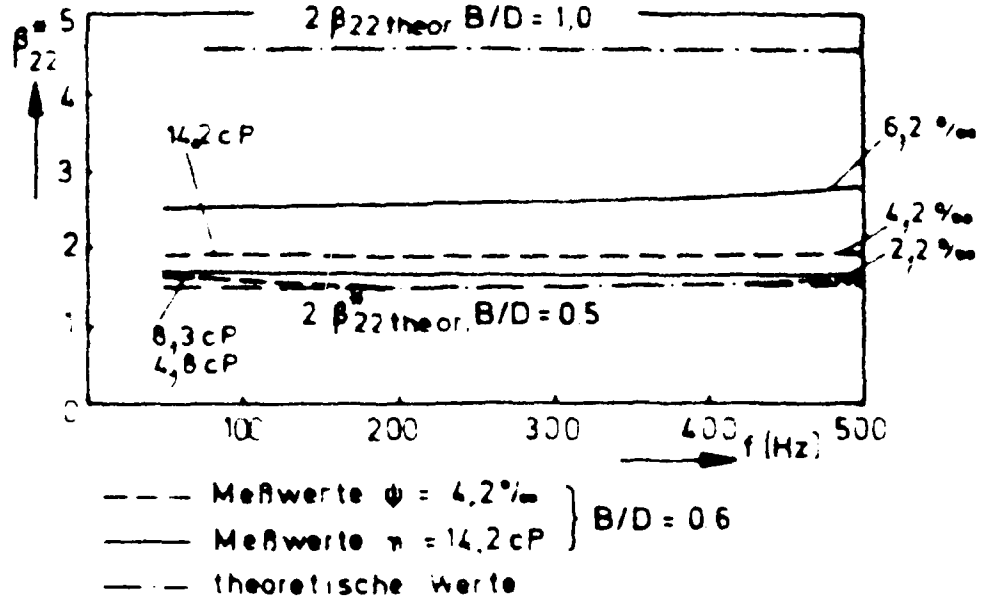

Fig. 6 Comparison with theory [3]

The experiments revealed also that two other parameters are of practical interest: 1) the end seal arrangement and 2) the oil supply pressure. The seal arrangement should ideally have no damping and stiffness properties however it was found that both O-ring type seals and piston ring type seal possessed som damping and thus influenced very much the results on the dampers which have a low absolute value. Secondly, the theory presented in [2] assumed atmospheric boundary conditions at the ends of the bearing. By having the seals, the boundary conditions are changed to at least those of the oil supply pressure and also the axial pressure profile from one of a parabolic shape to one of almost constant pressure across the length of the damper bearing. When comparing the test results with this background it then becomes easier to accept and expect higher values of the damping coefficients. Fig.5, which is obtained, from the test rig in Fig.1b, is a typical example of this situation.

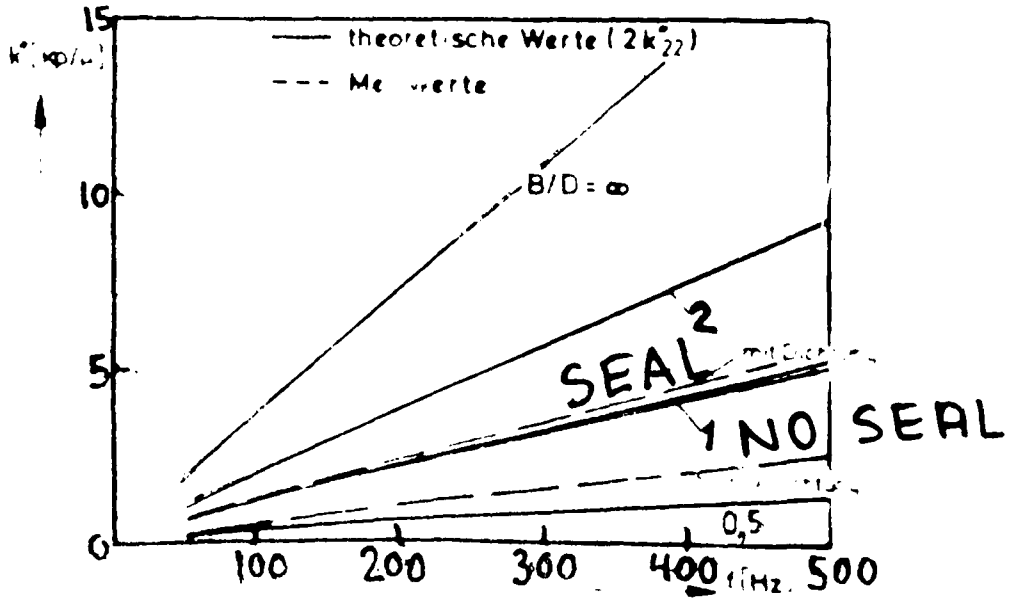

Fig.5 Influence of end seals [3]

Most damper bearings require some oil flow either for cooling purposes or as make-up oil due to leakage from the seals. The effect of flow, expressed as the oil supply pressure, is seen on Fig.6, which here relates to the test rig in Fig.1a. From Fig.6 it is seen that depending upon the orbit size, which is a function of the force/frequency combination, the damping coefficient varies a lot. This means that if the supply pressure is sufficiently high then at least a 180° deg film is maintained in the damper bearing which again means that the damper bearings behavior is predictable over a broader frequency range. What constitutes a sufficient oil supply pressure is difficult to answer and this is one of the areas where further research work needs to be done. The oil flow problems could be investigated using a test rig with a transparent bearing housing.

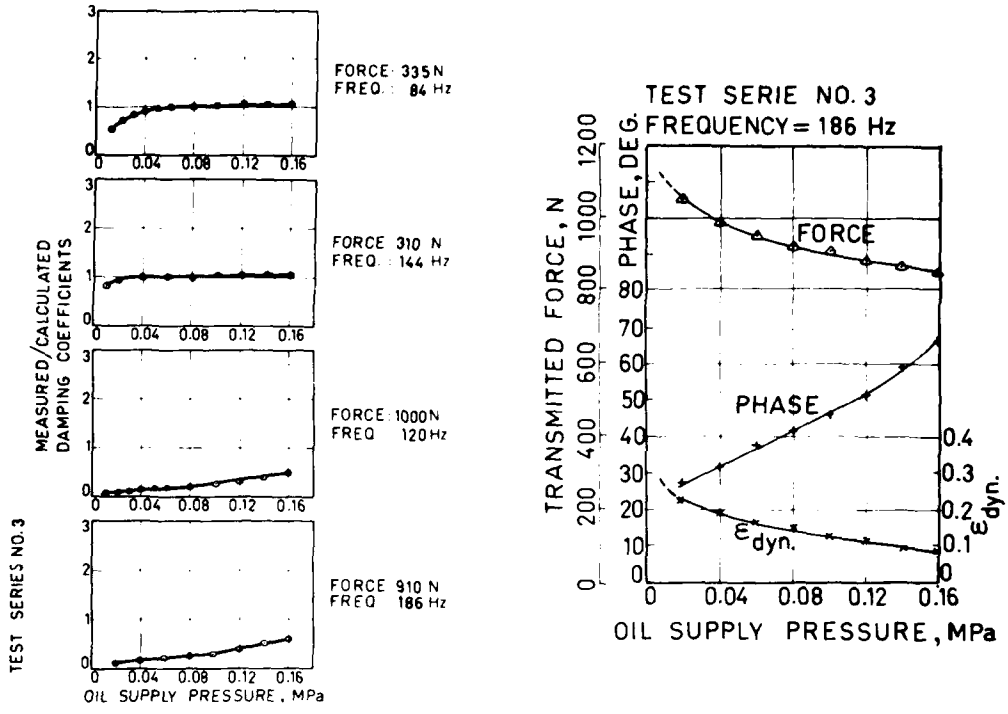

Fig.6 Influence of oil supply pressure

The expected peak oil pressure in the midplane of a damper bearing may be expressed as [2]:

$$|p|_{peak} = 1.5 \cdot \mu \cdot \frac{L^2}{C^3} \cdot \omega \cdot \Delta x \qquad (3)$$

where ω is the whirl frequency and Δx is the orbit amplitude. Fig.7 shows the measured oil pressures and comparison with the above equation (3) shows reasonable good agreement even for large whirl amplitudes.

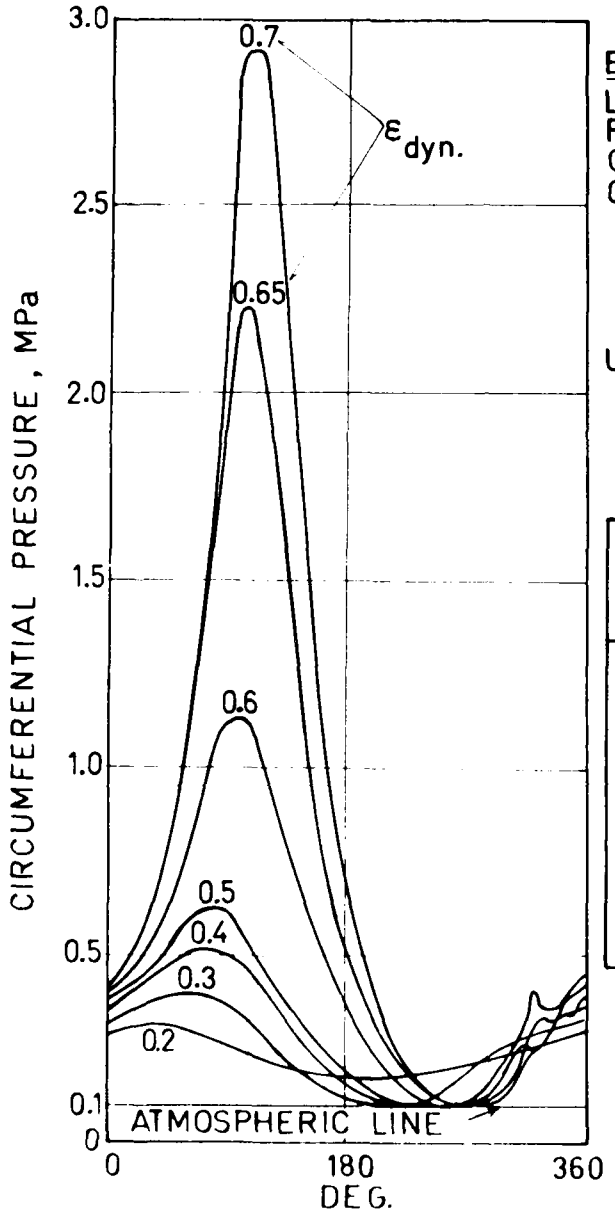

BRG. DATA:
LENGTH = 1.2 cm
RAD. CLEAR. = 132 μm
OIL VISCO. = 0.103 Pa·s
OIL SUPP. PRESS. = 0.1MPa

UNBAL. = 336 g·cm

WHIRL ORBIT $\varepsilon_{dyn.}$	FREQ. Hz	TRANS. FORCE N
0.2	48	250
0.3	61	500
0.4	69	620
0.5	73	700
0.6	84	1000
0.65	91	1250
0.7	97	1500

Fig.7 Measured midplane circumferential pressure distribution

Eccentric case

The operation of a damper bearing is typically in an eccentric position. This is caused by the built-in tolerances, operating conditions and manufacturing tolerance. Therefore, the eccentric case is more representative of the actual operation and the test results reveals also greater discrepancies when compared with the theory. Fig.8 shows typical test results obtained with the test rig in Fig.1a.

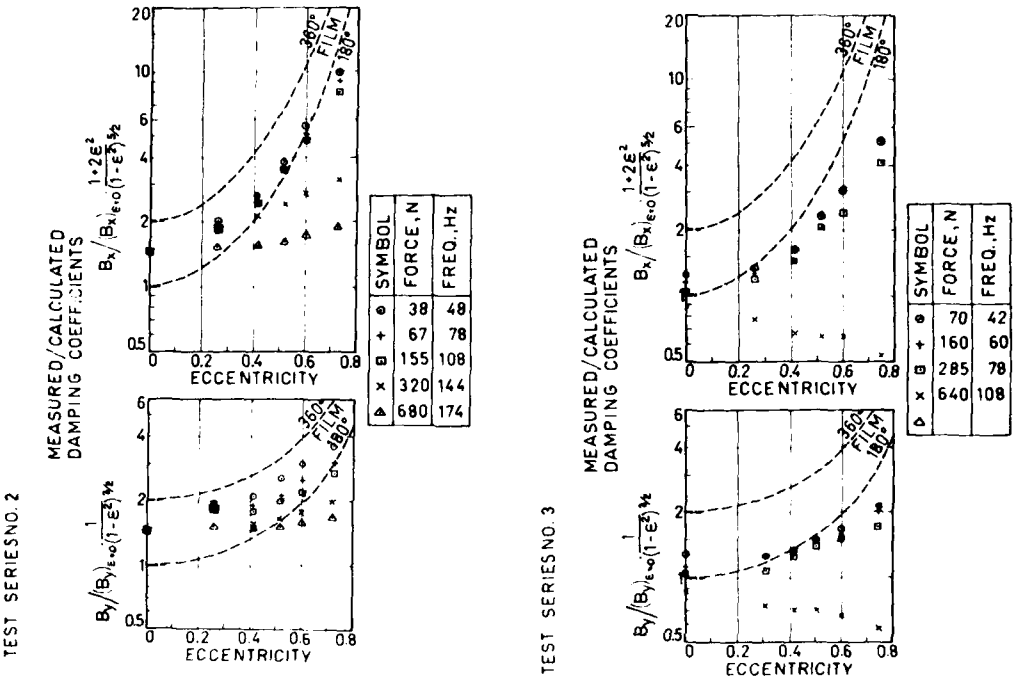

Fig.8 Influence of eccentricity ratio on the damping coefficient

At low to moderate force levels and at low eccentricities the trend is confirmed, but at higher values, which also means larger whirl amplitudes, the results clearly show that the theory does not apply anymore because small motions were asumed. At the same time any viscosity change may drastically alter the whirl orbit and this is shown on Fig.9 which shows in a extreme case, where the eccentricity is 0.75, that for a given force (unbalance here) and frequency, the whirl amplitude grows larger if the viscosity is lowered.

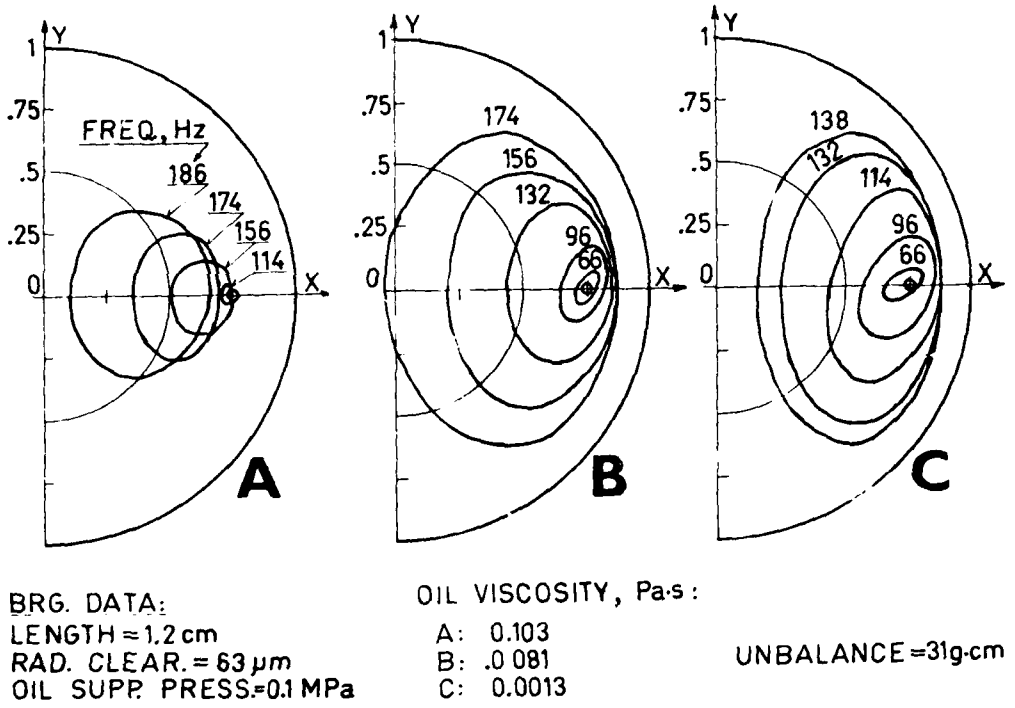

Fig.9 Influence of viscosity on the orbit amplitude

As an example in Fig.9a the whirl orbit at 114Hz is 5 per cent of the clearance and in Fig.9c is the orbit close to 40 per cent and at even higher frequencies (or lower viscosities) moves the center of the damper journal towards the center of the bearing housing and occupies almost the maximum clearance limit cycle [2]. This demonstrates that the behaviour under these conditions is nonlinear and should be treated accordingly [4].

APPLICATIONS

From a design viewpoint is it desirable to have the L/D ratio as small as possible, a typical range is 0.1 to 0.2 and the C/R should be no less than 2×10^{-3} assuming a given viscosity and supply pressure of the oil. Attention must be paid to changes in the actual operating conditions remembering that in equation (1) the damping coefficient is directly proportional to the viscosity and inversely proportional to the clearance to the 3rd power. Thus, a 15 percent viscosity change equals only a 15 per cent clearance change. The influence of the oil supply pressure on the film extent must also be considered when designing a squeeze film damper bearing and the influence may be termed as a "replenishment" factor. This area needs further investigation as do also the problems of the influence from the entrance loss from the supply groove to the much smaller oil film dimensions and the influence of operating outside the laminar flow regime.

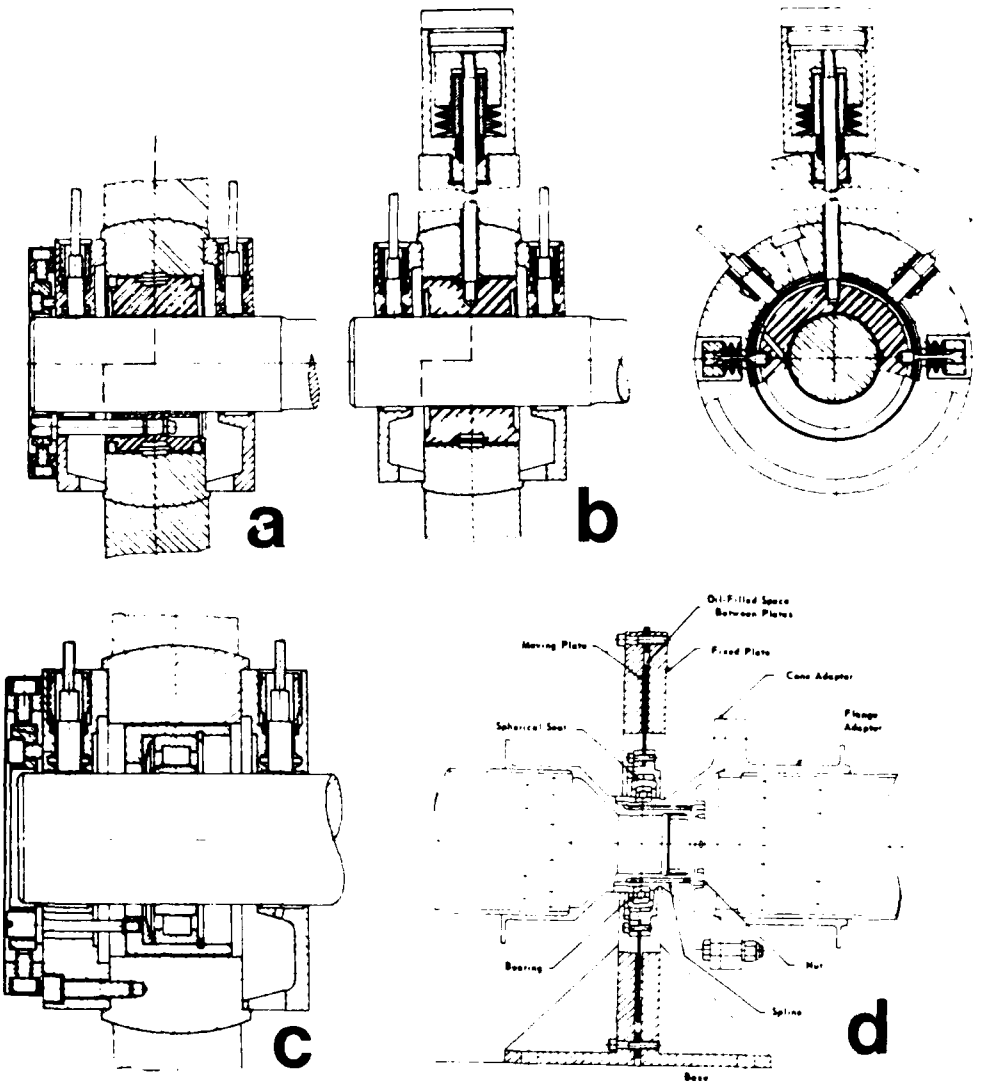

Fig.10 Cross-sectional view of squeeze film damper

Fig.10 and 11 show some typical lay-outs of damper bearing arrangements which have been and are presently being used in laboratory test rigs. Fig.10a and b shows application [3,5], in connection with fluid film bearings, where the purpose of the damper bearing is to supply external damping to a rotor which must run stable at high operating speeds, typically up to 30 - 50 Hz. Fig.10c and d [3,7] show installations where the damper bearings attenuate the critical speed vibrations of rotors supported in rolling element type bearings. In Fig.10d is the damper design of the type which employs a plate moving in a narrow gab between fixed plates.

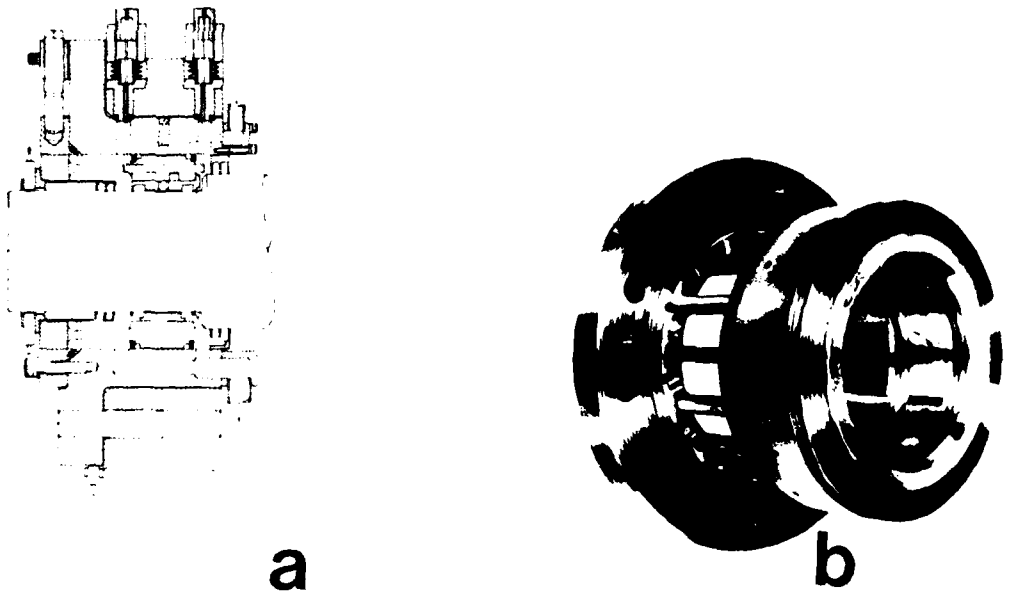

Fig.11 Arrangement of damper bearing [7]

Fig.11a shows the cross-sectional view of a bearing arrangement with damped flexible support and Fig.11b shows the flexible support structure with the journal bearing inside and the squeeze film damper surrounding it. Again, the purpose of the damper bearing is to stabilize up to 330Hz a rotor supported in fluid film bearings [7]. The damper bearing is fixed to an outboard member by 16 axial spokes which form an integral part of the arrangement. The L/D ratio is 0.23 the outside diameter is 100mm (~4in.) and C/R is 10^{-3}. Oil is fed at 0.2MPa (~30psig) to eight equally spaced holes in the midplane and the damper is sealed off at the ends by seals of the piston ring type. The damper bearing is centered in its housing by a pair of differential adjustment screws. If this is insufficient to compensate for the static deflection caused by the weight of the rotor, additional suspension is provided by a pair of externally located soft springs which pull through thin wires, an arrangement which is also used in Fig.10b.

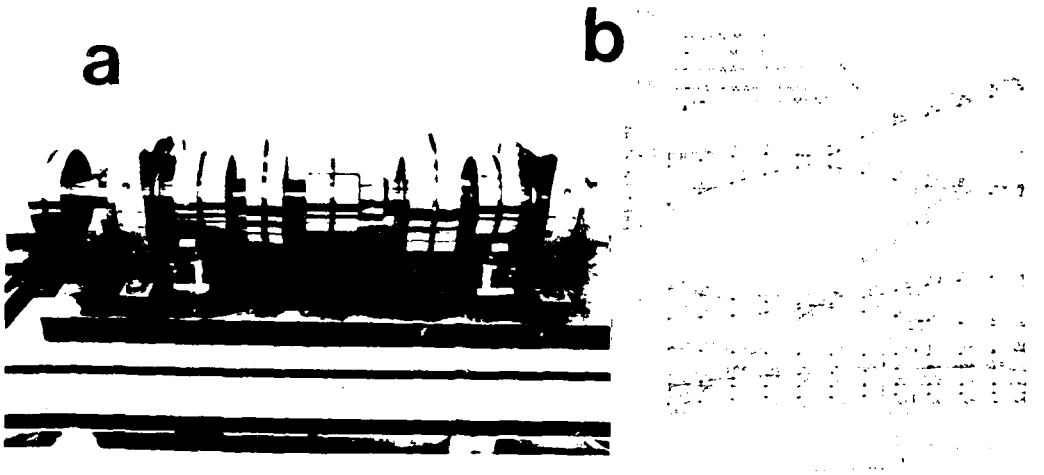

Fig.17 Rotor test stand and Lund stability map [8]

The bearing arrangements in Fig.11 are used on a test rig which is shown in Fig.17a where the rotor is 1190mm (~4feet) long, has a bearing centerline span of 950mm (~3feet), carries 6 heavy disks of which the largest is 300mm (~1 foot) in diameter and the total rotor weight is 136kg (~300 lbs). The damped natural frequencies of the system are calculated by the method of [8], and the resulting Lund map is given in Fig.17b. The rotor is seen to be stable over the entire speed range and test results [7] has confirmed this as well as the actual damping coefficients.

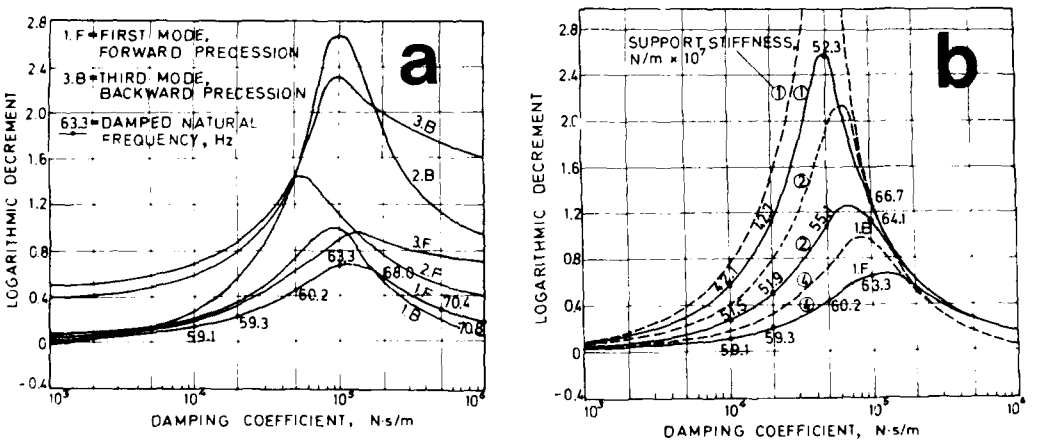

Fig.18 Optimization of squeeze film damper

However it must be emphasized, that the values of the damping coefficient shall be tuned to the particular rotor-bearing system and this is shown in Fig.13. Fig.13a shows, for a given support stiffness, how the 3 first forward and backward modes are stabilized as a function of the damping coefficient. No single optimum value is found, however a figure around 10^5 N·s/m (~500 lbs.sec/in.) seems reasonable. If the stiffness is reduced, however, the optimum for the lowest modes is shifted as shown in Fig.13b, and this means that the operating conditions (viscosity and clearance changes) must also be known with a reasonable margin since the support damping must be within a relatively narrow range.

It is obviously advantageous to make the support as soft as possible if the only consideration is the stability margin. On the other hand, in an actual application considerations of keeping the shaft centered and aligned dictate a stiff bearing support. Concerning the damping coefficient value it looks like, based on practical experience by others and the author, that a practical range for damper bearings of the present lay-out will be covered from $9x10^3$ to $5x10^5$ N·s/m (~30 to 3000 lbs sec/in.). For values lower than this the contribution of the seal arrangement and even material damping will dominate, and for larger values the damper begins to act as an additional spring on the vibrating system. In practice a compromise must be found and as shown by the above calculations and test results is it today possible to predict a damper bearings characteristics.

REFERENCES

1 Thomsen, K. K., and Andersen, H., "Experimental Investigation of a Simple Squeeze Film Damper," Journal of Engineering for Industry, Trans. ASME, Series B, Vol. [illegible], No. [illegible], May 1974, pp. 427-430.

2 Tonnesen, J., "Experimental Parametric Study of a Squeeze Film Bearing," Journal of Lubrication Technology, Trans. ASME, Series F, Vol. [illegible], No. [illegible], April 1977, pp. [illegible].

3 Gramkow, Uwe, "Bauelemente Für Die Äussere Lagerdämpfung," Dissertation, University of Karlsruhe, West Germany, 1975.

4 Han, Yeon H. T., and Tonnesen, J., "Eccentric Operation of The Squeeze-Film Damper," Journal of Lubrication Technology, Trans. ASME, Series F, Vol. [illegible], No. [illegible], July 1975, pp. 369-375.

5 Walle, Frank, "Unwuchtschwingung und Systemdämpfung Gleitgelagerte Rotoren Unter Praxisnahen Bedingungen," Dissertation, University of Karlsruhe, West Germany, 1975.

6 Prause, R. H., et al, "The Design and Evaluation of a Supercritical-Speed Helicopter Power-Transmission Shaft," Journal of Engineering for Industry, Trans. ASME, Series B, Vol. 89, No. 4, Nov. 1967, pp. 719-728.

7 Tonnesen, J., and Lund, J. W., "Some Experiments on Instability of Rotors Supported in Fluid-Film Bearings," Journal of Mechanical Design, Trans. ASME, Vol. 100, No. 1, Jan. 1978, pp. 147-155.

8 Lund, J. W., "Stability and Damped Critical Speeds of a Flexible Rotor in Fluid-Film Bearings," Journal of Engineering for Industry, Trans. ASME, Series B, Vol. [illegible], No. [illegible], May 1974, pp. [illegible].

SUPPRESSION OF SELF-EXCITED INSTABILITY USING A SQUEEZE FILM BEARING

M. A. Simpson
Research Engineer

L. E. Barrett
Research Assistant Professor

Department of Mechanical and Aerospace Engineering
School of Engineering and Applied Science
University of Virginia
Charlottesville, Virginia 22901

ABSTRACT

This work reports the design and application of a squeeze film damper for a single mass flexible rotor in journal bearings including experimental results. It is shown that the damper is extremely effective at eliminating subsynchronous vibrations due to self-excited hydrodynamic instability despite the presence of large instability mechanisms. The damper oil film was observed through a clear plastic damper housing. No uniform cavitation region was observed, although isolated bubbles appeared in the fluid at high unbalance levels.

INTRODUCTION

Advances in technology and more urgent demands on energy needs have had a direct effect on the development of high speed rotating machinery. The drive has been toward higher speeds, greater power-to-weight ratios and more flexible shafts. The combination of these factors often results in machinery which must pass through several critical speeds during regular cycles of motion. Machines which use rolling element bearings have very little damping and often experience high amplitude vibrations and large forces transmitted through the bearings and supports. The use of fluid film bearings often helps reduce the vibration amplitude and transmitted force but can also produce self-excited instability which often results in high amplitude whirl and possible interference of machine elements. Elimination of these problems is the major requirement of turbomachinery design and analysis.

One possible technique to avoid or improve any or all of the above problems which has seen considerable discussion in the literature is the use of flexible, damped bearing supports. As described in the noted references, the amount of stiffness and damping can and must be optimized

for each system considered. Improper application of support stiffness and damping can make the system worse by causing larger than normal forces to be transmitted or by generating unstable regions of operation (1, 2, 3).

One type of flexible damped bearing support which has seen increased use is the squeeze film damper bearing. A squeeze film damper bearing is basically a plain journal bearing where the journal is constrained from rotating but which can still have radial and precessional motion. The rotating shaft is then supported by a rolling element bearing or some type of fluid film bearing inside of the damper journal.

This paper describes the design and application of a squeeze film bearing for a single mass flexible rotor susceptible to self-excited whirl. Experimental results are included, and a visual study of the fluid film was made through the clear damper housing.

EXPERIMENTAL APPARATUS AND INSTRUMENTATION

The rotor system described is an experimental flexible rotor test rig susceptible to self-excited bearing whirl. The rig is essentially a single mass flexible rotor supported by two rigidly mounted journal bearings as shown in the schematic of Fig. 1. The 0.95 cm diameter shaft is 45.7 cm long with a bearing span of 41.3 cm. A central mass which weighs 8.23 N is fixed at the midspan. The total rotor weight is 11.39 N. This shaft is coupled to a zero to 10,000 RPM variable speed electric motor by a flexible coupling which includes a notch to provide the key phase pulse.

The motor end bearing is a plain porous bronze bushing supported by an O-ring in an aluminum housing. At the opposite end, an oversize plain journal bearing provides the support. The oversize bearing has 2.49 cm diameter, 0.71 cm land length and 5.6 mil radial clearance. This large bearing provides a particularly strong instability driving mechanism at an easily attainable speed. Oil is flood fed through the end of the bearing and flows freely out the inboard side into a reservoir.

Both the plain journal bearing and the squeeze film damper (to be described later) are supplied with SAE 10-weight oil which is recirculated after use. The tubing schematic for oil supply and recirculation is shown in Fig. 2. The main pump is a single-speed electric motor driven gear pump with adjustable bypass so that variable pressures may be maintained. Through the use of valves, the main pump can be used to suction the oil out of the damper and plain bearing reservoirs, or to pump oil from the main reservoir to the supply reservoirs, or to pressurize one or both of the supply reservoirs. In addition, the air compressor may be used to pressurize one supply reservoir so that each reservoir can be maintained at a different pressure. For variable static head without external pressure, the reservoirs may be moved up and down in the rack independent of the rotor rig.

The system vibration behavior is monitored with non-contacting displacement probes and the vibration data stored on FM magnetic tape for later analysis. A once-per-revolution key phase signal is also recorded for use in synchronous tracking and frequency spectrum analysis.

AD-A083 098 VIRGINIA UNIV CHARLOTTESVILLE DEPT OF MECHANICAL AND--ETC F/G 13/9
PROCEEDINGS OF THE CONFERENCE ON THE STABILITY AND DYNAMIC RESP--ETC(U)
1979 DAAG29-79-W-0061

UNCLASSIFIED ARO-16660.1-E NL

2 OF 3
AD
A083098

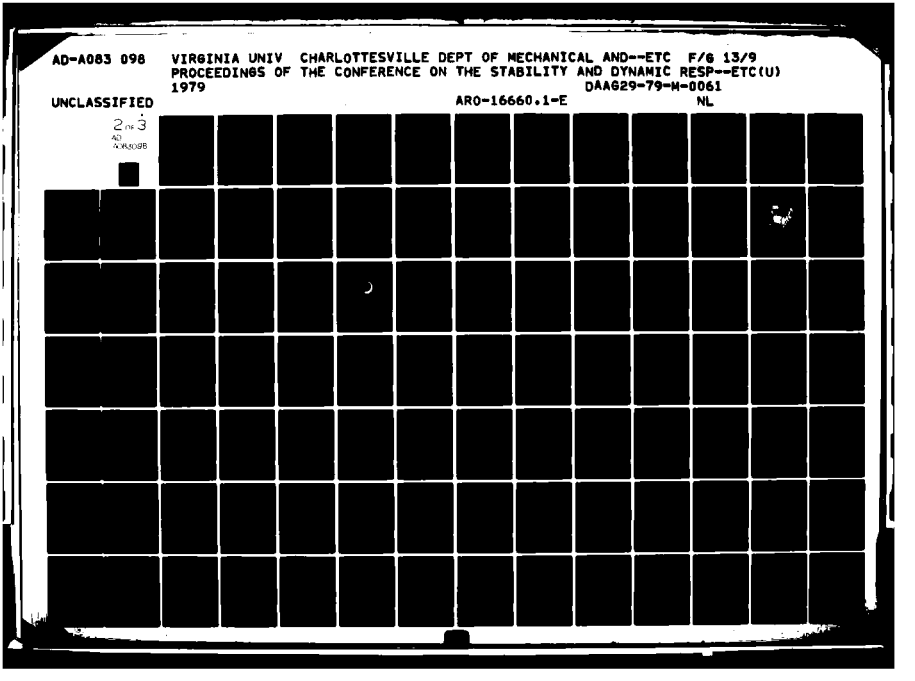

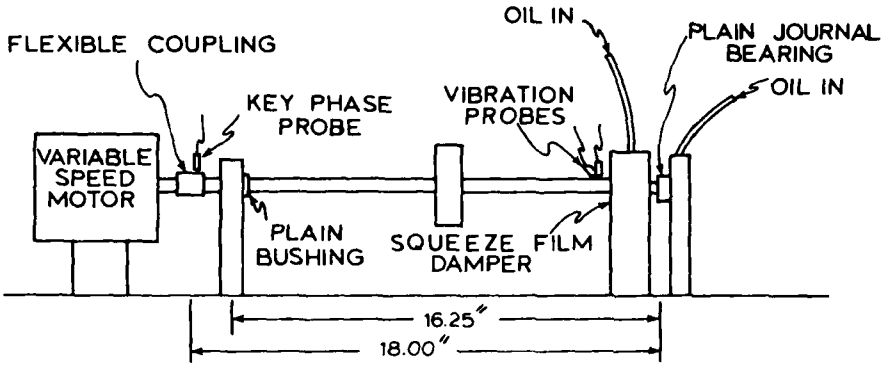

Fig. 1 Experimental Rotor Schematic Diagram

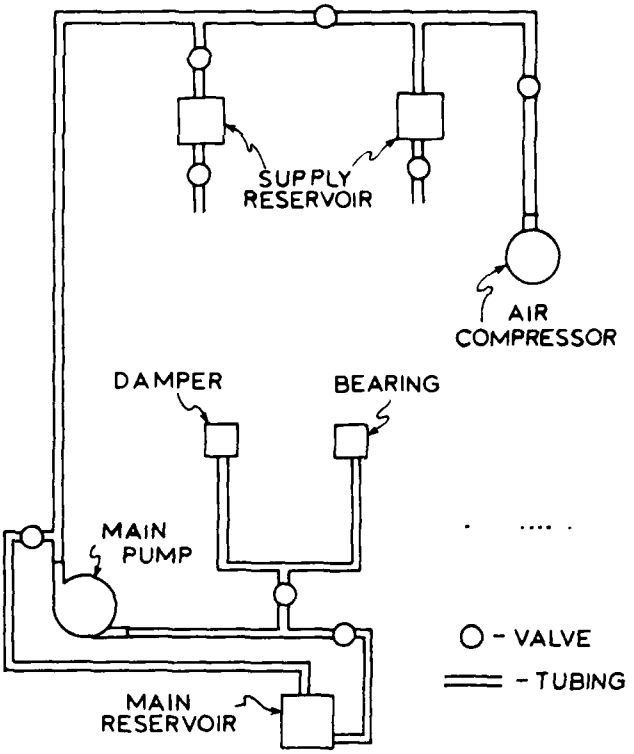

Fig. 2 Oil Supply and Return System Schematic

BASELINE EXPERIMENTAL RESULTS

The baseline response plots of amplitude and phase after final balance are shown in Figs. 3 and 4 for the horizontal and vertical directions respectively. The low speed amplitude of approximately one mil is primarily due to residual shaft bow. The rotor was balanced using vibration measurements from the horizontal probe, hence, the balance is slightly better in the horizontal than in the vertical plane. Since information about the response in whirl is desired, the amplitude plotted is the direct, unfiltered signal as opposed to the synchronous signal most often used on Bode plots. As is obvious in the figures, the synchronous tracking filter had difficulty tracking the true phase angle at some points. Amplified vibration signals did not improve the situation at all. The loss of phase angle tracking followed by the subsequent renewal of proper phase angle causes the abrupt changes in the phase angle on the response curves.

These baseline response curves indicate that the rotor operates smoothly at vibration levels of approximately one mil peak to peak up to a speed of 4000 RPM where the vibration suddenly jumps to almost twenty mils peak to peak in the horizontal plane and fifteen mils peak to peak in the vertical plane. The speed drops rapidly due to horsepower lost in the whirl action and the high vibration level locks in on the rotor natural frequency. It is possible to increase the speed beyond the 4000 RPM threshold, but this only aggravates the situation causing extremely high vibration. Even during deceleration, the locked in whirl motion exhibits strong excitation at the natural frequency of the system. This is only seen on the horizontal probe because of the orientation of the orbit ellipse at this speed. The high level whirl vibration remains locked in well below the first critical speed until approximately 1000 RPM where normal response returns.

The nature of this baseline response vibration is shown further in the "waterfall" plots of the frequency spectra of Figs. 5 and 6. Both curves were generated from horizontal probe vibration data but Fig. 5 is during acceleration and Fig. 6 is during deceleration. The major component of vibration during acceleration is the synchronous component, and there is absolutely no subsynchronous excitation below 4000 RPM. However, at 4000 RPM a very small half frequency component starts and just above 4000 RPM the one-half running speed frequency is the dominant frequency in the system. Because of the extremely large half frequency driver, it is necessary to scale the waterfall plots differently; however the scaling data is shown on each figure. As a result of scaling, the harmonics of the synchronous components are occasionally lost, but these are only of minor importance so no effort is made to retain them.

The subsynchronous vibration in Fig. 6 is referred to as half frequency vibration; however the frequency is actually about forty-four to forty-six percent of the running speed frequency. This relationship is also evident on the oscilloscope trace where the two timing marks per orbit "chase" one another around the orbit instead of standing still. As the speed decreases, the half frequency whirl tracks the running speed, but no synchronous component is seen due to the huge size of the half frequency peak. The response of the system to the critical speed during deceleration discussed earlier is also seen on the frequency spectrum by the synchronous peak

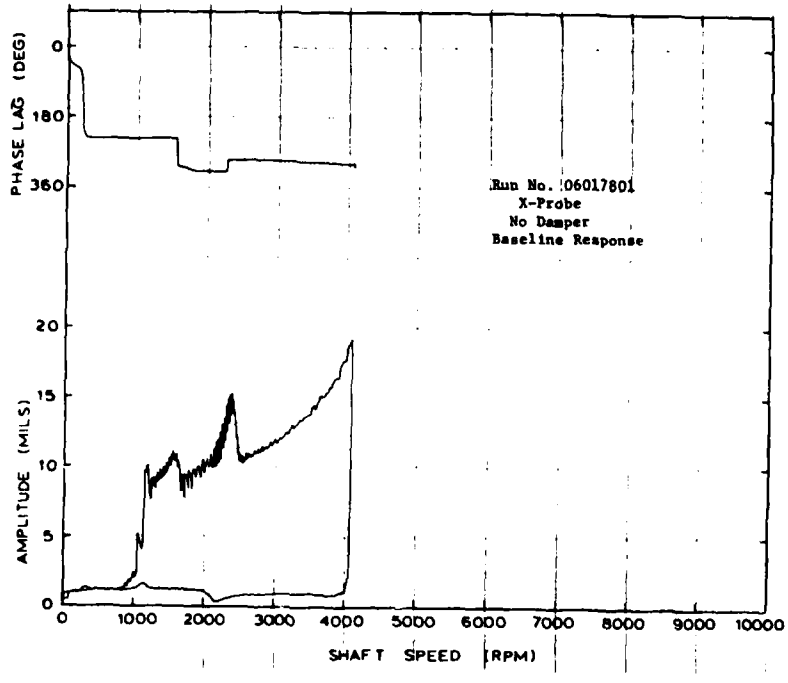
PHASE LAG (DEG)
0
180
360
Run No. 06017801
X-Probe
No Damper
Baseline Response
20
15
10
5
0
AMPLITUDE (MILS)
0
1000
2000
3000
4000
5000
6000
7000
8000
9000
10000
SHAFT SPEED (RPM)

Fig. 3

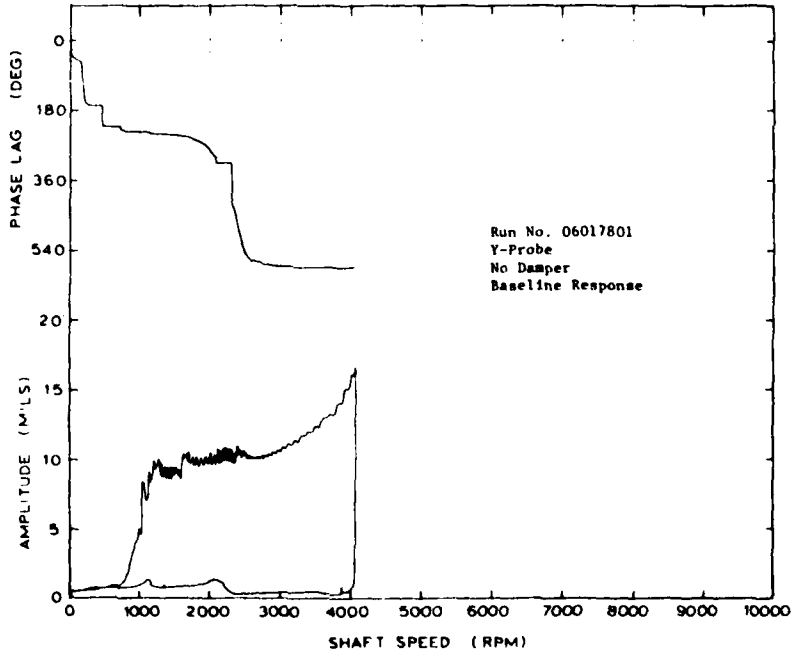
PHASE LAG (DEG)
0
180
360
540
Run No. 06017801
Y-Probe
No Damper
Baseline Response
20
15
10
5
0
AMPLITUDE (MILS)
0
1000
2000
3000
4000
5000
6000
7000
8000
9000
10000
SHAFT SPEED (RPM)

Fig. 4

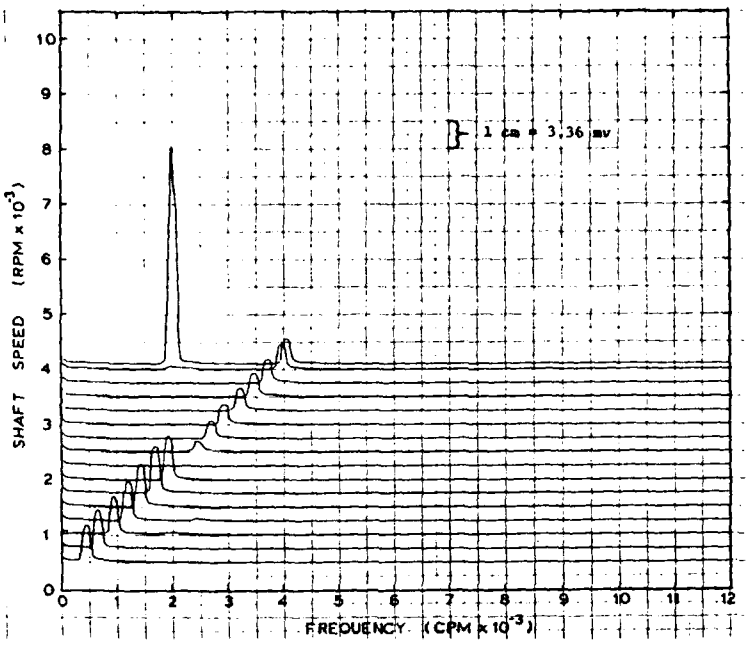

Fig. 5 Run No. 06017801, X-Probe, Acceleration, No Damper

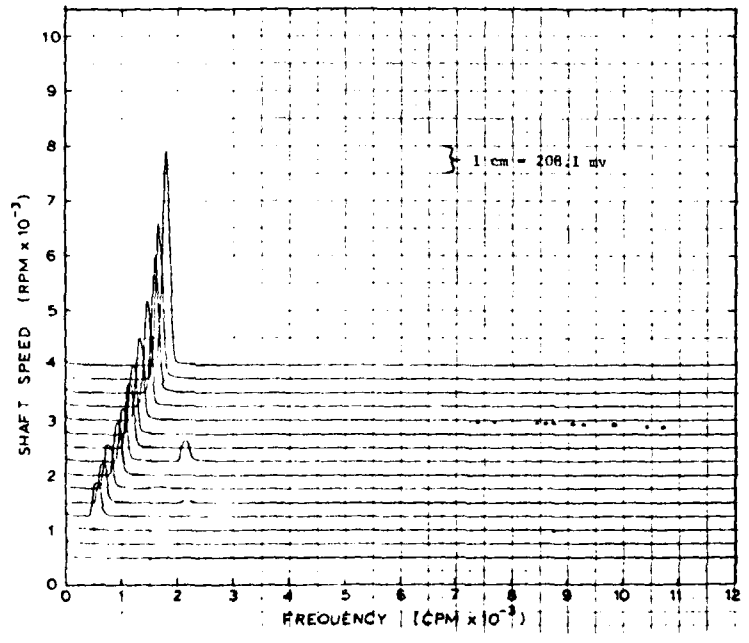

Fig. 6 Run No. 06017801, X-Probe, Deceleration, No Damper

occuring at 2250 RPM. Below 1000 RPM no response is seen because the half frequency motion has subsided and the synchronous trace is clipped due to scaling.

It has been demonstrated in the literature than an increase in bearing lubricant ambient pressure will increase the bearing attitude angle and decrease the instability threshold (4). Both of these phenomena are demonstrated in Figs. 7-10.

Figure 7 shows the change in attitude angle of the journal orbit center as the ambient supply pressure is increased with the rotor running at a constant speed of 1600 RPM. There are no probes in the journal bearing proper so these orbit locations were determined with probes looking at shaft motion inboard of the plain journal bearing. The idea was not to get exact values for eccentricity, but rather to get general behavior of the attitude angle and eccentricity for various operating conditions. The data was taken from photographs of the oscilloscope trace of the orbit as seen by the DC-coupled vertical and horizontal probe vibration signals. As expected from theory, the attitude angle increases toward 90° as the ambient supply pressure is increased from 1 to 15 psig.

The corresponding decrease in rotor instability threshold speed is shown in Figs. 8-10. The response curve with the bearing supply pressure at 5 psig is shown in Fig. 8 for the horizontal probe only. The baseline response is not much different from the unpressurized case except that the instability threshold speed has dropped to 3800 RPM. External bearing pressurization of 10 psig produces similar results except that the behavior at the critical speed has changed and the stability threshold has dropped to 2875 RPM, as shown in Fig. 9. Also, the subsynchronous whirl continues to a speed of 500 RPM instead of 1000 RPM, as before. When the bearing external pressure is increased to 15 psig, as in Fig. 10, the instability threshold drops to 2300 RPM and the whirl stays to below 500 RPM. In all of the pressurized runs, the amplitude of vibration during whirl is less than the corresponding unpressurized case.

Figures 11 and 12 show the "waterfall" frequency spectra associated with the 15 psig run. There are no subsynchronous components during acceleration to 2300 RPM, at which point a major half frequency component tracks downward at approximately 45% of the running speed, as before. Similar results were obtained for the 5 and 10 psig test runs, as well.

SYSTEM SIMULATION AND DAMPER DESIGN

Computer simulation of the rotor-bearing system is beneficial for predicting response to changes in the system configuration before hardware is actually changed. Two stability analyses were performed with this work to study the stability of the system before and after the application of the squeeze film damper. The first set of stability runs were made to predict the behavior of the rotor-bearing system without the damper to gain confidence in the system model. The second stability analysis was made to predict the effectiveness of the squeeze film damper in system stabilization.

A fourteen-mass station lumped-mass model with two bearing stations was

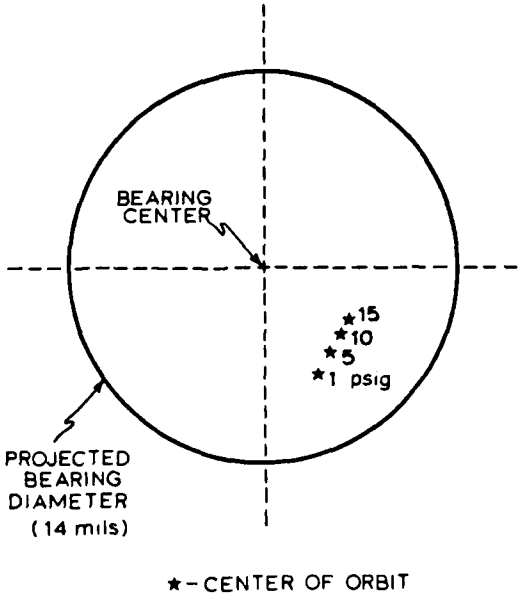

Fig. 7 Pressure Dependent Orbit Locus;
No Damper

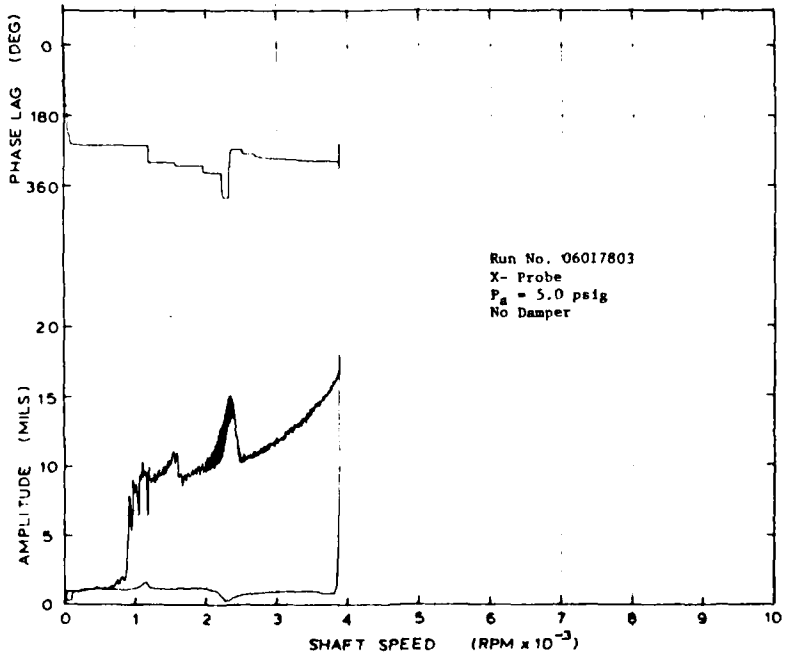

Fig. 8

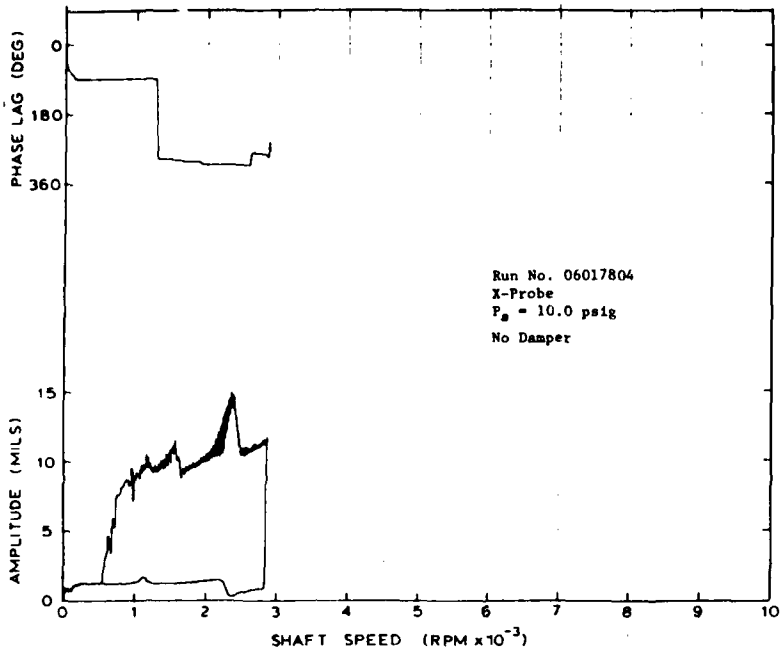
PHASE LAG (DEG)
0
180
360
Run No. 06017804
X-Probe
P_a = 10.0 psig
No Damper
AMPLITUDE (MILS)
15
10
5
0
0 1 2 3 4 5 6 7 8 9 10
SHAFT SPEED (RPM x 10^{-3})

Fig. 9

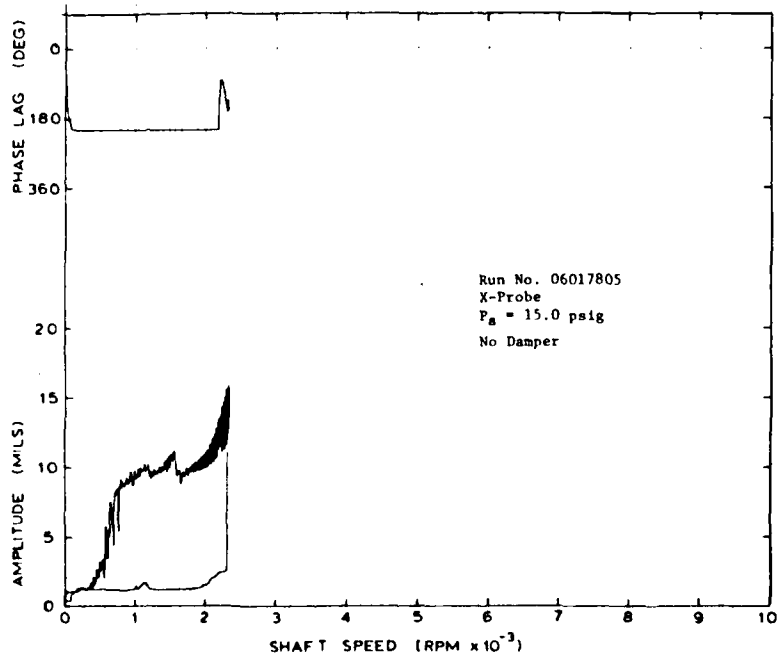
PHASE LAG (DEG)
0
180
360
Run No. 06017805
X-Probe
P_a = 15.0 psig
No Damper
20
AMPLITUDE (MILS)
15
10
5
0
0 1 2 3 4 5 6 7 8 9 10
SHAFT SPEED (RPM x 10^{-3})

Fig. 10

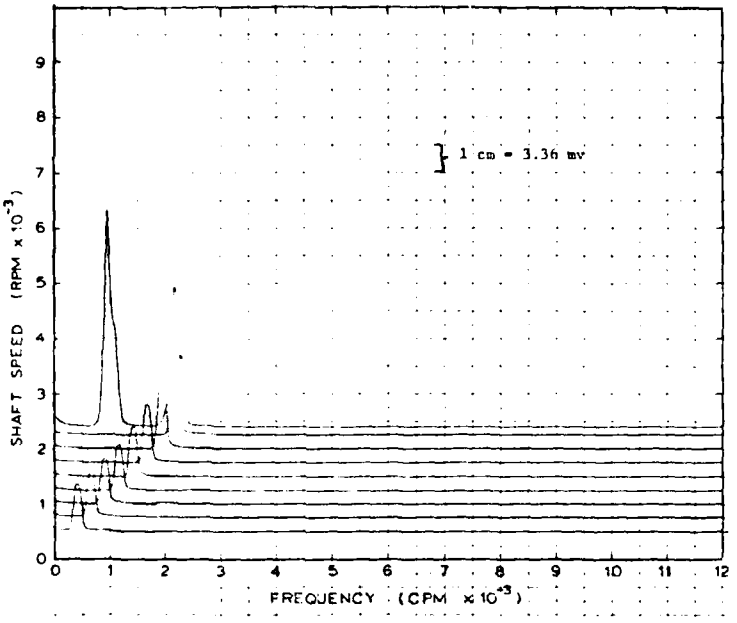

Fig. 11 Run No. 06017805, X-Probe, P_a = 15.0 psig, Acceleration, No Damper

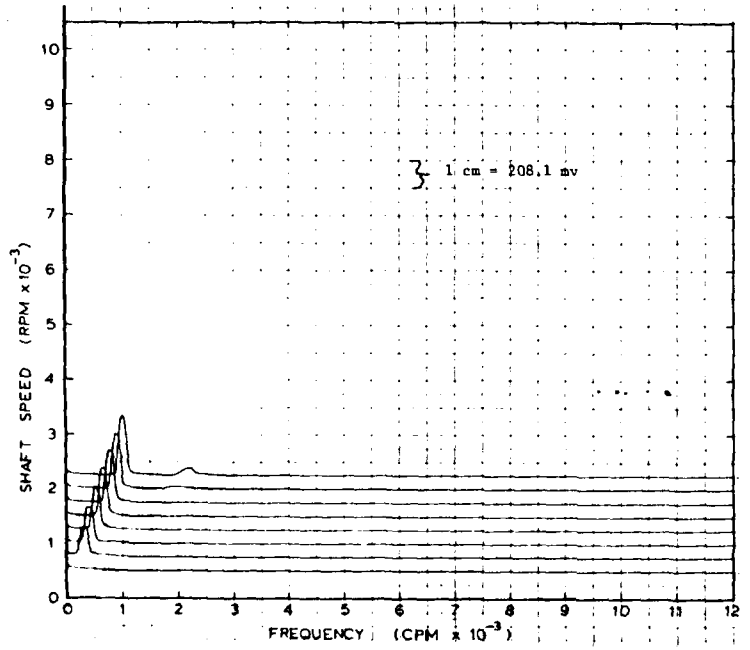

Fig. 12 Run No. 06017805, X-Probe, P_a = 15.0 psig, Deceleration, No Damper

used as the computer model. Since the length to diameter ratio of the plain journal bearing is 0.29, the short bearing approximation is valid, so short bearing coefficients may be used. The bearing coefficients for the plain bushing were determined by previous experimental work, as reported by Barrett and Li (5).

Figure 13 is a plot of damped natural frequency versus shaft speed for the first three modes of the system without the squeeze film damper. The log decrement values shown indicate how well the vibration is damped. A negative log decrement shows that the growth factor is positive and hence the system is unstable. Obviously this system is unstable above 4000 RPM because mode C, an even forward mode, develops a positive growth factor at this speed with a damped natural frequency of 2200 RPM. This frequency is also the first damped natural frequency of the system, as indicated by the intersection of the synchronous excitation line with mode C at 2200 RPM. This value is in good agreement with the experimental results of Figs. 3-6, which indicate a first natural frequency at about 2150 RPM. Figure 13 also predicts system damped natural frequencies at 2600 RPM and 4000 RPM, but these are not seen experimentally. The 2600 RPM mode is a backward mode and is not excited, and the 4000 RPM mode is well damped.

To eliminate the instability seen experimentally and predicted above, a squeeze film damper was designed for the system. Some of the constraints on the damper design were: no end seals, no retainer springs, central supply groove, clear housing to observe fluid film behavior. The damper was designed using short bearing theory and optimum bearing and support damping theory presented in the literature (6,7). In addition to the previous constraints, it was assumed that the damper would exhibit centered circular synchronous precession and that the fluid film would cavitate.

The final design of the damper selected is shown in Fig. 14 which shows the damper housing and Fig. 15 which shows the damper journal. The damper assembly was installed just inboard of the plain journal bearing at the non-drive end of the shaft. Due to the difference in the clearances of the damper (8 mils radial) and the bearing (5.6 mils radial), the shaft acted as a retainer spring to suspend the damper journal in the housing. Two lands, each of length 0.98 cm, form the inside surface of the damper housing. Oil is supplied to the central groove and from here it flows between the damper surfaces. The two outer grooves are used to carry oil away. Lucite was selected as the housing material to enable observation of the fluid film for cavitation effects. The journal of the damper is a smooth aluminum cylinder connected to the shaft by two shielded precision ball bearings. A stainless steel pin protrudes radially from one end of the journal and fits into the corresponding notch in the housing. This pin is used to prevent rotation of the journal. The damper journal and ball bearings weigh 1.07 N as a unit.

The addition of the damper to the system stability analysis produced the results shown in Fig. 16, which plots damped natural frequency versus shaft speed for the first three modes predicted. In this case, all of the modes are well damped and no instability is indicated. According to this analysis, the first damped frequency of the system should occur at approximately 3200 RPM.

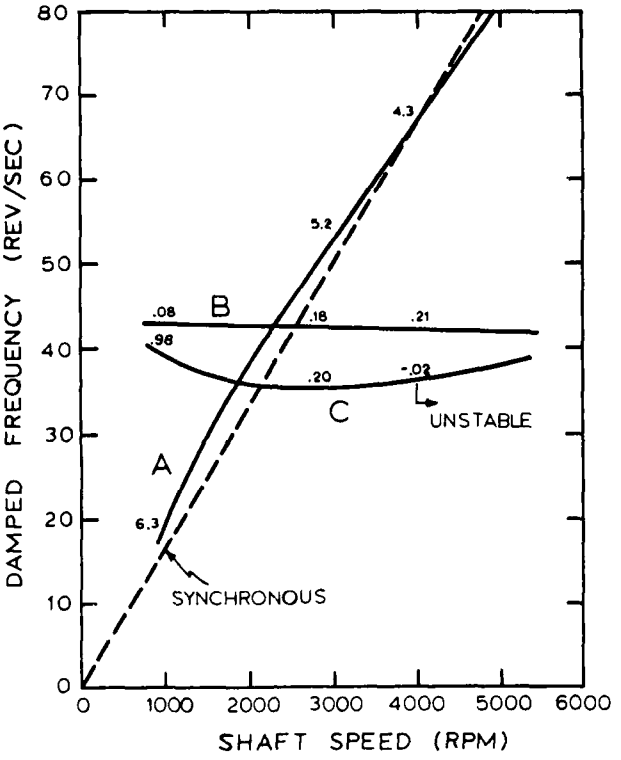

Fig. 13 Damped Frequency Versus Shaft Speed for the First Three Modes of the System with No Damper

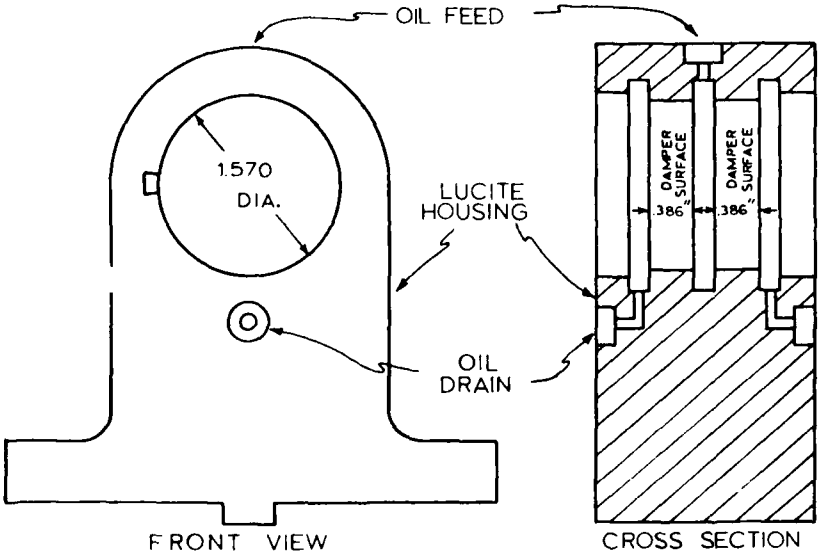

Fig. 14 Damper Housing Details

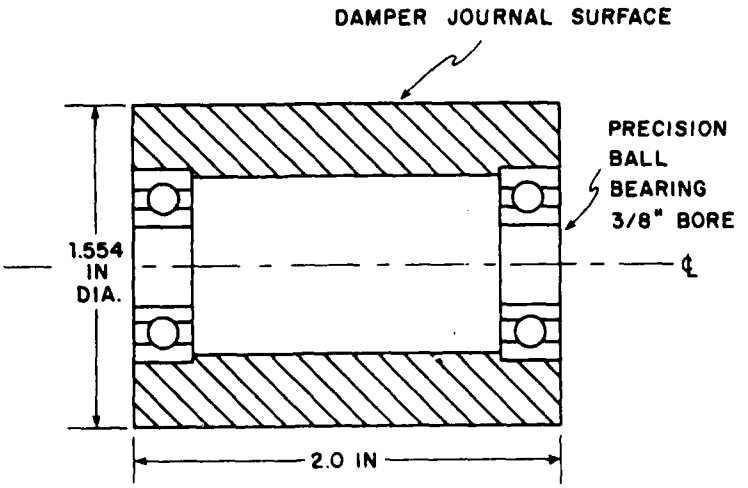

Fig. 15 Aluminum Damper Journal Cross Section

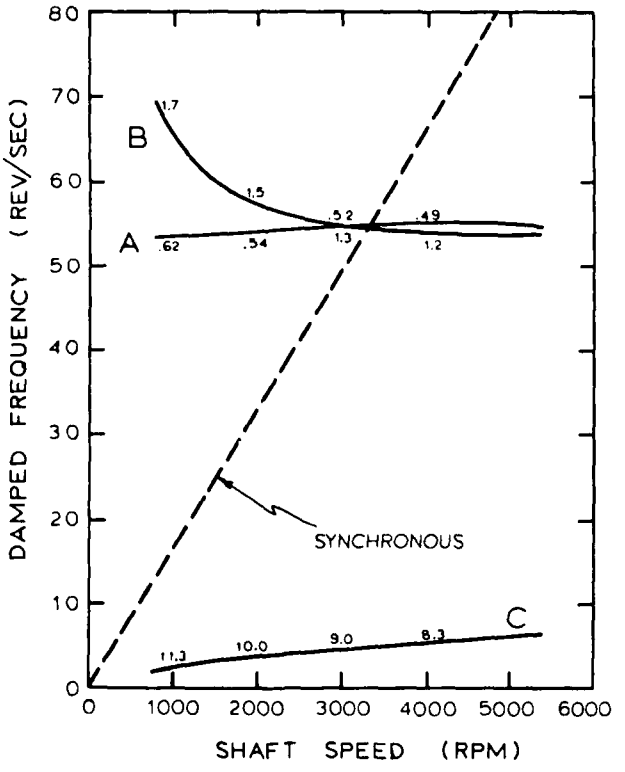

Fig. 16 Damped Frequency Versus Shaft Speed for the First Three Modes of the System with Damper Included

The above results indicate that the damper hardware described previously should effectively stabilize the system throughout the operating speed range.

EXPERIMENTAL RESULTS WITH DAMPER

The baseline response plots of the balanced rotor with squeeze film damper are shown in Figs. 17 and 18. The most obvious difference from the no-damper case is the lack of any instability throughout the entire operating range. The response curves for the horizontal and vertical planes are nearly identical. The system displays similar response to the no-damper case below the critical speed but has very low high speed response. The critical speed has shifted to 2800 RPM with a peak response of 1.25 mils. A dip in the response toward zero amplitude no longer exists since both the X and Y probes show small peaks at the critical. The effect of the damper is further seen in the frequency diagram of Fig. 19, which was taken from the horizontal probe vibration data. Only the acceleration run is shown in both the Bode-plots and the frequency spectra because the acceleration and deceleration curves are nearly identical with the addition of the damper. The scale factor in this figure is the same as that of the original baseline response with no damper. The peak amplitude at the critical is slightly larger in this case, but the synchronous component is the only contribution to the excitation as shown by the single 45° trace on the cascade plot. There are no subsynchronous components, whatsoever. Some higher harmonics are lost due to the scale factor applied. As far as being effective in eliminating instability, this damper has performed extremely well.

Increasing the ambient supply pressure in the journal bearing has very little effect on the system response when the damper is included, as shown in Figs. 20-22. These figures show response curves for values of ambient pressure ranging from 1 psig to 15 psig. The peak response speed shifts approximately 100 RPM over the range of pressures, but the amplitudes of vibration change only slightly. Similarly, the phase angle is nearly constant over all of the runs.

Figure 23 shows the frequency plot with the journal bearing pressurized to 15 psig. This is almost identical to Fig. 19, which is the corresponding plot for the zero external pressure case. As before, there are no subsynchronous components visible at all, and the synchronous harmonics are lost due to scaling. Only the acceleration data is shown since deceleration is identical.

From the above results, it is obvious that the squeeze film damper bearing designed and installed as described previously is extremely effective at stabilizing an otherwise unstable system. Even at high bearing supply pressures where the destabilizing mechanism is very large, no hint of instability is seen.

CAVITATION EFFECTS

As mentioned earlier, one of the damper design assumptions was that the fluid film would cavitate. This is one aspect of squeeze film dampers

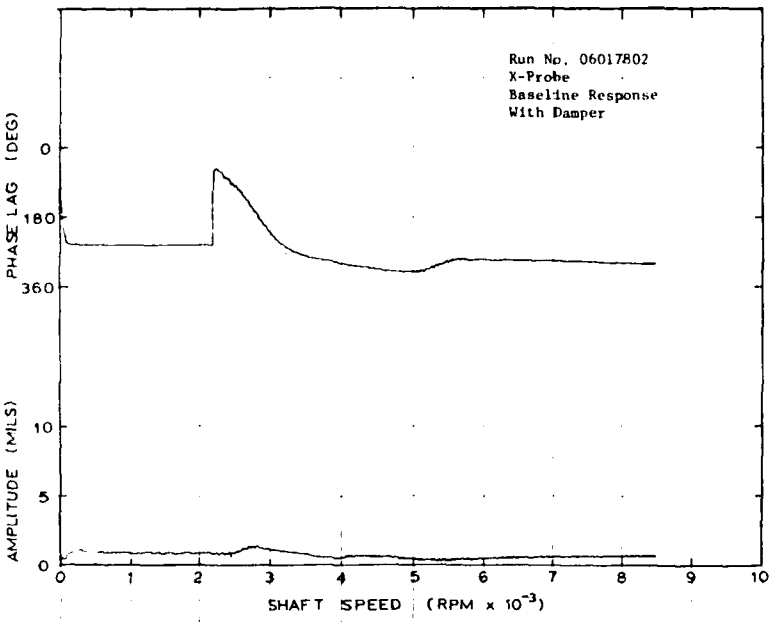
Run No. 06017802
X-Probe
Baseline Response
With Damper
PHASE LAG (DEG)
0
180
360
AMPLITUDE (MILS)
10
5
0
0 1 2 3 4 5 6 7 8 9 10
SHAFT SPEED (RPM x 10^{-3})

Fig. 17

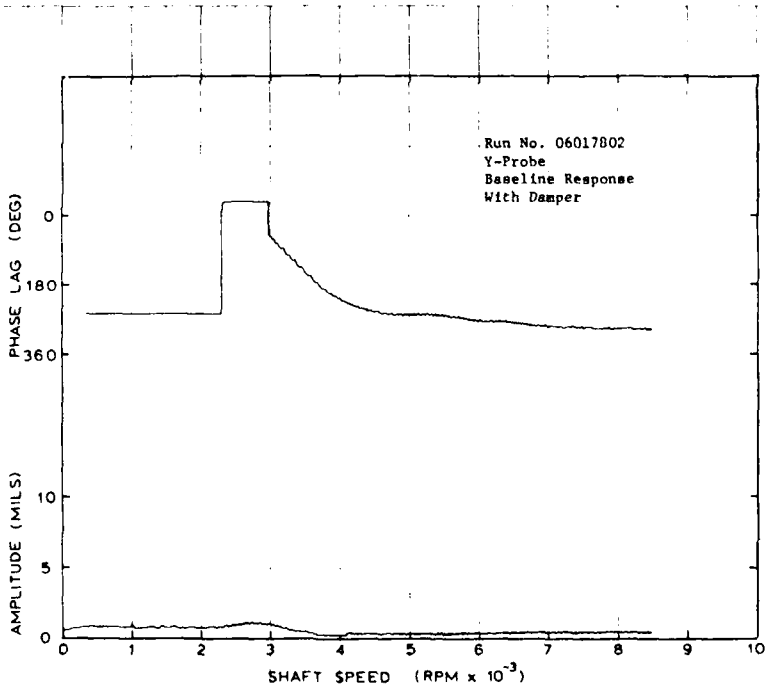
Run No. 06017802
Y-Probe
Baseline Response
With Damper
PHASE LAG (DEG)
0
180
360
AMPLITUDE (MILS)
10
5
0
0 1 2 3 4 5 6 7 8 9 10
SHAFT SPEED (RPM x 10^{-3})

Fig. 18

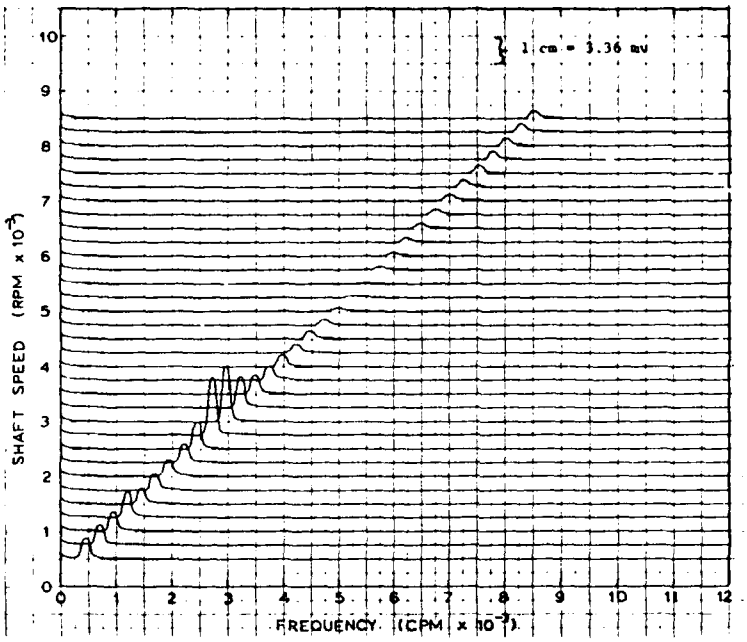

Fig. 19 Run No. 06017802, X-Probe, Acceleration, with Damper

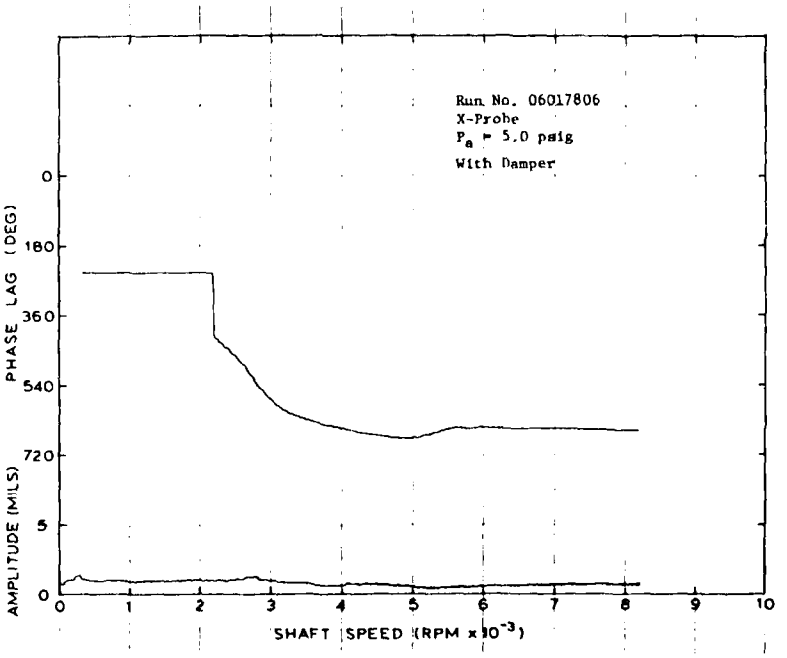

Fig. 20

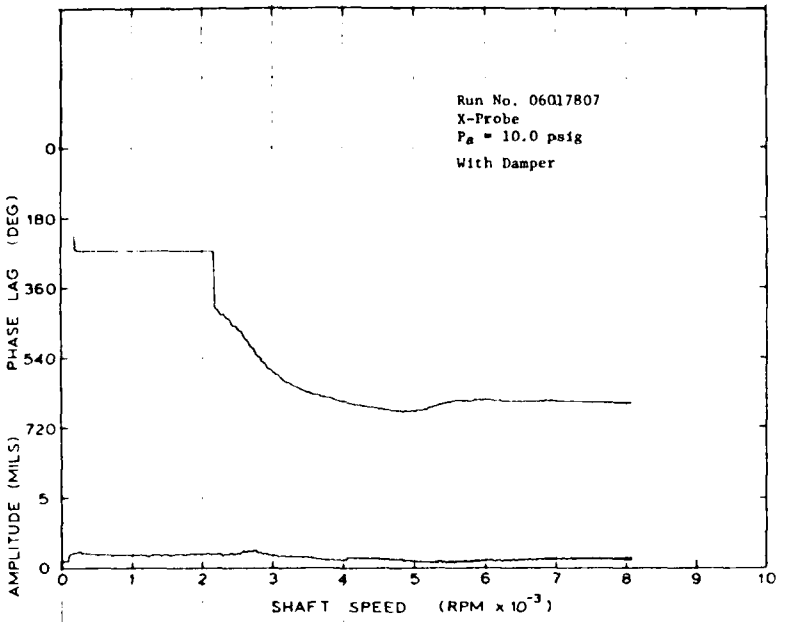
Run No. 06017807
X-Probe
P_a = 10.0 psig
With Damper
PHASE LAG (DEG)
0
180
360
540
720
AMPLITUDE (MILS)
5
0
0 1 2 3 4 5 6 7 8 9 10
SHAFT SPEED (RPM x 10^{-3})

Fig. 21

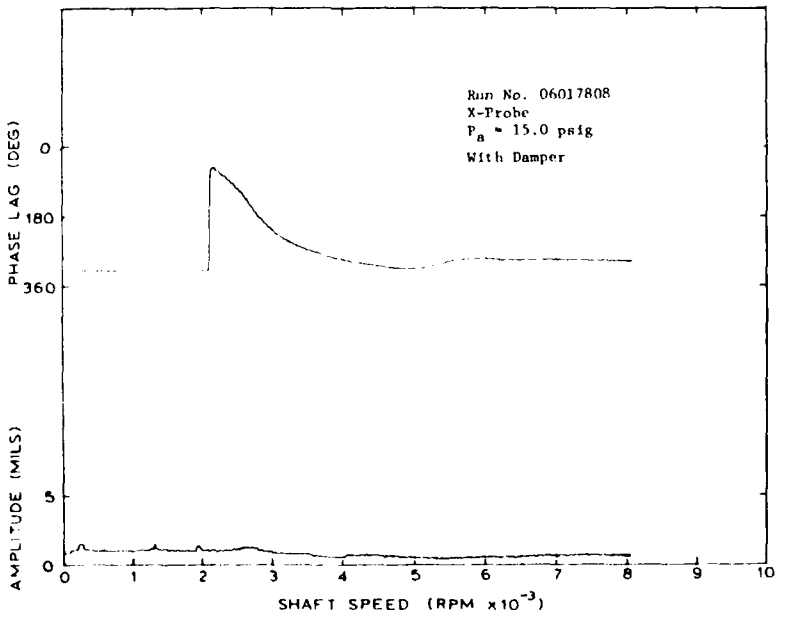
Run No. 06017808
X-Probe
P_a = 15.0 psig
With Damper
PHASE LAG (DEG)
0
180
360
AMPLITUDE (MILS)
5
0
0 1 2 3 4 5 6 7 8 9 10
SHAFT SPEED (RPM x 10^{-3})

Fig. 22

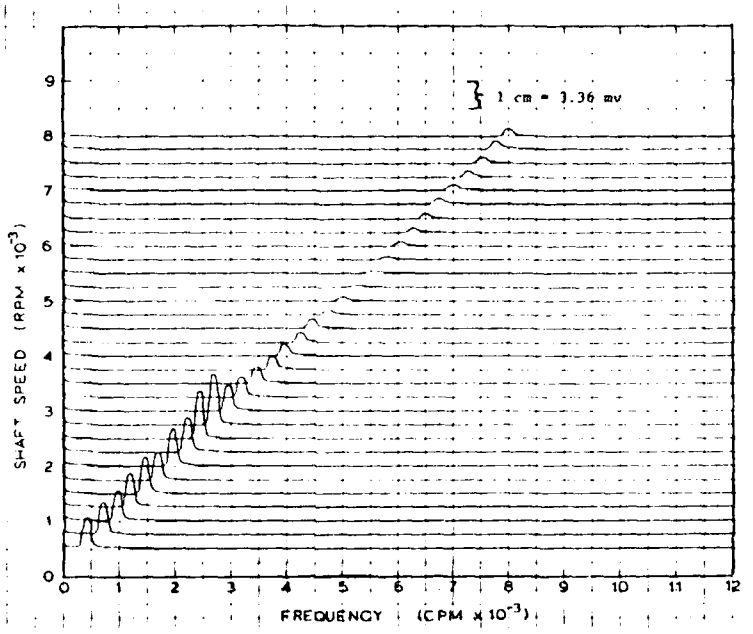

Fig. 23 Run No. 06017808, X-Probe, P_a = 15.0 psig, Deceleration, with Damper

that is often discussed but not well understood. The damper used in this study was made from lucite so that cavitation could be visually studied under various operating conditions. Several runs were made with added unbalances to load up the damper journal orbit radius.

In the studies made here, virtually no cavitation was seen under any operating conditions. This includes high unbalance loads where large circular precessions occurred. At the highest levels of unbalance (0.084 oz-in) a few small isolated bubbles formed in the oil but the pattern was random, and the bubbles quickly traveled with the oil out of the damper. This is similar to results reported by White (8), but the bubbles in this case were sporadic, not ordered as White observed. Using short bearing theory and assuming circular synchronous precession, the peak damper pressure for this case with 0.0874 oz-in unbalance is approximately 34 psig.

In case the bubbles rotated with the precession of the damper journal too fast to distinguish, a stroboscope was used to observe the film. Even when the strobe was triggered synchronous with the rotor running speed, no cavitation region was observed. It was noted, however, that the damper journal was precessing synchronously as assumed, and the orbit shown on the scope was circular. Therefore, the assumption of circular synchronous precession for dampers under high unbalance load is valid. However, the assumption of a cavitated film may not necessarily be valid.

CONCLUSIONS

The design of a squeeze film damper for a single mass flexible rotor was demonstrated and presented with experimental results. The study of the damper was not a parametric investigation under constrained operating conditions but instead showed the design of one fixed geometry damper for a specific application. The damper was extremely effective at stabilizing an unstable rotor-bearing system even when very large instability mechanisms were present. The instability driver was provided through a large clearance plain journal bearing with pressurized oil supply which caused large amplitude half frequency whirl motion which locked onto shaft operating speed.

No cavitation region was seen in the damper under any operating conditions. Small randomly spaced bubbles were seen under high unbalance conditions, but no cavitation region formed. Under large unbalance loads the damper exhibited circular synchronous precession as determined by oscilloscope and stroboscope.

Although squeeze film dampers are used frequently in industrial and commercial applications, their behavior is still not completely understood. Work is especially needed in the area of predicting the fluid film behavior more exactly. This would include predicting pressure profiles and peak pressures and comparing with experimental work, and also investigating and describing further the effect and behavior of damper cavitation.

ACKNOWLEDGEMENT

This research was supported by the U. S. Army Research Office, Grant No. DAG-29-77-C-0009,Dr. Edward A. Saibel, Project Monitor.

BIBLIOGRAPHY

1. Gunter, E. J., "Influence of Flexibly Mounted Rolling Element Bearings on Rotor Response: Part 1 - Linear Analysis," ASME Journal of Engineering for Industry, 1974.

2. Kirk, R. G. and Gunter, E. J., "Stability and Transient Motion of a Plain Journal Mounted in Flexible Damped Supports," ASME Journal of Engineering for Industry, 1976.

3. Lund, J. W., "The Stability of an Elastic Rotor in Journal Bearings with Flexible Damped Supports," ASME Journal of Applied Mechanics, December, 1965.

4. Barrett, L. E., Gunter, E. J., and Allaire, P. E., "Stability and Dynamics Response of Pressurized Journal Bearings with Nuclear Water Pump Application," Annals of Nuclear Energy, 1977.

5. Barrett, L. E., Li, D. F., and Gunter, E. J., "Second Mode Balancing without Phase Measurement Using the Three Point Method," from Selected Papers on Field Balancing of Rotating Machinery.

6. Barrett, L. E., Gunter, E. J., and Allaire, P. E., "Determination of Optimum Bearing Damping for Symmetric Rotor Bearing Systems," University of Virginia, RLES Report No.ME-543-130-76, 1976.

7. Black, H. F., "The Stabilizing Capacity of Bearings for Flexible Rotors with Hysteresis," ASME Journal of Engineering for Industry, 1975.

EFFECTS OF FLUID COMPRESSIBILITY ON VISCOUS DAMPER CHARACTERISTICS

by

D. H. Hibner*
P. N. Bansal**

PRATT & WHITNEY AIRCRAFT
UNITED TECHNOLOGIES CORPORATION
EAST HARTFORD, CONNECTICUT

ABSTRACT

The incompressible Reynolds equation is the basis for prediction of viscous damper and journal bearing hydrodynamic forces. The validity of this equation in situations where cavitation exists within the oil film is questioned. Compressibility could result from sub-atmospheric cavitation pressures liberating dissolved gases and creating a 2-phase, variable density fluid. The released gases in the form of bubbles would not readily re-dissolve but persist in the pressure region and reduce hydrodynamic pressures. A significant alteration of the pressure profile, and therefore the stiffness and damping characteristics would be expected.

This hypothesis, alluded to by various authors, is proposed as an explanation for reported, unusual fluid film behavior and is examined through additional experimental data. A viscous damper rig designed with a controlled orbit and fluid environment provided circumferential hydrodynamic pressures at various speeds and oil supply pressures. The analysis and interpretation of these data in comparison to current theory is addressed.

* Project Engineer
** Senior Analytical Engineer

NOMENCLATURE

c	radial clearance of damper bearing, in.
e	radial eccentricity of damper center, in.
F_R	radial force, lb
F_T	tangential force, lb
h	oil film thickness, in.
h_{min}	minimum thickness of oil film, in.
h_{max}	maximum thickness of oil film, in.
L	damper length, in.
P	damper pressure, psi
P_{max}	total peak pressure, psig
$\overline{P}_{max}$	normalized maximum pressure
P_{supply}	damper supply pressure, psig
R	damper radius, in.
ϵ	eccentricity ratio (e/c)
θ	angle referenced from h_{min}, deg
ρ	density, lb-S^2/in.
ω	angular speed of damper journal, rad/S

INTRODUCTION

The viscous (squeeze film) damper is commonly used in both industrial machinery and aircraft gas turbine engines to reduce vibration and bearing loads. Without sufficient damping, rotating equipment is apt to experience high bearing and static structure forces because of inherent or unusual shaft imbalance or dynamic instabilities within the system. The viscous damper provides increased tolerance to excitation forces, and for the gas turbine engine in particular, offers the opportunity to reduce weight and increase speed, and thereby improve performance and decrease fuel consumption. For these reasons an extensive effort to investigate viscous dampers both analytically and experimentally has been undertaken.

The basis of the lubrication theory for viscous damper and hydrodynamic bearing analysis is the Reynolds equation which was formulated in 1886. It results directly from the Navier-Stokes equation by imposing the following restrictions: a thin film, laminar flow, a Newtonian fluid, negligible inertia forces, no variation in pressure across the film, no external body forces, and no slip at the bearing surfaces. The generalized Reynolds equation for compressible fluids, which is discussed in 1, is

$$\frac{\partial}{\partial x}\left(\frac{\rho h^3}{\mu}\frac{\partial P}{\partial x}\right) + \frac{\partial}{\partial Z}\left(\frac{\rho h^3}{\mu}\frac{\partial P}{\partial Z}\right) = 6\left(U_1 - U_2\right)\frac{\partial(\rho h)}{\partial x} + 12\rho V \qquad (1)$$

By assuming an incompressible fluid, as normally expected in both dampers and hydrodynamic bearings, equation (1) becomes

$$\frac{\partial}{\partial x}\left(\frac{h^3}{\mu}\frac{\partial P}{\partial x}\right) + \frac{\partial}{\partial Z}\left(\frac{h^3}{\mu}\frac{\partial P}{\partial Z}\right) = 6\left(U_1 - U_2\right)\frac{\partial h}{\partial x} + 12V \qquad (2)$$

Both of these equations are nonhomogeneous partial differential equations in two variables and are difficult to solve directly. Specific assumption coupled with appropriate boundary conditions, however, have allowed the solution of these equations. Specifically, equation (2) has been solved by assuming (a) a sealed damper configuration wherein the bearing is infinitely long with no end leakage, i.e., the flow in the axial direction is negligible as compared to the circumferential direction, (b) open-ended conditions which assume negligible flow in the circumferential direction as compared to the axial direction, and (c) a finite length journal wherein flow in both the axial and circumferential directions is assumed. The infinite length solution as reported in 2 was used for the damper investigated in this program, an end-sealed type commonly used in gas turbine engine. Dampers without end seals have been used in some applications, but high oil flow requirements usually prohibit their use.

Various types of viscous dampers and hydrodynamic bearings have been experimentally investigated by several authors. Measured pressure profiles and forces have been compared with predictions based upon the solution of the Reynolds equation for an incompressible fluid. Correlation between test and theory has been shown to be good to excellent in some cases and poor in other instances. It is felt by the authors that an explanation for these differences is available and that it involves the issue of cavitation. A

survey of the early 20th century literature on the subjects of cavitation, sub-atmospheric pressures, and tensile stresses in fluids as summarized in [3] clearly shows that unusual and unexpected behavior within journal bearings was common. From a practical standpoint, the pressure within the cavitation region is usually ignored since the contribution of this pressure on the total force is negligible. But, this is not the discrepancy being addressed. The questions being raised are what is the nature of the cavitation region and what is its influence on the pressure region. On the basis of his review of works published during the first half of this century, Cole [3] speculated on sub-atmospheric bearing pressures and cavitation in journal bearings. He described three regions as shown in Fig. 1. In region A, liberation of dissolved gases within the lubricant would occur, and the resulting cavitated fluid would be compressible and probably of different viscosity. In region B, lubricant vapor would tend to be liberated. He thought that in both regions unstable states are possible with no gas liberation because of the absence of gas nuclei which are necessary to precipitate the change from a liquid to a liquid-gas phase. He went on to state that since gas liberation is not instantaneous, it is also possible that phase equilibrium may not be immediately attained after a pressure change. Region C, the true negative pressure region, is theoretically possible as a metastable state but except under transient dynamic conditions the liberation of vapor would cause conditions in region B to intervene. Cole went on to speculate that the cavitation pressure would most likely be between atmospheric and the lubricant vapor pressure under steady state conditions. In addition, he thought the time lag effects arising from the finite rates of gas liberation and re-solution could delay the formation of the pressure film at the point of maximum film thickness thereby introducing compressibility effects into the early portion of the pressure region. The similarity between the pressure profiles of journal bearings and viscous dampers suggests that compressibility effects noted in the bearing could also occur within the viscous damper.

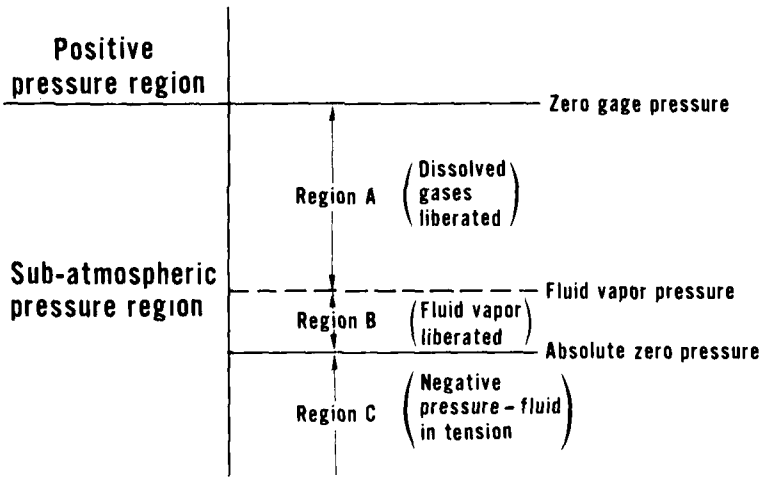

Fig. 1 Liquid/gas sub-atmospheric pressure regions

Later work on journal bearings by Marsh [4], Black & Walton [5], Nakahara et al [6], and Dyer & Reason [7] has shown cavitation to be responsible for reducing the load carrying capacity, producing cavities which persist in the high pressure region, creating a 2-phase compressible fluid, and inhibiting pressures below absolute zero. Nakahara et al specifically showed both cavitation pressure and zone width to be dependent upon air content of the fluid. In addition, at least four detailed publications concerning viscous dampers show lower-than-predicted dynamic pressures and good correlation only when cavitation was eliminated or dynamic pressures were low, viz, Tonnesen [8], Humes and Holmes [9], Jones [10], and White [11].

In order to explain the results of the viscous damper testing and the effects of cavitation on damper performance, an explanation of specific terms is necessary. A particularly instructive paper written by Swales [12] provides a detailed explanation of cavitation phenomena which occur in thin films. He specifically describes and defines gaseous and vaporous cavitation as being dependent upon the relative amounts of gas and vapor within the cavitation bubble. Bubbles with mainly vapor are thus defined as vaporous cavitation bubbles. When gas is the major constituent, the term gaseous cavitation is used. He goes on the state that "....even the longest lived vaporous cavities are transient phenomena and stability is only achieved when the contents are predominately of gas rather than vapor. Most types of cavitation observed in thin oil films are stable and ... from this evidence alone it would be possible to conclude that they are gas filled. The gas comes from free gas bubbles or the large amounts of dissolved air in oil (8-15 percent by volume). ...vaporous cavitation is only likely in situations where there is insufficient time for air to diffuse out of the oil."

It appears that cavitation may significantly alter the hydrodynamic characteristics of viscous dampers and bearings. The assumption of an incompressible, single-phase fluid may not be valid. Because of the unknown nature of gaseous and vaporous cavitation and the possibility of a 2-phase fluid within the oil film annulus, an explanation of the physics of the oil film is complex and possibly beyond the limits of analytical description. This paper will present a hypothesis and substantiating experimental results which add credence to the speculation and evidence of others.

THE PROBLEM AND A HYPOTHESIS

Early viscous damper testing [2] and Fig. 2 showed good correlation at low dynamic pressures. As higher speeds, larger eccentricity ratios, and smaller clearances were investigated, the amount of cavitation increased and deviation from theory became more pronounced. Specifically, peak dynamic pressures as low as 40% of the predicted values were observed. No obvious trend was noted except that, in general, decreasing the length of the circumferential cavitation zone improved the correlation.

A study of the test results led to the hypothesis of a 2-phase fluid consisting of the oil and gas bubbles created by the sub-atmospheric pressures within the cavitation region. The bubbles persist in the positive pressure region due to finite oil re-solution rates and create a compressible, variable density fluid. This fluid produces hydrodynamic pressures which are significantly lower than predicted by incompressible theory. Gaseous cavitation, which is probably unavoidable in most practical situations,

will therefore reduce hydrodynamic pressures within viscous dampers and, in addition, create similar effects in fluid bearings, particularly under whirl conditions.

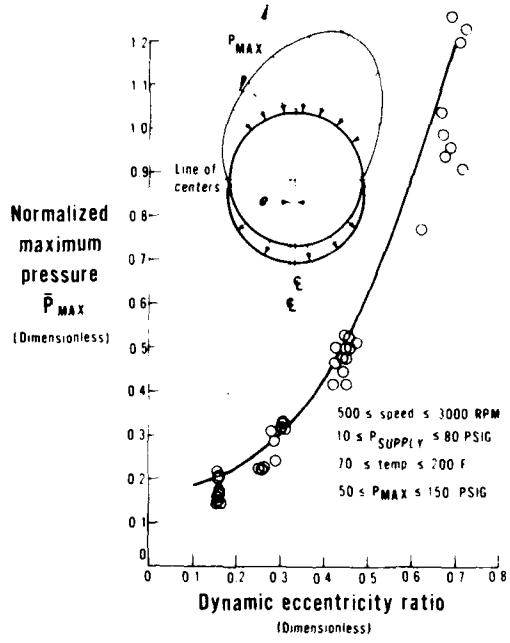

Fig. 2 Correlation of experimental data to theory for a 20 mil radial clearance viscous damper

A survey of the literature clearly shows similar trends. Humes and Holmes [9] stated "...as a result of the persistence of cavitation throughout a cycle, there appeared to be a limit to the maximum pressure attained during a cycle which was many times smaller than the pressure predicted using the Reynolds equation." It is interesting to note that the test damper was the open-ended variety and that maximum measured pressures were in the range of 100-150 psi. Similarly, Jones [10] also showed discrepancies between theory and practice, particularly at high eccentricity ratios. His damper was also the open-ended type. Comprehensive testing by White [11] with both open and sealed end conditions also showed experimental pressures significantly less than predicted. White pointed out that for the open-ended damper where the axial pressure profile is parabolic, cavitation was confined to the axial center line. This resulted in two dampers, each of length L/2 and a step change in total load capacity to one-quarter of that predicted for a length L damper. A sealed damper, which has a square axial pressure profile will cavitate over its entire width and reduce dynamic pressure uniformly, not in the manner observed and reported by White.

EXPERIMENTAL PROGRAM

To accurately assess the hydrodynamic characteristics of viscous dampers measurement of the pressure profile both axially and circumferentially under controlled environmental and orbit conditions is necessary. Since

forces can be calculated from the pressure measurements, this approach is superior to the alternate method of direct force measurement. The pressure profile can be directly compared to that predicted by the Reynolds equation. The test rig (Fig. 3) was the same rig as used for the results reported in 2 and 13 except for the modifications described below.

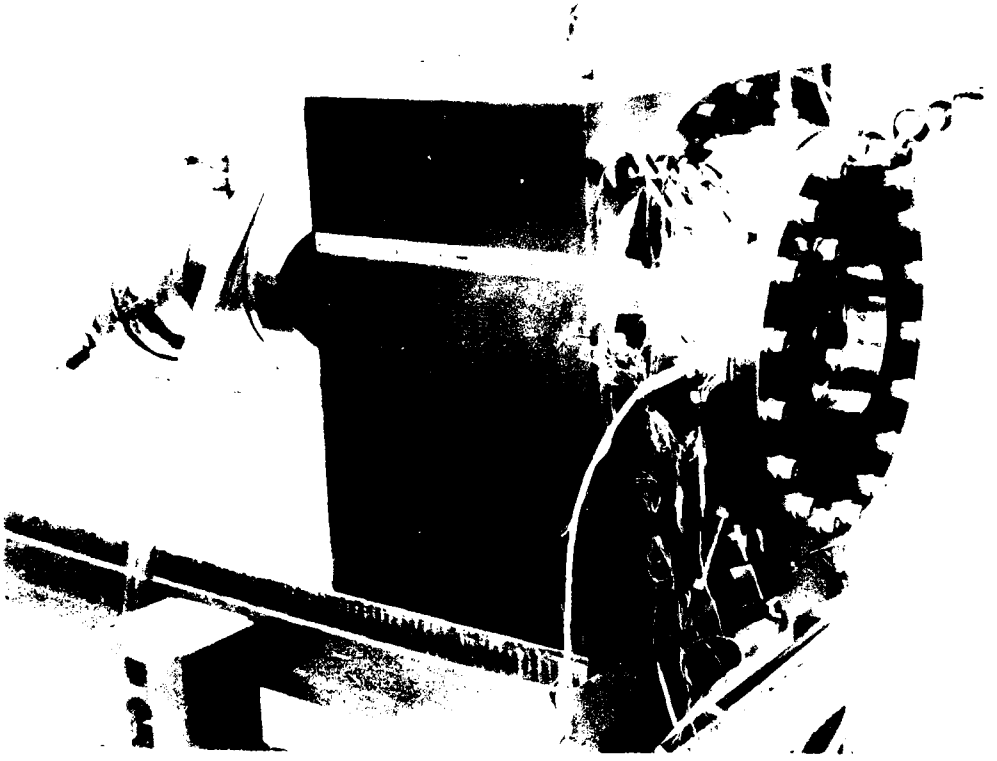

Fig. 3 Hydrodynamic test rig

To facilitate data reduction, circular centered orbits were essential. They were obtained by an off-set cam which was placed at one end of a simply supported shaft. A cross-section of the rig showing details of the shaft and damper assembly is illustrated in Fig. 4. The ball bearing supported shaft is driven by a variable speed motor which could accurately control the damper whirl speed to within ±2 rpm. The damper length and diameter chosen for the tests were 1.61 in. and 6.44 in. respectively. Measured radial clearance was 10.4 mils. Both ends of the damper were sealed with piston ring as well as "O" ring seals to facilitate collection of the return oil and to prevent air from being drawn in by the damper sub-atmospheric pressure in the cavitation zone. The piston rings were of the butt-joint type which are typically used in the gas turbine engine applications. The end leakage past the piston rings as compared to the flow through the butt joints was minute. Therefore, the damper was essentially operating with sealed end conditions except at the piston ring gaps which provided oil thru-flow. This arrangement allowed a direct comparison of the experimentally measured circumferential pressure profiles with those predicted by a long bearing solution of the Reynolds equation.

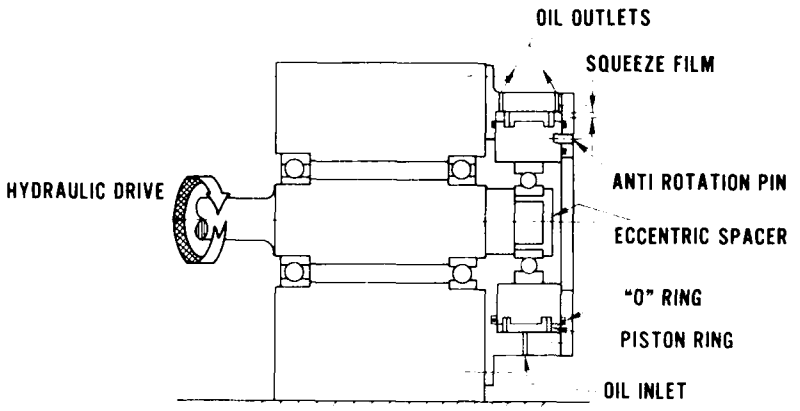

Fig. 4 Hydrodynamic test rig cross-section

Oil was supplied to the damper through a single .032 inch diameter hole located at the mid-plane of the damper. Two .032 inch diameter outlets 180° away from the inlet were located between the piston and "O" ring seals. Oil temperature was controlled within $\pm 1^{\circ}F$ and monitored by two quick response thermocouples which were placed in the oil film flush with the damper housing. Two proximity probes, 90° away from each other, were installed to obtain the shape of the damper orbit, dynamic eccentricity, and the instantaneous position of the line of centers (i.e., the line joining the bearing and damper centers). Several pressure transducers were positioned circumferentially and axially to measure the entire pressure profile. Preliminary testing showed that the axial pressure gradients were negligible and that pressure profiles measured at different circumferential locations were similar. Additionally, the traces of the two proximity probes were also similar. Therefore, for all subsequent tests, the damper orbit was assumed to be circular centered and the circumferential pressure data and eccentricity were obtained from one pressure transducer and one proximity probe, both of which were located at the same circumferential location.

DATA REDUCTION

For each test conducted, the output of the pressure transducer and proximity probes was stored in a digital memory system. This system provided a playback rate which was up to 1/200th of the input rate without amplitude or time phase distortion. An X-Y plotter was used to record the time history of damper pressure and radial clearance. With circular centered orbits, the pressure profile is synchronous with speed and fixed relative to the rotating shaft. Therefore, the pressure/time relationship could be transformed to a pressure/angular relationship. The line of centers was used as the reference line to determine the tangential and radial force components. The line of centers at the minimum damper gap also establishes the reference for both force and peak pressure phase angles. The pressure curve was digitized to obtain a pressure versus angular position tabulation, with respect to the line of centers, for one cycle of the damper. Experimental damper forces were determined by intergrating the pressure profiles using these equations:

$$F_T = RL \int_0^{2\pi} P \sin \theta \, d\theta$$

$$F_R = RL \int_o^{2\pi} P \cos\theta \, d\theta$$

Bearing clearances and shaft flexibilities introduced significant variations in the dynamic eccentricities. The change was more pronounced at higher speeds. The dynamic eccentricity ratio (ϵ) was, therefore, determined for each test from the proximity probe data using the equation

$$\epsilon = \frac{h_{max} - h_{min}}{2C}$$

Theoretical damper forces were calculated from the long bearing solution of the Reynolds equation using the test values of supply pressure, dynamic eccentricity, oil temperature, shaft speed, and damper geometry. Theoretical peak dynamic pressures were obtained using the equation

$$P_{max} = \frac{12\mu\omega R^2 \bar{P}_{max}}{C^2} + P_{supply}$$

where $\bar{P}_{max}$ is obtained from curves of $\bar{P}_{max}$ versus ϵ, 2 . Table 1 shows the experimental data together with predicted pressures and calculated forces.

EXPERIMENTAL RESULTS AND ANALYTICAL CORRELATION

As mentioned above and reported in 2 and 13 , the earlier research to ascertain the validity of the Reynolds equation for calculating viscous damper stiffness and damping coefficients showed good correlation over the range of variables tested. Likewise, work by Vance and Kirton 14 indicated good correlation, but their results were for a damper with no cavitation. If the data from 2 is presented as shown in Fig. 5, a delineation of the data with and without cavitation is clearly indicated. It will be noted that in general, good agreement with theory is apparent, but upon closer scrutiny it can be seen that better agreement was obtained within the uncavitated region. In the cavitation region theory over predicts the pressure, particularly as the extent of cavitation increases. The trend is subtle but apparent nevertheless.

Further investigation of the validity of the Reynolds equation required additional testing with smaller damper clearances, higher loads, and increased cavitation extent. Five preliminary tests at various eccentricity ratios showed significant deviation from theory (Fig. 6). Additional testing at various speeds, eccentricity ratios, and two oil supply pressures showed a general trend of improved correlation with both lower speeds and higher supply pressure (Fig. 7). It was not obvious what caused the variable correlation. Cavitation was suspected because the exiting oil was permeated with bubbles, unlike the inlet oil which was clear. With a greater range of shaft speed and supply pressure, nearly 100 tests were run to obtain the circumferential pressure profiles, the damper orbit, and the condition of

the fluid as it exited the damper. With these data fully analyzed, the trend of improved correlation between analytical and experimental data with minimum cavitation zone and minimum bubble production was clearly evident (Fig. 8). A 2-phase fluid with a compressibility dependent upon the extent of cavitation seemed probable.

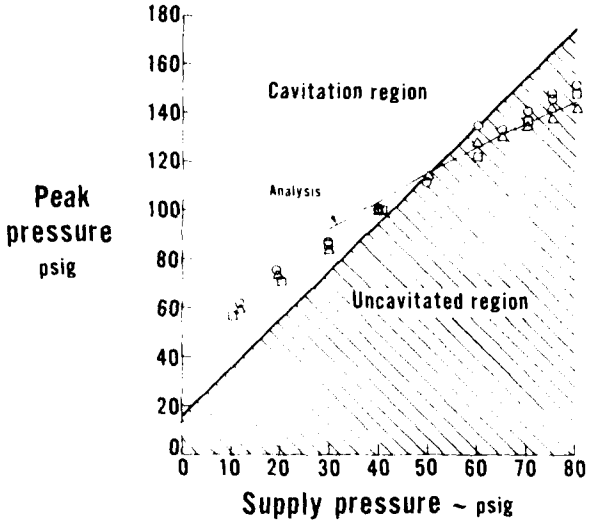

Fig. 5 Effect of cavitation upon analytical/experimental correlation

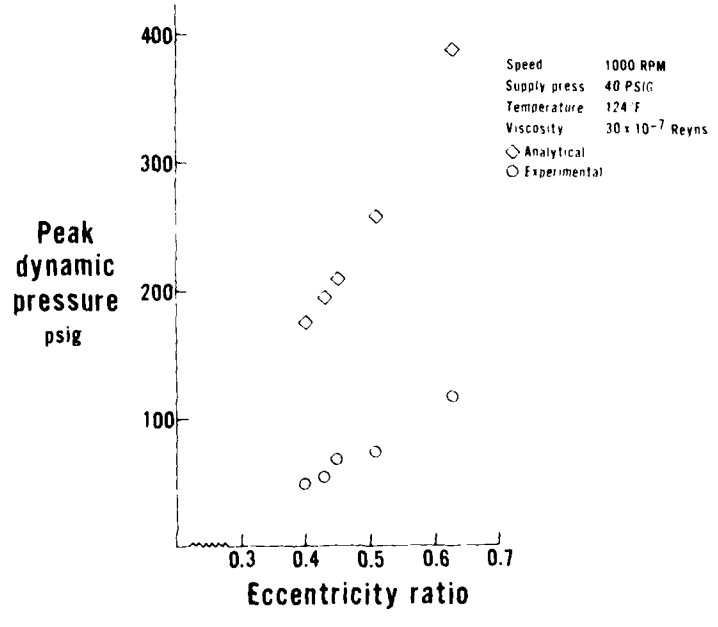

Fig. 6 Large deviation from theory observed with 10.4 mil radial clearance damper

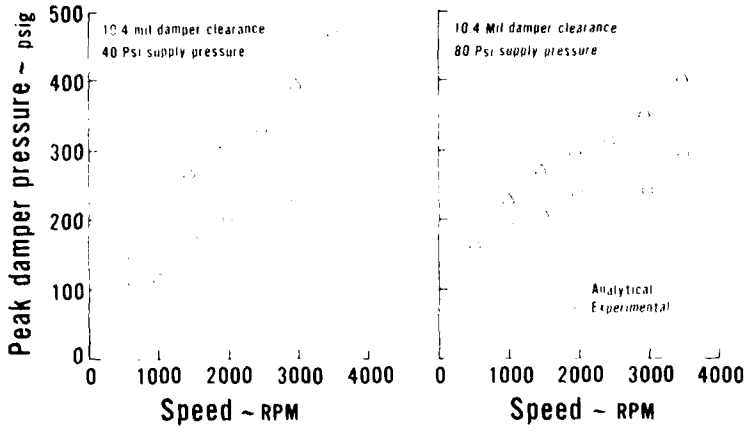

Fig. 7 Effect of speed and supply pressure upon analytical/experimental correlation

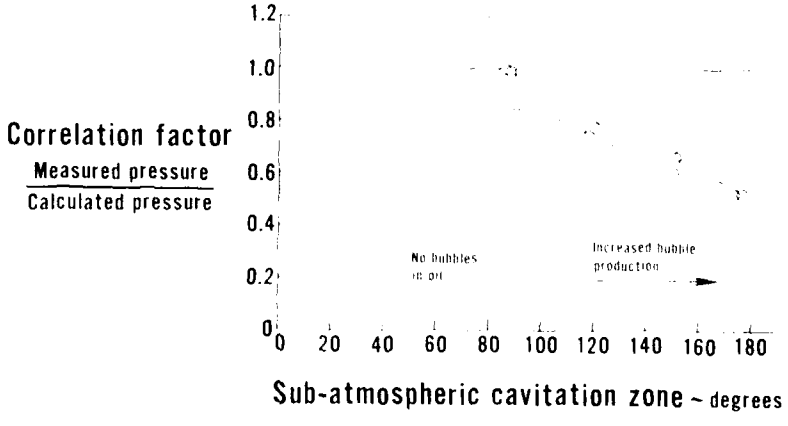

Fig. 8 Improved correlation results from a decreased cavitation zone

Evidence of compressibility is apparent in Fig. 9 which shows the circumferential pressure profiles for three oil supply pressures with speed and temperature held constant. If the fluid were incompressible, oil supply pressures should add linearly onto the 360° pressure profile. It can be seen, however, that the peak pressure increases by an amount greater than the supply pressure increment even though the eccentricity ratio decreased at higher pressures. The unexpected pressure rise was noted at all speeds and can be seen more clearly by a plot of the change in peak pressure versus the supply pressure increment (Fig. 10). The eccentricity ratio was not constant but decreased with increasing supply pressure (see Table 1). An even larger pressure rise would have occurred if eccentricity ratio had been held constant. This unusual behavior could be caused by a compressible 2-phase fluid which produces higher hydrodynamic pressures as it increases in density with increasing supply pressure.

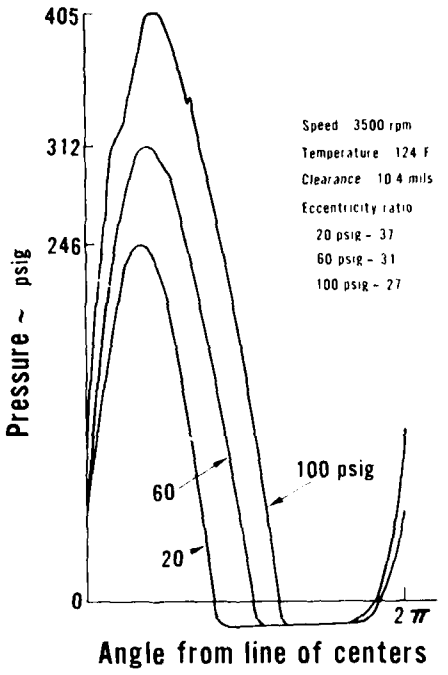

Fig. 9 Effect of supply pressure on damper peak pressure

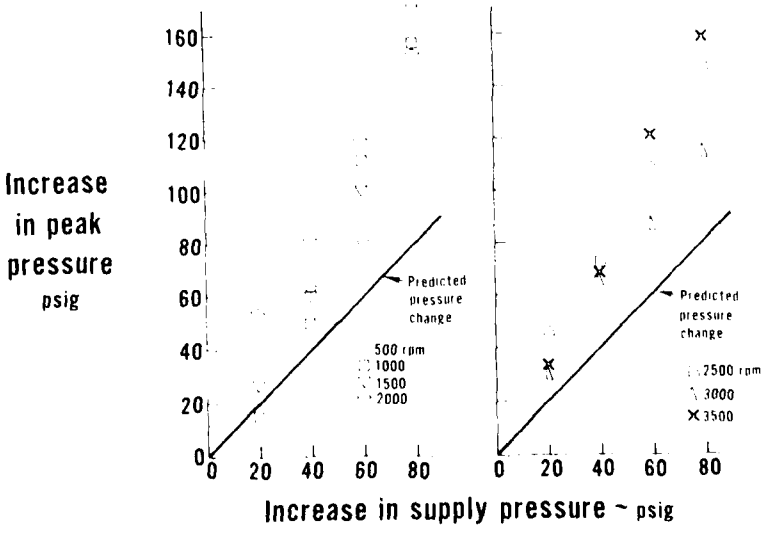

Fig. 10 Nonlinear effect of supply pressure for various speeds

TABLE 1 EXPERIMENTAL DATA AND PREDICTED PRESSURE FOR 10.4 MIL RADIAL CLEARANCE DAMPER

Test Number	Speed RPM	Supply Pressure (PSIG)	Dynamic Eccentricity	Angle of Peak Pressure From L.O.C. (Degrees)	Predicted Angle of Peak Pressure From L.O.C. (Degrees)	Peak Pressure (PSIG)	Peak Pressure Minus Supply Pressure PSIG	Predicted Peak Dynamic Pressure PSIG	Cavitation Region Sub Atmospheric (Degrees)	Total Force lbs	Radial Force (lbs)	Tangential Force (lbs)	Force Phase Angle (Degrees)
[illegible]	500	20	.529	67	45.5	104	84	[illegible]	[illegible]	[illegible]	[illegible]	[illegible]	[illegible]
[illegible]	500	40	.505	65	47.5	[illegible]	[illegible]	[illegible]	[illegible]	[illegible]	[illegible]	[illegible]	[illegible]
78	500	60	.515	70	46.6	168	[illegible]	[illegible]	[illegible]	[illegible]	[illegible]	[illegible]	[illegible]
[illegible]	500	80	.520	40	46.3	[illegible]	[illegible]	[illegible]	[illegible]	[illegible]	[illegible]	[illegible]	[illegible]
76	500	100	.539	40	44.8	220	[illegible]	[illegible]	[illegible]	[illegible]	[illegible]	[illegible]	[illegible]
[illegible]	1000	20	.424	[illegible]	54.3	140	[illegible]	[illegible]		[illegible]	[illegible]	[illegible]	[illegible]
[illegible]	1000	40	.427	[illegible]	[illegible]	155	[illegible]	[illegible]	[illegible]	[illegible]	[illegible]	[illegible]	[illegible]
[illegible]	1000	60	.429	[illegible]	54.0	190	[illegible]	[illegible]	[illegible]	[illegible]	[illegible]	[illegible]	[illegible]
[illegible]	1000	80	[illegible]	68	54.5	[illegible]	[illegible]	[illegible]	[illegible]	[illegible]	[illegible]	[illegible]	[illegible]
[illegible]	1000	100	[illegible]	78	55.2	[illegible]	46	[illegible]	[illegible]	[illegible]	[illegible]	[illegible]	[illegible]
[illegible]	1500	20	.404	69	55.6	183	[illegible]	[illegible]	[illegible]	[illegible]	[illegible]	[illegible]	[illegible]
110	1500	40	[illegible]	[illegible]	[illegible]	[illegible]	[illegible]	[illegible]	[illegible]	[illegible]	[illegible]	[illegible]	[illegible]
109	1500	60	[illegible]	69	56.8	[illegible]	[illegible]	[illegible]	[illegible]	[illegible]	[illegible]	[illegible]	[illegible]
99A	1500	80	[illegible]	[illegible]	[illegible]	[illegible]	[illegible]	[illegible]	[illegible]	[illegible]	[illegible]	[illegible]	[illegible]
[illegible]	1500	100	[illegible]	[illegible]	[illegible]	[illegible]	[illegible]	[illegible]	[illegible]	[illegible]	[illegible]	[illegible]	[illegible]
[illegible]	2000	20	[illegible]	[illegible]	[illegible]	[illegible]	[illegible]	[illegible]	[illegible]	[illegible]	[illegible]	[illegible]	[illegible]
[illegible]	2000	40	[illegible]	[illegible]	[illegible]	[illegible]	[illegible]	[illegible]	[illegible]	[illegible]	[illegible]	[illegible]	[illegible]
58	2000	[illegible]	[illegible]	[illegible]	[illegible]	[illegible]	[illegible]	[illegible]	[illegible]	[illegible]	[illegible]	[illegible]	[illegible]
[illegible]	2000	80	[illegible]	68	[illegible]	[illegible]	[illegible]	[illegible]	[illegible]	[illegible]	[illegible]	[illegible]	[illegible]
[illegible]	2000	100	[illegible]	[illegible]	[illegible]	[illegible]	[illegible]	[illegible]	66	[illegible]	[illegible]	[illegible]	[illegible]
[illegible]	2500	[illegible]	[illegible]	[illegible]	[illegible]	[illegible]	[illegible]	[illegible]	[illegible]	[illegible]	[illegible]	[illegible]	[illegible]
[illegible]	2500	[illegible]	[illegible]	[illegible]	[illegible]	[illegible]	[illegible]	[illegible]	[illegible]	[illegible]	[illegible]	[illegible]	[illegible]
[illegible]	2500	60	[illegible]	[illegible]	[illegible]	[illegible]	[illegible]	[illegible]	[illegible]	[illegible]	[illegible]	[illegible]	[illegible]
[illegible]	2500	80	.284	[illegible]	[illegible]	[illegible]	[illegible]	[illegible]	[illegible]	[illegible]	[illegible]	[illegible]	[illegible]
[illegible]	2500	100	.269		[illegible]	[illegible]	[illegible]	[illegible]	[illegible]	[illegible]	[illegible]	[illegible]	[illegible]
[illegible]	3000	20	[illegible]	[illegible]	[illegible]	[illegible]	[illegible]	[illegible]	[illegible]	[illegible]	[illegible]	[illegible]	[illegible]
[illegible]	3000	40	[illegible]	[illegible]	[illegible]	[illegible]	[illegible]	[illegible]		[illegible]		[illegible]	[illegible]
[illegible]	3000	60	.298	[illegible]	[illegible]	[illegible]	[illegible]	[illegible]		[illegible]	[illegible]	[illegible]	[illegible]
[illegible]	3000	80	[illegible]	[illegible]	[illegible]	[illegible]	[illegible]	[illegible]		[illegible]	[illegible]	[illegible]	[illegible]
[illegible]	3000	100	[illegible]		[illegible]	[illegible]	[illegible]	[illegible]	[illegible]	[illegible]	[illegible]		[illegible]
[illegible]	3500	20	[illegible]	[illegible]	[illegible]	[illegible]	[illegible]	[illegible]	[illegible]	[illegible]	[illegible]	[illegible]	[illegible]
[illegible]	3500	40	[illegible]	[illegible]	[illegible]	[illegible]	[illegible]	[illegible]	[illegible]	[illegible]	[illegible]	[illegible]	[illegible]
[illegible]	3500	60	[illegible]	[illegible]	[illegible]	[illegible]	[illegible]	[illegible]	[illegible]	[illegible]	[illegible]	[illegible]	[illegible]
[illegible]	3500	80	[illegible]	[illegible]	[illegible]	[illegible]	[illegible]	[illegible]	[illegible]	[illegible]	[illegible]	[illegible]	[illegible]
[illegible]	3500	[illegible]	[illegible]	[illegible]	[illegible]	[illegible]	[illegible]	[illegible]	[illegible]	[illegible]	[illegible]	[illegible]	[illegible]

A 2-phase fluid could also vary in density locally within the annulus. The variation would result from the time lag associated with gas re-solution rates and from the higher pressure within the converging oil annulus (see Fig. 11). With a variable density fluid in the pressure region the effect of supply pressure would depend upon the local density. In areas of high density the increase in pressure would approximately equal the supply pressure increase. Areas of low density would become denser, and the pressure would increase by an amount greater than the supply pressure due to an increase in hydrodynamic pressure. The experimental data shown in Fig. 12 on a polar plot clearly illustrate the effect. Each curve represents the pressure profile for a constant supply pressure at 20 psi increments. The pressure change in the high density (minimum clearance) region is approximately equal to the supply pressure increase. In the low density (maximum clearance) region a trend of significantly greater pressure change is evident. The increase above the supply pressure at various speeds and circumferential locations for an 80 psi supply pressure change is illustrated in Fig. 13. This pressure is calculated from the following equation:

$$P(\theta) = P_{100}(\theta) - P_{20}(\theta) - 80$$

At the four higher speeds a trend of increasing dynamic pressure with increasing film thickness and speed is apparent, while at the lower speeds the maximum dynamic pressure increase shows no discernable trend. These limited data suggest that the fluid density within the damper pressure region is variable and partially dependent upon time (speed) and pressure (position).

The forces obtained by integrating the pressure profiles provide additional information which suggests that incompressible fluid theory is not valid for a cavitated film. The phase angle of the total force increases

with increased supply pressure as predicted by theory except that it approaches (and exceeds) 90° with a supply pressure significantly less than predicted (Table 1). This is a direct result of the large increase in pressure within the maximum film thickness region caused by a variable density fluid. The phase angle of the peak pressure also increases with increased supply pressure. Theoretically, this angle should not change. It is, however, a function of eccentricity ratio which could not be held constant. Using the measured eccentricity ratios the pressure phase angles were calculated and compared to those observed. Significant deviations were evident, caused also by the larger than expected pressure changes in the maximum film thickness region. These additional observations suggest that the influence of a 2-phase fluid on viscous damper characteristics is complex and not as predicted by incompressible theory.

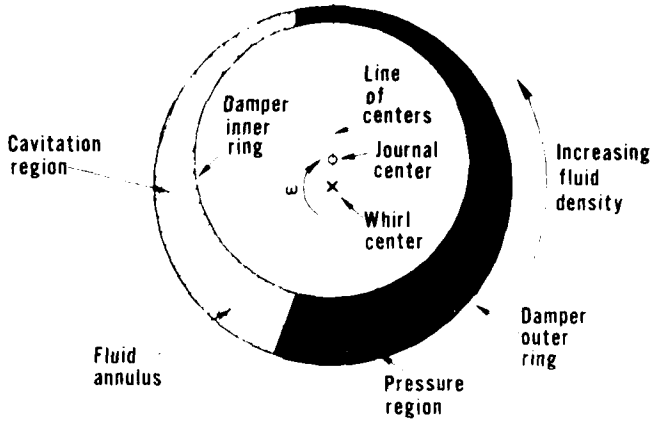

Fig. 11 Damper cross-section showing variable density fluid within pressure region

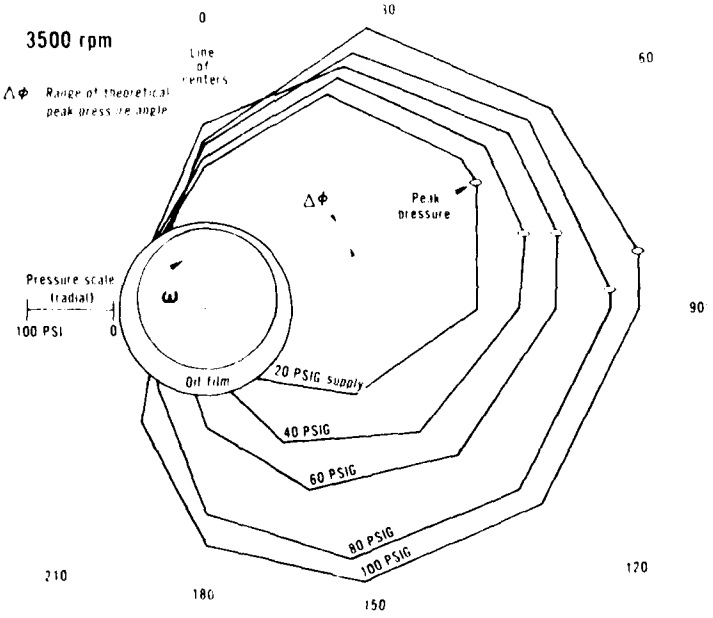

Fig. 12 Supply pressure effects on viscous damper pressure profile

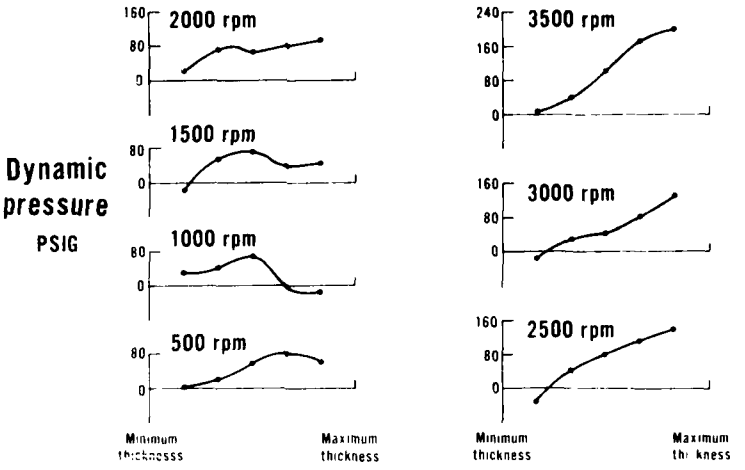

Fig. 13 Dynamic pressure increase versus circumferential location at various speed for an 80 psi supply pressure change

SUMMARY AND CONCLUSIONS

Experimental data obtained from a controlled orbit damper rig has provided additional evidence supporting the inadequacy of the incompressible Reynolds equation in predicting viscous damper pressures. It is hypothesized that the deviation from theory is due to fluid compressibility caused by sub-atmospheric cavitation pressures liberating dissolved gases and creating 2-phase fluid. The liberated bubbles, being primarily gaseous and not vaporous, do not readily re-dissolve but persist within the pressure region thereby reducing the hydrodynamic pressure. In addition, the 2-phase fluid has a variable density which is both pressure and time dependent, the density being affected by oil supply pressure, eccentricity ratio, and speed. Experimentally it has been shown that:

1. The correlation of experimental data with incompressible theory improves with a decreased extent of cavitation.

2. With a cavitated damper oil supply pressure can not be directly superimposed onto a pressure profile; an additional increase in hydrodynamic pressure results.

3. The damper pressure profiles which differ from those predicted by incompressible theory produce significant changes in the stiffness and damping characteristics of a cavitated damper.

The significance of the observed deviation in damper characteristics on rotor dynamic response can not in general be assessed. Because of extreme variations in damper operating conditions, the alteration of the hydrodynamic forces may be even greater than found in this program. Depending upon the dynamics of the system, gaseous cavitation may provide either vibration improvement or degradation. It is suggested that either viscous dampers be used within a range of parameters where the incompressible Reynolds equation is valid or specific testing be conducted for the damper in question to determine the degree of deviation from theory. Further research into the

effects of cavitation on both viscous dampers and fluid bearings is certainly warranted; equally important is the development of an analysis which can account for the compressibility effects.

ACKNOWLEDGMENT

Empirical studies to investigate controversial issues are usually influenced by technical dogma and an incomplete knowledge of relevant past efforts. Discussions with many fluid bearing and rotor dynamic experts provided encouragement and information useful for the understanding of the test results. In particular, the authors thank Mr. Donald Bently, Dr. Henry Black, Dr. Dara Childs, and Dr. Roy Holmes.

REFERENCES

1 Pinkus, O., and Sternlicht, B., "Theory of Hydrodynamic Lubrication", McGraw-Hill, 1961.

2 Feder, E, Bansal, P. N., and Blanco, A., "Investigation of Squeeze Film Damper Forces Produced by Circular Centered Orbits", Journal of Engineering for Power, January 1978. Vol. 100.

3 Cole, J. A., "A Note On the Low Pressure Regions Occurring In the Hydrodynamic Lubricating Films of Journal Bearings", Scientific Lubrication, January, 1951.

4 Marsh, H., "Cavitation In Dynamically Loaded Journal Bearings", 1st Leeds Tribology Symposium University of Leeds, England, September, 1974.

5 Black, H. F., and Walton, M. H., "Theoretical and Experimental Investigations of a Short 360° Journal Bearing In the Transition Superlaminar Regime", Journal Mechanical Engineering Science, Vol. 16, No. 5, 1974.

6 Nakahara, T., Kobayashi, T., and Masuko, M., "The Influences of Air Content of Lubricant On Cavitation In the Thrust Bearing With Closed Recesses", JSLE-ASLE International Lubrication Conference, Tokyo, Japan 1975, pp. 113-120.

7 Dyer, D., and Reason, B. R., "A Study of Tensile Stresses In a Journal-Bearing Oil Film", Journal Mechanical Engineering Science, Vol. 18, No. 1, 1976.

8 Tonnesen, J., "Experimental Parametric Study of a Squeeze Film Bearing", Transactions of the ASME, April, 1976.

9 Humes, B., "The Nonlinear Performance of Squeeze-Film Bearings", Ph.D Thesis , 1977, University of Sussex, England.

10 Jones, M. G., "An Experimental Investigation of Squeeze Film Hydrodynamics", NGTE Report R320, January, 1973.

11 White, D. C., "Squeeze Film Journal Bearings", (Ph.D dissertation), Churchill College, Cambridge, England, 1970.

12 Swales, P. D., "A Review of Cavitation Phenomena In Engineering Situations", 1st Leeds Tribology Symposium, University of Leeds, England, September 1974.

13 Bansal, P. N., and Hibner, D. H., "Experimental and Analytical Investigation of Squeeze Film Bearing Damper Forces Induced by Offset Circular Whirl Orbits", Journal of Mechanical Design, July 1978, Vol. 100.

14 Vance, J. M., and Kirton, A. J., "Experimental Measurement of the Dynamic Force Response of a Squeeze-Film Bearing Damper", Journal of Engineering for Industry, Trans, ASME, Vol. 97, pp. 1282-1290.

A DESIGN METHOD FOR AERODYNAMICALLY EXCITED ROTORS WITH SQUEEZE FILM BEARINGS

L. E. Barrett
Research Assistant Professor
Department of Mechanical and Aerospace Engineering
University of Virginia
Charlottesville, Virginia 22901

ABSTRACT

A method of analyzing the first mode stability and unbalance response of multimass flexible rotors is presented whereby the multimass system is modeled as an equivalent single mass modal model including the effects of rotor flexibility, general linearized hydrodynamic journal bearings, squeeze film bearing supports and rotor aerodynamic cross coupling. Expressions for optimum bearing and support damping are presented for both stability and unbalance response. The method is intended to be used as a preliminary design tool to quickly ascertain the effects of bearing and support changes on rotor-bearing system performance. Since the method can be quickly applied, it should realize a time and cost savings in analyzing the class of rotors considered.

An 8 stage industrial compressor is analyzed for stability and unbalance response. Linear and nonlinear analysis with squeeze film bearing supports are presented using nonlinear steady state and time transient techniques to verify the linear designs. The results indicate that the linear design method based on the optimum damping expressions presented herein leads to viable bearing and support designs for rotor-bearing stability and unbalance response.

NOMENCLATURE

Symbol	Description
A	Rotor amplification factor, dim.
A_o	Minimum rotor amplification factor, dim.
$[A]$	System coefficient matrix, FL^{-1}

$[B]$	System coefficient matrix, FL^{-1}
c	Bearing radial clearance, L
c_{ij}	Damping coefficient for i^{th} direction due to velocity in j^{th} direction, FTL^{-1}
c_p	Tilting pad bearing pad ground in clearance, L
c_r	Average radial damping coefficient, $(c_{ii} + c_{jj})/2$, FTL^{-1}
$[c]$	Matrix of damping coefficients, FTL^{-1}
D	Bearing diameter, L
$[D]$	$[A]^{-1}$ $[B]$, dim.
$[D_r]$	Real part of $[D]$, dim.
$[D_i]$	Imaginary part of $[D]$, dim.
k_{ij}	Stiffness coefficient for force in i^{th} direction due to displacement in j^{th} direction, FL^{-1}
k_o	Squeeze film bearing stiffness for circular centered orbit, FL^{-1}
k_r	Average radial bearing stiffness $(k_{ii} + k_{jj})/2$, FL^{-1}
k_{rs}	Fundamental shaft modal stiffness, FL^{-1}
k_s	Fundamental shaft modal stiffness, FL^{-1}
K	Ratio of total bearing principal stiffness to shaft stiffness, dim.
$[k]$	Stiffness matrix, FL^{-1}
L	Rotor length, L
l	Bearing length, L
m	Mass, FT^2L^{-1}
m	Tilting pad bearing preload, dim.
m_b	Bearing mass, FT^2L^{-1}

q	Aerodynamic cross coupling coefficient, FL^{-1}
Q	$2cq/W$, dim.
Q_m	Maximum value of Q, dim.
TRD	Dynamic force transmissibility factor, dim.
U	Rotor unbalance, FL
W_T	Total rotor weight, F
W_m	Rotor modal weight, F
	Bearing journal eccentricity ratio, dim.
	Imaginary part of eigenvalue, ω_d/ω, dim.
	Fluid viscosity, FTL^{-2}
	Angular location of journal in bearing, dim.
	Rotor speed, T^{-1}
$_{cr}$	Rotor rigid bearing critical speed, T^{-1}
$_d$	Damped natural frequency, T^{-1}
$_s$	Rotor instability onset speed, T^{-1}
$_s$	$_s \sqrt{c/g}$, dim.

INTRODUCTION

A method of analyzing the first mode stability and unbalance response of multimass flexible rotors is presented whereby the multimass system is modeled as an equivalent single mass modal model including the effects of rotor flexibility, general linearized hydrodynamic journal bearings, squeeze film bearing supports and rotor aerodynamic cross coupling. Expressions for optimum bearing and support damping are presented for both stability and unbalance response. The method is intended to be used as a preliminary design tool to quickly ascertain the effects of bearing and support changes on rotor-bearing system performance. Since the method can be quickly applied, it should realize a time and cost savings in analyzing the class of rotors considered.

An 8-stage industrial compressor is analyzed for stability and unbalance response. Linear and nonlinear analysis with squeeze film bearing supports are presented using nonlinear steady state and time transient techniques to verify the linear designs. The results indicate that the linear design method based on the optimum damping expressions presented herein leads to viable bearing and support designs for rotor-bearing stability and unbalance response.

A schematic of an 8 stage centrifugal compressor is shown in Fig. 1. The unit is to be used in an off-shore oil production facility. The rotating element has a total length of 279.4 cm, a bearing span of 228.6 cm and a total weight of 9341 N. The operating speed is 7000 RPM. The original design called for five pad tilting pad bearings with a 30% preload (1) at the main supports. A preliminary stability analysis (2) using a modified Myklestad-Prohl method (3) indicated the rotor would be unstable at speeds above 3900 RPM due to aerodynamic interaction of the gas flow with the impeller passages. The magnitude of the aerodynamic effects was anticipated to be q = 21024 N/cm at 7000 RPM. A speed squared variation of aerodynamic effects was assumed.

Subsequent stability analyses (2) indicated that modifications to the main bearings would not stabilize the system. In addition to the stability problem, the rotor was required to meet an unbalance response specification that the amplification factor not exceed A = 6 at the first critical speed. That is, the maximum vibrational amplitude of the rotor could not exceed 6 times the equivalent rotor mass eccentricity of the rotor unbalance. It was therefore decided to modify the bearing pedestals by the inclusion of squeeze film bearings. General squeeze film bearings of the type shown in Fig. 2 were selected which included a circumferential oil feed groove, end leakage seals and squirrel cage retainer springs. The original tilting pad bearings were not replaced by rolling element bearings as indicated in Fig. 2. The objective of the analysis was to determine the retainer spring stiffness and the length and clearance of the squeeze film bearings to simultaneously satisfy the stability and unbalance response requirements for the rotor.

Since the squeeze film journal does not rotate, the hydrodynamic squeeze film forces result only from translational motion of the journal which squeezes the lubricant. Thus, under steady state operating conditions without internal forcing functions acting on the rotor, the journal is stationary with respect to the damper housing and no hydrodynamic forces are produced.

It is this lack of hydrodynamic forces under unforced steady state operating conditions which produces the need for mechanical retainer springs in parallel with the lubricant film to support static loads imposed by gravitation and interaction of the rotor with the working fluid. These springs must be designed to prevent the damper journal from coming into contact with the damper housing when hydrodynamic forces are not present. Furthermore, the retainer springs must be carefully tuned to anticipated hydrodynamic forces under conditions of both small perturbations and cyclic orbital journal motion about the steady state journal position to produce the overall desired flexibility and damping characteristics. The hydrodynamic forces resulting from small perturbations about the static equilibrium position are utilized in stability analyses whereas those resulting from cyclic orbital motion are generally used in unbalance response analyses.

One of the major problems in analyzing and designing squeeze film bearings is that of nonlinearity of the hydrodynamic forces. Since translation of the journal is necessary to produce these forces, knowledge of the motion of the journal is necessary in order to accurately predict the forces which in turn affect the motion of the journal. If small perturbations about the static equilibrium position occur, one set of linear hydrodynamic force coefficients can be calculated (2). If cyclic orbiting about the static

equilibrium position occurs, a second set of linear coefficients, different from the first, can be calculated.

Fortunately, however, reasonable assumptions can be made about the journal motion and careful design techniques can be used to reasonably insure that the assumed journal motion will indeed occur, at least approximately, under normal operating conditions. This combination allows the linear design of dampers to be made to determine the feasibility of the application of squeeze film bearings in a particular situation and to calculate the necessary bearing parameters. The effects of bearing nonlinearity under normal and abnormal operating conditions can be analyzed separately to verify the linear design.

LINEAR DESIGN OF SQUEEZE FILM BEARINGS

For the purpose of a preliminary analysis, it is shown in References (2) and (5) that the general class of rotors described in the preceding section can be modeled as an equivalent single-mass flexible rotor which adequately represents first mode instabilities. The model consists of three components representing the original system: (1) a massless elastic shaft with an attached mass, (2) the bearings and supports, and (3) an equivalent destabilizing force on the rotor mass. The single-mass model is shown in Fig. 3. The major assumptions made are:

(1) The rotor is symmetric about the bearing mid-span.
(2) Mass rotary inertia and gyroscopic effects are negligible.
(3) The two bearings are identical and the coefficients are averaged.

The equivalent single mass representation is shown in Fig. 3. The modal mass and modal rotor stiffness are chosen such that the undamped natural frequency of the equivalent system is the same as that for the original system with rigid bearings. Figure 3 shows only the original bearings. The linearized representation of the squeeze film bearing supports will be subsequently included.

It can be shown (2) (5) that if the bearings do not possess cross coupled forces (as in the case of tilting pad bearings) and that asymmetry in the principal forces is negligible (as in the case of preloaded tilting pad bearings) relationships exist between the ratio of total bearing support to shaft stiffness and minimum unbalance amplification factor and maximum allowable aerodynamic cross coupling.

$$K = \frac{1}{4}\left[-3 + \sqrt{4A_o^2 + 1}\right], \quad A_o^2 > 2 \tag{1}$$

$$K = \frac{m\omega_{cr}}{2q_m} - 1 \tag{2}$$

These relationships assume that the optimum bearing-support damping is present.

Figure 4 schematically illustrates a flexible, damped bearing-support

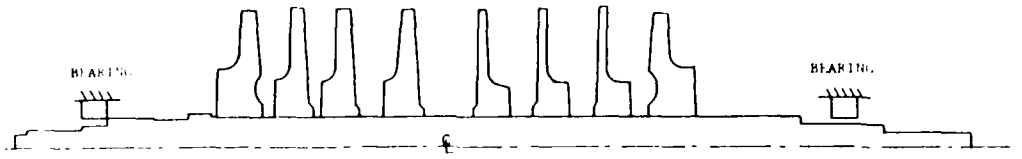

Fig. 1 Schematic of 8-Stage Centrifugal Compressor

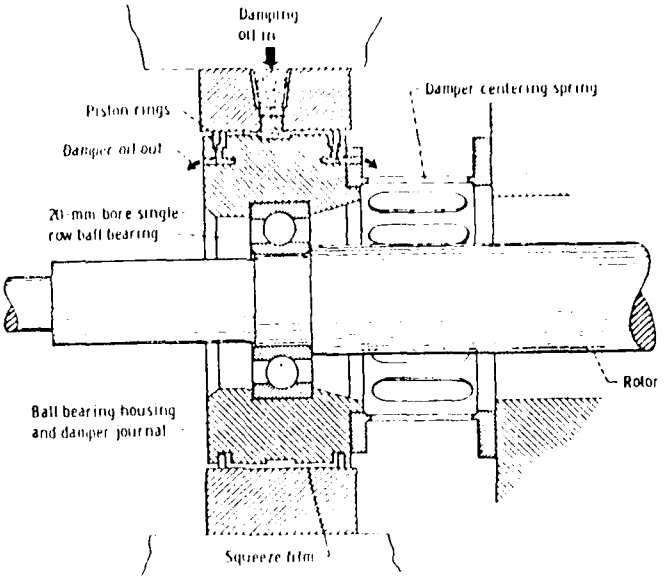

Fig. 2 Axial Cross Section of Squeeze Film Bearing Used in NASA Experimental Work. Ref. (4)

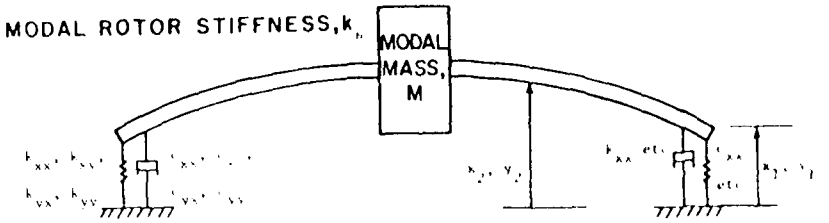

Fig. 3 Schematic of Single Mass Representation of Symmetric Multimass Rotors

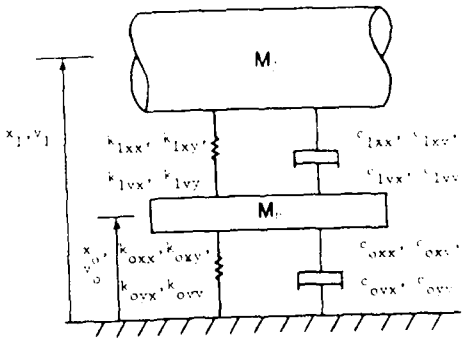

Fig. 4 Schematic of Bearing in Flexible, Damped Supports

component. The bearing and support are represented by general linearized stiffness and damping force coefficients. In many squeeze film bearing applications, the inner bearing mass, m_b, is statically supported in mechanical springs to align and preload the inner bearing within the squeeze film annulus. Therefore, the general support radial stiffness is represented by hydrodynamic stiffness coefficients, k_{oxx} and k_{oyy}, and by the mechanical retainer spring stiffness coefficients, k_{rsx} and k_{rsy}.

Reference (2) presents a completely general set of dynamical equations for the bearing-support system shown in Fig. 4. A set of equivalent linear stiffness and damping coefficients can be obtained from those equations which represent the original system

$$[k_{1e}] = [k_1] - [k_1] [D_r] + (\omega\lambda) [c_1] [D_i] \tag{3}$$

$$[c_{1e}] = [c_1] - [c_1] [D_r] - (1/\omega\lambda) [k_1] [D_i] \tag{4}$$

where

$$[k_i] = \begin{bmatrix} k_{ixx} & k_{ixy} \\ k_{iyx} & k_{iyy} \end{bmatrix} , \quad i = 0, 1$$

$$[c_i] = \begin{bmatrix} c_{ixx} & c_{ixy} \\ c_{iyx} & c_{iyy} \end{bmatrix} , \quad i = 0, 1$$

$[D_r]$ and $[D_i]$ are the real and imaginary parts of $[A]^{-1} [B]$

where

$$[A] = \left[[k_o] + [k_1] + [k_{rs}] - (\omega\lambda)^2 m_b [I] + i(\omega\lambda) \left[[c_o] + [c_1] \right] \right]$$

$$[B] = [k_1] + i(\omega\lambda) [c_1]$$

The design of squeeze film bearing supports for rotor-bearing systems involves the selection of support stiffness and damping coefficients which, in combination with the shaft bearing coefficients, produce overall bearing and support coefficients which will stabilize the system with a given amount of aerodynamic excitation at a given speed and will also result in satisfactory unbalance response characteristics at the unbalance resonant speed.

To conduct the preliminary design of squeeze film bearings for the compressor of Fig. 1, the modal properties must be calculated. These are summarized in Table 1.

TABLE 1 ROTOR PROPERTIES

Total Rotor Weight (W_T)	= 9340.8 N
Modal Weight (W_m)	= 4670.4 N
Operating Speed	= 7,000 RPM
Critical Speed	= 2204 RPM
Shaft Stiffness	= 253821 N/cm

Table 2 lists the stiffness and damping coefficients for the tilting pad bearings with 30% preload and pad clearance of 0.1092 mm.

TABLE 2 TILTING PAD BEARING CHARACTERISTICS

$m = 0.3$, $c_p = 0.1092$ mm

N RPM	k_{1xx} N/cm $x10^{-6}$	k_{1yy} N/cm $x10^{-6}$	c_{1xx} N-s/cm	c_{1yy} N-s/cm
1000	0.1602	5.0370	2070	20428
3000	0.3840	2.9756	1830	6337
5000	0.5749	2.3889	1701	3861
7000	0.7704	2.1109	1687	2986

The anticipated aerodynamic excitation at 7,000 RPM is q = 21024 N/cm. Since the actual level of excitation is unknown, a design value of q = 30,000 N/cm will be used to allow some margin for error. Using a maximum amplification factor of A = 6 at resonance, equations (1) and (2) give the maximum effective bearing-support stiffness values. These are presented in Table 3 together with the optimum effective bearing-support damping required. The optimum damping

TABLE 3
MAXIMUM EFFECTIVE BEARING-SUPPORT STIFFNESS AND OPTIMUM EFFECTIVE DAMPING

Specification	K (max)	k_{1re} N/cm	c_{1re} N-s/cm
$A \leq 6$ at resonance	2.26	286818	1948
$q \geq 30000$ N/cm at 7000 RPM	3.23	409921	2476

is given as (2)

$$c_{1re} = \frac{m\omega_{cr}}{2}\frac{(1+K)}{}\sqrt{\frac{2\ (1+K)}{1+2K}} \tag{5}$$

Equations (3) and (4) can be used to determine the proper squeeze film bearing coefficients. For initial design considerations, the bearing and support coefficients may be considered symmetric. If there is no bearing or support cross coupling, equations (3) and (4) then reduce to scalar equations which can be more easily manipulated. It is necessary, however, to estimate the whirl ratio for stability considerations and unbalance resonant speed for unbalance response considerations. Since the overall effective rotor damping ratio with optimum bearing-support damping is small (2) (5), the first unbalance resonant speed and first damped natural frequency whirl speed are very nearly the same. The whirl ratio, λ, can therefore be accurately approximated as (2)

$$\lambda = \frac{\omega_{cr}}{\omega} \sqrt{\frac{1+2K}{2(1+K)}} \tag{6}$$

This value of λ will be verified by comparison with the value calculated when the effective bearing-support coefficients are used to determine the actual rotor instability threshold. For unbalance response analyses, λ is unity, and the unbalance response resonant speed is predicted to be (2)

$$\omega_d = \omega_{cr} \sqrt{\frac{1+2K}{2(1+K)}} \tag{7}$$

For small perturbations of the journal about the static equilibrium position, the squeeze film bearing does not generate hydrodynamic forces that are represented by linear stiffness coefficients. Any restoring stiffness forces in the squeeze film bearing must be provided by mechanical retainer springs. Furthermore, the principal damping coefficients are symmetric, and cross coupled damping coefficients are zero if the static journal equilibrium position coincides with the bearing center. These characteristics are independent of the squeeze film bearing L/D ratio and may be advantageously used in the design process. By assuming that the squeeze film journal is centrally preloaded statically so that the equilibrium position is at the bearing center, the maximum radial deflection space in all directions in the damper is attained to allow for variations in the static load exerted on the retainer spring under various operating conditions. If the static equilibrium eccentricity ratio of the damper journal approaches unity, the damping coefficients become very large and effectively lock up the support regardless of the retainer spring rate.

For preliminary design purposes, the tilting pad bearing will be considered symmetric and the average stiffness and damping coefficients used. The asymmetry effects will be determined after the preliminary design has been made. The resulting support symmetry will reduce the asymmetry in the

overall effective bearing and support coefficients.

Figures 5 and 6 illustrate the variation in effective stiffness and damping coefficients with support damping for a range of retainer spring rates from 50,000 to 550,000 N/cm. A whirl ratio of $\lambda = 0.30$ was estimated using equation (6) with K = 3.23 from Table 3.. The weight of the tilting pad bearing is 89 N. For support damping less than 1,000 N-s/cm, the effective stiffness coefficient, k_{lre}, is nearly independent of the support damping. Similarly, the effective damping coefficient, c_{lre}, is relatively independent of the support stiffness over the same range of support damping values. For values of support damping greater than c_o = 1,000 N-s/cm, the effective stiffness and damping coefficients increase greatly. As c_o and/or k_{rs} approach infinity, the effective coefficients approach the tilting pad bearing values.

The effective coefficients can be used to determine the amount of allowable rotor aerodynamic excitation. Using the values of k_{lre} to determine K, the maximum allowable values of aerodynamic excitation as a function of support stiffness and damping can be determined. These values are shown in Fig. 7. The allowable aerodynamic excitation was calculated from (2)

$$q = \frac{2a}{(1 + a^2)}\, q_m \tag{8}$$

where q_m is given by equation (2) and a is the ratio of the effective bearing-support damping to the optimum value,

$$a = \frac{2c_{lre}}{m\omega_{cr}(1+K)} \sqrt{\frac{1+2K}{2(1+K)}} \tag{9}$$

As expected, the allowable values of q decrease with increasing retainer spring stiffness, and for each value of k_{rs} there is a value of c_o that maximizes q. From stability considerations alone, minimization of retainer spring stiffness maximizes q and also affords the greatest range of c_o for a given value of q. Figure 8 shows the variation in the optimum value of c_o with retainer spring stiffness and also the maximum value of allowable q for those conditions of k_{rs} and c_o. The retainer spring stiffness must be less than 425,000 N/cm for the rotor to withstand 30,000 N/cm aerodynamic cross coupling.

Figures 9 and 10 show the effective stiffness and damping coefficients for the compressor for unbalance response. An unbalance response resonant speed of 2028 RPM was calculated using equation (7) with K = 2.26 from Table 3. The whirl ratio is $\lambda = 1.0$. The support stiffness consists of the retainer stiffness, k_{rs}, and the hydrodynamic stiffness produced by the squeeze film because of journal orbiting, k_o. The same general variation of effective stiffness and damping occurs. By calculating K for each value of c_o and $(k_{rs} + k_o)$, the amplification factor, A, can be determined (2) from

$$A = \left(\frac{1+a^2}{2a}\right) A_o \tag{10}$$

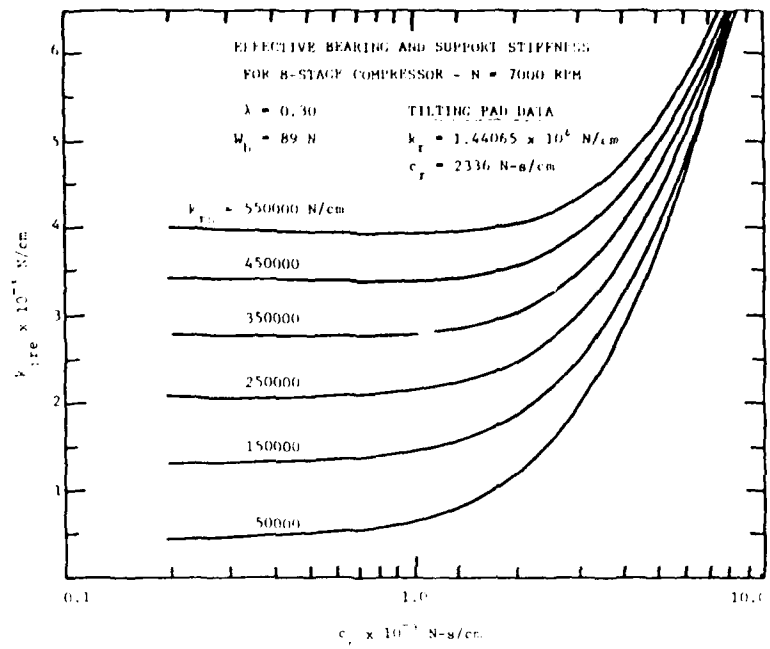
EFFECTIVE BEARING AND SUPPORT STIFFNESS
FOR 8-STAGE COMPRESSOR - N = 7000 RPM
λ = 0.30
W_b = 89 N
TILTING PAD DATA
k_r = 1.44065 x 10^5 N/cm
c_r = 2336 N-s/cm
k_rs = 550000 N/cm
450000
350000
250000
150000
50000
6
5
4
3
2
1
0.1
1.0
10.0

Fig. 5

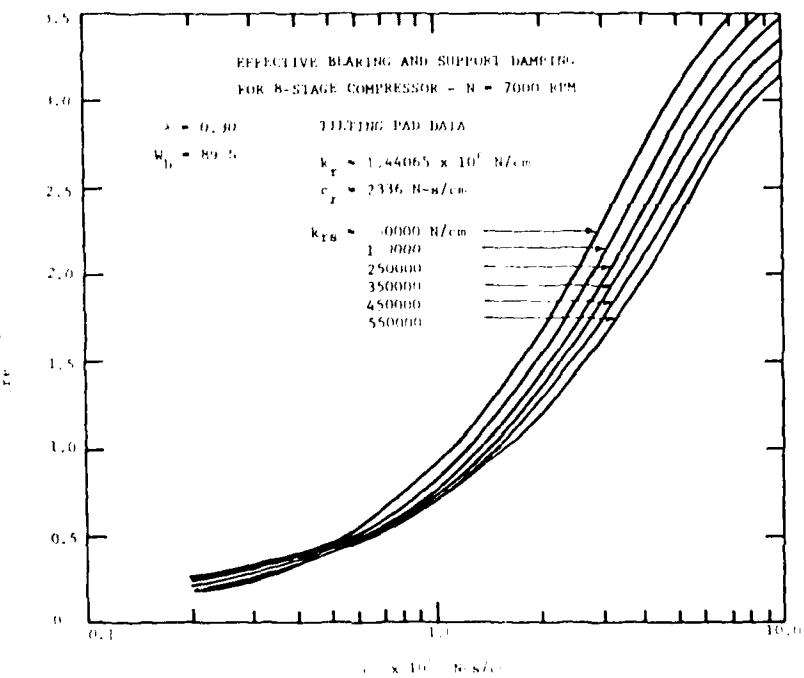
EFFECTIVE BEARING AND SUPPORT DAMPING
FOR 8-STAGE COMPRESSOR - N = 7000 RPM
λ = 0.30
W_b = 89.5
TILTING PAD DATA
k_r = 1.44065 x 10^5 N/cm
c_r = 2336 N-s/cm
k_rs = 550000 N/cm
450000
350000
250000
150000
50000
3.5
3.0
2.5
2.0
1.5
1.0
0.5
0
0.1
1.0
10.0

Fig. 6

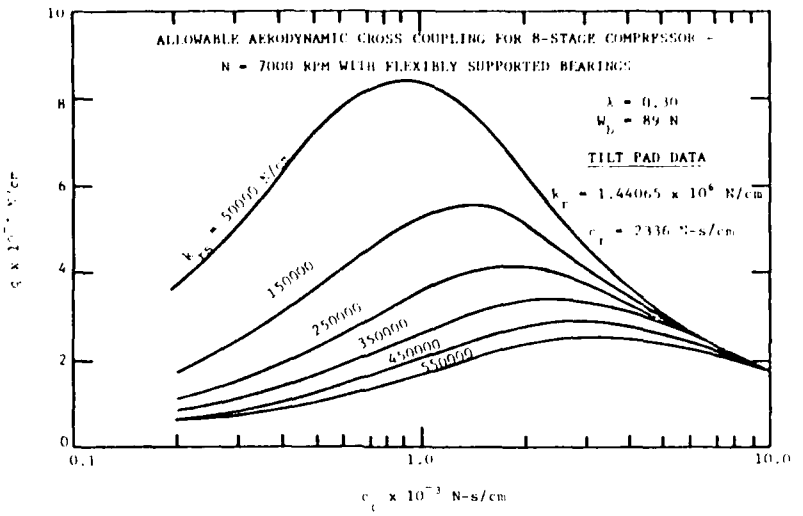
ALLOWABLE AERODYNAMIC CROSS COUPLING FOR 8-STAGE COMPRESSOR -
N = 7000 RPM WITH FLEXIBLY SUPPORTED BEARINGS
λ = 0.30
W_b = 89 N
TILT PAD DATA
k_E = 1.44065 x 10^6 N/cm
c_E = 2336 N-s/cm
k_ES = 50000 N/cm
150000
250000
350000
450000
550000
0.1
1.0
10.0
c_c x 10^-3 N-s/cm

Fig. 7

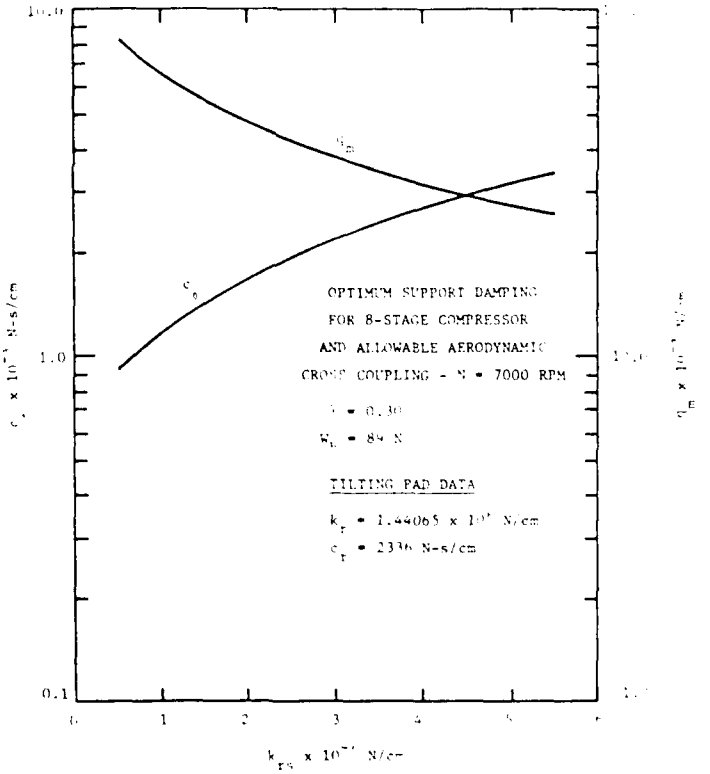
OPTIMUM SUPPORT DAMPING
FOR 8-STAGE COMPRESSOR
AND ALLOWABLE AERODYNAMIC
CROSS COUPLING - N = 7000 RPM
λ = 0.30
W_b = 89 N
TILTING PAD DATA
k_E = 1.44065 x 10^6 N/cm
c_E = 2336 N-s/cm
0.1
1.0
1
2
3
4
k_ES x 10^-4 N/cm

Fig. 8

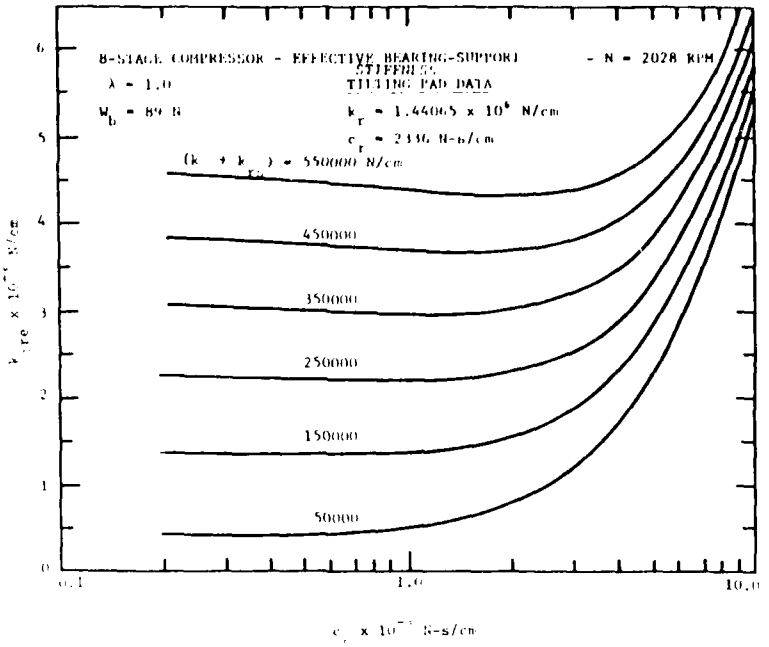
8-STAGE COMPRESSOR - EFFECTIVE BEARING-SUPPORT STIFFNESS
N = 2028 RPM
λ = 1.0
TILTING PAD DATA
W_b = 89 N
k_r = 1.44065 x 10^8 N/cm
c_r = 2336 N-s/cm
(k_xx + k_r) = 550000 N/cm
450000
350000
250000
150000
50000
0
1
2
3
4
5
6
0.1
1.0
10.0

Fig. 9

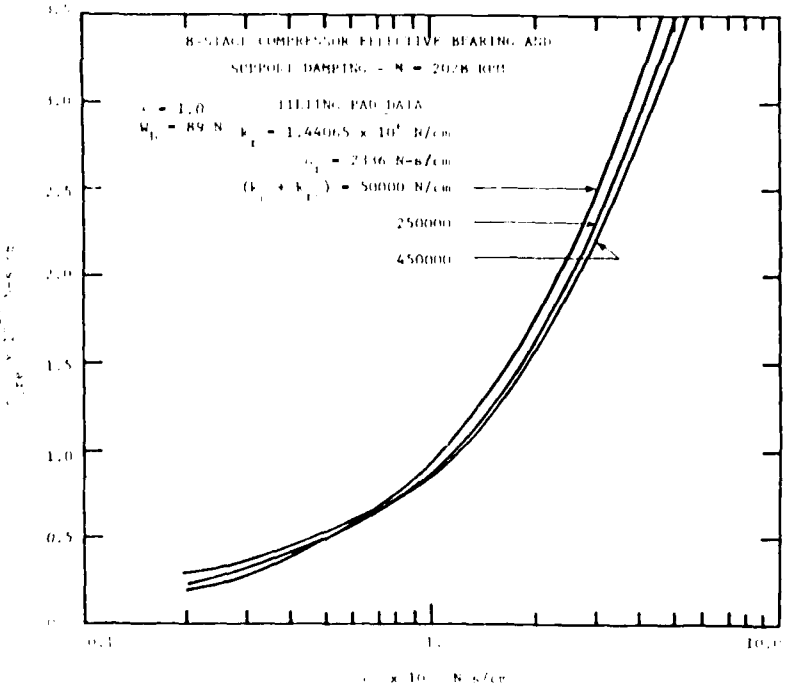
8-STAGE COMPRESSOR EFFECTIVE BEARING AND
SUPPORT DAMPING - N = 2028 RPM
λ = 1.0
TILTING PAD DATA
W_b = 89 N
k_r = 1.44065 x 10^8 N/cm
c_r = 2336 N-s/cm
(k_xx + k_r) = 50000 N/cm
250000
450000
0.5
1.0
1.5
2.0
2.5
3.0
0.1
1.
10.0

Fig. 10

where A_o is given by equation (1).

This is shown as a function of support stiffness and damping in Fig. 11. As in the stability case, amplification factor is improved by reducing the support stiffness. Figure 12 shows the optimum support damping as a function of support stiffness and the maximum amplification factor for those conditions. The total support stiffness must not exceed 325,000 N/cm for an amplification factor of $A \leq 6$.

This information can be used to determine the geometry of the squeeze film bearing support for the 8-stage compressor. The outer surface of the tilting pad bearing housings are to be used as the damper journal surface. The tilting pad bearings have outer dimensions R = 8.26 cm, L = 5.08 cm. The lubricating oil from the tilting pad bearings is to be used with viscosity $\mu = 1.24 \times 10^{-6}$ N-s/cm^2. Using a finite length solution to Reynolds equation (6), the squeeze film damping coefficients are shown in Fig. 13 for both cavitated and uncavitated films. Based upon a cavitated film, the squeeze film damping coefficient for a centrally preloaded journal with circumferential oil supply groove and end seals is

$$\frac{c_o}{\mu L (R/c)^3} = 0.60$$

Using the values for L, R, and μ given above, the damping coefficient as a function of damper clearance is

$$c_o = \frac{2.131 \times 10^{-3}}{c^3} \text{ N-s/cm}$$

where c is in cm.

For unbalance response analyses the squeeze film damping for circular orbiting about the bearing center is identical to the stability coefficient c_{tt} (2)(7). Noting from Fig. 13 that c_{tt} remains relatively constant for eccentricity ratios up to $\varepsilon = 0.4$, the unbalance response specification will be met for an assumed eccentricity of $\varepsilon = 0.4$. Since the stiffness coefficient, k_o, for a circular centered unbalance response orbit increases greatly with increasing orbital amplitude, meeting the unbalance response specification at $\varepsilon = 0.4$ will insure that the hydrodynamic stiffness, k_o, will not be too large over the eccentricity range for which the damping is constant, $0 \leq \varepsilon \leq 0.4$. It is shown in Reference (8) that the nondimensional hydrodynamic stiffness for unbalance response is the same as the nondimensional cross coupled damping coefficient for stability. Hence, for $\varepsilon = 0.4$, Fig. 13 gives

$$\frac{k_o}{\mu L (R/c)^3 \dot{\gamma}} = 0.40$$

Using the previous values of L, R, and μ and taking $\dot{\gamma} = 212$ rad/s (the unbalance response resonant speed), the hydrodynamic squeeze film stiffness

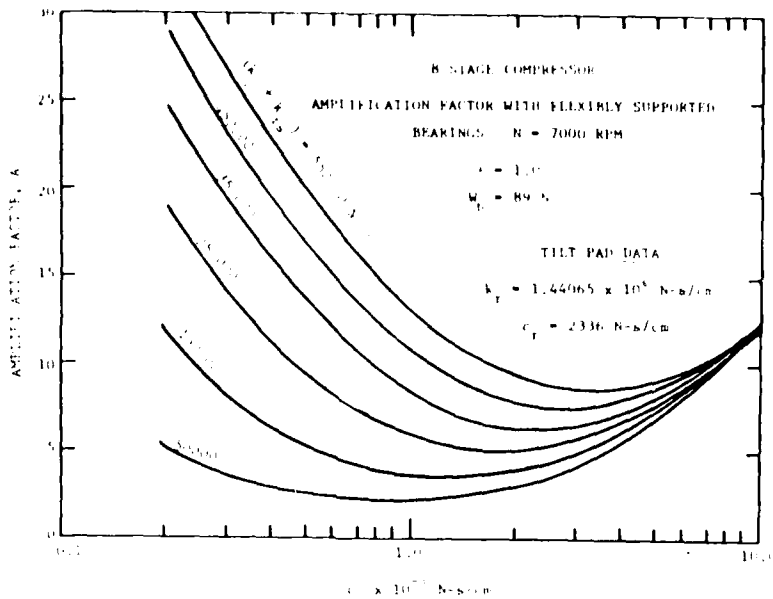
8-STAGE COMPRESSOR
AMPLIFICATION FACTOR WITH FLEXIBLY SUPPORTED
BEARINGS N = 7000 RPM
TILT PAD DATA
25
20
15
10
5
0
1.0

Fig. 11

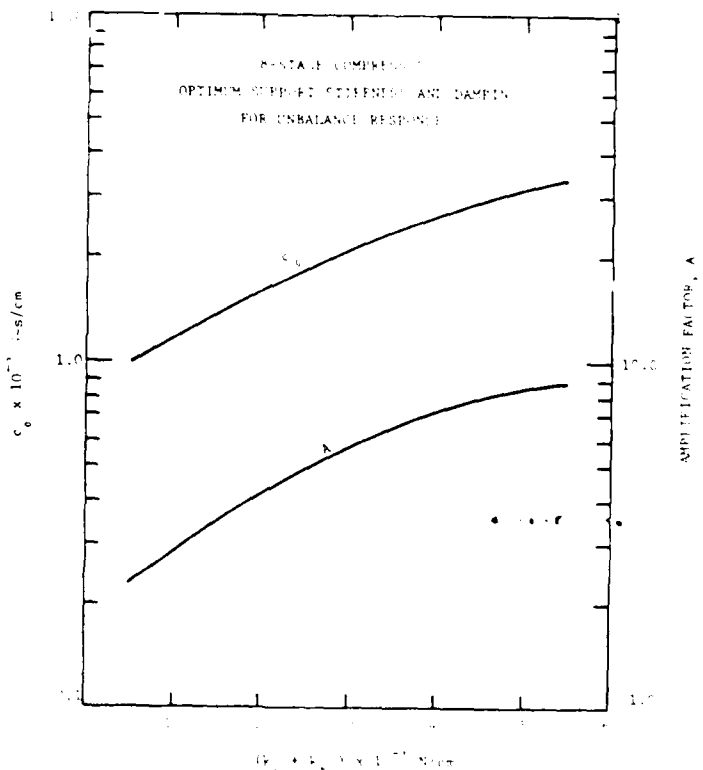
1.0

Fig. 12

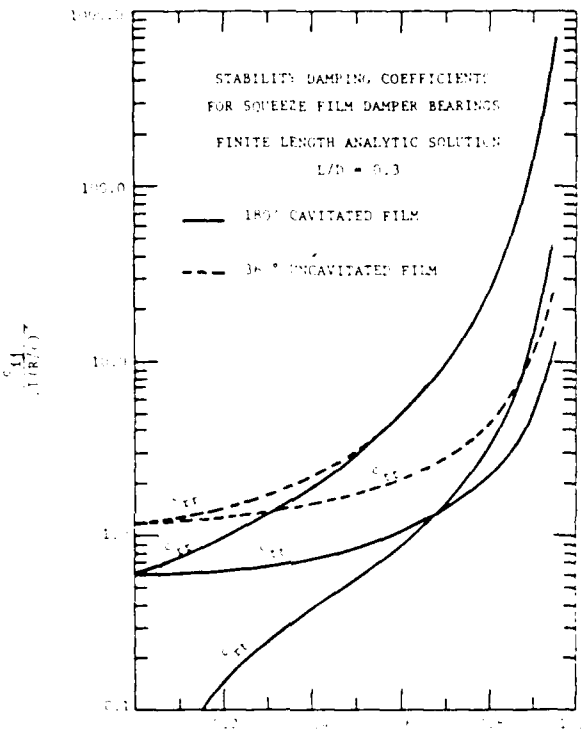
STABILITY DAMPING COEFFICIENTS
FOR SQUEEZE FILM DAMPER BEARINGS
FINITE LENGTH ANALYTIC SOLUTION
L/D = 0.3
180° CAVITATED FILM
360° UNCAVITATED FILM

Fig. 13

for unbalance response is

$$k_o = \frac{0.30}{c^3} \text{ N/cm}$$

where c is in cm. Figure 14 illustrates the variation in the squeeze film damping coefficient, c_o, and the stiffness coefficient for circular orbiting at γ = 0.4 with squeeze film bearing clearance.

The necessary information is now available to determine the as yet unknown damper clearance. From Fig. 11, the maximum value of total support stiffness, which will give an amplification factor of A $\leq$ 6, is determined and is plotted in Fig. 15. Similarly, the maximum value of retainer spring stiffness that will yield an allowable aerodynamic excitation of q $\geq$ 30,000 N/cm is found from Fig. 7 and is also plotted in Fig. 15. These curves are labeled $(k_o + k_{rs})$ max and k_{rs} max respectively. From Fig. 14, the unbalance response stiffness, k_o, is found as a function damping and is also shown in Fig. 15 by the curve labeled k_o. The difference between k_o and $k_o + k_{rs}$ represents the maximum allowable retainer spring stiffness from unbalance response considerations. The intersection of this curve with the stability k_{rs} curve gives values of retainer spring stiffness and squeeze film damping coefficients which will satisfy both the stability and unbalance response specifications. In this case, k_{rs} should not exceed 97500 N/cm and c_o should be 1180 N-s/cm. The damping coefficient is used to determine the damper clearance, which is c = 0.1200 mm.

Figure 16 shows the stability of the 8-stage compressor with k_{rs} = 97500 N/cm and c_o = 1180 N-s/cm using the actual asymmetric tilting pad bearing data. The whirl ratio, γ, was determined iteratively and is γ = 0.27 at the operating speed N = 7000 RPM. At the operating speed parameter, Ω_o = 2.45, the rotor can withstand Q = 0.3125 or q = 66815 N/cm aerodynamic excitation. Due to the restriction of retainer stiffness from unbalance response considerations, k_{rs} is sufficiently low to allow more than twice the design target value. For comparison, the stability of the rotor without squeeze film bearings is shown by the dashed curve. It is observed that the addition of squeeze film bearings has increased the allowable aerodynamic excitation by 650%.

The maximum allowable aerodynamic excitation as a function of rotor speed from 1000 to 7000 RPM is shown in Fig. 17. A very large margin between assumed and allowable excitation exists throughout the rotor operating speed range.

The squeeze film bearing design was based on a centrally preloaded, 180 deg cavitated bearing. If the static rotor load is such that static equilibrium position is eccentric, the squeeze film damping coefficients are no longer symmetric and cross coupled damping exists in the cavitated case. Figure 18 shows the allowable aerodynamic excitation for the 8-stage compressor at 7000 RPM for non-centrally preloaded dampers. The orientation of the damper journal eccentricity vector was chosen to be 315 deg with respect to the horizontal x-axis for convenience. Figure 18 shows a decrease in allowable aerodynamic excitation with increasing static equilibrium

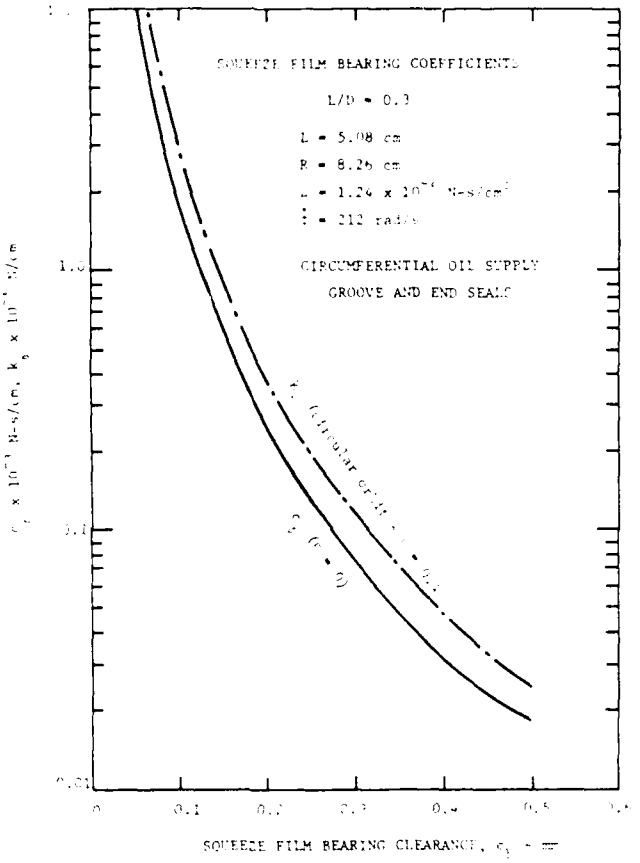
SQUEEZE FILM BEARING COEFFICIENTS
L/D = 0.3
L = 5.08 cm
R = 8.26 cm
CIRCUMFERENTIAL OIL SUPPLY
GROOVE AND END SEALS
1.0
0.1
0.01
0
0.1
0.2
0.3
0.4
0.5
SQUEEZE FILM BEARING CLEARANCE,

Fig. 14

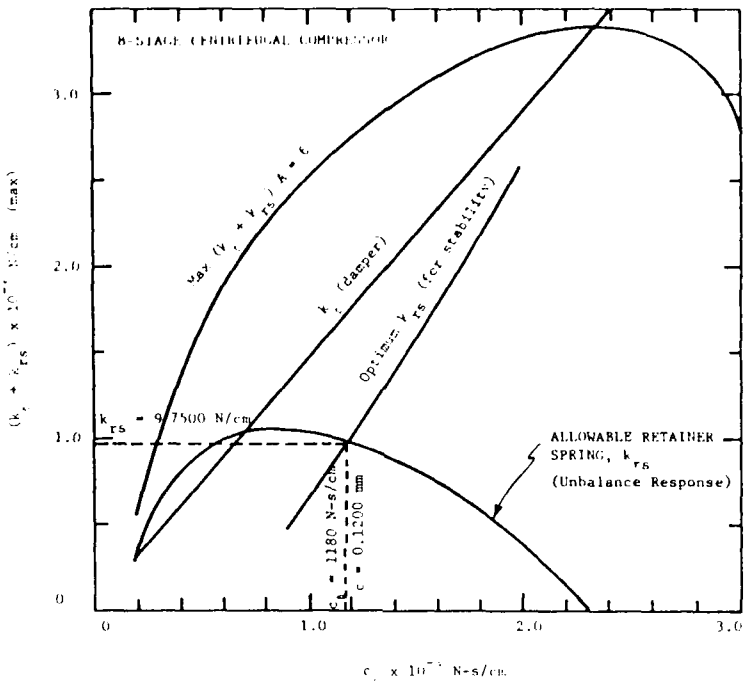
8-STAGE CENTRIFUGAL COMPRESSOR
3.0
2.0
1.0
0
1.0
2.0
3.0
k_{rs} = 97500 N/cm
k_d (damper)
Optimum γ_{rs} (for stability)
ALLOWABLE RETAINER SPRING, k_{rs} (Unbalance Response)
c_d = 1180 N-s/cm
c = 0.1200 mm

Fig. 15

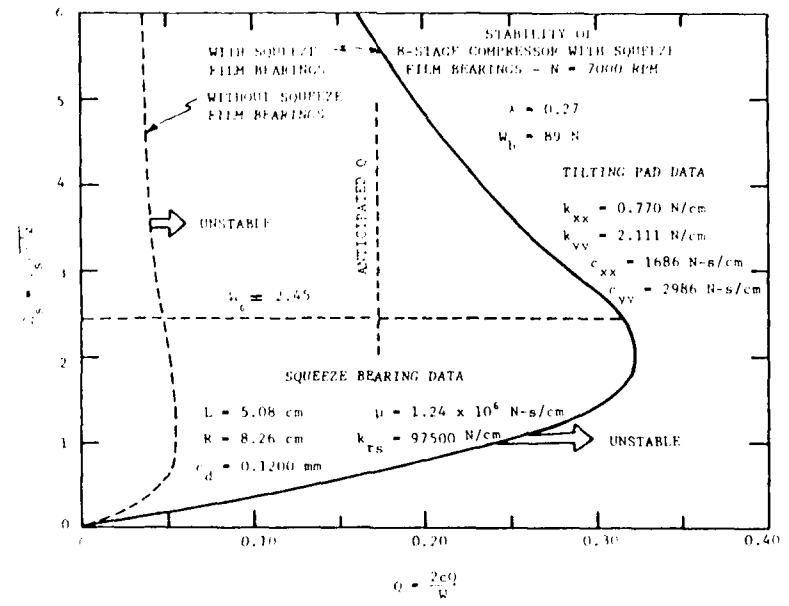
STABILITY OF 8-STAGE COMPRESSOR WITH SQUEEZE FILM BEARINGS - N = 7000 RPM
WITH SQUEEZE FILM BEARINGS
WITHOUT SQUEEZE FILM BEARINGS
UNSTABLE
ANTICIPATED C
γ_c = 2.45
A = 0.27
W_b = 89 N
TILTING PAD DATA
k_{xx} = 0.770 N/cm
k_{yy} = 2.111 N/cm
c_{xx} = 1686 N-s/cm
c_{yy} = 2986 N-s/cm
SQUEEZE BEARING DATA
L = 5.08 cm
R = 8.26 cm
c_d = 0.1200 mm
μ = 1.24 x 10^6 N-s/cm
k_{rs} = 97500 N/cm
UNSTABLE
0
1
2
3
4
5
6
0.10
0.20
0.30
0.40
$Q = \frac{2cQ}{W}$

Fig. 16

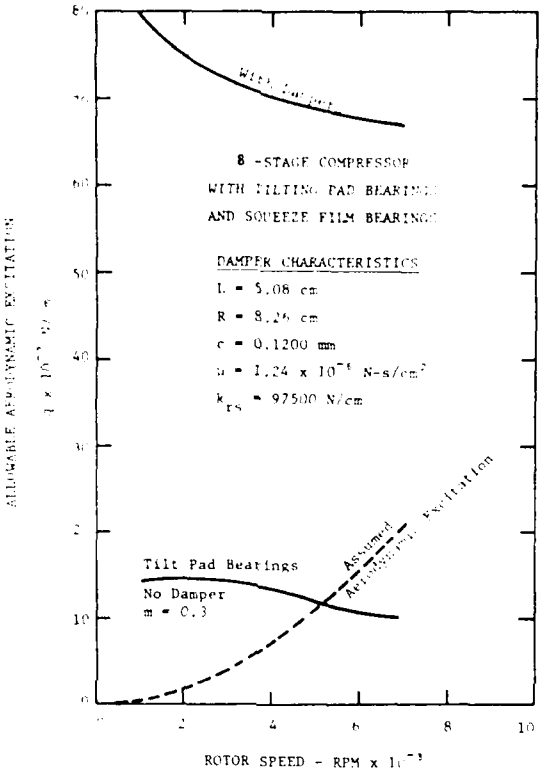

Fig. 17 Allowable Aerodynamic Excitation for 8-Stage Compressor with Squeeze Film Bearings

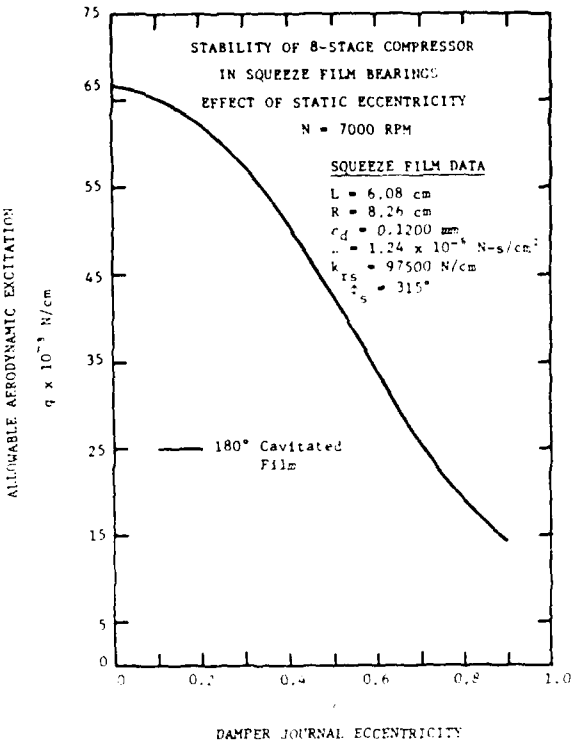
STABILITY OF 8-STAGE COMPRESSOR
IN SQUEEZE FILM BEARINGS
EFFECT OF STATIC ECCENTRICITY
N = 7000 RPM
SQUEEZE FILM DATA
L = 6.08 cm
R = 8.26 cm
c_d = 0.1200 mm
μ = 1.24 x 10^{-6} N-s/cm^2
k_{rs} = 97500 N/cm
θ_s = 315°
180° Cavitated Film
ALLOWABLE AERODYNAMIC EXCITATION
q x 10^{-3} N/cm
75
65
55
45
35
25
15
5
0
0
0.2
0.4
0.6
0.8
1.0
DAMPER JOURNAL ECCENTRICITY

Fig. 18

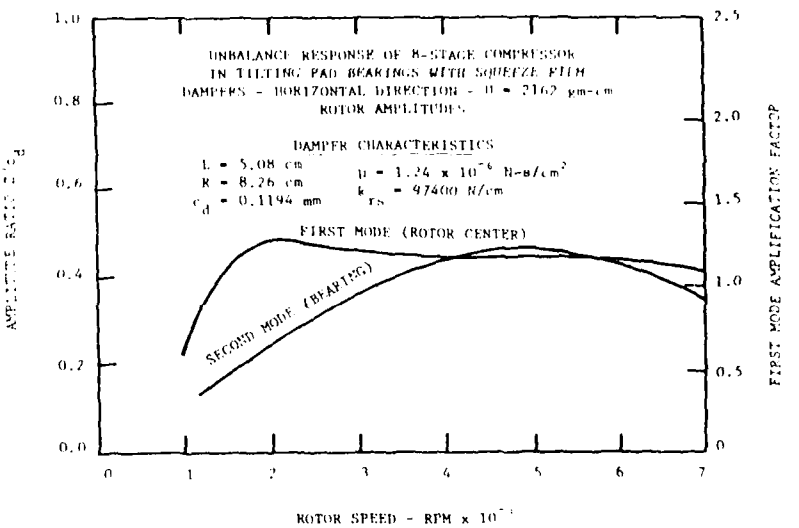
UNBALANCE RESPONSE OF 8-STAGE COMPRESSOR
IN TILTING PAD BEARINGS WITH SQUEEZE FILM
DAMPERS - HORIZONTAL DIRECTION - U = 2162 gm-cm
ROTOR AMPLITUDES
DAMPER CHARACTERISTICS
L = 5.08 cm
R = 8.26 cm
c_d = 0.1194 mm
μ = 1.24 x 10^{-6} N-s/cm^2
k_{rs} = 97400 N/cm
FIRST MODE (ROTOR CENTER)
SECOND MODE (BEARING)
1.0
0.8
0.6
0.4
0.2
0.0
2.5
2.0
1.5
1.0
0.5
0
FIRST MODE AMPLIFICATION FACTOR
0
1
2
3
4
5
6
7
ROTOR SPEED - RPM x 10^{-3}

Fig. 19

eccentricity. If $\varepsilon \geq 0.65$, the rotor will be unstable with $q \geq 30{,}000$ N/cm.

NONLINEAR UNBALANCE RESPONSE ANALYSIS

The design of squeeze film bearing supports was based upon both stability and unbalance response considerations. The near constancy of the squeeze film bearing damping coefficient for circular centered unbalance response orbits over the range $0 \leq \varepsilon \leq 0.4$ was used as a design criterion to select retainer spring stiffness coefficients. Since the equivalent squeeze film hydrodynamic stiffness coefficient is extremely nonlinear with respect to the amplitude of the forced response orbit, it is not certain from the analysis that the unbalance response vibration amplitude will necessarily meet the unbalance response specification.

Furthermore, the assumption of circular centered orbiting of the squeeze film bearing journal was based on the supposition that the static forces on the rotor were known and could be counteracted by preload forces on the journal. Static forces, in fact, are a function not only of the rotor weight, but also of interaction of the rotor with the working fluid and are not generally well known even under normal operating flow conditions. The static forces, therefore, may vary greatly over the machine operating speed range.

It is desirable to verify the linear squeeze film bearing design for nonlinear forced response with circular centered orbiting and for stability and forced response about a noncentered journal equilibrium position. The first case can be treated using steady-state response techniques whereas the second requires time transient simulation. Both steady-state response and time transient simulation have been used to analyze squeeze film supported rotors, but the response of anti-symmetric modes to unbalance and the effect of loss of journal preload have generally been neglected.

One of the major assumptions made to reduce the general multimass two-bearing rotor to a single-mass system was that the anti-symmetric rotor modes are generally well damped and may be neglected from the equations of motion. With this assumption, the motion at each end of the rotor is the same because of the symmetry of the rotor model. From stability considerations, this assumption is justified because instability of the system is almost always associated with the first damped natural frequency of the system (3). It is not clear, however, that the anti-symmetric modes will be well damped for forced vibrations although intuitively one might suspect that they would be based upon the arguments concerning forced first mode response. Even though the stability of higher modes may not be in question, it is conceivable that they may be excited by external forcing functions. It is important to verify the bearing-support designs for a particular rotor to insure that large forced vibrations do not occur within the operating speed range.

Table 4 shows the unbalance distribution used to analyze the nonlinear response for the first two modes of vibration for the 8-stage compressor.

TABLE 4 ROTOR UNBALANCE DISTRIBUTION

DISTRIBUTION	ROTOR MASS LOCATION		
	Quarter Span	Half Span	Three Quarter Span
First Mode	0	2162 gm-cm @ 0°	0
Second Mode	1081 gm-in.@ 0°	0	1081 gm-cm @ 180°

The rotor and damper journal amplitudes for the horizontal direction are shown in Figs. 19 and 20. Both the first and second mode horizontal amplitudes are low throughout the rotor speed range. The first mode horizontal amplification factor is less than A = 1.3 throughout the speed range, which is well below the design target of A = 6. The squeeze film journal eccentricity ratio is relatively constant at $\varepsilon = 0.2$ for the first mode and does not exceed $\varepsilon = 0.25$ for the second mode. Figures 21 and 22 illustrate the vertical response. The maximum vertical first mode amplification factor is A = 2.5 at 2000 RPM, and the second vertical mode is well damped with a maximum amplitude of 5.2×10^{-3} cm. The vertical damper amplitude for the first mode is $\varepsilon = 0.32$ for both the first and second vertical modes.

The forces transmitted through the squeeze film bearing are shown in Figs. 23 and 24. The maximum horizontal force and vertical force are 2800 and 4100 N at 6000 RPM with the second mode unbalance distribution. For both horizontal and vertical modes, the dynamic force transmissibility is less than unity at the operating speed indicating good force attenuation. The forces produced would be considerably less for normal unbalance magnitudes. It is concluded that the squeeze film bearing design is acceptable from unbalance response considerations for centrally preloaded circular orbiting.

Since both the stability and unbalance response specifications are met with a wide margin, it appears to be possible to increase both the retainer spring stiffness and squeeze film bearing clearance to aid in preloading the rotor and to prevent eccentric damper journal operation under large static loads.

NONLINEAR TRANSIENT ANALYSIS

Figure 25 shows the transient response of the squeeze film bearing journal and rotor center for the fully preloaded squeeze film bearing ($\varepsilon_{s_o} = 0.0$). The unbalance is zero and an aerodynamic excitation of $q_s = 105071$ N/cm is assumed to act at the rotor center. The motion of the tilting pad journals is almost identical to that of the squeeze film journal since the average tilting pad bearing radial stiffness is about 10 times the squeeze film bearing retainer spring stiffness. After an initial perturbation of the system, Fig. 25 shows that the motion is still confined to the vicinity of the static equilibrium position and the system is stable.

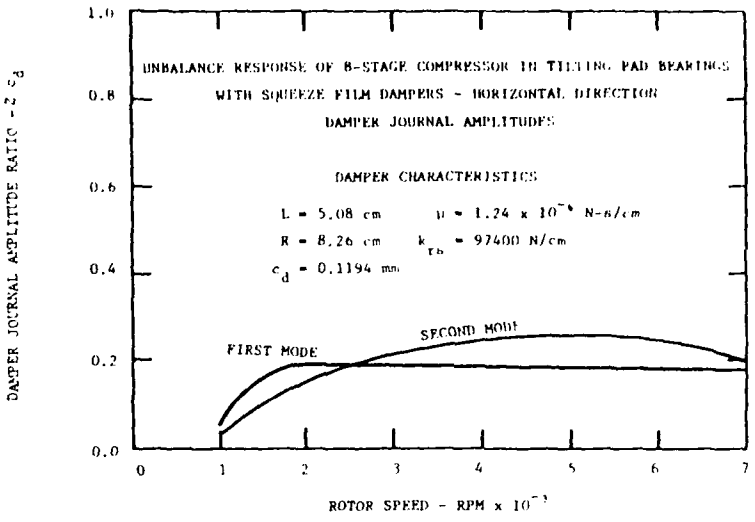
UNBALANCE RESPONSE OF 8-STAGE COMPRESSOR IN TILTING PAD BEARINGS
WITH SQUEEZE FILM DAMPERS - HORIZONTAL DIRECTION
DAMPER JOURNAL AMPLITUDES
DAMPER CHARACTERISTICS
L = 5.08 cm
R = 8.26 cm
c_d = 0.1194 mm
$\mu = 1.24 \times 10^{-6}$ N-s/cm
k_{rb} = 97400 N/cm
FIRST MODE
SECOND MODE
DAMPER JOURNAL AMPLITUDE RATIO - $2/c_d$
ROTOR SPEED - RPM x 10^{-3}

Fig. 20

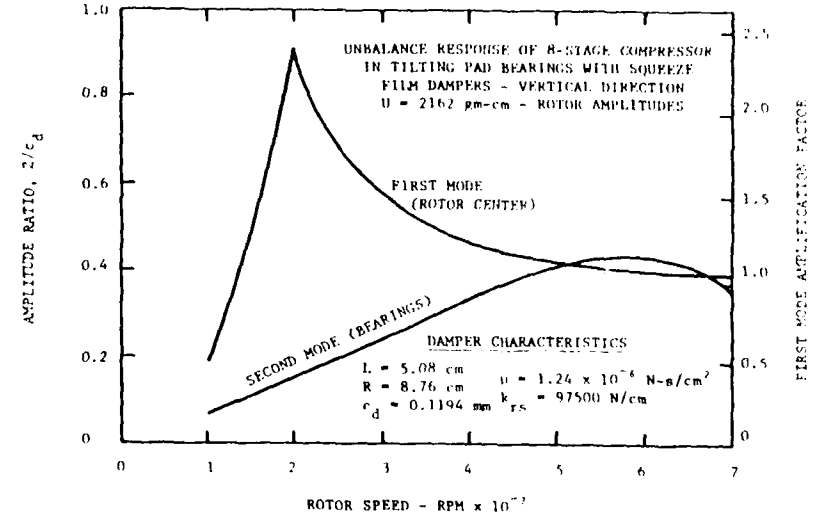
UNBALANCE RESPONSE OF 8-STAGE COMPRESSOR
IN TILTING PAD BEARINGS WITH SQUEEZE
FILM DAMPERS - VERTICAL DIRECTION
U = 2162 gm-cm - ROTOR AMPLITUDES
FIRST MODE
(ROTOR CENTER)
SECOND MODE (BEARINGS)
DAMPER CHARACTERISTICS
L = 5.08 cm
R = 8.76 cm
c_d = 0.1194 mm
$\mu = 1.24 \times 10^{-6}$ N-s/cm^2
k_{rs} = 97500 N/cm
AMPLITUDE RATIO, $2/c_d$
FIRST MODE AMPLIFICATION FACTOR
ROTOR SPEED - RPM x 10^{-3}

Fig. 21

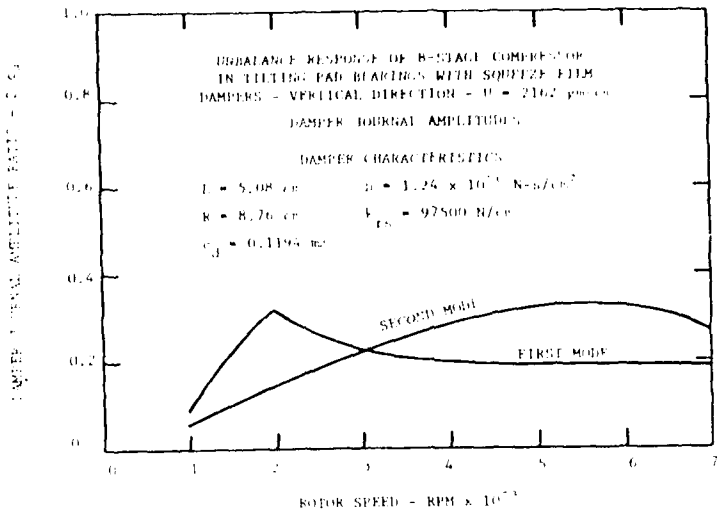
UNBALANCE RESPONSE OF 8-STAGE COMPRESSOR
IN TILTING PAD BEARINGS WITH SQUEEZE FILM
DAMPERS - VERTICAL DIRECTION - U = 210.2 gm-cm
DAMPER JOURNAL AMPLITUDE
DAMPER CHARACTERISTICS
L = 5.08 cm
R = 8.26 cm
c_b = 0.1194 mm
μ = 1.24 x 10^{-5} N-s/cm^2
k_{FS} = 92500 N/cm
SECOND MODE
FIRST MODE
0
0.2
0.4
0.6
0.8
1.0
1
2
3
4
5
6
7
ROTOR SPEED - RPM x 10^{-3}

Fig. 22

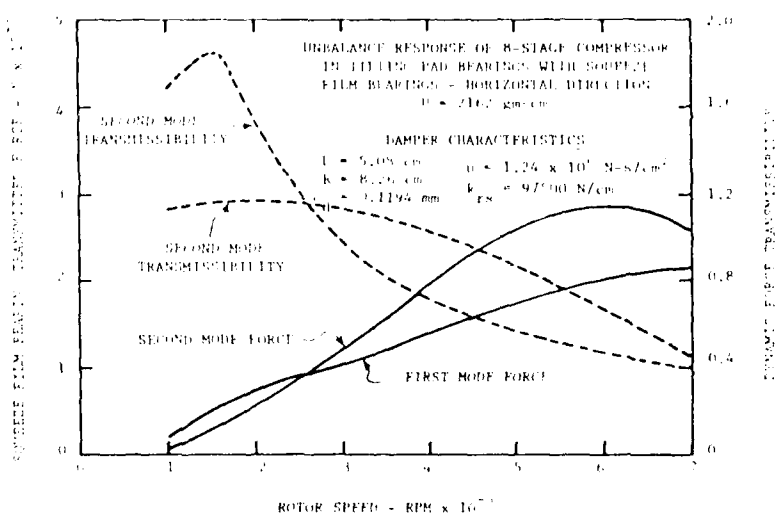
UNBALANCE RESPONSE OF 8-STAGE COMPRESSOR
IN TILTING PAD BEARINGS WITH SQUEEZE
FILM BEARINGS - HORIZONTAL DIRECTION
U = 210.2 gm-cm
DAMPER CHARACTERISTICS
L = 5.08 cm
R = 8.26 cm
c_b = 0.1194 mm
μ = 1.24 x 10^{-5} N-s/cm^2
k_{FS} = 92500 N/cm
SECOND MODE TRANSMISSIBILITY
SECOND MODE TRANSMISSIBILITY
SECOND MODE FORCE
FIRST MODE FORCE
0
1
2
3
4
5
6
0
0.4
0.8
1.2
1.6
2.0
ROTOR SPEED - RPM x 10^{-3}

Fig. 23

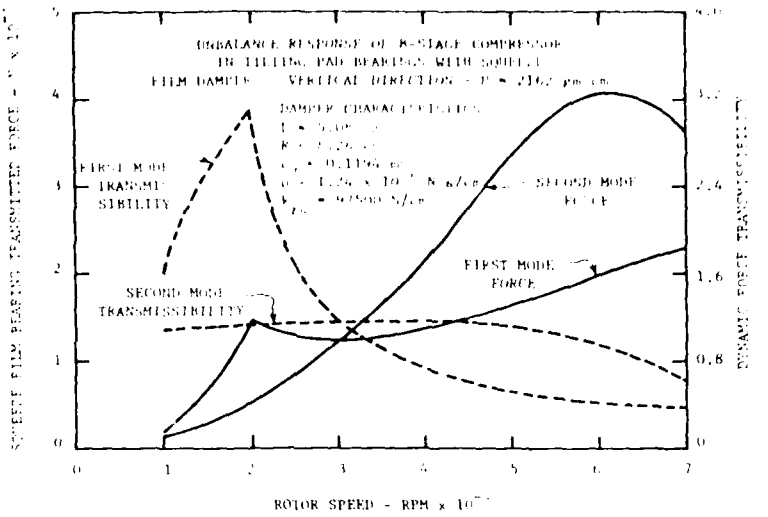
FIRST MODE
TRANSMI
SIBILITY
SECOND MODE
TRANSMISSIBILITY
FIRST MODE
FORCE
SECOND MODE
FORCE
ROTOR SPEED - RPM x 10

Fig. 24

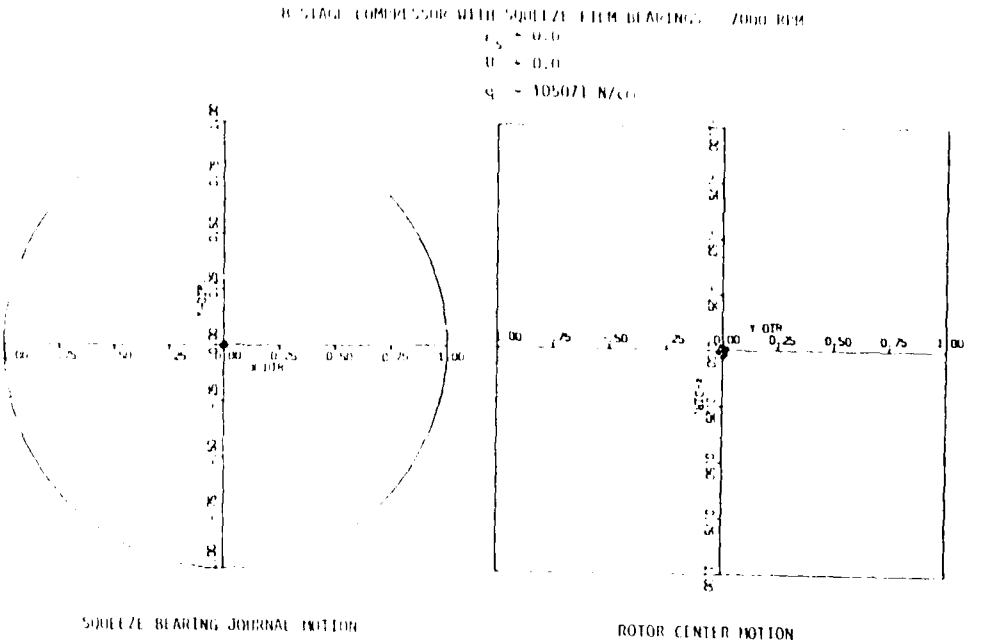
SQUEEZE BEARING JOURNAL MOTION
ROTOR CENTER MOTION

Fig. 25

Figure 26 shows the motion for the same conditions except that the aerodynamic excitation has been increased to q = 113827 N/cm. The system is observed to be unstable with fractional frequency whirl motion as shown by the small dots on the orbital trajectory which indicate the position after each shaft rotation. The amount of aerodynamic excitation required to produce instability is between 105071 and 113827 N/cm. This is larger than the value of 66000 N/cm which was obtained from linear theory. The increases in allowable aerodynamic excitation is due to the added mass at the ends of the rotor and to the relatively low retainer spring stiffness.

Figures 27 and 28 show the steady state response for a static equilibrium position of the squeeze journal of ε_s = 0.0600 mm). This static equilibrium position was produced by placing an unidirectional load of 476 N on the damper journal. The equilibrium attitude angle is ϕ_s = 315 deg. Figure 27 shows the steady state motion with a rotor unbalance of 216 gm-cm. The journal undergoes very small orbiting about the static equilibrium position. The rotor center orbits with a peak-to-peak amplitude of about 0.0085 mm. In Fig. 28 the unbalance has been increased to 2162 gm-cm. Both the journal and rotor center amplitudes have increased (nonlinearly) and the center of the orbits have shifted toward the bearing center by about 0.02 mm. This is a nonlinear effect of the squeeze film bearing and shows that although the forces are velocity dependent, there is net lifting force acting on the journal to counteract the static loading.

Figure 29 shows the resulting unstable motion with an aerodynamic excitation of q = 96315 N/cm acting on the rotor. The static equilibrium position is ε_s = 0.5, ϕ_s = 315 deg, and the unbalance is zero. This figure shows the reduction in allowable aerodynamic excitation with increasing static load (96000 N/cm compared with 110000 N/cm for ε_s = 0.0). The percentage reduction indicated by the transient analysis is less than that predicted using linear theory due to the additional mass in the transient representation.

Figure 30 shows the transient motion with q = 26250 N/cm acting on the rotor and ε_s = 1.0. This is about 2.5 times that predicted with rigidly mounted tilting pad bearings. The system is observed to be stable with an unbalance of 2162 gm-cm. With an aerodynamic excitation of q = 61250 N/cm, the rotor has become unstable as shown in Fig. 31. Although the allowable aerodynamic excitation is larger than that predicted with rigid supports, this also indicates the reduction in allowable excitation with increasing static load.

CONCLUSIONS

(1) The hydrodynamic squeeze film bearing provides a suitable option for stabilizing rotor-bearing systems provided the shaft flexibility is not too high.

(2) The design of nonlinear squeeze film bearing supports based on the assumption of a centrally preloaded squeeze film journal provides reasonable design values for squeeze film bearing geometry and journal retainer spring rates.

8 STAGE COMPRESSOR WITH SQUEEZE FILM BEARINGS - 7000 RPM

ϵ_s = 0.0

U = 0.0

q = 113827 N/cm

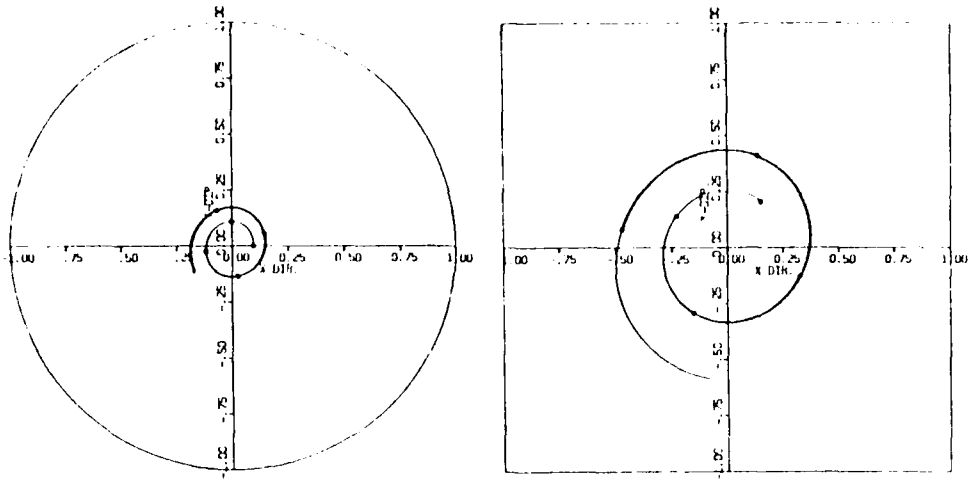

SQUEEZE BEARING JOURNAL MOTION

ROTOR CENTER MOTION

Fig. 26

8-STAGE COMPRESSOR WITH SQUEEZE FILM BEARINGS - 7000 RPM

ϵ_s = 0.5 ϕ_s = 31°

U = 216 gm cm

q = 0.0

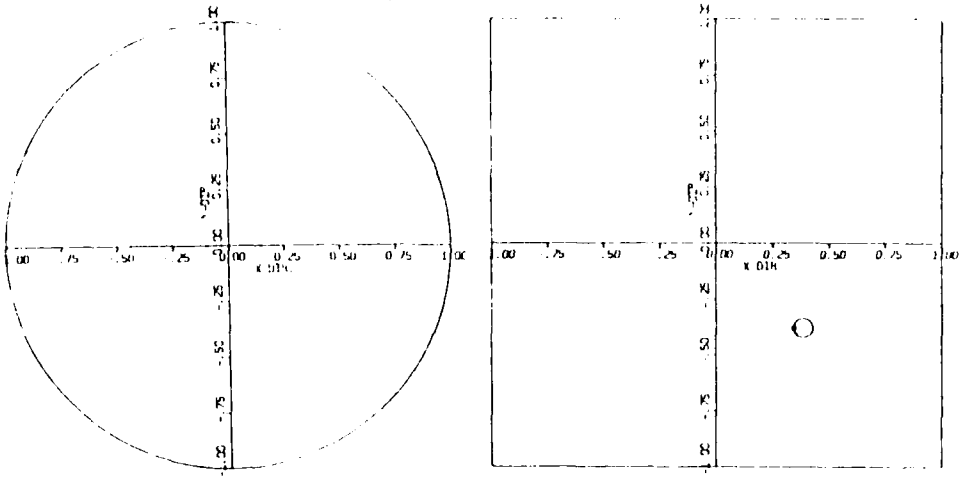

SQUEEZE BEARING JOURNAL MOTION

ROTOR CENTER MOTION

Fig. 27

8 STAGE COMPRESSOR WITH SQUEEZE FILM BEARINGS - 7000 RPM

c_s = 0.5 ϕ_s = 0°

U = 2162 cm/sec

q = 0.0

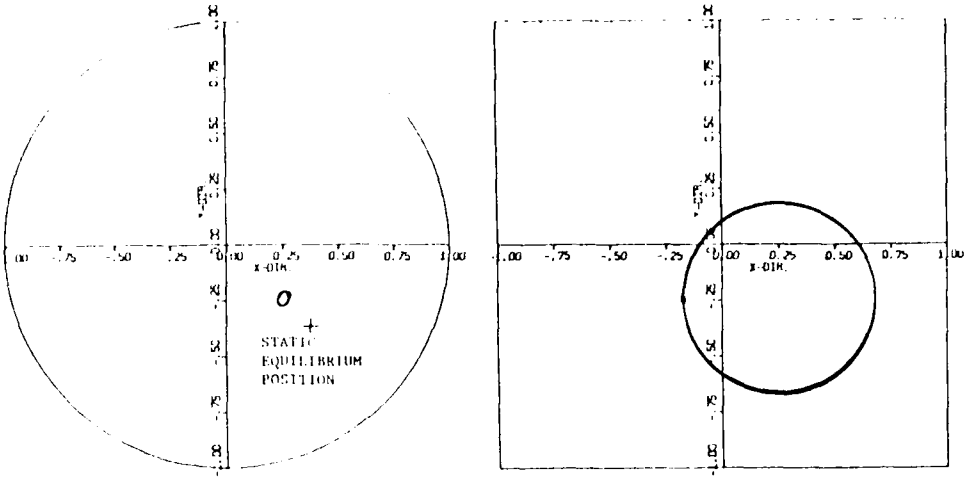

SQUEEZE BEARING JOURNAL MOTION ROTOR CENTER MOTION

Fig. 28

8 STAGE COMPRESSOR WITH SQUEEZE FILM BEARINGS - 7000 RPM

c_s = 0.5 ϕ_s = 0°

U = 2162 cm/sec

q = 96.815 N/cm

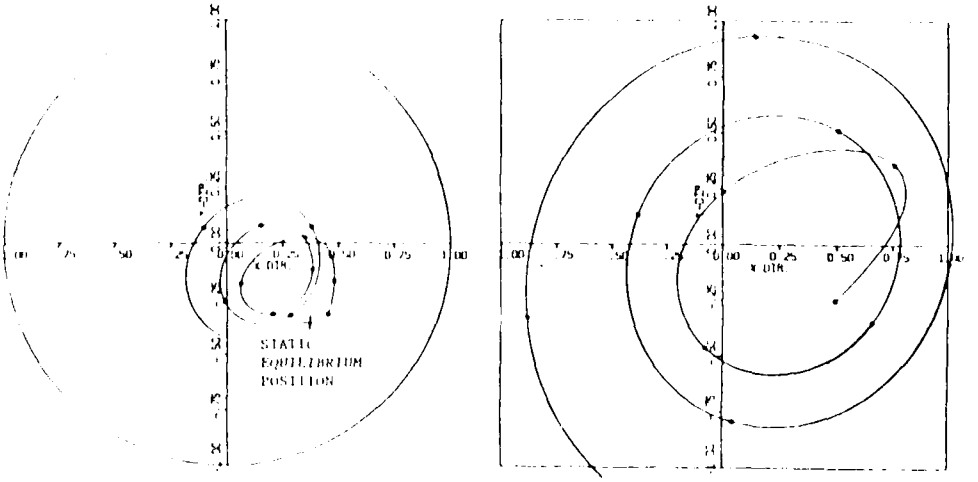

SQUEEZE BEARING JOURNAL MOTION ROTOR CENTER MOTION

Fig. 29

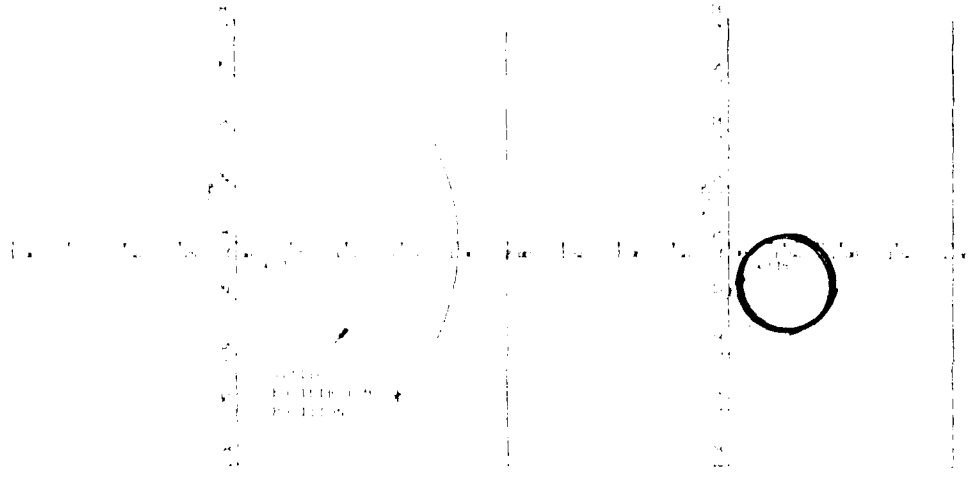

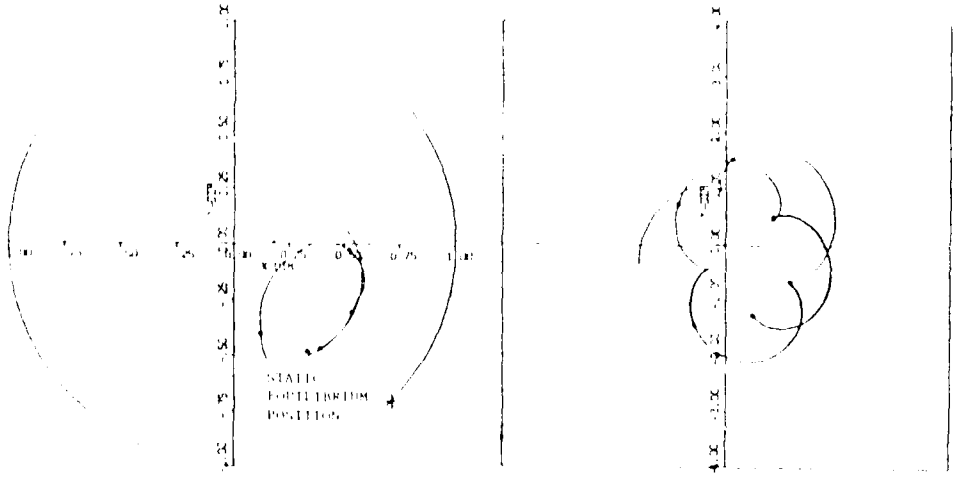

(3) For squeeze film bearings optimized for centrally preloaded operation and cavitated films, loss of preload decreases the allowable rotor aerodynamic excitation.

(4) Specifications on unbalance response amplification factor and aerodynamics excitation levels can be effectively used to determine suitable bearing and support stiffness and damping requirements and can be used to obtain squeeze film bearing geometry and retainer spring rates.

(5) Squeeze film bearings having suitable nonlinear response characteristics for centrally preloaded operation can be designed using linear characteristics for circular unbalance orbiting at a journal eccentricity ratio of $\varepsilon = 0.4$.

(6) Well designed systems for first mode stability and unbalance response are also generally well behaved with second and third mode unbalance excitations.

(7) Steady state orbits of noncentrally preloaded squeeze film bearings with cavitation move toward the bearing center with increasing unbalance forces. Thus unbalance tends to counteract the static forces and act as a dynamic preloading mechanism mechanism.

(8) Unbalance increases the allowable aerodynamic excitation on a rotor with squeeze film bearing supports with eccentric static equilibrium positions because of the dynamic preload with cavitation.

ACKNOWLEDGEMENT

The research reported herein was supported jointly by the U. S. Army Research Office, Grant No. DAG-29-77-C-0009, Dr. Edward Saibel, Project Monitor; NASA Lewis Research Center, Grant No. NSG-3105, Mr. Albert Kascak, Project Monitor; University of Virginia Industrially Supported Program on the Dynamic Analysis of Turbomachinery, Dr. E. J. Gunter, Director.

REFERENCES

1 Nicholas, J. C., Gunter, E. J., and Allaire, P. E., "Stiffness and Damping Coefficients for the Five-Pad Tilting-Pad Bearing," Trans. ASLE, Paper No. 77-LC-3A-2, 1977.

2 Barrett, L. E., "Stability and Nonlinear Response of Rotor-Bearing Systems with Squeeze Film Bearings," Ph.D. Dissertation, University of Virginia, August 1978.

3 Lund, J. W., "Stability and Damped Critical Speeds of a Flexible Rotor in Fluid Film Bearings," Trans. ASME, Journal of Engineering for Industry, Vol. 96, 1974, pp. 509-517.

4 Cunningham, R. E., Fleming, D. P., and Gunter, E. J., "Design of a Squeeze Film Damper for a Multimass Flexible Rotor," Trans. ASME, Journal of Engineering for Industry, 1976.

5 Barrett, L. E., Gunter, E. J., and Allaire, P. E., "Optimum Bearing

and Support Damping for Unbalance Response and Stability of Turbo-machinery," Trans. ASME, Journal of Engineering for Power, Jan. 1978, pp. 89-94.

6 Allaire, P. E., Barrett, L. E., and Gunter, E. J., "Variational Method for Finite Length Squeeze Film Damper Dynamics with Applications," Wear, No. 42, 1977, pp. 9-22.

7 Barrett, L. E. and Gunter, E. J., "Steady State and Transient Analysis of a Squeeze Film Bearing for Rotor Stability," NASA CR-2548, May 1975.

8 Kirk, R. G. and Gunter, E. J., "Nonlinear Transient Analysis of Multi-mass Flexible Rotors - Theory and Application," NASA CR-2300, September 1973.

CALCULATION OF THE FORCES IN A CLOSED-END SQUEEZE FILM DAMPER

by

Dr. B.J. Stephens

Senior Analytical Engineer
Pratt & Whitney Aircraft
Government Products Division
P. O. Box 2691
West Palm Beach, Fla. 33402

ABSTRACT

This paper presents a method for determining the forces generated in a closed-end squeeze film damper as a function of the location and velocity of the journal and damper geometry. This method, which follows the "long bearing" simplification of the incompressible Reynolds equation with steady fluid properties, uses a numerical integration scheme to calculate the resulant forces once the discrete pressure distribution has been obtained from analytic expressions. Flow of fluid across the boundaries of the damper is accounted for in the formulation of the pressure distribution by considering ports as axial slots which extend over the entire length of the damper. The calculations required are straight forward and once implemented, the method can provide considerable time savings over methods that numerically obtain the pressure distribution. A two port damper along with associated non-dimensional damping and stiffness plots are presented as an example and indication of the usefulness of the procedure.

NOMENCLATURE

C	port flow coefficient (in.^{3}/sec-psi)
c	nominal radial clearance (in.)
F_x, F_y	damper forces in the x and y directions (lb)
G	constant of integration
h	film height (in.)
I, J, K	functions of ϕ as defined in equations (21) (22) (23)
L	damper length (in.)
P	pressure (psi)
P_o	static pressure maintained in a port (psi)
Q	flow coefficient associated with damper annulus (in.^{3}/sec-psi)
R	radius (in.)
U_o, V_o	journal surface velocity components (in./sec)
x, y	journal location components (in.)
$\dot{x}$, $\dot{y}$	journal velocity components (in./sec)

Greek letters

μ	viscosity (lb-sec/in.^{2})
ϕ	independent angular coordinate

Subscripts

i	subscript indicating the variable associated with the i^{th} interval or the i^{th} port

Numerical solutions of the incompressible Reynolds equations for the prediction of the forces generated in a squeeze film damper are highly time consuming. Even in the case where the damper may be considered one-dimensional this time requirement becomes prohibitive when considering time transient or non-linear solutions of rotor dynamic problems. The solution method presented here minimizes this time requirement by first analytically solving a simplified form of the Reynolds equation for the pressure distribution and then numerically integrating for the resultant forces.

The "long bearing" form of the incompressible Reynolds equation with constant fluid properties for a squeeze film damper is:

$$\frac{1}{R}\left\{\frac{\partial}{\partial\phi}\left(h^3\,\frac{1}{R}\,\frac{\partial P}{\partial\phi}\right)\right\} = 6\mu\left\{\frac{1}{R}\,\frac{\partial}{\partial\phi}\left(U_o h\right) - 2V_o\right\} \qquad (1)$$

where $P = P(\phi)$ is the pressure in the fluid, R is the radius of the journal, $U_o(\phi)$ is the tangential velocity of the journal surface, $V_o(\phi)$ is the radial velocity of the journal surfaces, μ is the viscosity of the fluid, ϕ is the independent angular coordinate, and h is the height of the film given by:

$$h = c - x\cos(\phi) - y\sin(\phi) \qquad (2)$$

Here c is the nominal radial clearance and x and y are the cartesian components of the location of the journal in the non-rotating coordinate systems as in figure 1. Since the journal may only experience translational motion, the velocities U_o and V_o may be related to the velocity of the center of the journal by:

$$U_o = \dot{x}\sin(\phi) + \dot{y}\cos(\phi) \qquad (3)$$

$$V_o = \dot{x}\cos(\phi) + \dot{y}\sin(\phi) \qquad (4)$$

where $\dot{x}$ and $\dot{y}$ are the cartesian components of the velocity of the journal. After the substitution of equation (2), (3), and (4) into equation (1), and the integration with respect to ϕ the variation of pressure with angular location may be expressed as:

$$\frac{\partial P}{\partial\phi} = \frac{6\mu R\,(\dot{y}\cos(\phi) - \dot{x}\sin(\phi))}{(c - x\cos(\phi) - y\sin(\phi))^2} + \frac{12\mu R^2\,(\dot{y}\cos(\phi) - \dot{x}\sin(\phi)) + G}{(c - x\cos(\phi) - y\sin(\phi))^3} \qquad (5)$$

where G is a constant of integration. Noting that the first term of equation (5) is smaller than the second by a factor of c/R, which for typical dampers is less than 0.01, equation (5) may be reduced to:

$$\frac{\partial P}{\partial\phi} = \frac{12\mu R^2\,(\dot{y}\cos(\phi) - \dot{x}\sin(\phi)) + G}{(c - x\cos(\phi) - y\sin(\phi))^3} \qquad (6)$$

In the case of a damper with multiple fluid ports that act undiminished along the entire axial length of the damper, the variation of the pressure

distribution between each pair of ports is unique. This requires that equation (6) be written as:

$$\left(\frac{\partial P}{\partial \phi}\right)_i = \frac{12\mu R^2 \left(\dot{y}\cos(\phi) - \dot{x}\sin(\phi)\right) + G_i}{\left(c - x\cos(\phi) - y\sin(\phi)\right)^3} \tag{7}$$

where i denotes the subinterval of interest. With the pressure variation so defined, the pressure distribution within each respective subinterval may be defined as:

$$P(\phi) = P_i + \int_{\phi_i}^{\phi} \left(\frac{\partial P}{\partial \phi}\right)_i d\phi \qquad \phi_i \leq \phi \leq \phi_{i+1} \tag{8}$$

where P_i is the pressure in the film at the beginning of the i^{th} subinterval.

By examining equations (7) and (8), it may be seen that if there are n subintervals then there are 2n unknown that must be evaluated. These unknowns may be evaluated by considering the continuity of flow at the n fluid ports and the continuity of pressure at the beginning of each subinterval. The continuity of flow may be expressed as:

$$Q_i \left\{ \left(\frac{\partial P}{\partial \phi}\right)_i \Big|_{\phi_i} - \left(\frac{\partial P}{\partial \phi}\right)_{i-1} \Big|_{\phi_i} \right\} = C_i \left(P(\phi_i) - P_{oi}\right) \tag{9}$$

where P_{oi} is the static pressure maintained in the i^{th} port, C_i is the flow coefficient associated with the i^{th} port, and:

$$Q_i = \frac{L}{12\mu R}\left(c - x\cos(\phi_i) - y\sin(\phi_i)\right)^3 \tag{10}$$

where L is the length of the damper. The continuity in the pressure requires that:

$$P_{i+1} = P_i + \int_{\phi_i}^{\phi_{i+1}} \left(\frac{\partial P}{\partial \phi}\right)_i d\phi \tag{11}$$

However, successive substitution of equations (11) into equations(9) leads to flow conditions of the form:

$$Q_1 \left\{ \left(\frac{\partial P}{\partial \phi}\right)_1 \Big|_{\phi_1} - \left(\frac{\partial P}{\partial \phi}\right)_n \Big|_{\phi_1} \right\} = C_1 \left(P_1 - P_{o1}\right) \tag{12}$$

$$Q_i \left\{ \left(\frac{\partial P}{\partial \phi} \right)_i \Big|_{\phi_i} - \left(\frac{\partial P}{\partial \phi} \right)_{i-1} \Big|_{\phi_i} \right\} = \tag{13}$$

$$C_i \left(P_1 - P_{o1} + \sum_{j=2}^{i} \int_{\phi_{j-1}}^{\phi_j} \left(\frac{\partial P}{\partial \phi} \right)_{j-1} d\phi \right)$$

$$i = 2,3,4 \ldots n$$

while the combination of equations (11) leads to the continuity condition:

$$\sum_{j=2}^{n} \int_{\phi_j}^{\phi_{j+1}} \left\{ \frac{\partial P}{\partial \phi} \right\}_j d\phi = 0 \tag{14}$$

where: $$\phi_{n+1} = \phi_1 \tag{15}$$

It may be seen that (n-1) unknown pressures have been eliminated and only (n+1) unknown remain to be evaluated fron the simultaneous equations.

Once the unknowns are evaluated, the pressure in the i^{th} subinterval may be calculated from:

$$P(\phi) = P(\phi_i) + G_i \; I \Big|_{\phi_i}^{\phi} - 12\mu R^2 \; (\dot{x} \; J \Big|_{\phi_i}^{\phi} - \dot{y} \; K \Big|_{\phi_i}^{\phi}) \tag{16}$$

$$\phi_i \leq \phi \leq \phi_{i+1}$$

where: $$P(\phi_1) = P_1 \tag{17}$$

$$I \Big|_{\alpha}^{\beta} = \int_{\alpha}^{\beta} \frac{d\phi}{(c - x \cos(\phi) - y \sin(\phi))^3} \tag{18}$$

$$J \Big|_{\alpha}^{\beta} = \int_{\alpha}^{\beta} \frac{\sin(\phi) \; d\phi}{(c - x \cos(\phi) - y \sin(\phi))^3} \tag{19}$$

and:

$$K\Big|_{\alpha}^{\beta} = \int_{\alpha}^{\beta} \frac{\cos(\phi)\ d\phi}{(c - x\cos(\phi) - y\sin(\phi))^3} \tag{20}$$

The indefinite form of these integrals (I, J, and K) are given by Gradshteyn and Ryzhik (1) as:

$$I(\phi) = \frac{x\sin(\phi) - y\cos(\phi)}{2(c^2 - x^2 - y^2)(c - x\cos(\phi) - y\sin(\phi))^2} + \frac{3cx\sin(\phi) - 3cy\cos(\phi)}{2(c^2 - x^2 - y^2)^2(c - x\cos(\phi) - y\sin(\phi))} + \frac{2c^2 + x^2 - y^2}{(c^2 - x^2 - y^2)^{2.5}} \tan^{-1}\left\{\frac{(c + x)\tan\left(\frac{\phi}{2}\right) - y}{\sqrt{c^2 - x^2 - y^2}}\right\} \tag{21}$$

$$J(\phi) = \frac{x - c\cos(\phi)}{2(c^2 - x^2 - y^2)(c - x\cos(\phi) - y\sin(\phi))^2} + \frac{2xy\sin(\phi) - (c^2 + 2y^2)\cos(\phi) + cx}{2(c^2 - x^2\ y^2)^2(c - x\cos(\phi) - y\sin(\phi))} + \frac{3cy}{(c^2 - x^2 - y^2)^{2.5}} \tan^{-1}\left\{\frac{(c + x)\tan\left(\frac{\phi}{2}\right) - y}{\sqrt{c^2 - x^2 - y^2}}\right\} \tag{22}$$

$$K(\phi) = \frac{c\sin(\phi) - y}{2(c^2 - x^2 - y^2)(c - x\cos(\phi) - y\sin(\phi))^2} + \frac{(2x^2 + c^2)\sin(\phi) - 2xy\cos(\phi) - cy}{2(c^2 - x^2 - y^2)^2(c - x\cos(\phi) - \sin(\phi))} + \frac{3cx}{(c^2 - x^2 - y^2)^{2.5}} \tan^{-1}\left\{\frac{(c + x)\tan\left(\frac{\phi}{2}\right) - y}{\sqrt{c^2 - x^2 - y^2}}\right\} \tag{23}$$

With the I, J, and K integrals so defined, the pressure distribution about the damper may be readily calculated from equation (16) by starting at ϕ_1 and then proceeding in the positive ϕ direction.

After the calculation of the discrete pressure distribution about the damper the resultant forces may be obtained with one numerical integration.

Kirk and Gunter (2) suggest Weddle's Rule as an accurate and efficient formula for numerical integration in bearing applications, i.e.;

$$\int_{\phi_0}^{\phi_6} F(\phi)d\phi = 0.3\Delta\phi \ (f_0 + 5f_1 + f_2 + 6f_3 + f_4 + 5f_5 + f_6) \tag{24}$$

where f_j, j=0,1,2,3,4,5,6, are seven equally spaced discrete values of $F(\phi)$ on the interval ϕ_0 to ϕ_6 inclusive and:

$$\Delta\phi = \frac{\phi_6 - \phi_0}{6} \tag{25}$$

As an example of the method consider the two port damper illustrated in figure 2. The analytic expressions for the determination of the pressure distribution may be written as:

$$P(\phi) = P_1 + G_1 \, I\Big|_{\phi_1}^{\phi} - 12\mu R^2 \, (\dot{x} \, J\Big|_{\phi_1}^{\phi} - \dot{y} \, K\Big|_{\phi_1}^{\phi}) \tag{26}$$

$$\phi_1 \leq \phi \leq \phi_2$$

and

$$P(\phi) = P(\phi_2) + G_2 \, I\Big|_{\phi_2}^{\phi} - 12\mu R^2 \, (\dot{x} \, J\Big|_{\phi_2}^{\phi} - \dot{y} \, K\Big|_{\phi_2}^{\phi}) \tag{27}$$

$$\phi_2 \leq \phi \leq \phi_1$$

where the integration with respect to ϕ must always proceed in the positive direction. The flow conditions at the two ports may be expressed as:

$$Q_1 \left\{ \left(\frac{\partial P}{\partial \phi} \right)_1 \Big|_{\phi_1} - \left(\frac{\partial P}{\partial \phi} \right)_2 \Big|_{\phi_1} \right\} = C_1 \, (P_1 - P_{o1}) \tag{28}$$

and

$$Q_2 \left\{ \left(\frac{\partial P}{\partial \phi}\right)_2 \Big|_{\phi_2} - \left(\frac{\partial P}{\partial \phi}\right)_1 \Big|_{\phi_2} \right\} = C_2 \left(P_1 - P_{o2} + \int_{\phi_1}^{\phi_2} \left(\frac{\partial P}{\partial c}\right)_1 d\phi \right) \tag{29}$$

The continuity of the pressure distribution requires that:

$$\int_{\phi_1}^{\phi_2} \left(\frac{\partial P}{\partial \phi}\right)_1 d\phi + \int_{\phi_2}^{\phi_1} \left(\frac{\partial P}{\partial \phi}\right)_2 d\phi = 0 \tag{30}$$

where again the integration with respect to ϕ must always proceed in the positive direction.

Once the pressure field and forces have been generated, damping and stiffness characteristics may be determined. The damping and stiffness characteristics of the two port damper of figure 2 have been determined and are presented in non-dimensional form in figures 3 and 4. In this example, the flow coefficients C_1 and C_2 were set to a very small number so the ports would not affect the characteristics of the damper. In general, however, the method may be used to generate similar curves for dampers which exhibit port flow effects.

ACKNOWLEDGEMENTS

The author would like to thank Dr. J. M. Vance for his invaluable assistance in the formulation of this work. The author would also like to thank M. J. Wehner for his help in generating the non-dimensional damping and stiffness curves for the two port damper.

REFERENCES

1. Gradshteyn and Ryshik, Tables of Integrals, Series, and Products, Acedemic Press, New York, 1965, pg. 149.

2. Kirk and Gunter, "Transient Journal Bearing Analysis," NASA CR 1549 June 1970.

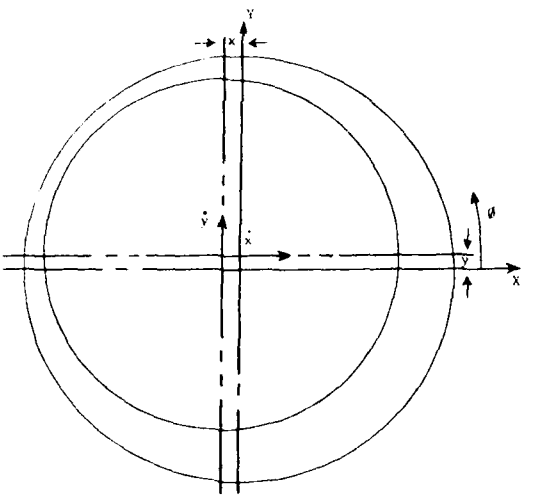

Fig.1 Damper coordinate system

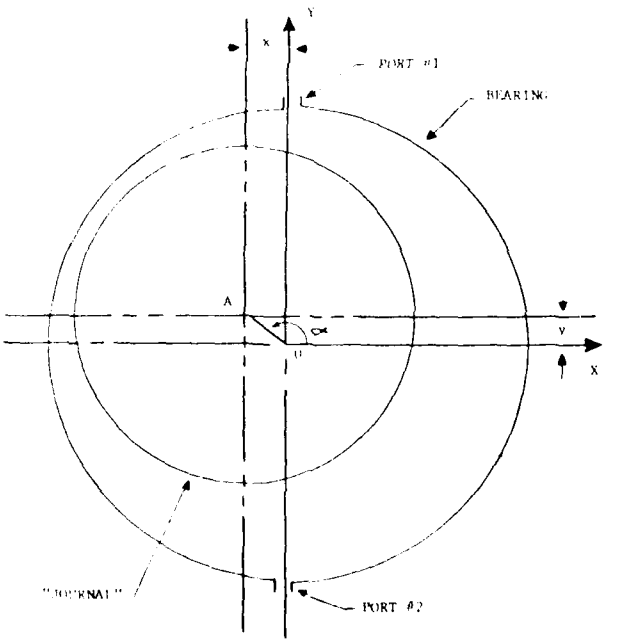

Fig.2 Two port damper

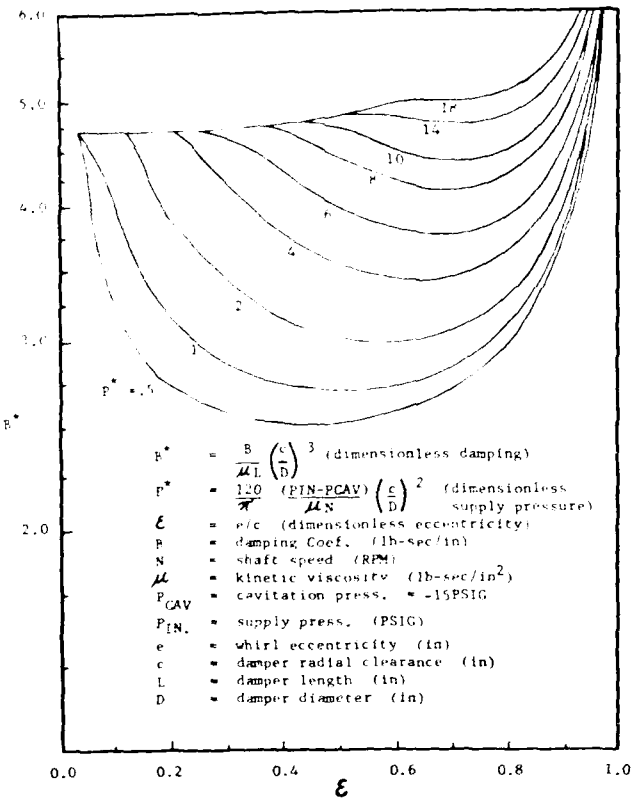

Fig.3 Non-dimensional damping characteristics of two port damper

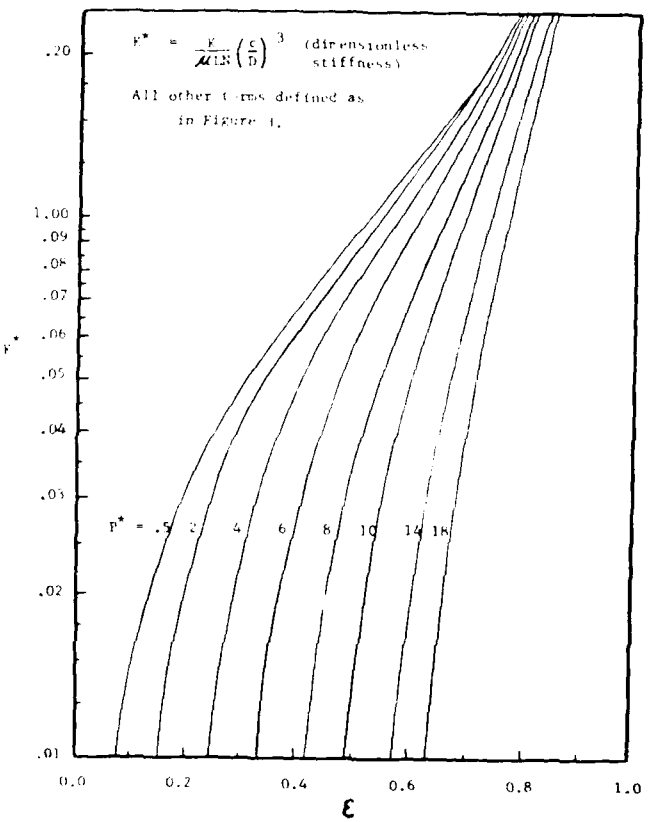

Fig.4 Non-dimensional stiffness characteristics of two port damper

UNBALANCE BEHAVIOUR OF SQUEEZE FILM SUPPORTED RIGID ROTORS

E.J. HAHN

Senior Lecturer, University of New South Wales,
Kensington, New South Wales, Australia.

ABSTRACT

Appropriately designed squeeze film dampers can act as excellent vibration isolators for unbalanced rigid rotors. This paper presents the equilibrium load capacity and transmissibility data over a wide range of operating conditions for both unloaded vertical and centrally preloaded rigid rotors mounted in either one or two squeeze film supported rolling element bearings. Their applicability to ensure effective vibration isolation consonant with acceptable rotor vibrations is discussed. It is shown that with unpressurized bearings, bistable operation can and must be avoided; significant vibration isolation is possible but limited by the degree of unbalance; and there is no need for external support for unloaded vertical rotors. With fully pressurized bearings, such support is essential. However, bistable operation is eliminated and vibration isolation is possible for any degree of unbalance, though effectiveness decreases with increasing unbalance.

NOMENCLATURE

a = $1/U$

b = $2\mu RL^3/(mC^3\omega_r U)$

B = load number = $2\mu RL^3/(mC^3\omega)$

C = radial clearance

d = rotor shaft span between bearing supports

d_0 = axial distance between bearing station 1 and the rotor mass center

d_1 = 0 for conical motions, = ∞ for cylindrical motions

D = journal diameter

e = journal orbit eccentricity

f_r, f_t = fluid film forces on journal in $\hat{r}$ and $\hat{t}$ directions

g_r, g_t = defined in equations (4) and (5)

I_X, I_Z = rotor moments of inertia about the transverse and longitudinal axes through the bearing center O_{b_1} at bearing station 1

k = equivalent retainer spring stiffness = $[d_1^2/(d_1+d)^2+1]K$

K = retainer spring stiffness at flexible supports

L = bearing length

m = equivalent rotor mass = $(I_X-2I_Z)/d^2$ for conical motions, = M for cylindrical motions

M = rotor mass

Q = defined in equation (9)

$\hat{r}, \hat{t}$ = unit vectors along and transverse to the line of centres $O_{b_2}O_{j_2}$ in Fig. 1

R = journal radius

T = unbalance transmissibility

U = unbalance parameter = $\omega^2(d_1+d)/[C(d_1+d_0)]$

β = phase angle between unbalance force and rotor displacement

λ = nondimensional speed = ω/ω_r

Λ = $(1-1/\lambda^2)/U$

ε = journal orbit eccentricity ratio = e/C

μ = absolute viscosity of lubricant at the mean lubricant temperature

ρ = unbalance eccentricity

ω = rotor speed

ω_r = $\sqrt{k/m}$

INTRODUCTION

Owing to their relative constructional simplicity and the wide range of damping attainable, hydrodynamic squeeze film bearings show excellent potential as vibration isolators and attenuators (1). The satisfactory performance of such bearings is, however, very much dependent on their design, being greatly influenced by the degree of unbalance and damping in the system, the operating speed as well as the degree of pressurization of the lubricant supply. This is well exemplified by the available design data on the steady state vibration amplitude and unbalance transmissibility of such squeeze film supported rotors (2-7). These data presume that either the rotor is centrally preloaded (e.g. via retainer springs), or that the rotor is vertical and free from all external loading. The resulting circular journal orbits offer analytical simplicity, avoid the need for transient analysis (8,9) and are realisable in practice (10-11).

The potential user of the available design data may, however, justly complain that the system parameters utilised in centrally preloaded rotor situations cannot be easily extrapolated to encompass the vertical rotor situation (data for which utilise slightly different parameters), so that the advantages (if any) in providing external support stiffness (e.g. retainer springs) for unloaded vertical rotors are not readily apparent. Nor can an overall view be so readily obtained. This paper will attempt to rectify the situation for the case of squeeze film supported rigid rotors, i.e. the purpose of this paper is to present in a generalised but compact form the equilibrium load capacity data (in the form of the equilibrium journal orbit eccentricity ratio) and the unbalance transmissibility data for vertical and centrally preloaded rigid rotors, over a wide range of operating conditions and for any degree of unbalance.

THEORETICAL MODEL

A general hydrodynamic squeeze film damper mount for a rotor running in rolling element bearings is schematically depicted in Fig. 1. The following assumptions are made: (a) the rotor is rigid; (b) excitation forces from the rolling element bearings are negligible; (c) the Reynolds equation for constant lubricant properties is applicable; (d) the short bearing (Ocvirk) approximation is valid; (e) steady state conditions have been attained with the journal centres describing synchronous circular orbits about the bearing centres; (f) if necessary to offset any resultant unidirectional loading, the rotor is centrally preloaded with constant radial stiffness; (g) the rotor speed is constant; (h) the rotor is axially symmetric in spite of rotor unbalance; (i) the rotor is either symmetric and exhibits symmetric motions and is mounted in two squeeze film supported rolling element bearings, or the rotor is mounted in rigidly supported rolling element bearings at one end and squeeze film supported rolling element bearings at the other.

Assumption (a) defines the operation to well below the first bending critical speed. Assumptions (c) and (d) are typical and allow one to obtain [illegible] analytical expressions for the lubricant forces for bearings having [illegible] length to diameter ratios of 2.0 or less (10,11). The major approximation inherent in assumption (c) is that the cavitating region forms and collapses [illegible] as dictated by the solution of the Reynolds equation. Assumptions (e) and (f) are justified in (8,9), [illegible] to the steady state

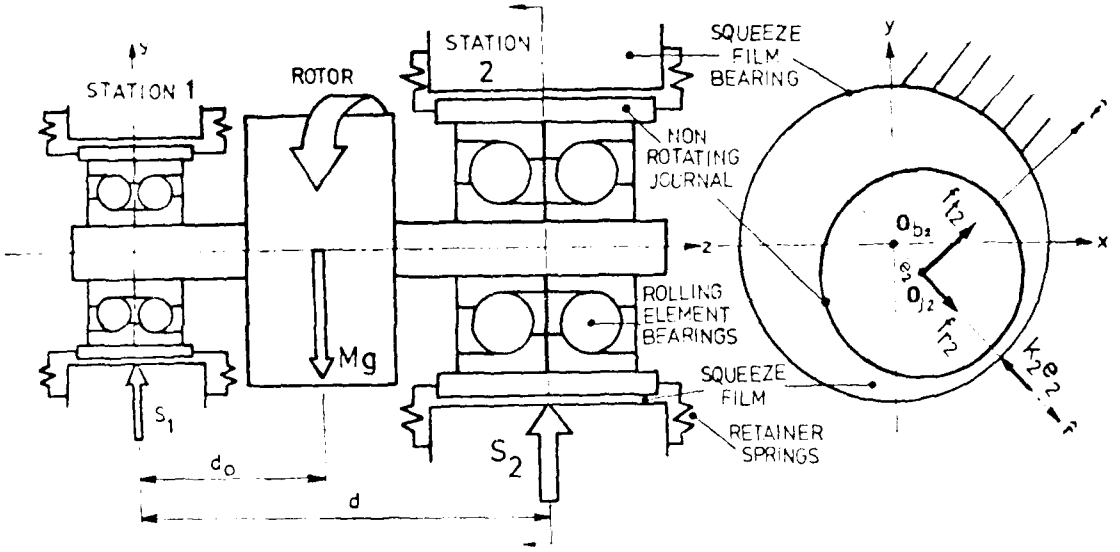

Fig. 1 General hydrodynamic squeeze film damper supported rotor bearing system showing external forces

solutions obtained were of the synchronous circular orbit type. Whilst centrally preloading the rotor appears to yield no undesirable effects on the system performance, it reduces the number of possible system parameters, enables theoretical solutions to be more simply obtained, and ensures the avoidance of possible potential squeeze film start up problems. Hence, its prescription is felt justified and advantageous, even if not necessary. Assumption (g) implies a large moment of inertia about the rotor longitudinal axis. Assumptions (h) and (i) simplify the analysis considerably. Journal vibration amplitude predictions based on the [illegible] (a)-(i) have been verified experimentally (9,11).

As shown in (11), the nondimensional equations of motion for such a system may be written as:

$$[illegible] = F\cos\ldots \qquad (1)$$

and

$$[illegible] = F\sin\ldots \qquad (2)$$

The fluid film forces f_r and f_t are given by:

$$f_{r,t} = -\frac{\partial V}{\partial r,t} \qquad (3)$$

where, for unpressurized or pressurized bearings respectively,

$$g_r = \frac{2\varepsilon^2}{(1-\varepsilon^2)^2} \quad \text{or} \quad 0 \tag{4}$$

$$g_t = \frac{\pi\varepsilon}{2(1-\varepsilon^2)^{3/2}} \quad \text{or} \quad \frac{\pi\varepsilon}{(1-\varepsilon^2)^{3/2}} . \tag{5}$$

Upon eliminating δ from eqns. (1) and (2) one finally obtains:

$$(g_t B/U)^2 + (g_r B/U - \varepsilon)^2 = 1. \tag{6}$$

The corresponding value for the unbalance transmissibility T is then given by:

$$T = \sqrt{1 + 2\varepsilon g_r B - \varepsilon^2(1-2/\delta^2)}/U . \tag{7}$$

PRESENTATION OF DATA

Since g_t and g_r are functions of ε only, it is possible to represent the load capacity data in terms of two independent parameters. A simple choice appears to be the parameter combination of B/U and ε, although $B/(1-1/\delta^2)$ and ε would seem to be equally satisfactory. One should note that with either parameter combination, both parameters are speed dependent.

For ease of interpretation of the final data, it is important that the operating line be easily determined. This latter consideration suggests that for data portrayal, the independent parameters (i.e. B/U and ε or $B/(1-1/\delta^2)$ and ε) should be the ordinate and abscissa variables, rather than ε. Thus, the load capacity data given in Fig. 4 in (7) ostensibly for unloaded vertical rotors only, may in fact be generalised to encompass centrally preloaded rotors, if, in the notation of (7), (B) is replaced by $(B)/(1-1/\delta^2)$ and U is replaced by $1/\delta$. However, the determination of ε as the rotor varies in speed is unduly complicated by the need to continually switch from one $1/\delta$ line to another.

Orbit Eccentricity Data

Choosing B/U and ε as the independent parameter combination, eqn. (6) was solved to give the equilibrium load capacity charts of Figs. 2 and 3 for unpressurised (" film) and fully pressurized (2" film) bearings. Note that for (fully) pressurized bearings, $g_r = 0$, so the sign of ε does not influence the solutions. Thus, Figs. 2 and 3 display in compact form all the equilibrium journal orbit eccentricity ratios ε of both unloaded vertical rotors and centrally preloaded rotors for operating conditions encompassed by the system parameters varying over the range $10^{-3} \leq B/U \leq 10$ and $-30 \leq \varepsilon \leq 30$. Such a range is adequate to cover all operating conditions of practical interest. In all cases, as $B/U \to 0$, the constant ε lines approach $\varepsilon = 1/\delta$.

Determination of Operating Line

Since in general both B/U and ε (and of course δ) are speed dependent, it is not possible to follow any given line on the design maps as

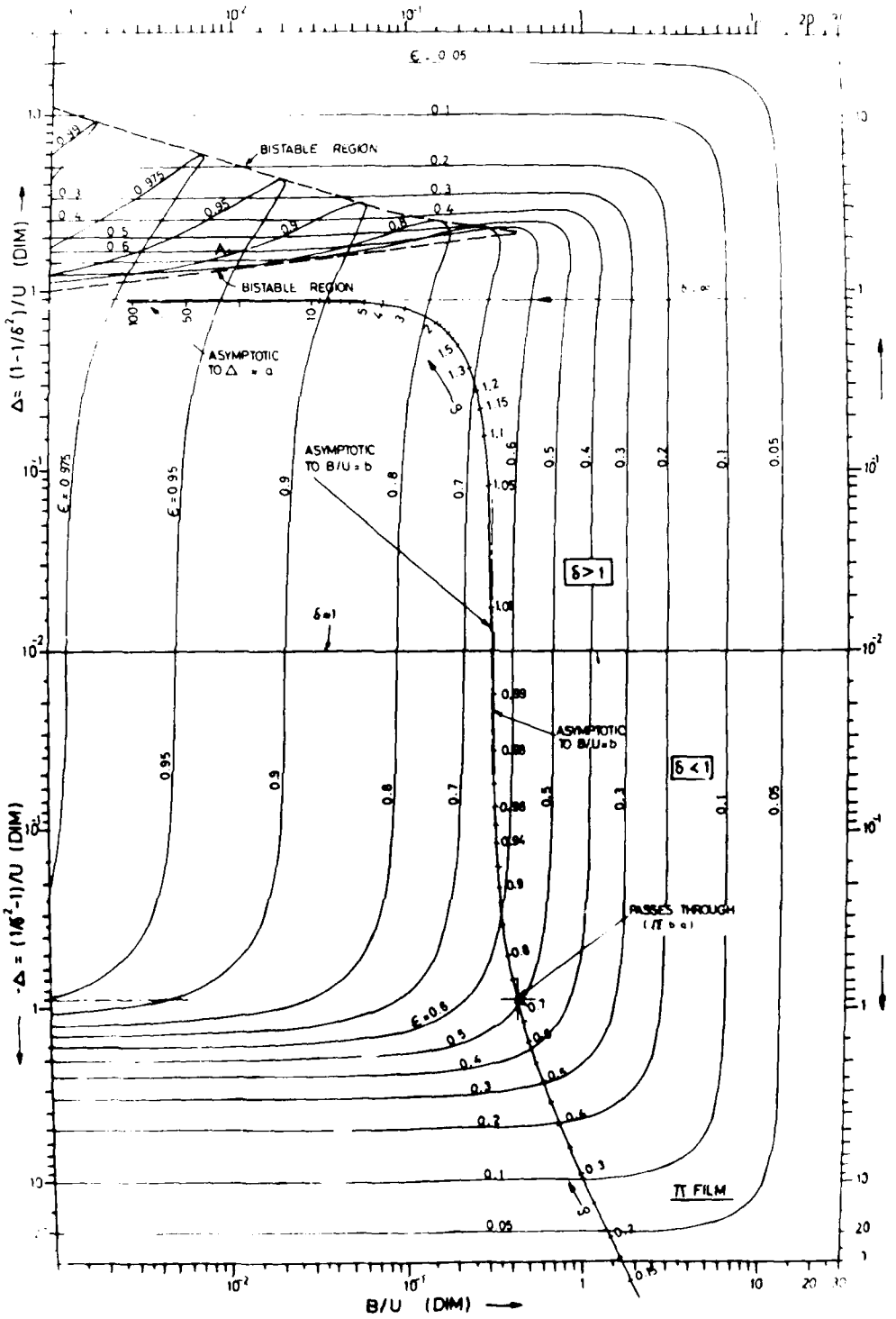

Fig. 2 Equilibrium load capacity for unpressurized squeeze film supported rotors

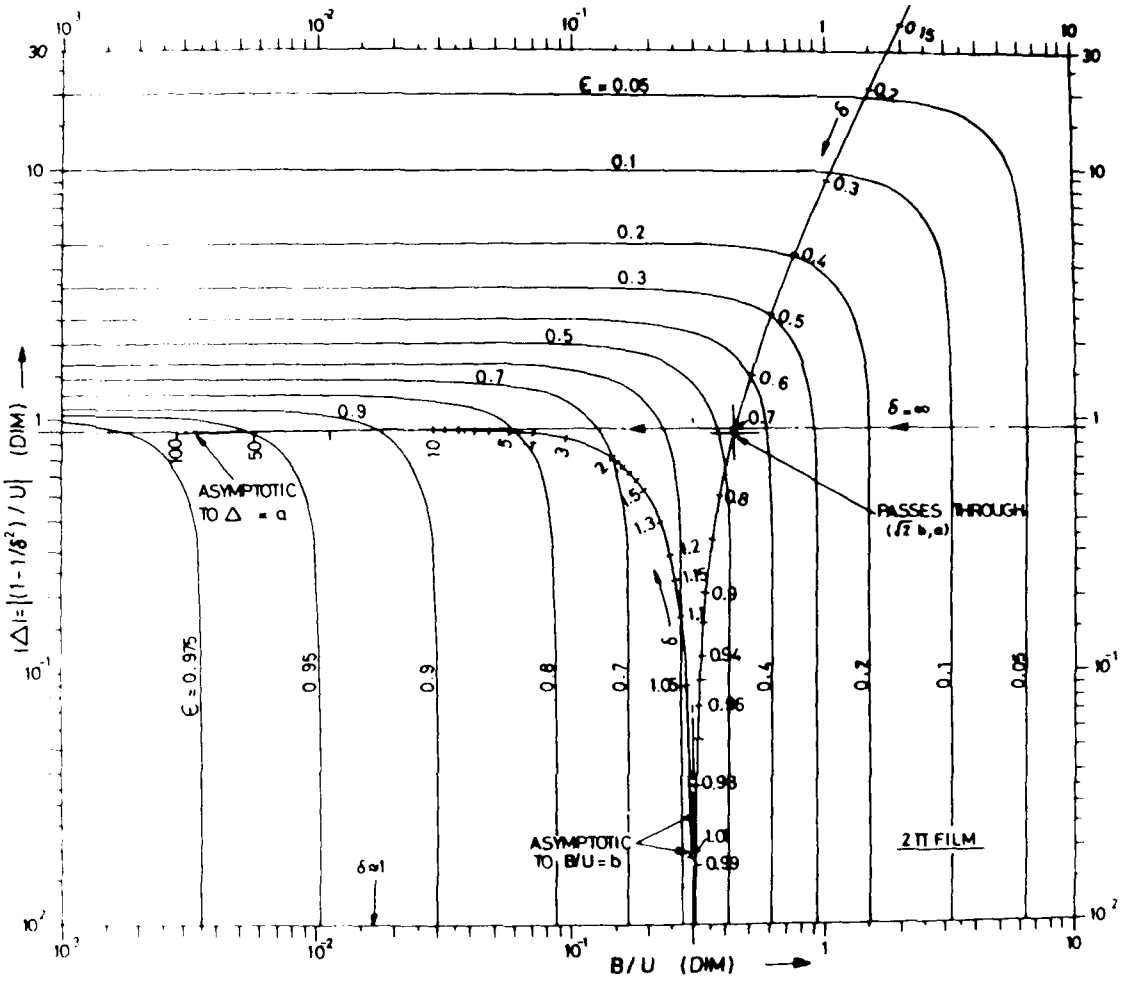

Fig. 3 Equilibrium load capacity for fully pressurized squeeze film supported rotors

the operating line for a given rotor bearing system. Since knowledge of the variation of the journal vibration amplitude with speed for a given system is of paramount importance for the design of such systems, a reasonably simple means of determining this is required. This is not a problem for unloaded vertical rotors, since [illegible] and operation is along lines of constant [illegible], moving from right to left with increasing speed (i.e. decreasing B/U) as shown in Figs. 2 and 3 for [illegible] = 0.9 (i.e. F = 1.11).

For centrally preloaded rotors however, since both B/U and [illegible] are speed dependent, determination of the operating line is more complicated. Thus, one can write [illegible] and B/U = b/[illegible] where 'a' and 'b' are speed independent, so that one can plot the operating line as [illegible] increases from 0 to [illegible] as shown in Figs. 2 and 3. Note that over the range [illegible],

the operating line is asymptotic to [illegible] = a as [illegible] and asymptotic to B/U = b as [illegible] 1. Also, when [illegible] = $1/\sqrt{2}$, B/U = $\sqrt{2}$b, [illegible] = a and the operating line passes through this point.

Further, since both the [illegible] and B/U scales are logarithmic, the magnitudes actually being plotted are log [illegible] = log a + log [illegible] and log (B/U) = log b + log 1/[illegible]. Hence the shape of the operating curve is independent of the particular values of a and b, which values do however specify its position, so the asymptocity requirements and ease of locating the co-ordinate ($\sqrt{2}$b,a) enable the operating line for any system to be rapidly located.

Transmissibility Data

Transmissibility data is more difficult to portray conveniently for, as may be seen from eqn. (7), T is in general a function of three independent parameters, such as B, [illegible], and U or B, [illegible], and U or various combinations therefrom. As a rapid guide to whether T is less than or greater than unity, eqn. (7) may be written in the form:

$$T^2 + Q^2 = 1 \qquad (8)$$

where $$Q^2 = \frac{[illegible]}{U^2} - \frac{2gB}{U^2} . \qquad (9)$$

This variation of T with Q is shown in Fig. 4. For pressurized bearings, such a description is adequate, but for unpressurized bearings, the

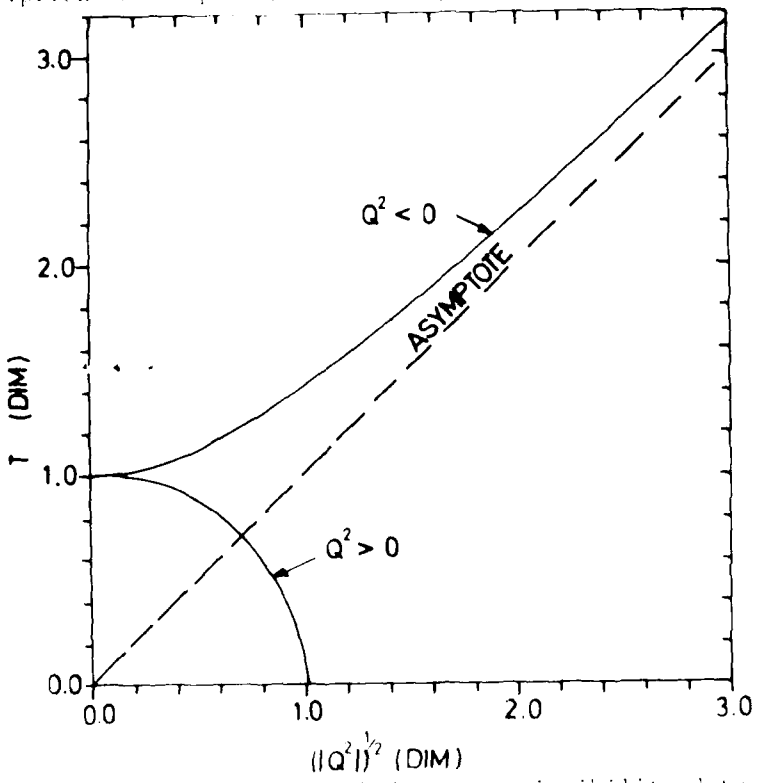

Fig. 4 General equilibrium transmissibility data

determination of the sign, let alone the magnitude of Q^2 is difficult to present.

For unloaded vertical rotors, or for high values of δ (say $\delta > 5$), Figs. 2 and 3 (and eqn. (6)) show that the differences in ε between its value for unloaded vertical rotors ($\delta = \infty$) and its value for centrally preloaded rotors at increasing speeds (i.e. speeds such that $\delta \geq 5$ say) become increasingly insignificant. Hence, eqn. (7) simplifies to:

$$T \approx \sqrt{1 + 2\varepsilon g_r B - \varepsilon^2}/U \quad \text{for} \quad \delta \geq 5 \qquad (10)$$

In such cases T is a function of only two independent parameters, say U and ε. Fig. 5 illustrates this dependence for $U \leq 1.4$. It corresponds to the transmissibility data for unpressurized unloaded vertical rotors given in (7), and may be used provided $\delta \geq 5$.

DISCUSSION OF DATA

Design Considerations - General

The major reason for supporting rolling element bearing mounted rotors on flexible damped supports is to achieve vibration isolation, so that as low a T as possible, and in any case, $T < 1$ is attained at design speed. Such vibration isolation can significantly extend rolling element bearing life, as well as result in noise attenuation. The transmissibility at resonance is generally of little concern since the actual load on the bearings is usually higher at the design speed. Such vibration isolation can only be achieved at the expense of increasing the vibrations of the rotor itself, so an added consideration is to maintain rotor vibration amplitudes as low as dictated by other design constraints. (e.g. blade tip clearances in compressors). The added benefit of flexible damped supports in cushioning against shock loading (such as resulting from a sudden increase in unbalance due to a blade loss in a turbine) may also be partly inferred from the design data in this paper.

Bistable Operation

Referring to the load capacity data for unpressurized bearings in Fig. 2, there exists a region, termed the bistable region. For example, suppose operation is at A. Possible equilibrium solutions for ε are 0.60, 0.91 and 0.955. As shown in previous investigations (6, 7, 10), in the case of three equilibrium orbits, the intermediate orbit is always unstable (in the linear sense), while the others are stable. High values of ε are always undesirable in their own right, indicating high vibration amplitudes. Also they are associated with undesirably high values of T, as may be seen in Fig. 5. Hence operating conditions should be such as to avoid the bistable region altogether.

Whether a change from one stable orbit to another occurs (i.e. whether 'jump' occurs) depends on conditions at entry into or exit from the bistable region. Thus, entry into the bistable region from above poses the possibility of a jump up to the higher stable orbit, while entry below would necessitate a jump down (a rather unlikely event). Under certain operating conditions, one could enter the bistable region from below, then exit and

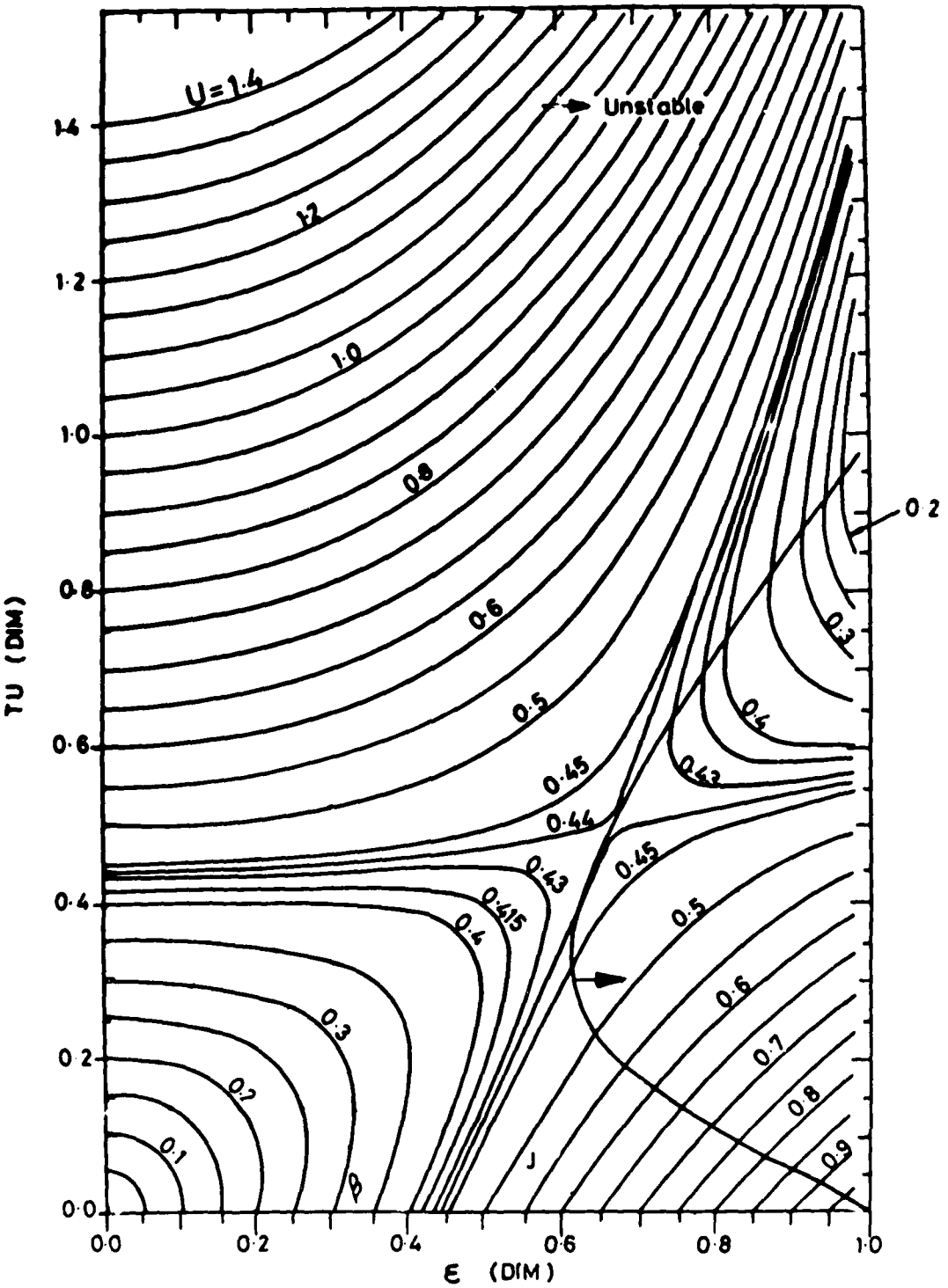

Fig. 5 Equilibrium transmissibility data for unpressurized squeeze film supported rotors with $\delta > 5$

reenter from above. A detailed investigation of these complicated multijump possibilities is reported in (2,6) and such multijump predictions have been observed experimentally (6,11).

One can see from Fig. 2 that no bistable operation is possible once U exceeds 1. However, for unpressurized bearings, such high values of U result in T > 1 (see Fig. 5). For lower values of U, bistable operation is always possible if the operating speed is high enough, i.e. if B/U is small enough. Least leeway occurs around the cusp of the bistable region when $\lambda \approx 2.2$ and $B/U \approx 0.42$. Note that for rotors operating at $\sigma > 5$, this corresponds to $U \approx 0.45$ and $B \approx 0.18$. A more precise determination of the exact position of the cusp requires B to exceed 0.14 (7). The sharpness of the cusp explains why $U \approx 0.45$ has often been regarded as a critical unbalance parameter.

With fully pressurized bearings on the other hand, bistable operation is not possible, as may be seen from Fig. 3 or from an examination of eqn. (6). This is a major plus if operating conditions cannot be sufficiently controlled to avoid possible entry into the bistable region with unpressurized bearings.

Design Considerations - Unpressurized Bearings

With unpressurized bearings, choice of parameters should be such that under all conditions of likely operation, the bistable region is avoided. In addtion, at design speed, one requires $T < 1$. From eqn. (9), a necessary, though by no means sufficient condition for this is that $\sigma > \sqrt{2}$. Qualitatively, one can see that Q^2 increases (and hence, T decreases) as speed increases, particularly if operation is in a region where σ is no longer greatly speed dependent and one would normally pick σ_r so that $\sigma > \sqrt{2}$ at design speed. If $\sigma > 5$, Fig. 5 is applicable, and one can readily see that for $T < 1$, conditions at design speed require $\lambda > 0.55$ and $U < 0.43$ (or $\lambda > 2.4$). Hence, operation should be such as to avoid the cusp of the bistable region and remain generally in the area above the bistable region and above $\lambda = 2.4$. An alternative description of transmissibility frequency responses for centrally preloaded bearings is given in (6).

To ensure low maximum vibration amplitudes, the parameters specifying the operating line must be chosen accordingly. This will also indicate whether the maximum vibration amplitude occurs at design speed or is passed while accelerating up to design speed.

No advantage can be seen in providing external radial support stiffness to unloaded vertical rotors. Not only is the transmissibility somewhat lower in the absence of retainer springs but under certain conditions of operation, entry into the bistable region is likely to be delayed as the avoidance of the cusp is less difficult. As regards vibration amplitudes, the provision of external support stiffness appears to have negligible effect.

Design Considerations - Fully Pressurized

With fully pressurized bearings, no bistable region problems exist. However, stability (in the linear sense) of the equilibrium solutions

requires some external radial support stiffness (5-7) so that otherwise unloaded vertical rotors must be provided with retainer springs.

As may be seen from Fig. 4 or eqn. (9), for pressurized bearings, where $g_r = 0$, the necessary and sufficient condition for $Q^2 > 0$ is that $\lambda > \sqrt{2}$. Hence, with pressurized bearings, values of $T < 1$ are always possible once $\lambda > \sqrt{2}$, regardless of the magnitude of U. However, the minimum T attainable is $\sqrt{1-(\lambda/U)^2}$, so that only minimal vibration isolation (say $T > 0.94$) is possible once $U > 4$. A more detailed description of transmissibility frequency response is given in (6).

Both pressurized and unpressurized bearings exhibit similar orbit eccentricity behaviour and similar comments are applicable in choosing the operating line to minimise the maximum vibration amplitudes as for unpressurized bearings.

The apparent advantages of fully pressurized bearings need to be weighed against the additional cost of the pressurized oil supply. The minimum supply pressure and oil flow rates required to achieve full pressurization are given in (2), taking due note of the slight difference in the definition of B.

CONCLUSIONS

(a) Equilibrium load capacity and transmissibility data are presented in a compact form over a wide range of operating conditions and unbalance and encompass both unloaded vertical and centrally preloaded squeeze film supported rotors.

(b) The choice of independent system parameters enables the operating line to be easily located on the equilibrium load capacity chart.

(c) The data may be used to ensure avoidance of bistable operation and obtain effective vibration isolation at design speed while maintaining induced rotor vibration amplitudes at an acceptable level.

(d) Once the speed exceeds five times the undamped system natural frequency (i.e. once $\lambda > 5$) there is negligible difference between the data for unloaded vertical and centrally preloaded rotors.

(e) With unpressurized bearings, bistable operation is possible and must be avoided; significant vibration isolation is possible up to a limited degree of unbalance (up to $U \approx 0.43$); and no advantages can be seen in providing external support stiffness to otherwise unloaded vertical rotors.

(f) With fully pressurized bearings, some support stiffness is essential; no bistable operation is possible; and once $\lambda > \sqrt{2}$, some vibration isolation is possible for any degree of unbalance, though the effectiveness is minimal for $U < 4$.

REFERENCES

1 Glienicke, J. and Stanski, U., "External Bearing Damping - A Means of Preventing Dangerous Shaft Vibrations on Gas Turbines and Exhaust Turbo Chargers", International Council on Combustion Engines Congress, Barcelona, 1975, pp. 287-311.

2 Simandiri, S. and Hahn, E.J., "Effect of Pressurization on the Vibration Isolation Capability of Squeeze Film Bearings", Journal of Engineering for Industry, Trans. ASME, Vol. 98, No. 1, February, 1976, pp. 109-117.

3 Simandiri, S. and Hahn, E.J., "Vibration Isolation Using Pressurized Squeeze Film Bearings", Vibration and Noise Control Engineering, The Institution of Engineers Australia, National Conference Publication No. 76/9, 1976, pp. 51-55.

4 Rabinowitz, M.D. and Hahn, E.J., "Steady State Performance of Squeeze Film Damper Supported Flexible Rotors", Journal of Engineering for Power, Trans. ASME, Vol. 99, No. 4, 1977, pp. 552-558.

5 Rabinowitz, M.D. and Hahn, E.J., "Stability of Squeeze Film Damper Supported Flexible Rotors", Journal of Engineering for Power, Trans. ASME, Vol. 99, No. 4, 1977, pp. 545-551.

6 Simandiri, S., "A Study of Squeeze Film Bearings", Ph.D. Thesis, UNSW, 1978.

7 Hahn, E.J., "Stability and Unbalance Response of Centrally Preloaded Rotors Mounted in Journal and Squeeze Film Bearings". To be published in Journal of Lubrication Technology, Trans. ASME, Vol. 101, 1979, 9 pp.

8 Mohan, E. and Hahn, E.J., "Design of Squeeze Film Damper Supports for Rigid Rotors", Journal of Engineering for Industry, Trans. ASME, Vol. 96, No. 3, 1974, pp. 976-982.

9 McLean, L.J. and Hahn, E.J., "The Transient Response of a Balanced Rigid Rotor Running in Squeeze Film Supported Journal Bearings". Topics in Fluid Film Bearing and Rotor Bearing System Design and Optimization, ASME 1978, pp. 203-229.

10 White, D.C., "The Dynamics of a Rigid Rotor Supported on Squeeze Film Bearings", Conference on Vibration in Rotating Systems, Proceedings of the Institution of Mechanical Engineers, 1972, pp. 213-229.

11 Simandiri, S. and Hahn, E.J., "Experimental Evaluation of the Predicted Behaviour of Squeeze Film Bearing Supported Rigid Rotors", UNSW Report No. 1979/AM/3.

Bearing Parameter Identification

by

Emerson Woomer, Research Assistant
Walter D. Pilkey, Professor

Department of Mechanical and Aerospace Engineering
School of Engineering and Applied Science
University of Virginia
Charlottesville, Virginia 22901

ABSTRACT

The problem of identifying unknown bearing parameters in a linear rotor-bearing system model is discussed. The measurements of displacements caused by a trial mass unbalance applied to the rotor are used along with the linear algebraic equations which describe the rotor steady - state sinusoidal motion to provide a means of selecting values of model parameters such that the fit between the measured and computed rotor responses is optimized. Several approaches to the optimization are discussed, and two example problems are included.

NOMENCLATURE

A	Cross-sectional area of the shaft
C1	Left pedestal damping constant
C2	Left bearing damping constant
C3	Right pedestal damping constant
C4	Right bearing damping constant
[c]	Matrix of viscous damping constants (2N + 2, 2N + 2)
E	Young's modulus of the shaft material
f(t)	Vector of applied forces and moments (2N + 2)
F(s)	Vector of Laplace transformed applied forces and moments (2N + 2)
G	Shear modulus of the shaft material
[G(s)]	Matrix of transfer functions
I	Transverse area moment of inertia of the shaft
IP	Polar mass moment of inertia of an intermediate shaft mass

K1	Left pedestal spring constant
K2	Left bearing spring constant
K3	Right pedestal spring constant
K4	Right bearing spring constant
[K]	Matrix of linear spring stiffnesses (2N + 2, 2N + 2)
l	Length of a massless elastic section joining two lumped masses
M	Magnitude of a lumped mass between the shaft end masses
MBL	Left bearing mass
MBR	Right bearing mass
MSL	Magnitude of the left end shaft mass
[m]	Matrix of translational mass and moments of inertia (2N + 2, 2N + 2)
N	Number of lumped masses in the shaft model
PR	Poisson's ratio of the shaft material
{q}	Vector of displacements and rotations (2N + 2)
{q(s)}	Vector of Laplace transformed displacements and rotations (2N + 2)
r	Outer radius of the rotor shaft
R	Transverse mass moment of inertia of an intermediate shaft mass
ri	Inner radius of the rotor shaft
RL	Transverse mass moment of inertia of the left end shaft mass
RP	Polar mass moment of inertia of the right end shaft mass
RR	Transverse mass moment of inertia of the right end shaft mass
s	Complex variable in the Laplace transformation
SF	Shear shape factor
SP	Polar mass moment of inertia of the left end shaft mass
[Z(s)]	Impedance matrix
Ω	Rotor spin angular frequency

INTRODUCTION

The usefulness of mathematical models which depict the behavior of physical systems is sometimes impaired by a lack of knowledge of the correct values of constants which appear in the equations. Spring stiffnesses, damping coefficients, and masses are examples of constants which are encountered in models of linear mechanical systems. For rotors in particular, an accurate mathematical model can be important for conducting response studies [illegible] and asynchronous whirl stability analyses. A method is described herein for estimating the parameters in a linear rotor-bearing system model from measurements of influence coefficients taken in the same manner as in the influence coefficient method of balancing (1).

The parameter identification process involves three principal steps: modeling, measurement, and optimization. That is, a mathematical model containing

some unknown parameters is devised to provide a means of computing the system properties such as its natural frequencies or its response for a known excitation. Then, because the physical system exists, these properties can also be experimentally measured; finally, the values of the unknown model parameters are adjusted to obtain the best agreement between the computed and measured values. Often, best agreement is defined as a minimum of the sum of the squares of the differences between the theoretical and experimental results.

Previous publications on estimating bearing coefficients appear to concentrate on the bearing alone as it is subjected to sinusoidal, step, impulse, or other inputs [2], [3], [4], [5], [6]. Schlenzel and Zahrenfeldt [7] have proposed an estimation process based on the shaft response, but in their approach the excitation is the unknown intrinsic shaft unbalance. Assumptions must be made about the value of the unbalance, and "borrowed" forces or coefficients result.

In the following presentation an estimation method is described which involves the application of an optimization algorithm to the linear algebraic equations which govern the rotor steady - state sinusoidal response to an applied unbalance weight. The response of the shaft to applied unbalance is required when the influence coefficient method of balancing is used; therefore the balancing and estimation problems become related. The optimization is conducted at a single frequency and requires that at least as many displacement measurements be obtained as there are unknown parameters to be estimated. Because the actual response characteristics of the rotor bearings are known to be non-linear, the confinement of the optimization to a single frequency should result in a linear model which is useful in some range about the frequency. Of course, if the linear model is to apply over a wide range of frequencies, the optimization can be performed using measurements taken at a number of rotor speeds.

MODEL

For the rotor-bearing system chosen to demonstrate the estimation method, the important assumptions made in modelling are those of linearity, isotropy, and the absence of bearing forces which couple the motions in the horizontal and vertical directions. Only the assumption of linearity is essential to the parameter estimation process; the other two serve to decrease the complexity of the problem presented here. The rotor is treated as an assemblage of rigid masses connected by massless elastic sections, and the bearings are represented as combinations of linear springs, rigid masses, and viscous dampers. In addition a rotary spring acts at one end of the rotor. The rotor-bearing system model is shown schematically in Fig. 1. The unknown model constants are chosen to be MBL, MBR, E1, E2, E3, E4, KE, C1, C2, C3, and C4 (C2 and C4 are often fixed at zero).

For this model type the behavior of the system is described mathematically by a set of ordinary, linear differential equations with constant coefficients:

$$[m]\{\ddot{q}\} + [c]\{\dot{q}\} + [k]\{q\} = \{f(t)\}$$

In these equations the effects of rotary inertia, shear deformation, and gyroscopic moments can all be included, and they have been taken into account

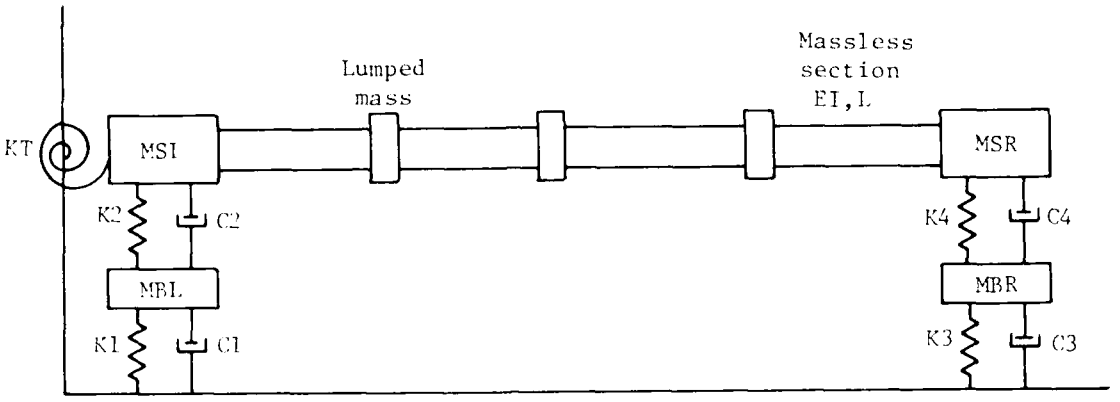

Fig. 1 Schematic diagram of a rotor-bearing model with five shaft masses

for the numerical results given here. If the bearing forces are assumed to be isotropic, the system response can be described by considering one direction of motion only. Also, we choose to neglect the rotary energy of the bearing masses and the effects of axial and torsional loads.

MEASUREMENTS

As a basis for parameter estimation the same experiment has been chosen that is used in the influence coefficient method of balancing. The rotor is first operated in its unmodified state, and measurements are taken of displacement and bending direction at stations along the rotor as it undergoes synchronous whirl caused by intrinsic unbalance inertia forces. Then a small trial mass is placed at a specified station on the rotor, and the measurements are repeated. If the trial mass is very small compared to the lumped rotor mass, by the principle of superposition the increment of motion due to the trial mass should be independent of the intrinsic shaft unbalance distribution. The additional motion caused by the trial mass can be found by vectorially subtracting the original measurements from those made with the trial mass applied to the rotor. The required information is depicted on the sketch shown in Fig. 2.

Since the unbalance excitation caused by the trial mass is sinusoidal with amplitude $mr\omega^2$, the equations of motion can be solved for the system steady-state sinusoidal response. Starting with the differential equations and applying the Laplace transform, the results become:

$$[[m]s^2 + [c]s + [k]]\ \{Q(s)\} = \{F(s)\}.$$

The impedance matrix is defined as $[Z(s)] = [m]s^2 + [c]s + [k]$, and the matrix of transfer functions is defined as the inverse of the impedance matrix, $[G(s)] = [Z(s)]^{-1}$. For steady-state sinusoidal response, $s = j\omega$. $(j = \sqrt{-1})$. Suppose for example that the trial mass is placed at the second shaft mass from the left in a model with five shaft masses, and that the rotor response to the mass unbalance is determined as previously described. The following set of linear algebraic equations applies to the steady-state response:

$$\begin{bmatrix} \\ \\ \\ Z(j\omega) \\ \\ \\ \\ \\ \\ \\ \\ \\ \\ \\ \end{bmatrix} \begin{Bmatrix} G_{13}(j\omega) \\ G_{23}(j\omega) \\ G_{33}(j\omega) \\ \vdots \\ G_{73}(j\omega) \\ G_{83}(j\omega) \\ \vdots \\ G_{12,3}(j\omega) \end{Bmatrix} = \begin{Bmatrix} (0,0) \\ (0,0) \\ (1,0) \\ (0,0) \\ \vdots \\ \\ \\ \\ \\ \\ \\ \\ (0,0) \end{Bmatrix}$$

In this example the third column of the matrix of transfer functions enters into the equations because the trial mass was located at the third mass station. The complex elements of this vector are related to the measured quantities in the following manner:

$$G_{i3} = \frac{X_{i3}}{mr}, \quad i = 1,2, \ldots, 7$$

in which X_{i3} is the amplitude of displacement or rotation which results at mass station i when the trial mass is at station 3.[1] For $i = 1$ through 7, X_{i3} is a displacement, and for $i = 8$ through 12, X_{i3} is a rotation. Also, ARG $(G_{i3}(j\omega))$ is the difference in phase between a displacement or rotation and the applied exciting unbalance force.

By making the appropriate measurements of displacements, rotations, and phases, some or all of the elements of the vector $\{G_{i3}\}$ can be determined. The set of linear algebraic equations which relates the impedance matrix to one column of the matrix of transfer functions will be used as a basis for estimating the unknown parameters in the rotor-bearing model.

OPTIMIZATION

Depending on the number and type of experimental measurements available, several possible approaches exist for estimating the unknown model parameters. These approaches range from iterative search methods, which require a computer,

[1] This formula applies when the unbalance is placed on the rotor surface; if the unbalance is not on the surface, r would be the distance from the center to the unbalance location.

AD-A083 098 VIRGINIA UNIV CHARLOTTESVILLE DEPT OF MECHANICAL AND--ETC F/G 13/9
PROCEEDINGS OF THE CONFERENCE ON THE STABILITY AND DYNAMIC RESP--ETC(U)
1979 DAAG29-79-M-0061

UNCLASSIFIED ARO-16660.1-E NL

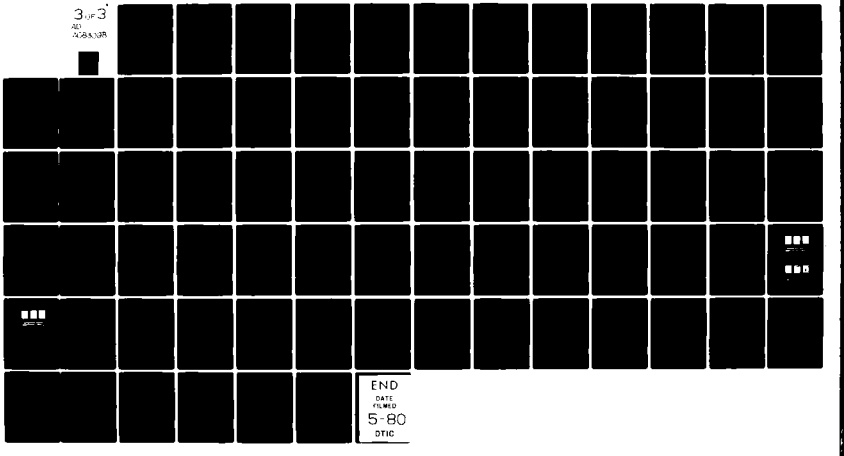

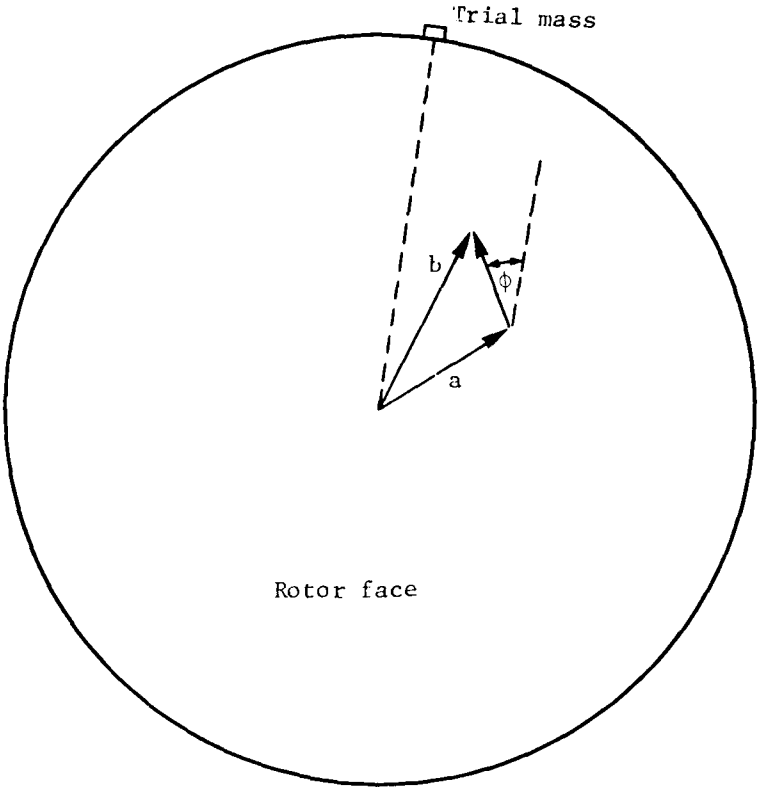

$\bar{a}$ = Deflection without trial mass

$\bar{b}$ = Deflection with trial mass

$\bar{b} - \bar{a}$ = Effect of trial mass

: = Phase difference between deflection and force

Fig. 2 Measurements required for determining the response to a trial mass (all directions are fixed on the rotor face)

to simply solving directly or in a least squares sense a set of linear algebraic equations. Because iterative searches increase rapidly in computational expense as the number of shaft masses in the model is increased and because convergence can be slow and somewhat uncertain, it is advantageous to either avoid them completely or, if they must be used, to obtain the best possible initial parameter estimates before resorting to the iterative search.

For a five mass shaft model the complete (12x12) system impedance matrix is shown in Fig. 3. The elements of this matrix were derived from stiffness matrices given in reference (8). The impedance matrix can readily be expanded for models with more than five masses because for masses between the shaft ends the rows of the matrix contain the same elements but shifted one position to the right of the previous row element. The important facts to note are that the unknown parameters occur linearly in the impedance matrix rows and that the unknown parameters appear in only five rows of the matrix. Thus if the column vector of transfer functions were measured, five complex equations (ten real) would be available to solve for some of the unknown parameters. More equations could be obtained by placing the trial mass at different stations or by operating the rotor at different speeds. The constants of the

D1	(-K2,-ωC2)										
(-K2,-ωC2)	D2	(-X,0)					(Y,0)	(Y,0)			
	(-X,0)	D3	(-X,0)				(-Y,0)		(Y,0)		
		(-X,0)	D3	(-X,0)				(-Y,0)		(Y,0)	
			(-X,0)	D3	(-X,0)				(-Y,0)		(Y,0)
				(-X,0)	D4	(-K4,-ωC4)				(-Y,0)	(-Y,0)
					(-K4,-ωC4)	D5					
	(Y,0)	(-Y,0)					D6	(ST,0)			
	(Y,0)		(-Y,0)				(ST,0)	D7	(ST,0)		
		(Y,0)		(-Y,0)				(ST,0)	D7	(ST,0)	
			(Y,0)		(-Y,0)				(ST,0)	D7	(ST,0)
				(Y,0)	(-Y,0)					(ST,0)	D8

BLANK SPACES ARE (0,0)

LET D = ((SF)AGL^2+12EI)

SF = $6(1+PR)(1+(ri/r)^2)^2/\{(7+6PR)(1+(ri/r)^2)^2+(20+12PR)(ri/r)^2\}$

SF = (2EI/L)((SF)AGL^2-6EI)/D

Z2 = (4EI/L)((SF)AGL^2+3EI)/D

Y = 6EI(SF)AG/D

*X = 2Y/L

X2 = 4Y/L

Z4 = 2Z2

D1 = $(-\omega^2$MBL+K1+K2, ω(C1+C2))

D2 = $(-\omega^2$MSL+K2+X, ωC2)

D3 = $(-\omega^2$MSR+X2,0)

D4 = $(-\omega^2$MSR+K3+K4, ω(C3+C4))

D5 = $(-\omega^2$MBR+K3+K4, ω(C3+C4))

D6 = $(-\omega^2$(RL-SP)+KT+Z2,0)

D7 = $(-\omega^2$(R-IP)+Z4,0)

D8 = $(-\omega^2$(RR-RP)+Z2,0)

Fig. 3 Impedance matrix for a five mass shaft model in steady-state sinusoidal motion

left bearing appear in the first two rows of the matrix, the constants of the right bearing in the N + 1 and N + 2 rows (N = number of shaft masses), and the rotary spring occurs only in the N + 3 row.

These five complex equations contain displacements, rotations, and phases (here, phase refers to the phase difference between displacement or rotation and the unbalance excitation). If the displacements and phases of the first three masses and the last three masses were known, and the rotations and phases of the first two shaft masses were known, then enough information could be gathered to solve for the unknown parameters either directly or in a least squares or minimax sense, depending on whether the number of equations equalled or exceeded the number of unknowns.

The difficulty with this solution is that measurements of rotations and their phases are evidently rarely if ever made. Also, it could be that a displacement measurement could not be taken due to the inaccessibility of some portion of the rotor. If rotations have not been measured, it is possible to eliminate them from the problem by solving for them in terms of displacements using rows of the matrix which contain no unknown parameters. Because of the sparseness of the impedance matrix, this procedure would not entail an overwhelming amount of algebraic manipulation, especially for rotor models with a small number of lumped masses.

If the available experimental data is such that only displacements are known, then an iterative solution is a feasible alternative. A steepest descent gradient algorithm was developed to demonstrate the estimation process. With this method an error function consisting of the sum of the squares of the differences between computed and measured displacements is found, and the partial derivatives of that error with respect to the unknown parameters are used to seek values of constants which result in smaller errors. Beginning at an initial estimate of the constants, the negative gradient direction is followed until the error begins increasing; then a new gradient is computed, and the procedure is repeated.

The gradient search method has the advantage that eventually some low point must be reached; however, convergence can be slow, and no guarantee exists that the low point reached will be the absolute minimum point of a multi-modal objective function. Another difficulty associated with the gradient method is that of scaling the variables such that all the partial derivatives in the gradient have the same order of magnitude. In a case in which the pedestal spring is much smaller than the bearing spring (K2>>K1) for example, the problem cannot be properly scaled because both constants have the same units and the rotor response is much more sensitive to the smaller pedestal spring than to the bearing spring.

Two example problems illustrating some of the difficulties involved in parameter estimation are discussed on the following pages. The steepest descent method used in the examples, despite its simplicity, is generally not regarded as a good optimization tool. In reference (9) several alternative optimization techniques are described which might be applied to the parameter estimation problem. The PARTAN methods, the method of conjugate gradients, or the variable metric method might offer improved performance over that obtained from the steepest descent search. These methods are modified gradient techniques developed to very efficiently optimize a quadratic function,

but they can also improve the efficiency of optimization of non-quadratic functions.

EXAMPLES

Two sample runs of the parameter estimation problem are presented. The first two problems use the steepest descent gradient search. The gradient search method can be used to the best advantage when fairly good estimates of the unknown parameters are initially available.

All of the example problems use the same rotor model, the same trial mass, and the same displacement data. This information is summarized in Table 1. The rotor has been modeled with ten concentrated shaft masses, and the trial mass is 10g placed at the third mass station. The displacement values shown in Table 1 were computed rather than measured, and the number of significant figures shown exceeds any that actually would be measured.

TABLE 1

PROPERTIES OF THE ROTOR USED IN THE EXAMPLE PROBLEMS

ROTOR PHYSICAL PROPERTIES	
Length = 2.54m	Young's modulus = 69.56GN/m^2
Outer radius = 0.127m	Shear modulus = 6.956GN/m^2
Inner radius = 0.1245m	Poisson's ratio = .3
Mass/volume = 4188.9kg/m^3	
(The end cap masses and moments of inertia are zero in the example rotor.)	

TRUE PARAMETER VALUES	
MBL = .883kg	K1 = 8.834MN/m
MBR = .883kg	K2 = 88.34MN/m
C1 = 8834.6Ns/m	K3 = 7.068MN/m
C2 = 0.0	K4 = 70.68MN/m
C3 = 5300.8Ns/m	KT = 11399.5Nm/rad
C4 = 0.0	

DISPLACEMENTS CAUSED BY A 10g TRIAL MASS AT STATION 3 (OPERATING FREQUENCY = 100Hz)						
STATION NUMBER	1	2	3	4	5	6
DISPLACEMENT (mm)	.0251816	.0276634	.0176305	.0315312	.0645451	.0916482
STATION NUMBER	7	8	9	10	11	12
DISPLACEMENT (mm)	.107037	.108043	.0947153	.0698863	.0397836	.0362853

Problem 1

In the first example problem the gradient search method is applied to estimate the four pedestal parameters K1, K3, C1, and C3. The initial estimate of each parameter is 50% below its true value. The other model parameters are held fixed at their true values.

The results of the run are summarized in Table 2. The constants converged to within 3% of their true values in 173 iterations. Using the computed values of the constants, values of displacements are obtained which agree with the actual values to three significant figures at five mass stations and to two significant figures at the remaining seven stations. The root mean square of the differences between the computed and the true displacements is .51836μm.

TABLE 2

SUMMARY OF THE RESULTS OF EXAMPLE NO. 1

PARAMETER	INITIAL ESTIMATED VALUE	TRUE VALUE	COMPUTED VALUE	PERCENT ERROR	DISPLACEMENTS (mm) (STATIONS 1 THROUGH 12)	
					COMPUTER VALUES	TRUE VALUES
C1 (Ns/m)	4,417.3	8,834.6	8,562.4	-3.08	.025090	.025182
C3 (Ns/m)	2,650.4	5,300.8	5,259.3	-.78	.027534	.027663
K1 (KN/m)	4.4173	8.8346	9.0180	+2.08	.017536	.017630
K3 (KN/m)	3.5338	7.0677	7.0366	-.44	.031318	.031531
					.064414	.064545
					.091592	.091648
					.10703	.10704
					.10812	.10804
					.085725	.094715
					.070078	.069886
					.040005	.039784
					.036525	.036285

The fairly good success obtained in this problem is attributable to the high sensitivity of the rotor response to the pedestal constants and to the choice of a time scale which made the gradient components with respect to the damper constants approximately the same magnitude as those with respect to the spring constants.

Problem 2

In the second problem the gradient search is also applied, but in this example nine of the eleven model constants are included in the search. The initial estimates of the parameters have all been chosen close to their true values in order to have a good chance of converging to the true minimum. The optimization was performed in an alternating sequence beginning with the four pedestal constants, then the two bearing masses, and finally the rotary and bearing springs. The two bearing dampers were held fixed at zero. The results are summarized in Table 3.

TABLE 3

SUMMARY OF THE RESULTS OF EXAMPLE NO. 2

PARAMETER	INITIAL ESTIMATED VALUE	TRUE VALUE	COMPUTED VALUE	PERCENT-ERROR	DISPLACEMENTS (mm) (STATIONS 1 THROUGH 12)	
					COMPUTED	TRUE
MBL (kg)	.7951	.8835	.7589	-14.1	.025135	.025182
MBR (kg)	.7951	.8835	1.0327	+16.9	.027669	.027663
C1 (Ns/m)	7,951.2	8,834.6	8,559.0	-3.1	.017418	.017630
C3 (Ns/m)	4,417.3	5300.8	5,229.0	-1.3	.031279	.031531
k1 (KN/m)	7.9512	8.8346	8.9509	+1.3	.064458	.64545
k2 (KN/m)	79.512	88.346	87.270	-1.2	.091649	.091643
k3 (KN/m)	6.1842	7.0677	7.1582	+1.3	.10708	.10704
k4 (KN/m)	61.842	70.677	73.280	+3.7	.10811	.10804
KT (Nm/rad)	9,689.6	11,399.5	4,118.9	-63.9	.094767	.094715
					.069888	.069886
					.039662	.039784
					.036284	.036285

Of the nine constants in the search six came to fairly good agreement with their true values; two MBL and MBR converged to incorrect values which did not differ too greatly from their true values, while the rotary spring reached a value more than 60% less than its true magnitude. Despite the disparity between the values of three of the constants and their true values, the computed and measured displacements agree to two or three significant figures, and the root mean square of the differences between the two sets of displacements is .37759mm, which is a smaller error than that of example 1. These results emphasize the difficulties which arise in estimating parameters such as the rotary spring constant when the rotor response is highly insensitive to the constant magnitude.

SUMMARY AND CONCLUSIONS

The problem of estimating parameters in a linear rotor-bearing model is discussed. A particular estimation technique involving measurements of influence coefficients is proposed. Several example problems illustrating the application of a gradient search technique to the estimation problem are presented. Although the results are generally good for parameters to which the rotor response is most sensitive, some difficulty is encountered in finding accurate estimates for parameters which do not strongly influence the rotor rotor response. The principal problem area is the convergence of the gradient search method to a local rather than an absolute minimum when the initial estimates of the parameters are far from the correct values. Also, the success of steepest descent optimization depends strongly upon the scales chosen for the units in which the unknown parameters are specified. Several alternative optimization techniques such as the PARTAN methods, the method of conjugate gradient, and the variable metric method are suggested as approaches which might be more efficient than the steepest descent algorithm used in these examples.

ACKNOWLEDGEMENT

This work was supported by the U.S. Army Research Office, Research Triangle.

REFERENCES

1 Goodman, T. P., "A Least-Squares Method for Computing Balance Corrections", Journal of Engineering for Industry, Trans. ASME, Vol. 86, Series B, Aug. 1964. pp. 273-279.

2 Morton, P. G., "Measurement of the Dynamic Characteristics of a Large Sleeve Bearing", Trans. ASME, 93 (F), 143-50 (1971).

3 Thomsen, R. K. and Anderson, H., "Experimental Investigation of a Simple Squeeze-Film Damper," Trans. ASME, 96 (B), 427-30 (1974).

4 Tonnesan J., "Experimental Parametric Study of a Squeeze - Film Bearing", Trans. ASME, 98 (F), 206-13 (1976).

5 Burrows, C. R. and Stanway, R., "Identification of Journal Bearing Characteristics," Trans. ASME., 99 (G) 167-173 (1977).

6 Stranway, R., Burrows, C. R., and Holmes, R., "Pseudo - Random Binary Sequence Forcing in Journal and Squeeze - Film Bearings" American Society of Lubrication Engineers, Dearborn, Mich., 1978.

7 Schlegel, V. and Mahrenholtz, O. "Identification of a Rotor System", Dynamics of Multibody Systems, Springer Verlag Berlin Germany, 1977.

8 Azar, J. J., Matrix Structural Analysis, New York, Pergamon Press Inc., 1972.

9 Gottfried, B. S., and Weismann, J., Introduction to Optimization Theory, Englewood Cliffs, New Jersey: Prentice-Hall Inc., 1973.

TRANSIENT DYNAMICS OF SQUEEZE FILM BEARING SYSTEMS

Anthony J. Smalley

Mechanical Technology Incorporated
968 Albany-Shaker Road
Latham, New York 12110

ABSTRACT

This paper reviews methods available for analyzing transient response of squeeze film damper bearing systems, including treatment of the rotor and the fluid film. Important considerations in choosing a method are discussed, and limitations in the published state-of-the-art are identified.

NOMENCLATURE

C	Damping
C_D	Total residual matrix in modal space
C_D'	Residual damping matrix in modal space
C_n	Constant of integration
$f_n(t)$	Forcing function in damped modal space
f_r	Forcing function in modal space
$f(t)$	Excitation vector
h	Film thickness
k	Stiffness
$[K]$	Generalized stiffness matrix
M	Mass
$[M]$	Generalized inertia matrix

N	Non-linear excitation vector
n	Mode number; also time step count
N_n	Modal norm
p	Pressure
q_n	Damped modal coordinate
r	Radius
S_n	Constant of integration; also nth damped natural frequency
t	Time
Δt	Time step
V	Velocity
{X}	Generalized displacement vector
$\{X_n^*\}$	Complex modal vector for nth damped mode
β	Newmark's coefficient
ζ	Damping ratio
η	Modal coefficient
θ	Circumferential coordinate
λ	Growth component
μ	Viscosity
ξ	Modal velocity vector
τ	Time parameter for convolution integrals
ϕ	Mode shape
ω	Frequency; also rotational speed
$[\omega^2]$	Diagonal Eigenvalue matrix
ω_n	Frequency component

INTRODUCTION

The dynamic behavior of damped rotor bearing systems can be predicted for the majority of conditions by frequency domain analysis; for linear systems, the majority of design and analysis questions can be answered by performing critical speed, unbalance response, nonsynchronous response, and damped natural frequency analyses. These frequency domain algorithms are economical; they provide compact and comprehensible output; they are convenient for parametric studies; and direct cause/effect relationships can normally be established by the use of these techniques. However, frequency domain analysis does not directly answer all questions.

Time domain analysis is required in a number of situations which are becoming increasingly important; for example:

- Response of linear systems to non-periodic excitation such as:
  - Seismic excitation
  - Maneuver loads
  - Shock loads
- Response to periodic excitation of systems with non-linear elements such as:
  - Spline couplings
  - Squeeze film dampers
  - "Dead bands"
  - Fluid bearings in which vibration amplitudes are significant compared with the clearance
- Response to periodic excitation of time-varying linear systems such as:
  - Flexurally asymmetric shaft in asymmetric bearings
  - Intershaft fluid film bearings without circumferential symmetry
  - Floating ring bearings without circumferential symmetry
  - Accelerating or decelerating rotors under any excitation
- Response of non-linear systems to non-periodic excitation
- Free vibration response of non-linear or time-varying systems to initial disturbance for stability and limit cycle evaluation

The objective of this paper is to present the major options available for transient analysis of damped rotor systems. The paper will emphasize squeeze film damper supported systems, but many of the points made will be more generally applicable. Some advantages and disadvantages of the available options will be discussed. Limitations of the present state-of-the-art will be defined, and areas needing further work, analysis, and evaluation will be defined. The thrust of the paper is to provide information for the engineer interested in establishing a meaningful, computer-assisted basis for engineering design decisions.

ANALYTICAL METHODS

In the following paragraphs, some major groupings of analytical methods for predicting transient response of a rotor bearing damper system are

described and discussed. The methods considered are:

- Modal methods (damped and undamped)
- Direct numerical methods
- Hybrid computation methods

These are discussed in turn in the following paragraphs.

Modal Methods

The basis for modal methods of predicting transient response is that the deflected shape of the rotor at any instant in time can be expressed as the sum of its natural modes of vibration, each multiplied by a weighting factor or modal coordinate. Since natural modes satisfy orthogonality relationships, the response of individual modes to the imposed excitation may be computed independently. As shown by reference (1), the system of equations:

$$[M]\{\ddot{X}\} + [K]\{X\} = \{f(t)\} \tag{1}$$

may be replaced by:

$$\{\ddot{\eta}\} + [\omega^2]\{\eta\} = \{f_r(t)\} \tag{2}$$

where η is the vector of modal coordinates which measures the participation of each mode in the response and may be mapped into real space as follows:

$$\{X\} = [\phi]\{\eta\} \tag{3}$$

where $[\phi]$ is the matrix of modes, normalized so that $[\phi]\, m[\phi] = I$, the identity matrix, and $f_r(t)$ is the vector in modal space mapped from the real space excitation as follows:

$$\{f_r(t)\} = [\phi]^t \{f(t)\} \tag{4}$$

$[\omega^2]$ is the diagonal matrix of system natural frequencies or eigenvectors.

Clearly, each row of the matrix equation (2) is uncoupled from any other row since the only operator is a diagonal matrix. Thus, the equation for each modal coordinate may be solved independently of the equations for all other modal coordinates.

The general solution to equation (2) is for any modal coordinate:

$$\eta_n = C_n \cos(\omega_n t) - S_n \sin(\omega_n t) + \frac{1}{\omega_n}\int_0^t f_{rn}(\tau)\sin\omega_n (t-\tau)d\tau \tag{5}$$

where C_n and S_n are constants delineated to match the initial boundary conditions; ω_n is the nth modal frequency; and $f_{rn}(t)$ is the nth component of $\{f_r(t)\}$.

Solution in modal space has the additional advantage that the number of modes considered can be less than the total number of system modes, and, generally, accurate results can be obtained by considering only a small number of modes (e.g., 3 or 4).

The response of a linear rotor system in linear, time-invariant bearings may be described by an equation of the general form of equation (1), except for two complicating features:

- Damping, which adds the term $[C]\{X\}$ to equation (1)
- Gyroscopic terms

Provided the damping matrix satisfies necessary relationships to the mass or stiffness matrices, the same operations which led to diagonalization in equation (1) (pre- and post-multiplication of each matrix by $[\ ]^t$ and $[\ ]$ respectively) can be used to diagonalize the damping term, giving an equation of the form:

$$\{\ddot{\eta}\} + [2\zeta\omega] \{\dot{\eta}\} + [\omega^2] \{\eta\} = \{f_r(t)\} \tag{6}$$

Unfortunately, in most rotor situations, the damping matrix does not rigorously satisfy the required relationships, and the diagonalization operation leaves stray terms, so that the full equation is of the form:

$$\{\ddot{\eta}\} + [2\zeta\omega] \{\dot{\eta}\} + [\omega^2] \{\eta\} + [C_D^1] \{\dot{\eta}\} = \{f_r(t)\} \tag{7}$$

Gyroscopic effects give rise to off-diagonal, damping-like terms which likewise are not diagonalized by the operation leading to equation (2). Thus, the full rotor system has the form:

$$\{\ddot{\eta}\} + [2\zeta\omega] \{\dot{\eta}\} + [\omega^2] \{\eta\} + [C_D] \{\dot{\eta}\} = \{f_r(t)\} \tag{8}$$

where C_D is now a matrix of residual terms accounting for some damping and gyroscopic effects and is generally neither diagonal nor sparse. Further development of this equation and the content of C_D can be obtained from Dennis, et al. (2) or Choy, et al. (3). The treatment of the residual terms embodied in the C_D matrix offers several options, which are summarized as follows, and are then discussed in more detail.

- Neglect the residual terms.
- Transfer the residual terms to the right-hand side of equation (4) and treat them as part of the excitation function.
- Transfer residual damping terms to the right-hand side, but account for gyroscopic effects by the undamped modal analysis method for asymmetric matrices described by Lund (5).
- Leave the residual terms on the left-hand side of the equation and incur the problem of coupling between equations or matrix inversion for the limited number of modes (as discussed, typically 3 or 4) which result.
- Use damped modes of vibration as described by Lund (6).

Neglect of the residual terms can, in some cases, be quite satisfactory; this generally requires that damping be relatively light and that the dynamics of the rotor be governed more strongly by the mass distribution rather than

by localized or distributed rotary inertias. In this case, the considerable advantages of the simple, normal mode treatment can be preserved. However, in cases where there is significant localized damping or rotary inertia, this course of action is not satisfactory.

Treatment of the residual terms as right-hand side excitations has been shown by Dennis (2) to be an effective approach. However, on the right-hand side, these terms have the characteristics of non-linearity; a "pseudo-excitation", which is a function of the state variables. The evaluation for the terms requires values for the state variables; this feature enforces a step-by-step procedure in time. At any stage in the process (current time), the state variable values at current and past time provide a basis for evaluating the pseudo-excitation so that the step-by-step process may be advanced to a future time. The accuracy and stability of any computational procedure will be a function of the frequency with which the pseudo-forcing functions are updated. Dennis reports the potential for oscillating solution to what should be a stable problem apparently associated with the gyroscopic terms. An approach based on Lund's work (5) will eliminate the problem of gyroscopic terms in return for considering the pairs of modes introduced by asymmetry.

If an explicit numerical integration scheme capable of handling non-linearities is chosen, the handling of the pseudo-forcing functions falls naturally into place. Thus, defining $\{\dot{\xi}\} = \{\eta\}$, we have:

$$\{\frac{d\dot{\xi}}{dt}\} = \{f_r(t)\} - [2\zeta\omega]\{\dot{\xi}\} - [C_D]\{\dot{\xi}\} - [\omega^2]\{\eta\} \tag{9}$$

and

$$\{\frac{d\eta}{dt}\} = \{\dot{\xi}\} \tag{10}$$

and any number of numerical integration methods (self-starting schemes, such as Euler, Runge-Kutta, Kutta-Merson, and predicter-corrector methods, such as Adams, Milne, or Hamming) may be used. A piecewise continuous approach is also possible and will be discussed in relation to non-linear systems in equations (21) through (23). The question can be asked, "Has the modal formulation gained anything if the additional complexity of approximate numerical integration is required?" The answer must be a definite yes. The powerful flexibility remains to employ only as many modes as accuracy requirements impose.

The fourth option for treatment of damping, namely evaluation and use of damped system modes, is a powerful one, pioneered by Lund (6). It readily handles arbitrarily distributed damping, bearing cross-coupling terms, gyroscopic terms, isotropy, and asymmetry in the bearings. Each damped mode is characterized by a complex frequency:

$$S_n = \cdot_n + i\cdot_n \tag{11}$$

where $\cdot_n$ is a growth term and by a set of complex modal vectors.

$\{X_n^*\}$ which implicitly contains the lateral displacements in two orthogonal directions and angular displacements in two orthogonal directions.

It is shown by Lund that the response of a rotor system can be evaluated by solution of equations of the form:

$$\frac{dq_n}{dt} - S_n q_n = f_n(t) \tag{12}$$

for each damped mode, where q_n is the modal coordinate (analogous to the modal coordinates for the undamped modal approach) for the nth mode, and $f_n(t)$ is a modal excitation function developed as follows:

$$f_n(t) = \frac{1}{N_n} \{X_n^*\}^t \{f(t)\} \tag{13}$$

where $f(t)$ is the total excitation function, including excitations in two lateral and two angular directions. The modal norm N_n depends on the manner in which each mode is normalized (two options are to set the largest amplitude to 1, or to require $N_n = 1$, and normalize the mode accordingly).

The general solution to equation (12) is:

$$q_n(t) = q_n(t=0)\, e^{S_n t} + \int_0^t e^{S_n(t-\tau)} f_n(\tau)\, d\tau \tag{14}$$

As shown by Lund for systems where the stiffness matrix is asymmetric, it is necessary to include in the evaluation the adjoint modes and adjoint modal functions obtained by replacing the stiffness and damping matrices by their transposes and by changing the sign of terms containing polar moments of inertia. A similar approach was presented by Pilkey (19).

The damped modes option has the advantage of implicitly handling the general damping matrix gyroscopic terms and asymmetric cross-coupling stiffness terms. The disadvantage of this approach is that the computational algorithm to find the damped modes is clearly more involved than that for planar undamped modes, and the need to include adjoint modes in the time transient algorithm is an additional complexity in the software development. In practice, it is also found that additional care is needed to ensure that all modes are found before initiating the time integration process and that the higher modes (above the third or fourth pair of backward and forward modes) are subject to numerical instability if computed by the popular transfer matrix algorithm. In this case, an alternative method such as the Ricatti transform (7) is then required. It is found that, with the transfer matrix method, circular orbit and undamped modes can be obtained to much higher order than non-circular orbit damped modes.

To illustrate the use of damped, modal, transient analysis, the response to a step increase in velocity of one bearing support of a flexible helicopter power transmission shaft (as described in reference (8)) is shown in Figures 1, 2, and 3. Such an excitation function might result from a maneuver or hard landing involving angular velocity of the aircraft. The shaft has a damped bearing at one end, and it is at this location that the step increase in velocity is applied. Figure 1 shows the response at the shaft center computed in two ways: first with the first four modes (two forward, two

backward) considered; and second with the first eight modes (four forward, four backward) included. Interestingly, for this point on the shaft, predicted response as a function of time is negligibly influenced by the number of modes used. (The predicted peak amplitude is approximately two percent higher with the four modes than with the eight.) Clearly, the only participation of any import comes from the fundamental mode.

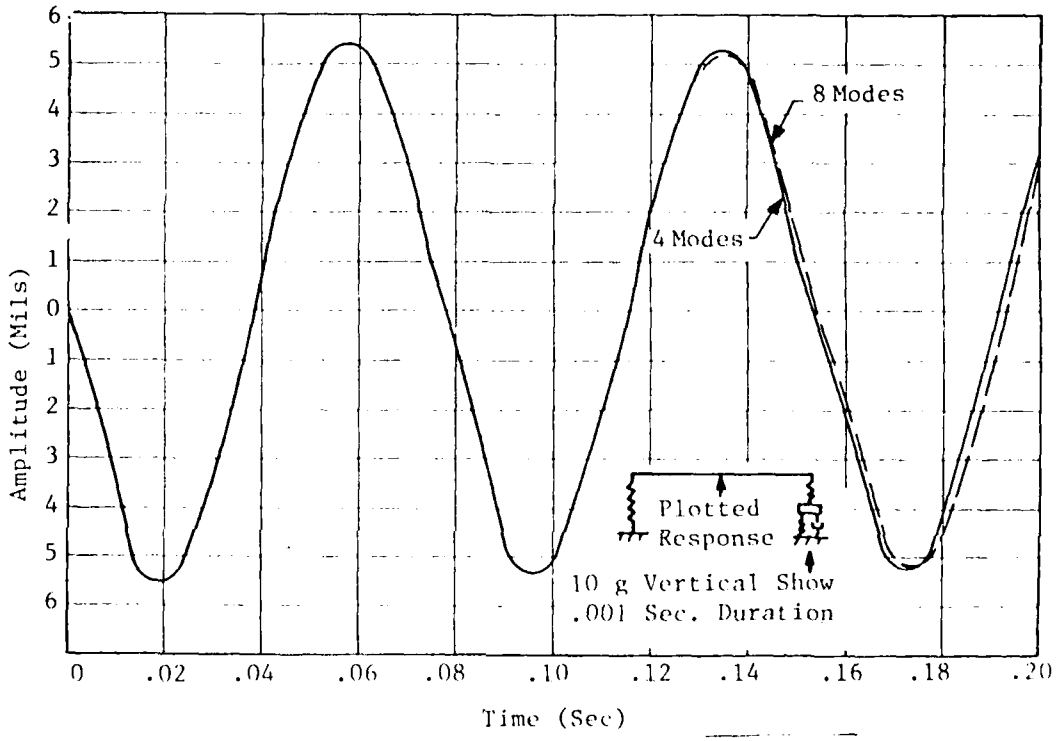

Figure 1. Damped Modal Time Integration Influence on Solution of Number of Modes Considered. Shaft Center.

In Figure 2, the effect of damping on the peak amplitude at shaft center is shown. Three conditions are compared:

- Support damping = 25 lb·sec/in.; support stiffness = 2500 lb/in.
- Support damping = 50 lb·sec/in.; support stiffness = 2500 lb/in.
- Support stiffness = ∞; support damping = zero

These comparisons are intended to be illustrative of the trade-off design studies which can be performed with this transient analysis capability.

It may be seen for the shaft in question that peak amplitude is negligibly affected by damping, perhaps by less than one percent. What is clear, however,

is that the rate of decay of vibration amplitude is affected by the presence of damping. Within three cycles, either of the damped cases have dropped in amplitude by 10 percent.

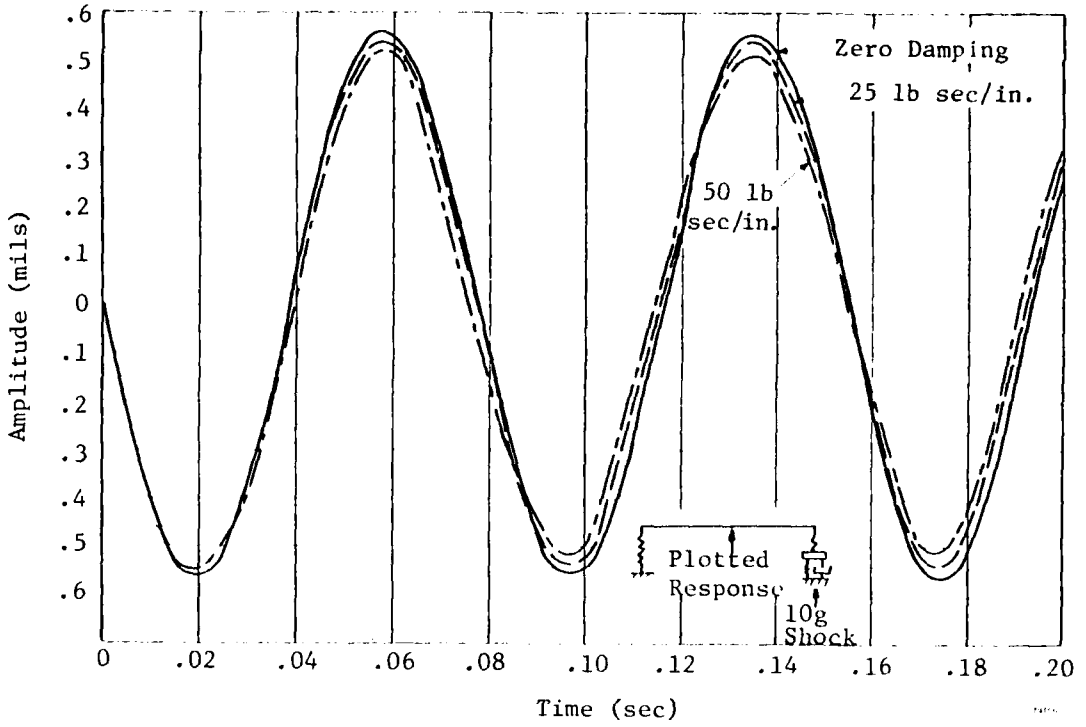

Figure 2. Damped Modal Response. Effect of Damping (Four Modes)

In Figure 3, the response of the shaft at the damped bearing is shown. Here the participation of the modes, other than the fundamental, is much more apparent. However, the choice of number of modes does not affect the predictions qualitatively or quantitatively except in one regard, the ability to precisely match initial boundary conditions. While not affecting the peak amplitude to any degree, and, therefore, of little importance from an engineering point of view, this feature of the damped modal transient method is one of its minor disadvantages. Since the number of modes does affect the match of initial conditions to zero, it is assumed that a sufficient number of modes will achieve a satisfactory match.

Direct Numerical Integration Method (Digital)

The basis for direct numerical integration methods is to substitute for equations containing continuous time derivatives an equivalent algebraic equation which replaces the continuous derivatives with discrete approximations and performs a step-by-step solution of the resultant equation. Alternative approaches to direct numerical integration are listed on the following page.

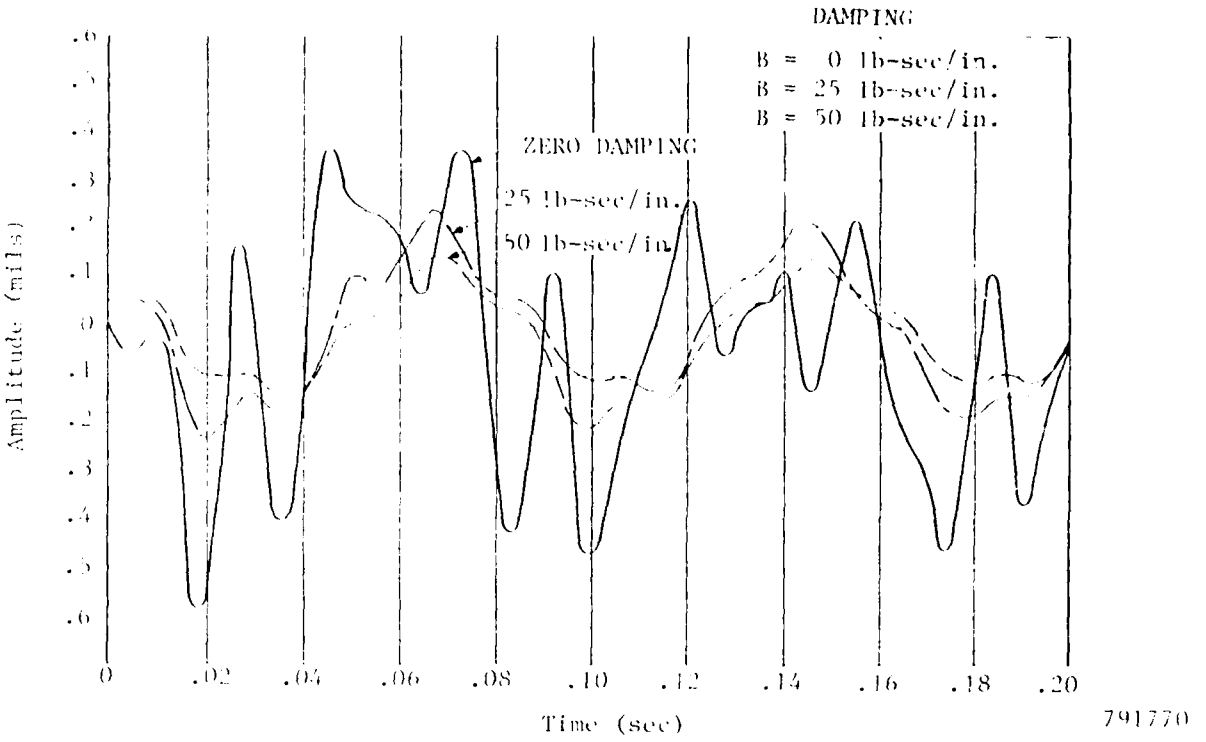

Figure 3. Damped Modal Response, Influence of Damping on Shaft End Response (Four Modes)

- Explicit methods, such as the Euler, Runge-Kutta, or Adams method
- Implicit methods, such as the Newmark Beta Algorithm

A common approach to applying an explicit integration is to treat both the displacements and the velocities as unknowns and to develop explicit expressions for the first time derivatives of these unknowns in terms of current values of velocities and displacement. These expressions are evaluated at each step and sub-step of the process as the state variables of velocity and displacement are advanced. For example, considering the general equation of motion:

$$[M]\{\ddot{X}\} + [C]\{\dot{X}\} + [K]\{X\} = \{F(t)\} \tag{15}$$

a vector of unknown velocities, V, is defined so that:

$$\frac{dV}{dt} = -[M]^{-1}\left\{[C]\{V\} + [K]\{X\} - \{F(t)\}\right\} \tag{16}$$

and

$$\frac{dX}{dt} = V \tag{17}$$

For most explicit integration methods, there exit efficiently coded, well tested subroutines which will perform a single step or multiple steps of these algorithms. The user of these subroutines would interface via the argument list and via a user-developed subroutine which evaluates the derivatives of velocity and displacement. Thus, convenience is a clear advantage of this approach. Gunter and Kirk (9) describe the application of the Euler method to rotor transients.

As with any numerical method, care must be taken to preserve accuracy. The time step must be sufficiently small that truncation errors in the discrete representation of the equations of motion are negligible for the phenomenon and application under investigation. A further significant problem with explicit methods is the potential for numerical instability. If the time step is too large to provide between two and three time steps per cycle of the highest system frequency, numerical instability occurs, manifesting itself by answers which are usually very large and physically meaningless. Thus, a system with a wide range of system natural frequencies, in order to be stable for the highest frequency, may require hundreds or thousands of time steps per cycle of the lowest natural frequency, even though far fewer time steps would be adequate from accuracy considerations.

The advantage of explicit methods is their simplicity of implementation and the convenient handling of non-linearities. The latter feature will be discussed further in a later section of this paper.

Implicit numerical integration methods require a set of spatially coupled equations for the vector of state variables at the next step in the process (future time) in terms of values of state variables at current and past time. For example, in the frequently used Newmark Beta method (10), the same equation referred to with respect to explicit integration methods is replaced by the following:

$$[M]\left\{\ddot{X}_{n+2} - 2\ddot{X}_{n+1} + \ddot{X}_n\right\}\frac{1}{\Delta t^2} + [C]\left\{\dot{X}_{n+2} - \dot{X}_n\right\}\frac{1}{2\Delta t} + [K]\left[\beta X_{n+2} + (1-2\beta)X_{n+1} + \beta X_n\right] \tag{18}$$

$$= \left[\beta f_{n+2} + (1-2\beta) f_{n+1} + \beta f_n\right]$$

where a value for β of 1/3 has been found to be satisfactory.

In this equation, time step (n+1) is current time and time step (n+2) is future time. The equation is re-arranged to give the operation for advanding from known state vector values at time steps n+1 and n to the unknown state vector at future time.

$$X_{n+2} = \left[\frac{M}{\Delta t^2} + \frac{C}{2\Delta t} + \beta K\right]^{-1}\left\{\left[\frac{2M}{\Delta t^2} + (2\beta-1)K\right]X_{n+1} - \left[\frac{M}{\Delta t^2} - \frac{C}{2\Delta t} + \beta K\right]X_n + \beta F_{n+2} + (1-2\beta) f_{n+1} + \beta f_n\right\} \tag{19}$$

To start the process, the usual assumption is that of zero acceleration prior to and including time 0, so that:

$$\{X_{-1}\} = \{X_0\} - \{\dot{X}_0\}\,\Delta t$$

$$\{f_{-1}\} = [K]\{X_{-1}\} + [C]\{\dot{X}_0\} \tag{20}$$

$$\{f_0\} = [K]\{X_0\} + [C]\{\dot{X}_0\}$$

The Newmark Beta integration process firstly requires availability of the inverse matrix $\left[\frac{M}{\Delta t^2} + \frac{\beta}{2\Delta t} + \beta K\right]^{-1}$, and for linear systems this can be set up at the beginning of the process and used thereafter without further inversion. Secondly, the process involves three separate multiplications of square matrices of order N (where N is the number of degrees of freedom), by vectors of order of N. This series of multiplications governs the computational cost of the Newmark Beta method in most cases.

In general, the cost of the Newmark method is more per time step than for simple explicit methods, particularly something as simple as the Euler method. However, numerical stability can be achieved with fewer time steps. In fact, for linear systems, the method is absolutely stable, although the requirement to ensure accuracy by means of sufficient time steps does remain.

In one example comparing the Newmark method to the Runge-Kutta method, with system frequency spread (highest to lowest) of 50:1, it was found that a solution accurate within two percent could be found with the Newmark method for one quarter the computer cost of the cheapest stable solution with the Runge-Kutta method.

Figures 4 and 5 show orbits computed by the Newmark Beta method for a flexible rotor excited by a sudden applied unbalance representative of a blade loss. Figure 4 is for an isotropic support where the asymptotic solution is a circular orbit. Figure 5 is for an anisotropic support where the asymptotic solution is an elliptical orbit.

Hybrid Computation

In hybrid computation, the continuous time variation or each state variable is simply replaced by a continuously variable analog: specifically, an electrical voltage. The values for the time derivatives are, however, evaluated digitally. To effect this process, both analog-to-digital and digital-to-analog conversions are required at various stages. The digitally evaluated time derivatives are converted to voltages, which are then integrated using analog integrators. The state variable voltages which result from the integrations are periodically sampled and digitized. Each time this digitizing occurs, a digital calculation of the time derivatives is performed, and these updated time derivatives are then fed back into the continuous integration process as analog values. It has some similarities to an explicit integration method, except that the discrete advancement in time is replaced by continuous advancement in time. The process is illustrated very simply in Figure 6.

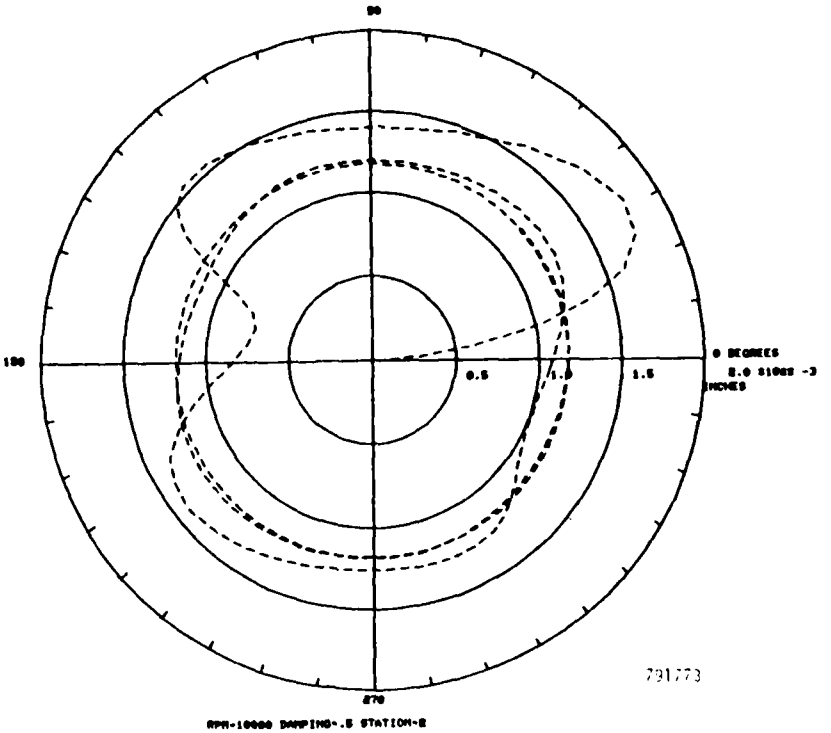

Figure 4. Damped Rotor Response to Blade Loss, Symmetric Suspension, Newmark Method Solution

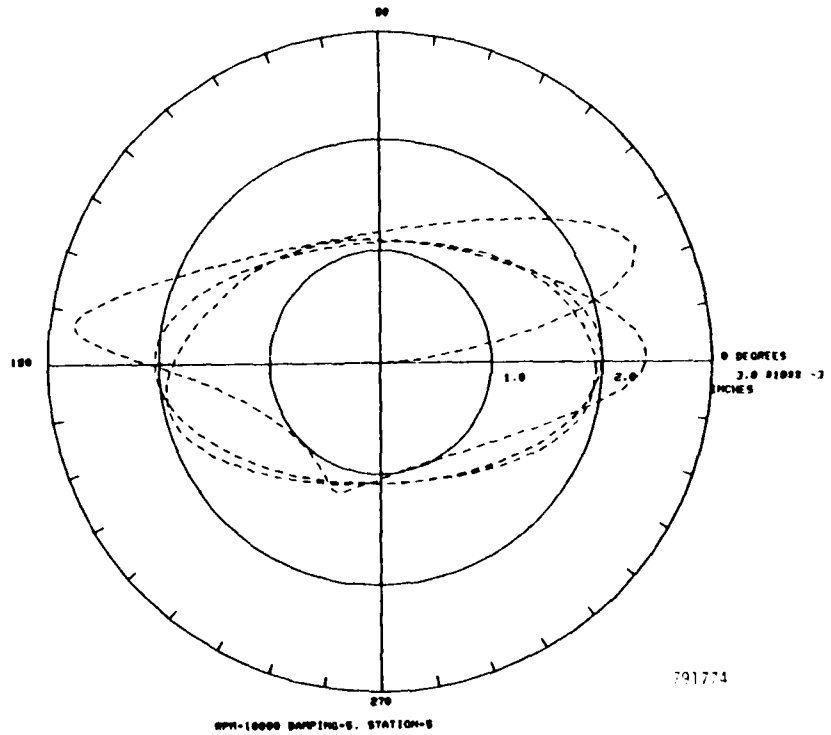

Figure 5. Damped Rotor Response to Blade Loss, Unsymmetric Suspension, Newmark Method Solution

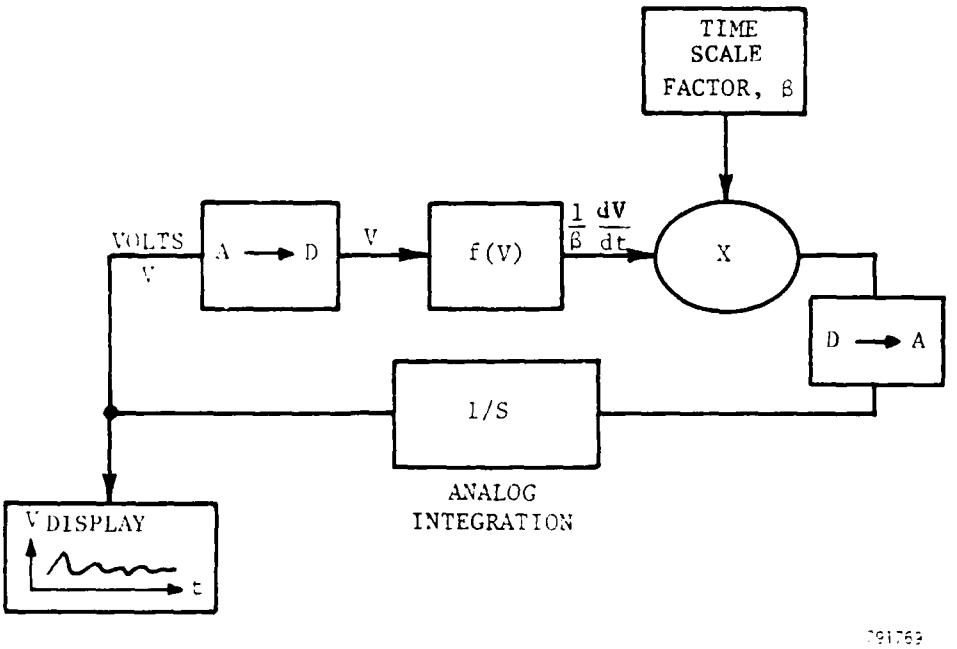

Figure 6. Hybrid Computation Schematic

Clearly, the time between sampling must be kept long enough for the digital calculations to be completed. At the same time, the accuracy of the computation process is controlled by the amount by which the calculated time derivative values, based on state variables at the instant when sampled, differ from those values which would result if they could be instantaneously evaluated at the instant when they are fed back into the analog portion of the system. Thus, since the elapsed time for digital calculations may be treated as a fixed quantity (assuming efficient programming) for a given number of degrees of freedom, it may be necessary to make the computation time different from the problem time. A given solution accuracy requirement will dictate the ratio between computation time and problem time. As reported by McLean and Hahn (11), some scaling of the computation time frame is required even for a small system (involving four degrees of freedom). It is to be presumed that such techniques as extrapolation could be used to reduce the time scaling requirement, but the requirement clearly cannot be avoided. The more degrees of freedom involved in this system, the greater the digital computation time per sampling will be and the greater the time scaling. While firm data is not available, it is normally to be expected that satisfactory accuracy will require 10 to 50 evaluations (samples) per cycle of the highest system frequency of interest.

A major benefit of hybrid computation appears to be that numerical stability problems are eliminated and that analog graphic displays can be readily used. For given accuracy, the elapsed computer time per problem, however, must be similar to digital computation time for an explicit solution since digital evaluation of the derivatives is the pacing item.

Maslo and Rieger (12) have also described the use of hybrid computation for a simple rotor model. They focus on dynamic stability of a fluid film mounted rotor. McLean and Hahn's work involves stability analysis of a simple rigid rotor mounted in a sleeve bearing, which is itself mounted in a squeeze film damper. As yet, no published results indicate that the hybrid method is being applied to large-scale, multi-degree of freedom, rotor bearing systems.

TREATMENT OF NON-LINEARITIES

As discussed in the Introduction, a major motivation for performing transient analysis is to handle non-linearities. When non-linearities are significant, frequency domain methods are generally inadequate.

A non-linear system of equations can, in general, be described by the following equation:

$$[M]\{\ddot{X}\} + [C]\{\dot{X}\} + [K]\{X\} = \{f(t)\} + \{N(t,X,\dot{X},\ddot{X})\} \qquad (21)$$

where $\{N\}$ is a vector of non-linear forcing functions. The contributors to N may be true excitation functions which vary with vibration amplitude (e.g., a mass unbalance which shifts at certain force levels) or "pseudo" forcing functions which actually represent the deviation of actual stiffness, damping, or inertial forces from those given by the linear system defined by M, C, and K. For example, if a squeeze film damper at a particular eccentricity and velocity generates a force of 125 pounds in the $-X_j$ direction, but the value given by the product of C_{jj} and the current value of X_j is 80 pounds, then the contribution to the instantaneous value for N_j is -45 pounds. Alternatively, if a stiffness value, k_{jj}, is, at a particularly instant, in the system response history, 20 percent lower than the basic reference value (due, for example, to rotation of a flexurally asymmetric shaft), then there is a contribution to N_j of $+0.2\ k_{jj}$ times X_j. It is to be noted that one of the simplest treatments of arbitrary damping with undamped modal analysis discussed earlier involved such a pseudo-forcing function approach.

Written in continuous differential form, this equation can clearly be an exact reproduction of the dynamic system force relationship. However, as will be seen, efforts to perform numerical evaluation of the time history of system state variables introduce approximations in the treatment of non-linear terms. The practical problem is this: whatever integration method is applied, the availability of values for the non-linear excitation function always lags behind the incremental advancement of state variables by the integration method.

The major options previously discussed for analyzing linear systems may be extended to treatment of non-linear systems:

- Undamped modal integration
- Damped modal integration
- Explicit numerical integration in real space
- Implicit numerical integration in real space

Features and problems of each approach are discussed in the following paragraphs.

Undamped Modal Methods for Non-Linear Systems

As equation (5) shows, the general solution to the undamped modal system of equations requires that the integral:

$$\frac{1}{\omega_n} \int_0^t f_{rn}(\tau) \sin(\omega_n(t-\tau))d\tau \tag{22}$$

be evaluated, where $f_{rn}(t)$ is the full excitation function in modal space. Since the evaluation of each component of the non-linear excitation function requires knowledge of the state vector, this evaluation presents a problem. A step-by-step procedure may be defined where advancement from time step t to time step t + Δt involves solution of the following equation:

$$\begin{aligned} \eta_n(t+\Delta t) = \; & \eta_n(t) - (C_n \sin(\omega_n t) - S_n \cos(\omega_n t)\omega_n \Delta t \\ & + \Delta t \int_0^t f_{rn}(\tau)\cos(\omega_n(t-\tau))d\tau \\ & + \frac{1}{\omega_n} \int_t^{t+\Delta t} f_{rn}(\tau)\sin(\omega_n(t+\Delta t-\tau))d\tau \end{aligned} \tag{23}$$

The first integral now involves known quantities at time t even though some form of quadrature may be required for its evaluation. The second integral still contains a quantity f_{rn}, unknown at time t + Δt. However, the integrand as a whole is known to be 0 at $\tau = t + \Delta t$ because sin (0) = 0. Thus, a reasonable approximation to the integral is obtained by assuming linear variation of the integrand from t to t + Δt. The resultant value of the integral is $\frac{\Delta t^2}{2} f_{rn}(t)$. The quality of the approximation clearly improves as Δt is reduced.

Evaluation of $f_{rn}(t)$ will involve transformation of the modal coordinates into real space, evaluation of all non-linear functions for all degrees of freedom in real space, and then transformation back into modal space at each time step.

For mild and moderate non-linearities, the use of undamped modes is probably effective. Where it is likely to give problems is for non-linearities severe enough to induce operating regimes where the original modes are totally unrepresentative of the current system. Consider, for example, the case of a rolling element bearing in a clearance space or "dead band" to which no fluid is directed. While the rolling element bearing outer race is in metal-to-metal contact, the stiffness of the contact is very high and the system modes for a hard-mounted rotor would apply. When the transient vibrations are sufficiently high for separation to occur, the stiffness of the contact is reduced essentially to 0 and free body modes would apply. Although answers for such a system can probably be forced from an undamped modal solution, the results will be expected to be strongly time step dependent and unsatisfactory.

Damped Modal Methods for Non-Linear Systems

As shown in equation (14), the solution to the damped modal equations of motion for a particular modal coordinate is:

$$q_n(t) = q_n(t=0)e^{S_n t} + \int_o^t e^{S_n(t-\tau)} f_n(\tau)d\tau \tag{24}$$

Again, the integral in this solution creates a problem since it calls for evaluation of the excitation function which is itself a function of the solution. The integral may be expanded so that:

$$q_n(t+\Delta t) = q_n(t) + q_n(t=0)S_n e^{S_n t}\Delta t + \Delta t S_n \int_o^t e^{S_n(t-\tau)} f_n(\tau)d\tau + \int_t^{t+\Delta t} e^{S_n(t+\Delta t-\tau)} f_n(\tau)d\tau \tag{25}$$

In this expression, all quantities are known except the term $f_n(\tau)$ in the final integral. An effective approach to the problem is to approximate variation of the integrand in the integral t to t+Δt as a linear extrapolation from the values at t and t-Δt. As a result, the last integral is approximately:

$$\frac{\Delta t}{2}\left(f_n(t)(3+S_n\Delta t) - f_n(t-\Delta t)\right) \tag{26}$$

The right-hand side is now completely known, once the point t is reached. Note that it is necessary at each time step to translate the modal coordinates into real space so that the non-linear excitation functions may be evaluated and then to translate back into modal space to provide the value for $f_n(t)$.

Similar comments apply to use of damped modes as to undamped modes. They are likely to be effective up to the point where they are no longer representative of the system whose response they are treating. At this stage, however, there has been no formal comparison of damped and undamped modes for non-linear transient analysis and, in particular, for squeeze film systems. Likewise, there has not been guidance provided as to how far one can take either method into non-linear regimes before running into difficulties.

Explicit Integration Methods for Non-Linear Systems

Explicit integration methods are affected little by non-linearities as far as implementation is concerned. The extra term simply has to be added to the expressions for time derivatives of velocity, i.e.,

$$\{\frac{dV}{dt}\} = -[M]^{-1}\left\{[C]\{V\} + [K]\{X\} - \{f(t)\} - \{N(t,X,\dot{X},\ddot{X})\}\right\} \tag{27}$$

The disadvantages of explicit methods with regard to numerical stability remain. However, an important additional point in favor of explicit methods arises for certain classes of problems. Where the non-linearity is strong and important, there is no option but to track accurately the detailed

short-term behavior of the solution as it interacts with the non-linearity. Inevitably a large number of small time steps are required to achieve accurate treatment of the solution and, under these conditions, the method with lower cost per time step is at an advantage: for example, when the physics of the problem rather than the idiosyncrasies of the algorithm dictate a small time step, explicit methods can have an advantage.

Implicit Integration Methods for Non-Linear Systems

The mechanics of handling a non-linear excitation function with an implicit integration algorithm are really no more complicated than with an explicit method. Using the Newmark Beta method again as an example, the expression for advancement by one time step is added to as follows:

$$X_{n+1} = \left[\frac{M}{\Delta t^2} + \frac{C}{2\gamma\Delta t} + \alpha K\right]^{-1} \left\{\left[\frac{2M}{\Delta t^2} + (2\gamma-1)K\right] X_{n+1}\right.$$

$$- \left[\frac{M}{\Delta t^2} - \frac{C}{2\gamma\Delta t} + \alpha K\right] X_n + \alpha f_{n+2} + (1-2\alpha) f_{n+1} \qquad (28)$$

$$\left. + \alpha f_n + N_{n+1}\right\}$$

This treatment of N preserves the order Δt^2 numerical accuracy of the method. It is similar to an evaluation of a linear excitation term with α set equal to 0. When N is a function of velocity or acceleration, it is necessary to use a $O(\Delta t^2)$ numerical differentiation method to calculate the necessary derivatives since the Newmark method directly generates values only for displacements and not for time derivatives of displacement.

With non-linearities present, the Newmark Beta method cannot guarantee numerical stability. However, if, when the basic system structure encounters a non-linearity, the "system" matrix inverse $\left[\frac{M}{\Delta t^2} + \frac{C}{2\gamma\Delta t} + \alpha K\right]^{-1}$ is recalculated, it would be intuitively reasonable to expect the stability present in using the method with linear systems to be maintained. What is not presently available is a good criterion on which to base a decision to re-invert the system matrix.

NON-LINEARITIES FROM SQUEEZE FILM DAMPERS

Squeeze film dampers give rise to non-linearities, firstly, because the solution to the governing equations is a function of the location of the damper journal within the clearance space and, secondly, because the velocity of the damper journal gives rise to pressures in the fluid film, some of which result in cavitation of the film and the location of the cavitated region is a function of journal velocity. The question can be asked, "Are these non-linearities significant since the vast majority of fluid film bearing analyses rely on linearized data with good effect?" It is worth reviewing why the linearized treatment is effective in journal bearings. The rotation of the journal at a particular eccentricity ratio and attitude angle generates pressures, and, because some of these pressures tend to be negative, a cavitated region is established. Thus, under a static load, there is an established

operating condition defined by an eccentricity, an attitude angle, and a cavitated region extent. Dynamic loads superimposed upon the static load give rise to perturbations about this established condition. It is for this reason that a linearized treatment is effective in journal bearings.

In a squeeze film damper, the nature of the operating condition which is established under a steady load is somewhat different. Considering first the situation where the design incorporates mechanical springs in parallel with the fluid film, the static load will cause the mechanical springs to deflect and the damper will establish some displacement under which the spring force equals the applied load. Thus, the damper journal will have an eccentricity ratio, and, if the mechanical springs are symmetric, the attitude angle will be zero. The difference between this and the journal bearing is that there is no established cavitated region. Only when dynamic loads are applied on top of the static load are pressures generated in the fluid film. Where the journal motion acts to decrease the clearance, the pressures are created positive, and, where the clearance is increasing, the pressures tend to go negative, causing cavitation. Since a dynamic load gives rise to an orbit, it is clear that the cavitated region is continually shifting around, following the motion of the journal. As the cavitated region moves around the clearance space, sometimes it is in the region of high clearance, sometimes in the region of low clearance. As a result, linearized damping coefficients analogous to those used in journal bearings are harder to conceive and to define. The problem is inherently non-linear.

Considering the case where there are no mechanical springs in parallel with the fluid film, the arguments presented earlier are greatly exaggerated. Under a static load, the damper journal sits at the bottom of the clearance space. *Small dynamic* loads will cause some small rolling motion about this metal-to-metal equilibrium condition, but no orbit will be established. Once the magnitude of the dynamic loads becomes greater than the static load, it is likely that, during part of the loading cycle, the damper journal will lift as the net force momentarily acts upward. However, at other points in the load cycle, the net force is clearly downward and the question as to whether an orbit is established is governed by the fluid film characteristics. It is found that, in a fluid film with cavitation effects suppressed, a continuous fluid film orbit is not effectively established. However, the presence of cavitation in the film and its attendant non-linearities provides a basis for carrying a net static load as the journal undergoes a stable orbit generated by dynamic forces. Clearly, the fluid film damper without parallel mechanical springs only works as a result of non-linearities. Pan and Tonneson (13) have shown that this non-linear problem is susceptible to linearization if the orbit which is established is treated as a small perturbation from a circular orbit. Holmes has treated the problem as a non-linearity soluble by step-by-step integration and has demonstrated encouraging agreement with test data in terms of orbit size and shape. Childs performed a similar analysis with similar results. Figure 7 shows an orbit generated by the author in response to a suddenly applied unbalance for a fluid film damper without parallel mechanical springs.

Non-linearities are, thus, an essential feature of squeeze film damper analysis. How to handle these non-linearities in design analysis and how to interpret the results will now be discussed.

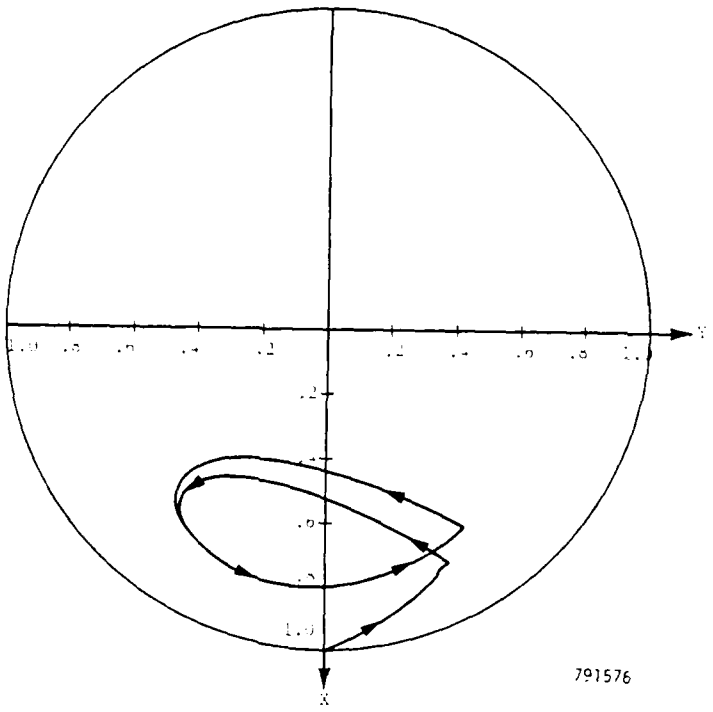

Figure 7. Non-Linear Response of Squeeze Film Damper without Mechanical Springs — 1 g static load plus suddenly applied 1g unbalance force

Fluid Film Analytical Treatment

The basic governing equation is the Reynolds equation:

$$\frac{1}{r}\frac{\partial}{\partial\theta}\left[\frac{h^3}{12\mu r}\frac{\partial p}{\partial\theta}\right] + \frac{\partial}{\partial z}\left[\frac{h^3}{12\mu}\frac{\partial p}{\partial z}\right] = \frac{\partial h}{\partial t} + \frac{\omega}{2}\frac{\partial h}{\partial\theta} \qquad (29)$$

Note that the last term is zero for the most common case of a non-rotating outer member of the damper. (In the special case of an intershaft squeeze film damper, the effects of rotation as well as squeezing must be included.) Considering only the simpler case without rotation effects, at a particular location in the film (assuming the presence of oil in the film) for a particular journal velocity magnitude and direction, direct solution of the governing equation yields a pressure field with pressures which are both above and below zero. The limited ability of the fluid to support tension gives rise to cavitation or rupture in the region of sub-zero pressures. The most common assumption for the region of sub-zero pressures is that each sub-zero pressure location sees a pressure of zero. This assumption is variously termed the "π" or half film treatment since in the absence of supply pressure effects half of the film is normally cavitated as a result of this treatment. More

complicated treatments of the cavitation problem have been proposed based on zero oil flow into the cavitated region, and this assumption requires zero pressure gradient as well as zero pressure as a boundary condition for the cavitated region. It is generally more difficult to establish this more sophisticated boundary condition, and it is found that the difference in force magnitude between the two assumptions is less than 10 percent. This not withstanding the fact that the phenomena relating to fluid conservation in an orbiting, cavitating, squeeze film damper are not well understood. Further work is definitely needed here to investigate what really happens to the fluid film and its cavitated region.

Accepting for the purposes of discussion the half film assumption, we are concerned with the mechanics of generating fluid film forces exerted by a cavitating film for use in rotor transient analysis. What is needed, in general, is a means of determining fluid film force as a function of location vector and velocity vector. The complexity of the particular problem under consideration dictates the computational strategy and quantity of data which must be generated. It is generally desirable to avoid solving the Reynolds equation at every step in the integration process and most computational strategies involve pre-calculation and storage of pertinent data either in tabular or in fitted functional form.

For a rotationally symmetric damper geometry with rotationally symmetric fluid supply, the only location parameter which influences the Reynolds equation solution is the eccentricity ratio. Once the velocity direction is established, the shape of the pressure distribution is also established so that the cavitation boundary locations for a particular eccentricity ratio are a function of the velocity direction only. Figure 8 illustrates the extent of cavitated and positive pressure regions for the particular cases of radial and tangential velocity of a damper journal. In these two cases, the positive pressure region extends 90 degrees on either side of the positive velocity vector. The cavitated region extends between 90 and 270 degrees from the positive velocity vector.

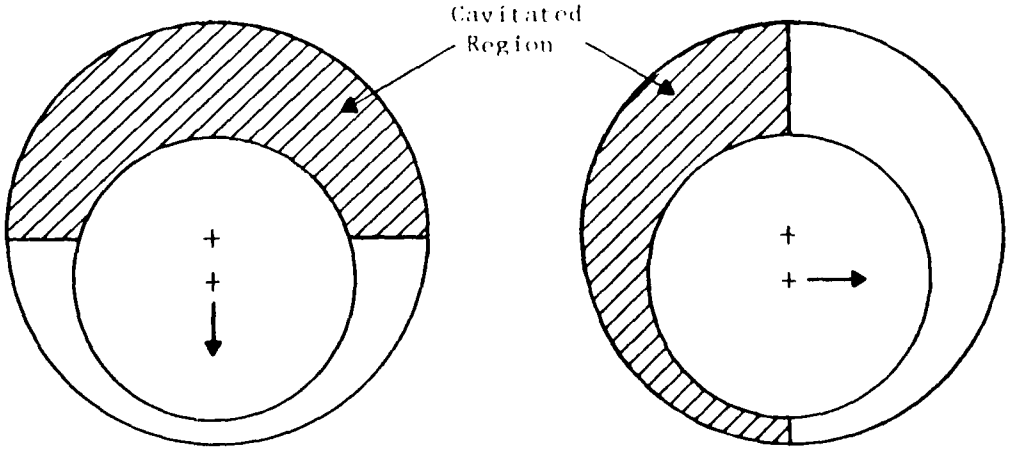

a) Radial Velocity b) Tangential Velocity 792031

Figure 8. Influence of Velocity Direction on Location of Cavitated Region of Squeeze Film Damper

While a number of people have done work in this area, three papers provide most of the important inputs with regard to computational strategy. Some of the earliest work was done by Lloyd (14) who was interested in computing the response of diesel engine bearings to applied dynamic loads. Lloyd solved the Reynolds equation by two-dimensional finite difference methods. At each eccentricity ratio, he calculated the pressure distributions due to radial velocity, that is velocity in line with the eccentricity vector, and, due to tangential velocity, that is motion at 90 degrees to the eccentricity vector. Because his journal was rotating, he also calculated pressure distributions due to rotation at that eccentricity and, because he was supplying oil to the bearing, he calculated the pressure distribution due to supply pressure. All these pressure distributions were stored prior to executing a step-by-step integration. During the process of the step-by-step integration in time, for whatever journal location and journal velocity was required, the various pressure distributions were added in the required proportions and all sub-ambient pressures from the result were set to zero. This work was very effective for the analysis of diesel engine bearing dynamics.

The work of Booker (15) was also directed at dynamically loaded journal bearings for diesel engine applications. Booker's name has been associated with a computational approach termed the Mobility Method. Booker pointed out that, for any combination of rotational speeds of male and female members in a fluid film, there exists a rotating coordinate frame (specifically with angular velocity equal to the average angular velocity of the two members) in which all relative motion appears as squeezing; that is, in this particular frame, the effects of surface rotation are zero because the average surface velocity relative to the coordinate frame is zero. In this coordinate frame, if one axis of the frame is aligned with the current load vector, then the direction in which the journal will move under the action of the applied load is a function strictly of journal location within the frame and the velocity with which it will move is proportional to the applied load.

The basis for this statement is the argument presented earlier that the shape of the pressure distribution and location of the cavitation boundaries is independent of applied load or velocity magnitude and simply a function of applied load or velocity direction. Implementation of the mobility method requires a map defining the direction of journal motion under a vertical load as a function of journal location within the coordinate frame (the squeeze frame). A second map defines the ratio between journal velocity and applied force, again as a function of the journal location within the coordinate frame. With these maps, the solution to diesel engine bearing dynamics is readily accomplished. In this problem, shaft inertia is not important and the problem is one of tracking the journal path under a known load history. The mobility method is ideal for this purpose. Mobility maps may be generated either by short bearing theory or by finite length numerical methods.

Childs (16) makes the important point that, in a rotor dynamics transient analysis, the shaft inertia is usually important and that, to solve the equations of motion, it is necessary to know fluid film force as a function of velocity as opposed to velocity as a function of applied force. The latter has been termed a mobility; the former is conventionally termed an impedance. Childs points out that there exist impedance maps which are analogous to the mobility maps except now that one axis of the coordinate system is aligned with the squeeze velocity direction. One map provides the direction of the resultant fluid film

force; a second map provides the ratio of fluid film force to journal velocity. Again, the impedance maps may be generated either from short bearing theory or by finite length numerical methods or by an improved asymptotic solution to the finite length Reynolds equation such as that proposed by Barrett, Allaire, and Gunter (17) or by Smalley, Lloyd, McCallion, and Horsnell (18).

It reduces somewhat to a matter of personal preference, whether an impedance map format is selected for storage of the damper characteristics or whether a table of force to velocity ratios is tabulated as a function of eccentricity ratio and velocity direction relative to the eccentricity vector. The latter approach reduces the number of individual coordinate frames. For illustration purposes, a computational strategy using the latter type of data format is presented in the following steps. Figure 9 illustrates the process in schematic form.

1. Execute a step of the rotor integration algorithm in response to applied forces.

2. Extract X, Y, $\dot{X}$, $\dot{Y}$ at damper locations. Calculate eccentricity and eccentricity ratio from X,Y of the damper journal and from the damper clearance.

3. From $\dot{X}$ and $\dot{Y}$, calculate magnitude and direction of velocity vector.

4. Calculate angle between velocity vector and eccentricity ratio vector.

5. From table of data, interpolate force to velocity ratio, and force direction, as a function of eccentricity ratio and velocity direction.

6. Multiply force to velocity ratio by velocity to get force.

7. Rotate force direction back into XY frame.

8. Calculate non-linear pseudo-forcing function at current time.

9. Repeat from Step 1.

The execution of a step of the integration algorithm is accomplished by one of the algorithms described earlier for non-linear rotor systems.

INTERPRETATION

An unavoidable aspect of transient dynamics analysis of rotor damper systems is a large volume of output; the computation generates complete state vectors at every time step for every station of the rotor system. Thus, the ratio of useful engineering information to the total volume of data is relatively low. The use of graphical output goes some way toward reducing the magnitude of this problem; visual interpretation of an orbit or time history plot can readily inform the observer of such important items as:

- Peak amplitudes
- Rates of decay
- Minimum film thickness
- Major frequency components

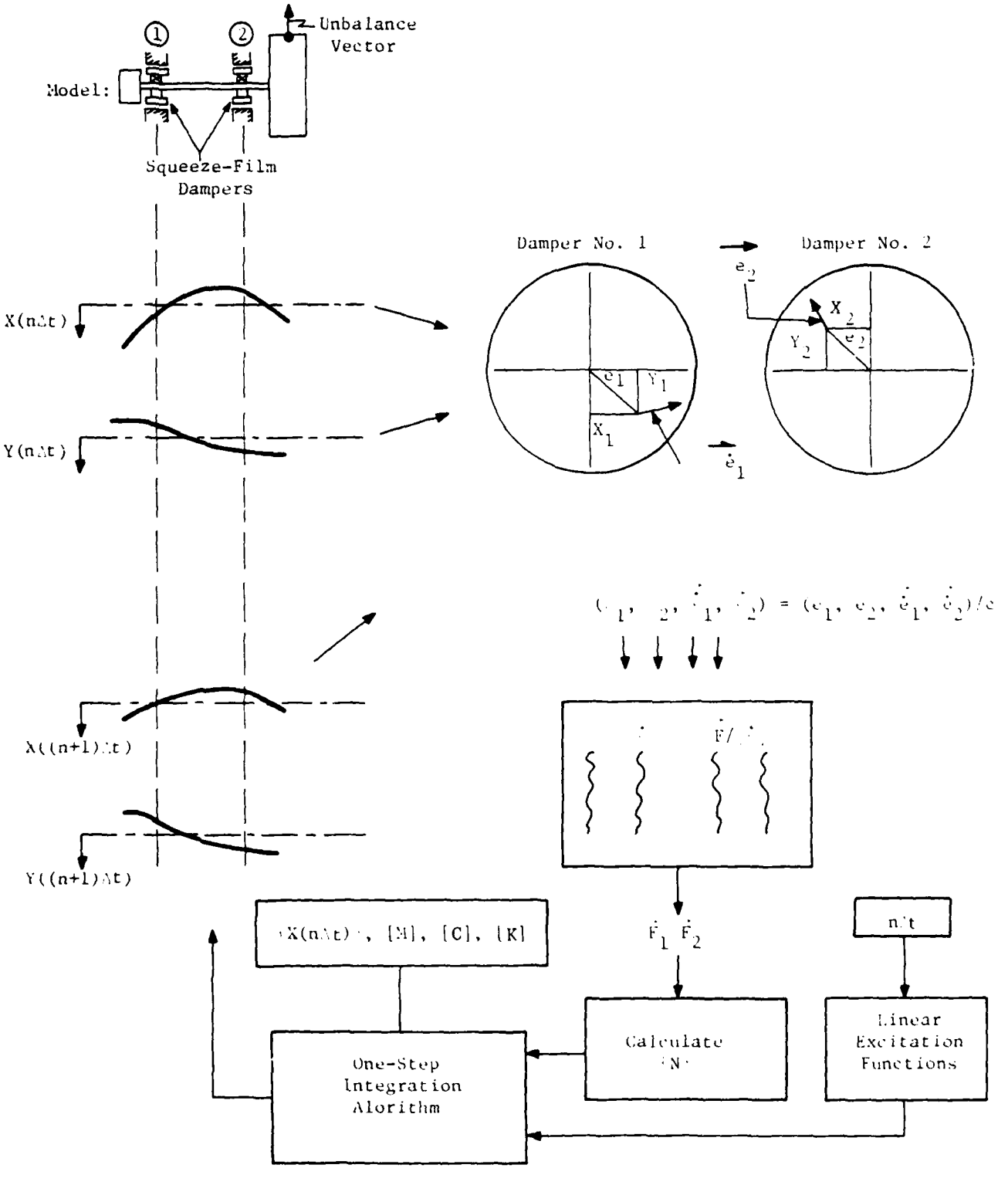

Figure 9. Integration Loop for Rotor System with Squeeze Film Damper

The use of summary tables listing such items as peak amplitudes and minimum film thicknesses and the times at which they occur are of additional help to the engineer who must make use of transient dynamics information.

A recent contribution by Choy, Gunter, and Allaire (3) was to develop frequency domain information from the results of time integration analysis by performing a Fourier transform (using the FFT algorithm) on the time series data. If, for example, time transient response information is available at a series of speeds showing the response of the rotor to both rotating unbalance and an initial displacement, this transformation can be used to develop the waterfall type plots normally generated in real-time analysis of measured vibration data. The presence of large forced response amplitude is shown by peaks in the diagonal, order-related lines on the waterfall plot. The presence of subsynchronous instability is revealed by speed-independent peaks in the waterfall plot. Figure 10 shows these two characteristics of a waterfall plot.

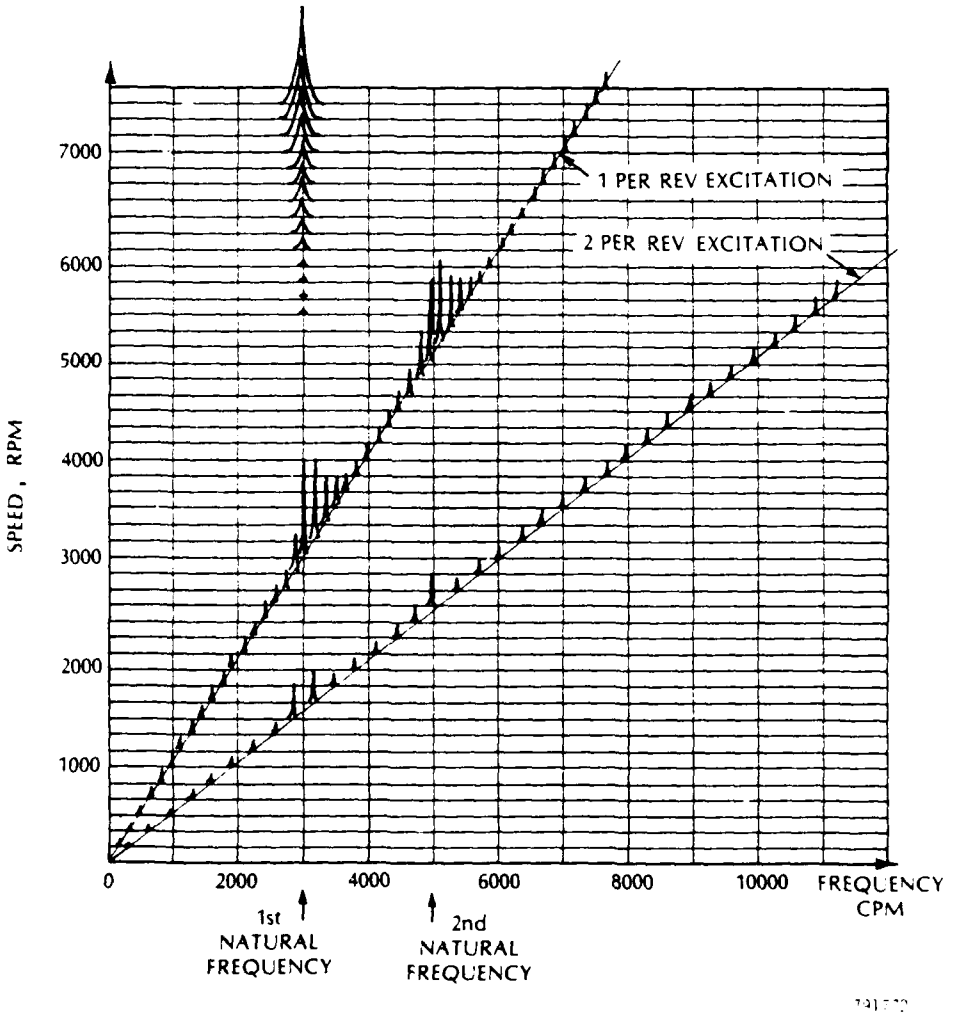

Figure 10. Waterfall Plot of Shaft Displacement Sensor Output

Another approach used at Mechanical Technology Incorporated (MTI) to bridge the gap between non-linear time domain information and frequency domain linearized analysis for squeeze film dampers is to interpret the characteristics of hysteresis plots for X and Y force and X and Y displacement for a damper to yield effective X and Y stiffness and damping values. Figure 11 reveals the approach by means of a hysteresis plot of X force as a function of X displacement generated by a non-linear squeeze film transient response (using a mobility representation of the fluid film). An effective stiffness is calculated by locating the points of maximum positive displacement and maximum negative displacement and the associated force values and dividing the force difference by the displacement difference to give an effective stiffness. Damping is determined by measuring the area of the hysteresis loop and equating this to the energy dissipation generated with a linear damper and an elliptical hysteresis loop. While not rigorous, this approach yields quantities which can be applied in linearized rotor dynamics, namely, stiffness and damping coefficients. These should be generated for different levels of excitation on the damper so that the set of amplitude-dependent coefficients is obtained. It must then be ensured that, when response analysis is performed with these effective coefficients, that the computed response agrees reasonably with the orbital amplitude from which the coefficients were extracted. Figure 12 illustrates effective damping values generated in this way as a function of frequency and amplitude. A nominal "safe" operating limit corresponding to a 75 percent maximum eccentricity ratio is superimposed.

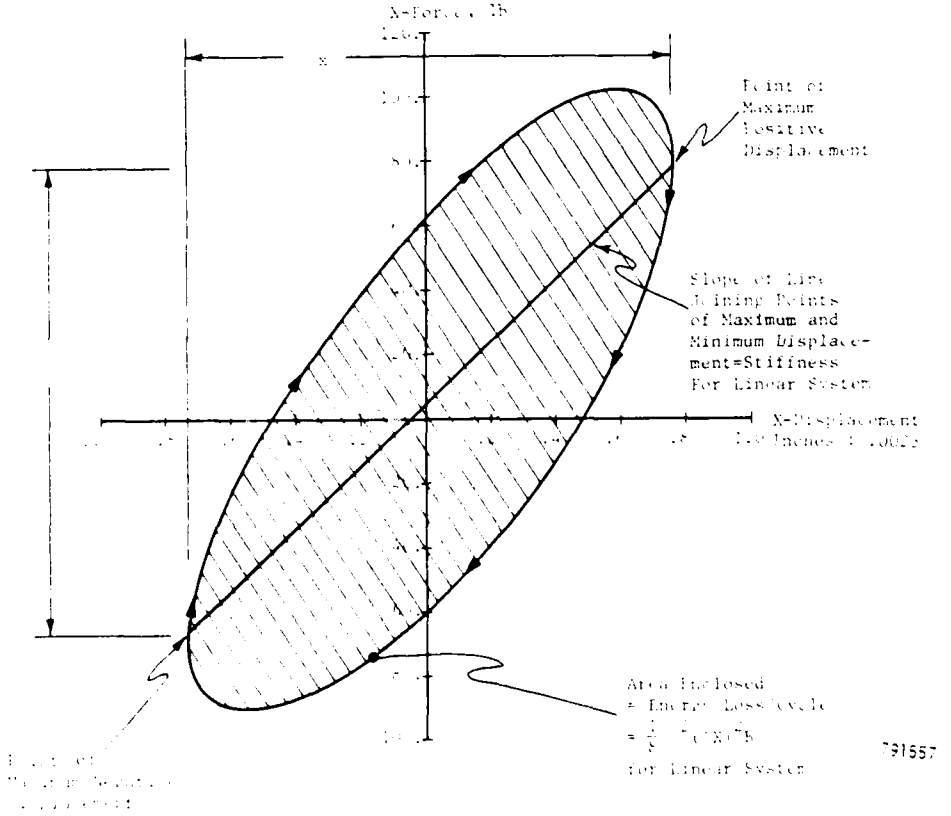

Figure 11. Typical Hysteresis Loop with Definitions of Quantities Used for Calculation of Stiffness and Damping

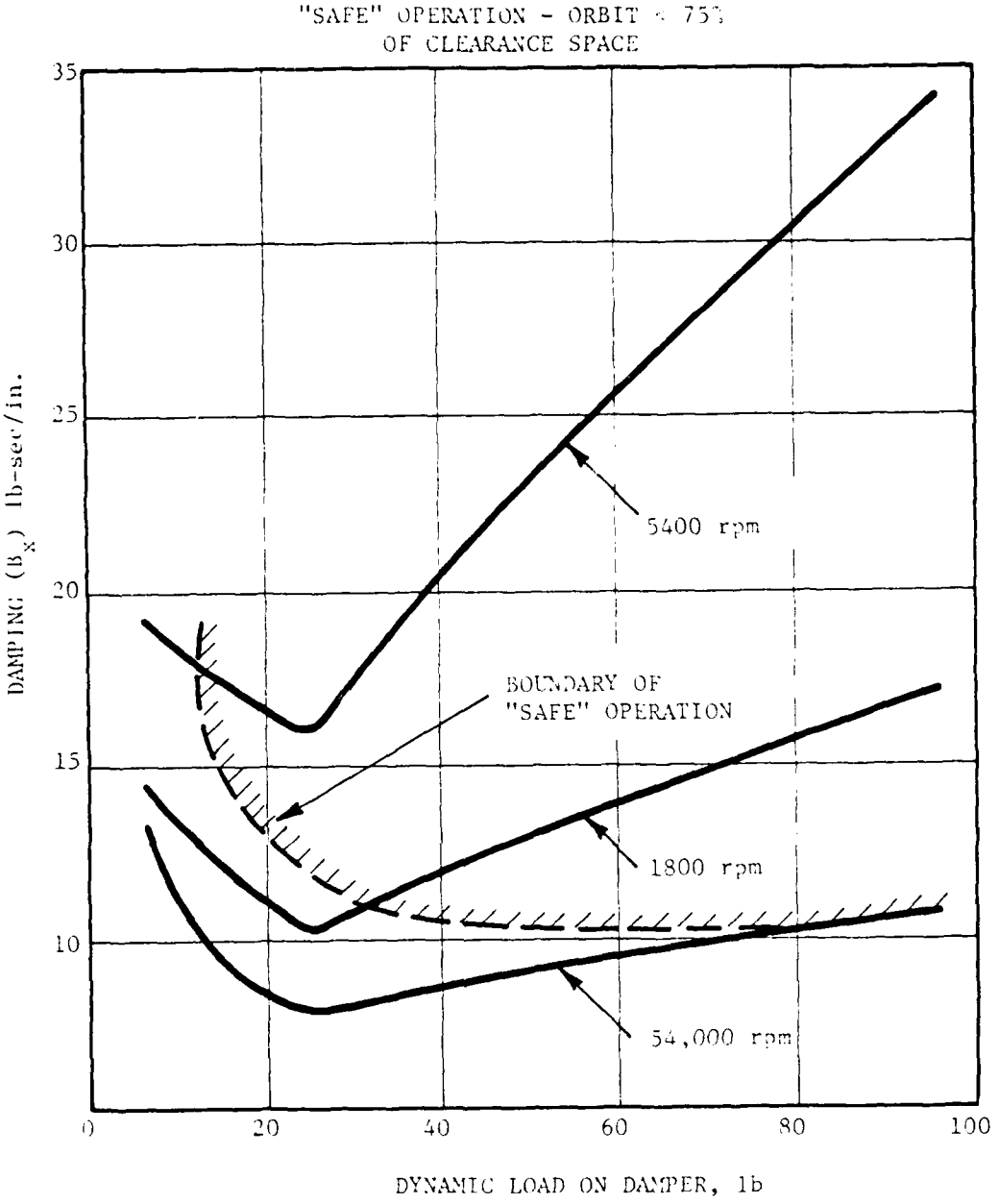

Figure 17. Effective X-Damping Determined from Hysteresis Loop for Non-Linear Fluid Film Response. Static Load = 6 lb.

The topics discussed briefly in this section indicate a real need for further effective work to improve the interpretability of rotor transient information. There is additional need for documentation of studies in which rotor transient information has been effectively applied in design with demonstrations of how trade-offs between design alternatives were influenced by transient dynamic considerations. As a particular example, there is a need for combined optimization for attenuation of normal unbalance excitation, subsynchronous excitation, and the abusive loading which results from loss of a blade and vehicle maneuvers.

CONCLUSIONS

In this paper, various methods available for analyzing the transient dynamics of squeeze film bearing systems have been discussed. The information contained should make the reader aware of his options and of the considerations to be applied in choosing one method over another.

The following general observations can be made:

1. Modal methods are very economical from a computational cost point of view.

2. Non-linear problems can be handled with modal methods.

3. Criteria as to the extent of non-linearity which can be handled by the different modal methods are not available.

4. Comparisons of effectiveness of damped and undamped modal methods are not available.

5. For severely non-linear problems, explicit integration methods have advantages when the time step is dictated by the physics of the problem rather than by idiosyncrasies of the numerical algorithm.

6. The Newmark algorithm is a very powerful method of implicit integration which avoids stability problems for linear and moderately non-linear problems.

7. Criteria for re-evaluation of the system matrix inverse in implementing the Newmark method for strongly non-linear problems are not readily available.

8. The fluid film portion of the non-linear problem is readily handled by any sensible variant on the mobility of impedance methods.

9. Choices of the fluid film method are mainly choices of detail, although economical handling of the fluid film calculation does require careful organization of the problem.

10. The true boundary condition for a squeeze film damper remains an uncertainty, although the half-film assumption is an effective approach.

Clearly the guidelines for time integration methods presented above are general and inconclusive. This emphasizes a state-of-the-art needed in

this area, namely, an objective, quantitative evaluation of the available methods with such outputs as:

- Computation time
- Criteria for use on non-linear problems
- Accuracy
- Volume of input and output
- Computational convenience

for a number of different classes of problems.

In summary, the following investigative work is needed:

- Comparison of alternative algorithms for different classes of problems.
- Development of criteria for selection of one method over another.
- Development of additional methods for effective interpretation of time transient information.
- Documentation of applications experience with time transient methods in design.

REFERENCES

1. Meirovitch, L. "Analytical Methods in Vibration,", MacMillan, New York, 1967.

2. Dennis, A.J., Erickson, R.H., Seitelman, L.H., "Transient Response Analysis of Damped Rotor Systems by Normal Mode Method," ASME Paper #75GT50.

3. Choy, K.C., Gunter, E.J., Allaire, P.E., "Fast Fourier Transform Analysis of Rotor Bearing Systems," Topics in Fluid Film Bearing and Rotor Bearing System Design and Optimization, ASME Publication Presented at Design Engineering Conference, Chicago, Illinois, April 17-20, 1978, p. 245.

4. Childs, D.W., Bates, J.B. III, "Residual Flexibility Corrections for Transient Modal Rotor Dynamic Models," American Society of Mechanical Engineers, ASME Paper #77-DET-31.

5. Lund, J.W., "A Method for Using the Free Shaft Modes in Rotor Balancing," Institute of Mechanical Engineers, Paper #C169/76.

6. Lund, J.W., "Modal Response of a Flexible Rotor in Fluid Film Bearings," ASME Paper #73DET98.

7. Horner, G.C. and Pilkey, W.D., "The Ricatti Transfer Matrix Method," ASME Vibration Conference, 1977.

8. Darlow, M.S. and Smalley, A.J., "Design and Test of a Squeeze Film Damper for a Flexible Power Transmission Shaft," Topics in Fluid Film Bearing and Rotor Bearing Systems Design and Optimization, ASME Publication presented at Design Engineering Conference, Chicago, Illinois, April 17-20, 1978, p. 43.

9. Gunter, E.J. and Kirk, R.G., "Transient Response of Rotor Bearing Systems," ASME Transactions, Journal of Engineering for Industry, Vol. 96, No. 2, Series B, pp. 682-693.

10. Newmark, N.M., "A Method of Computation for Structural Dynamics," Proceedings of ASCE, Journal of Engineering Mechanics, Division EM-3, July 1959, pp. 67-94.

11. McLean, L.J. and Hahn, E.J., "The Transient Response of a Balanced Rigid Rotor Running in Squeeze Film Supported Journal Bearings," Topics in Fluid Film and Rotor Bearing System Design and Optimization, ASME Publication presented at Design Engineering Conference, Chicago, Illinois, April 17-20, 1978, p. 203.

12. Maslo, R.N. and Rieger, N.F., "A New Way to Analyze Rotor Stability," Machine Design, October 2, 1975.

13. Pan, C.H.T. and Tonnesen, J., "Eccentric Operation of the Squeeze Film Damper," ASME Paper #77-LUB-22.

14. Lloyd, T., Horsnell, R., McCallion, H., "An Investigation into the Performance of Dynamically Loaded Bearings: Theory," Symposium on Journal Bearings for Reciprocating and Turbomachinery, ISME Proceedings, September 1966.

15. Booker, J.F., "Dynamically Loaded Journal Bearings," Numerical Application of the Mobility Method, Transaction of the ASME, Journal of Lubrication Technology, January 1971, pp. 168-176.

16. Childs, D.W., Moes, H., Vanleeuwen, H., "Journal Bearing Impedance Descriptions for Rotor Dynamic Applications," ASME Transactions, Journal of Lubrication Technology, April 1977, p. 198.

17. Barrett, L.E., Allaire, P.E., Gunter, E.J., "The Dynamic Analysis of Journal Bearings Using a Finite Length Correction for Short Bearing Theory," Topics in Fluid Film Bearing and Rotor Bearing System Design and Optimization, Presented at the Design Engineering Conference, Chicago, Illinois, April 17-20, 1978, p. 29.

18. Smalley, A.J., Lloyd, T., Horsnell, R., and McCallion, H., "Comparison of Performance Predictions for Steadily Loaded Journal Bearings," Proceedings of the Institute of Mechanical Engineers, Vol. 180, Part 3K, 1965-66, pp. 133-144.

19. Pilkey, W.D., Strenkowski, J.P., and Chang, P.Y., "Transient Response of a Rotor in Damped Bearings," ASME Paper #77-DET-21.

DIRECT INTEGRATION OF TRANSIENT ROTOR DYNAMICS

by Albert F. Kascak

National Aeronautics and Space Administration
Lewis Research Center
Cleveland, Ohio 44135

ABSTRACT

A study was conducted to develop an implicit method for integrating the equations of motion of a lumped-mass model of a rotor bearing system. The approach was, first, to use a Nordsieck-like numerical integration directly on the second-order equations of motion and, second, to assume that the forces and torques on the rotor are functions of the position and velocity at the point of application and its nearest axial neighbors. This allows the variables to be arranged so that the Jacobian of the set of nonlinar equations is block tridiagonal. Therefore the computational time is proportional to the number of elements in the rotor dynamics model rather than to the cube of the number. Numerical stability was demonstrated for any linearized homogeneous mode.

To decrease computational time, a closed-form solution to the short-bearing theory was derived for a damper with arbitrary motion. Explicit results were presented for no cavitation and for full cavitation.

The vast amount of data generated by the computer code was displayed in a motion picture showing an oblique view of the rotor bearing system. The motion of the rotor could be easily interpreted.

An example problem of a rotor accelerating through three critical speeds with 19 mass elements in the rotor dynamics model took 0.7 second of central processing unit time per time step on an IBM 360-67 computer in a time-sharing mode. The mode shapes at the first and third critical speeds were similar to the predicted mode shapes and occurred at the predicted speed. Because of the unbalance distribution, the second mode was not excited. Above the third critical speed the rotor bearing system operated as a self-centering device. This was also observed experimentally.

The computer code, for the first time, allows us to look at a complex rotor bearing system with nonlinear transients and displays the vast amount of results in an easily understood motion-picture format. A 10-minute 16-millimeter, color, sound motion-picture supplement is available on loan.

SYMBOLS

$A_{\pm j}$	coefficients used in partial-fraction expansion
$a_{\pm}$	property of shaft between mass stations defined in eq. (18a)
$b_{\pm}$	property of shaft between mass stations defined in eq. (18b)
C	radial clearance
$c_{\pm}$	property of shaft between mass stations defined in eq. (18c)
D	diameter
E	modulus of elasticity
F	force
G	torque
h	clearance in direction $\hat{n}$
I	moment of inertia
j	index
k	index
L	axial length between mass stations
m	mass of a rotor segment
N	number of rotor segments
n	radial direction at angle θ
O	order of error in Taylor series
P	pressure
q	order of Taylor series
r	radial displacement
S	stability matrix
s_{kj}	element of S
t	time
Δt	time step
u	defined in eq. (5)

V	nondimensional velocity of journal in rotating coordinates
x	real part of radial displacement
y	imaginary part of radial displacement
Z	independent variable
z	axial coordinate
α_k	given set of constants
Γ	angle defined in eq. (43)
ϵ	eccentricity ratio
ζ	damping ratio
θ	circumferential angle
λ	eigenvalue of stability matrix
μ	viscosity
ω	frequency

Subscripts:

B	bearing
J	journal
P	polar
T	transverse
$\pm$	associated with nearest axial neighbor or root of eq. (45)
0	start of integration
1	end of integration

Superscripts:

$\dot{(\ )}$	time derivative
$(\ )'$	axial derivative
$\bar{(\ )}$	average or conjugate
(k)	k^{th} time derivative
$\rightarrow$	vector
$\hat{\ }$	unit vector

INTRODUCTION

Nonlinear transients that are important in flexible, rotating equipment are difficult to analyze. Such things as blade tip rubs, spline friction, and squeeze-film dampers are difficult to predict with a linear model. Some of the transients that are important are locked rotor starts, blade loss, and rapid deceleration due to bearing failures.

There are two basic methods for studying transient rotor dynamics. The first method is the modal method (refs. 1 and 2). It is best suited to linear rotor bearing systems running at a constant speed. The second method is the direct integration of the equations of motion. It can be applied easily to nonlinear systems that are varying in speed. The problem with the direct method is that it is limited by either computer running time or numerical stability.

The equations of motion for rotor dynamics can be integrated directly in either of two ways, explicit or implicit integration. The explicit integration method solves the equations of motion at the present time for higher order derivatives and then extrapolates the displacements and velocities with a Taylor series to the advanced time (ref. 3). The implicit method solves the equations of motion (implicitly) at the advanced time step for the displacements and velocities, such that an extrapolation backward in time gives the previous results.

The explicit method tends to be unstable when the product of the critical frequency (for any mode numerically possible) and the time step is large (ref. 4). Since the highest frequency is related to the square of the number of elements in the rotor dynamics model, the computational time will be related to the square of the number of elements. Approximately five or six elements seems to be a practical limit to the explicit method (ref. 2); that is, it can only be applied to simple assemblies.

In contrast to the explicit method, the implicit method tends to be stable for large time steps (ref. 5); but it requires the solution of a large number of nonlinear simultaneous equations at each time step. For every element in the rotor dynamics model there are four degrees of freedom. For each degree of freedom there is an associated displacement and velocity. Therefore the total number of nonlinear equations to be solved at each time step is eight times the number of elements in the rotor dynamics model. The number of computations necessary to solve these equations is proportional to the cube of the number of equations. Therefore the computational time is proportional to the cube of the number of elements.

This study was conducted to develop an implicit method for integrating the quations of motion in a reasonable amount of computational time. The approach is first to use a Nordsieck-like numerical integration directly on the second-order equations of motion[1] and second to assume that the forces and torques on the rotor are functions of the position and velocity of the point where the force or torque is applied and its nearest axial neighbors. This allows the variables to be arranged so that the Jacobian of the set of nonlinear equations is block tridiagonal. The computational time is proportional to the number of elements in the rotor dynamics model rather than to the cube of the number of elements.

---

[1]This method of numerical integration was developed by Frank J. Zeleznik of the Lewis Research Center. For a set of first-order equations, it reduces to Gear's method.

Besides the problems associated with integrating the equations of motion, there is a problem of describing the nonlinar damper force at each instant of time for an arbitrary orbit. In the past this was done by numerically integrating the Reynolds equation around the damper (ref. 6). This required a considerable amount of computational time. As an aside, a closed-form solution to the short-bearing theory was derived for a damper with arbitrary motion.

NUMERICAL INTEGRATION

Given an arbitrary function, $Z_k(t)$, whose derivatives exist, $Z_k^{(j)}(t)$, a Taylor series expansion can be written:

$$Z_k(t + \Delta t) = \sum_{j=0}^{q-k} \frac{(\Delta t)^j}{j!} Z_k^{(j)} + O_{q-k} \tag{1}$$

with Lagrange's remainder of order O_{q-k}. If the arbitrary function is chosen as

$$Z_k = \frac{(\Delta t)^k}{k!} r^{(k)} \tag{2}$$

the Taylor series for this function becomes

$$Z_k(t + \Delta t) = \sum_{j=0}^{q} \binom{j}{k} Z_j(t) + O_q \tag{3}$$

where the binomial coefficients are defined as

$$\binom{j}{k} = \begin{cases} \dfrac{j!}{k!(j-k)!} & \text{for } j \geq k \\ 0 & \text{for } j < k \end{cases} \tag{4}$$

If the form of the remainder is chosen as

$$O_q = \alpha_k u \tag{5}$$

the Taylor series becomes

$$Z_k(t + \Delta t) = \sum_{j=0}^{q} \binom{j}{k} Z_j(t) + \alpha_k u \tag{6}$$

where α_k is a given set of constants and u can be determined from the equation of motion at the advanced time. The equation of motion at the advanced time is

$$\Sigma F(r, \dot{r}, \ddot{r}, t + \Delta t) = 0 \tag{7}$$

From the definition of z, the various derivatives become

$$r^{(k)} = \frac{k!}{(\Delta t)^k} Z_k \tag{8}$$

Substituting for the various derivatives into the equation of motion and knowing the values at the previous time result in the equation of motion being a function of

$$\Sigma F(u, t + \Delta t) = 0 \tag{9}$$

This equation can be solved for u and, from this value of u, the remainder can be used as an error estimate to control the time step.

NUMERICAL STABILITY

The analysis of the stability of the numerical integration technique assumes a model of a rotor bearing system that is linearized at some instant of time. The homogeneous equation of motion for any mode is

$$\ddot{r} + 2\omega\zeta\dot{r} + \omega^2 r = 0 \tag{10}$$

where ω is the natural frequency and ζ is the damping ratio for the mode. For every mode that is numerically possible, with nonnegative damping ratio, the amplitude must either remain constant or decay in time. The numerical integration is defined as unstable if the amplitude grows in time.

From the definition of z the modal equation becomes

$$2Z_2 + 2\omega\,\Delta t\zeta Z_1 + (\omega\,\Delta t)^2 Z_0 = 0 \tag{11}$$

Substituting the Taylor series into the modal equation at the advanced time results in

$$u = -\sum_{j=0}^{q} \left[\frac{j(j-1) + 2j\omega\,\Delta t\zeta + (\omega\,\Delta t)^2}{2\alpha_2 + 2\alpha_1\omega\,\Delta t\zeta + \alpha_0(\omega\,\Delta t)^2}\right] Z_j(t) \tag{12}$$

For this value of u, the Taylor series expresses the solution at the advanced time in terms of the solution at the present time as

$$Z_k(t + \Delta t) = \sum_{j=0}^{q} \left\{ \binom{j}{k} - \frac{\alpha_k[j(j-1) + 2j\omega\,\Delta t\zeta + (\omega\,\Delta t)^2]}{[2\alpha_2 + 2\alpha_1\omega\,\Delta t\zeta + \alpha_0(\omega\,\Delta t)^2]} \right\} Z_j(t) \qquad (13)$$

Defining the matrix element s_{kj} to be

$$S_{kj} = \binom{j}{k} - \frac{\alpha_k[j(j-1) + 2j\omega\,\Delta t\zeta + (\omega\,\Delta t)^2]}{[2\alpha_2 + 2\alpha_1\omega\,\Delta t\zeta + \alpha_0(\omega\,\Delta t)^2]} \qquad (14)$$

and the q-dimension vector $\vec{z}$ gives the eigenvalue equation as

$$S\vec{Z} = \lambda\vec{Z} \qquad (15)$$

If the $|\lambda| > 1$, the amplitude grows and the method is numerically unstable. For $q = 2$, the given α's are $\alpha_0 = 2$, $\alpha_1 = 3$, and $\alpha_2 = 1$. In the limit as $\omega\,\Delta t \to \infty$, the maximum $|\lambda| \to 0$. Therefore if the time step Δt is much larger than ω^{-1} for a mode, the amplitude of that mode will approach zero. If a mode is to have a nonzero amplitude, h must be small. In the limit as $\omega\,\Delta t \to 0$, the maximum $|\lambda| \to 1$. Therefore the method is numerically stable in the two limits.

EQUATIONS OF MOTION

A model of the shaft showing the complex number representation of the radial displacemebt r is shown in figure 1. The radial displacement is the distance between the shaft centerline and the axis of rotation. It can be represented by

$$r = x + iy \qquad (16a)$$

where the real and imaginary axes are fixed in space perpendicular to the axis of rotation. The slope of the shaft along the axis of rotation is

$$r' = x' + iy' \qquad (16b)$$

The position of the shaft is then described by r and r' at all the axial locations.

The lumped-mass model of a rotor divides the rotor into N segments. The mass and inertia of each segment are assumed to be concentrated at a point. These points are then assumed to be connected by massless elastic beams that model the stiffness of the rotor.

The equations of motion for the lumped-mass model were derived in reference 7. The sum of the forces ΣF at a point, must be zero, where

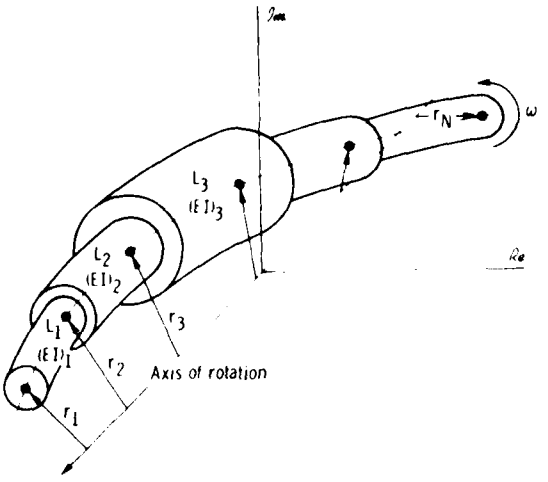

Figure 1. - Model of shaft showing complex number representation of radial displacements.

$$
0 = \begin{bmatrix} \Sigma F_{x_1} \\ \Sigma F_{y_1} \\ \Sigma G_{x_1} \\ \Sigma G_{y_1} \\ \hline \bullet \\ \hline \bullet \\ \hline \bullet \\ \hline \Sigma F_{x_N} \\ \Sigma F_{y_N} \\ \Sigma G_{x_N} \\ \Sigma G_{y_N} \end{bmatrix} + \left[\begin{array}{ccccc} B_1 & C_1 & 0 & \bullet & 0 \\ \hline A_2 & B_2 & C_2 & \bullet & \bullet \\ \hline 0 & \bullet & \bullet & \bullet & 0 \\ \hline \bullet & \bullet & A_{N-1} & B_{N-1} & C_{N-1} \\ \hline 0 & \bullet & 0 & A_N & B_N \end{array}\right] \begin{bmatrix} u_{x_1} \\ u_{y_1} \\ u_{x_1'} \\ u_{y_1'} \\ \hline \bullet \\ \hline \bullet \\ \hline \bullet \\ \hline u_{x_N} \\ u_{y_N} \\ u_{x_N'} \\ u_{y_N'} \end{bmatrix}
$$

Figure 2. - Newton-Raphson technique that leads to a linear set of block-tridiagonal equations.

$$\Sigma F = -m\ddot{r} + a_- r_- - (a_- + a_+)r + a_+ r_+$$

$$+ b_- r'_- + (b_- - b_+)r' - b_+ r'_+ + F = 0 \tag{17a}$$

and the sum of the torques ΣG about a point must be zero, where

$$\Sigma G = -I_T \ddot{r}' + i\omega I_p \dot{r}' - \dot{\omega} I_p r'$$

$$- b_- r_- + (b_- - b_+)r + b_+ r_+$$

$$- c_- r'_- - 2(c_- + c_+)r' - c_+ r'_+ + G \tag{17b}$$

The $+$ or $-$ refer to the next or previous axial location; and a, b, and c are properties of the shaft between these locations:

$$a = 12EI/L^3 \tag{18a}$$

$$b = 6ET/L^2 \tag{18b}$$

$$c = 2EI/L \tag{18c}$$

If the nonlinear force F and the nonlinear torque G are functions of displacements and velocities of the point and its nearest neighbors, the ΣF and ΣG are functions of the displacements and velocities of the point and its nearest neighbors. If the Taylor series of the numerical integration technique is substituted into the equations of motion for the acceleration, velocity, and displacement, the form of the equations of motion becomes

$$0 = \Sigma F(u_-, u, u_+, u'_-, u', u'_+) \tag{19a}$$

$$0 = \Sigma G(u_-, u, u_+, u'_-, u', u'_+) \tag{19b}$$

These equations form a set of 2N complex nonlinear equations in 2N unknowns. These equations are solved by rewriting them as 4N real equations in 4N real unknowns and then using a Newton-Raphson iterative technique to obtain a numerical solution. The Newton-Raphson technique assumes a solution, linearizes the equations about that solution, and then solves the linear set of equations for a correction to the assumed solution. The form of the equations of motion results in the linear set of equations being block tridiagonal (fig. 2). The block-tridiagonal form allows the set of equations to be solved in a very efficient manner. The computational time is proportional to N rather than N^3 as in the general method.

SQUEEZE-FILM DAMPER BEARING

The configuration of the squeeze-film damper is shown in figure 3. The same configuration can be used to analyze journal bearings where the journal and the bearing are allowed to rotate. If ω_J is the rotational speed of the journal and ω_B is the rotational speed of the bearing, the average rotational speed is

$$\bar{\omega} = \frac{1}{2}(\omega_B + \omega_J) \tag{20}$$

For a damper this average rotational speed would be zero.

If C is the radial clearance and $\vec{r}$ is the displacement of the journal center with respect to the bearing center, the clearance h in the direction $\hat{n}$ is

$$h = c - \vec{r} \cdot \hat{n} \tag{21}$$

If $\dot{\vec{r}}$ is the velocity of the journal,

$$\frac{\partial h}{\partial t} = -\dot{\vec{r}} \cdot \hat{n} \tag{22}$$

If $\hat{n}$ is at an angle θ,

$$\frac{\partial \hat{n}}{\partial \theta} = \hat{k} \times \hat{n} \tag{23}$$

where $\hat{k}$ is a unit vector along the axis of the damper bearing in the z-direction. If $\vec{\omega}$ is defined as

$$\vec{\omega} = \bar{\omega}\hat{k} \tag{24}$$

then

$$\bar{\omega}\frac{\partial h}{\partial \theta} = (\vec{\omega} \times \vec{r}) \cdot \hat{n} \tag{25}$$

The Reynolds equation for the short, plain damper journal bearing is presented in reference 6 as

$$\frac{\partial}{\partial z}\left(\frac{h^3}{12\mu}\frac{\partial P}{\partial Z}\right) = \bar{\omega}\frac{\partial h}{\partial \theta} + \frac{\partial h}{\partial t} \tag{26}$$

If the boundary conditions in the damper bearing are

$$P(0, \theta, t) = 0 \tag{27a}$$

$$P(L, \theta, t) = 0 \tag{27b}$$

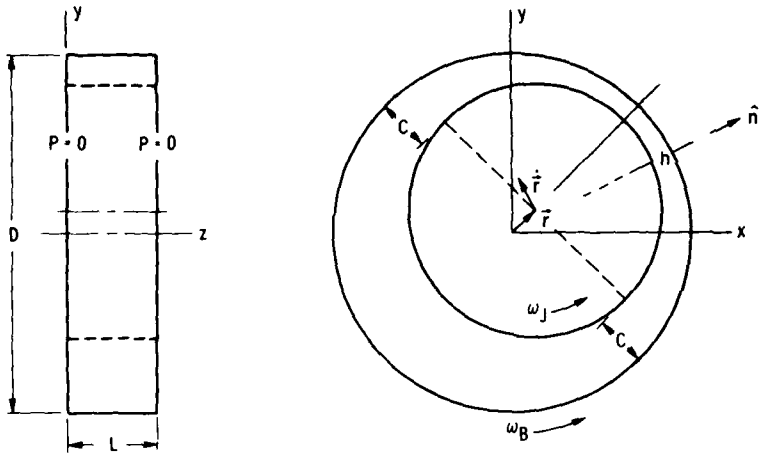

Figure 3. - Damper bearing geometry.

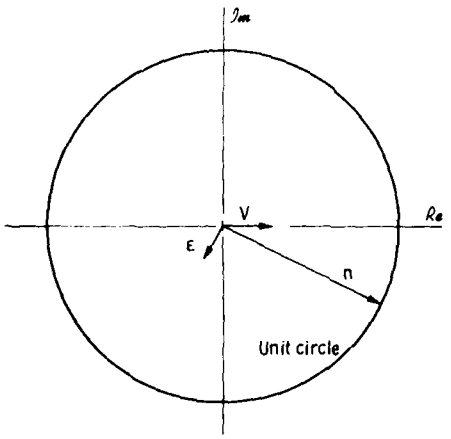

Figure 4. - Complex plane.

and if h is not a function of z,

$$P = -\frac{6\mu z(L - z)}{h^3}(\vec{\omega} \times \vec{r} - \dot{\vec{r}}) \cdot \hat{n} \tag{28}$$

The eccentricity ratio is

$$\vec{\varepsilon} = \frac{\vec{r}}{C} \tag{29}$$

so that

$$\dot{\vec{\varepsilon}} = \frac{\dot{\vec{r}}}{C} \tag{30}$$

If $\vec{V}$ is defined as

$$\vec{V} = \dot{\vec{\varepsilon}} - \vec{\omega} \times \vec{\varepsilon} \tag{31}$$

$$P = \frac{6\mu z(L - z)}{C^2(1 - \vec{\varepsilon} \cdot \hat{n})} \vec{V} \cdot \hat{n} \tag{32}$$

The pressure is zero when $\hat{n}$ is perpendicular to $\vec{V}$, and the pressure is greater than zero when $\vec{V} \cdot \hat{n} > 0$.

The force on the journal due to the pressure in a segment of the film extending from θ_0 to θ_1 is

$$\vec{F} = -\frac{D}{2}\int_{\theta_0}^{\theta_1}\int_0^L P\hat{n}\, dz\, d\theta \tag{33}$$

This expression for the force can be integrated axially and becomes

$$\vec{F} = -\frac{\mu DL^3}{2C^2}\int_{\theta_0}^{\theta_1} \frac{(\vec{V} \cdot \hat{n})\hat{n}}{(1 - \vec{\varepsilon} \cdot \hat{n})^3}\, d\theta \tag{34}$$

The angular integral can be integrated by transforming the integral to the complex plane (fig. 4). Let $\vec{V}$ be in the real direction, $\vec{\varepsilon}$ be at an angle ϕ, and $\hat{n}$ be at an angle θ so that

$$V = |V| \tag{35a}$$

$$\varepsilon = |\varepsilon| e^{i\phi} \tag{35b}$$

$$n = e^{i\theta} \tag{35c}$$

Differentiating the expression for n yields

$$d\theta = -i\, n^{-1} dn \tag{36}$$

and using the definition of the complex cosine yields

$$\vec{V} \cdot \hat{n} = \frac{V(n + n^{-1})}{2} \tag{37}$$

$$\vec{\varepsilon} \cdot \hat{n} = \frac{(n\bar{\varepsilon} + \varepsilon n^{-1})}{2} \tag{38}$$

The expression for the force becomes

$$F = -i\left(\frac{2\mu DL^3}{C^2}\right) V \oint \frac{n^2(n^2 + 1)dn}{(\bar{\varepsilon}n^2 - 2n + \varepsilon)^3} \tag{39}$$

where the integral is around the unit circle from n_0 to n_1, where

$$n_0 = e^{i\theta_0} \tag{40a}$$

$$n_1 = e^{i\theta_1} \tag{40b}$$

The pressure is zero at $n = \pm i$, and the pressure is greater than zero when $Re(n)$ is greater than zero.

For no cavitation the integral extends completely around the journal; and by using the theory of residues, the force becomes

$$F = 4\pi\left(\frac{\mu DL^3}{C^2}\right)\left(\frac{V}{\bar{\varepsilon}^3}\right) A_{-1} \tag{41}$$

For cavitation the integral extends from $-i$ to $+i$; and, by using a partial-fraction technique, the force becomes

$$F = 4\left(\frac{\mu DL^3}{C^2}\right)\left(\frac{V}{\bar{\varepsilon}^3}\right)\left\{\Gamma A_- + \sum_{j=2}^{3}\left[\frac{(-n_+)^{j-2} A_{+j}}{(1 + n_+^2)^{j-1}} + \frac{(-n_-)^{j-2} A_{-j}}{(1 + n_-^2)^{j-1}}\right]\right\} \tag{42}$$

where Γ is defined as

$$\Gamma = \tan^{-1} \frac{\sqrt{1 - |\varepsilon|^2}}{-Re(\varepsilon)} \tag{43}$$

and Γ is in the first or second quadrant. The partial-fraction expansion coefficients are

$$A_{\pm 3} = \frac{n_{\pm}^2(n_{\pm}^2 + 1)}{(n_{\pm} - n_{\mp})^3} \tag{44a}$$

$$A_{\pm 2} = \frac{2n_{\pm}(2n_{\pm}^2 + 1)}{(n_{\pm} - n_{\mp})^3} - \frac{3A_{\pm 3}}{n_{\pm} - n} \tag{44b}$$

$$A_{\pm 1} = \frac{6n_{\pm}^2 + 1}{(n_{\pm} - n_{\mp})^3} - \frac{3A_{\pm 2}}{n_{\pm} - n_{\mp}} - \frac{3A_{\pm 3}}{(n_{\pm} - n_{\mp})^2} \tag{44c}$$

where the roots of the denominator of the force equation are

$$n_{\pm} = \left(\frac{1 \pm \sqrt{1 - |\varepsilon|^2}}{|\varepsilon|^2} \right) \varepsilon \tag{45}$$

DISCUSSION OF EXAMPLE

The rotor bearing system described in reference 8 was used as the example problem. This rotor bearing system consisted of a shaft with three disks mounted on two axially preloaded ball bearings (fig. 5). The bearings were mounted in a squeeze-film damper journal, and the journal had a centering spring.

The first three critical speeds for the rotor bearing system without oil in the damper are shown in figure 6. All the modes are bent-shaft modes. The "classical" hierarchy only applies to stiff shafts; therefore, the classical mode shapes do not characterize the actual mode shapes. The first mode, about 7581 rpm, classically would be the cylindrical mode. But in this case, it has a large amount of bending outward near the shaft center. The second mode, about 9235 rpm, classically would be the conical mode. In this case, it has a slight amount of bending outward near the shaft ends. The third mode, about 11 248 rpm, classically would be the bending mode. In this case, it has a large amount of bending throughout the shaft.

Experimentally the rotor was accelerated from rest through the three critical speeds. The Lissajous patterns for the three disks were displayed on three side-by-side cathode ray tubes. A motion picture was taken of the CRT's plus a speed counter. The Lissajous patterns at the three critical

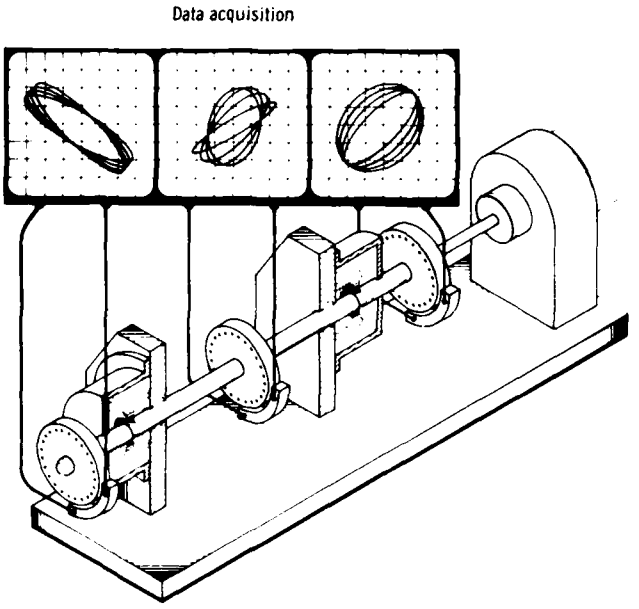

Figure 5. - Rotor bearing system used as example problem.

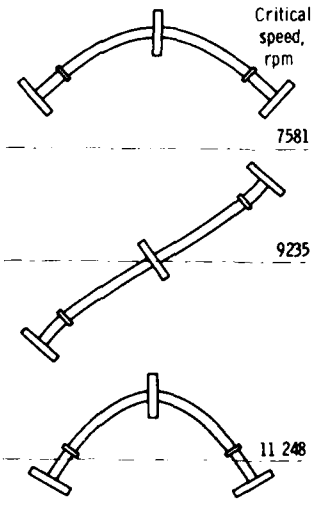

Figure 6. - Undamped critical speeds.

speeds are shown on figures 7 to 9. The three critical speeds occurred at about the predicted speeds, and the Lissajous patterns corresponded to the three mode shapes.

The rotor bearing system was modeled by using 19 elements. The rotor was assumed to have a uniform, in-line unbalance, with a mass eccentricity of 0.00254 centimeter (1 mil). The equations of motion for this system were programed in FORTRAN IV on an IBM 360-67 computer in a time-sharing mode. The equations of motion were directly integrated by the implicit integration method, with a fixed time step of 0.12 millisecond. The transient analyzed was the rotor accelerated from rest through the three critical speeds. The rate of acceleration was 8727 rad/sec^2. Each time step took about 0.7 second of CPU time.

The output at each time step of the calculation was displayed on a CRT. The display showed an oblique view of the rotor bearing system, with the bearing centerline as the oblique axis. The transverse vibration is indicated by a series of dots. Each dot represents a location of an element in the rotor dynamics model. The scale of the transverse vibration exaggerates the amplitude of the vibration. The display on the CRT was photographed at each time step. These photographs were then shown as a motion picture.

The computer-generated displays on the CRT at the first and third critical speeds and at a speed much greater than the third critical speed are shown in figures 10 to 12. The mode shapes at the first and third critical speeds were similar to the predicted mode shapes and occurred at the predicted speed. Because of the unbalance distribution, the second mode was not excited. The only indication of the second mode was a traveling wave superimposed on the first mode shape. This traveling wave decayed when the rotor went through the third critical speed. Above the third critical speed, the rotor bearing system operated as a self-centering device. The mass centerline coincided with the bearing centerline. Therefore, the rotor displacement was uniform and in line, with an amplitude of 0.00254 centimeter (1 mil).

In conclusion, this computer code for the first time allows us to look at complex rotor bearing systems experiencing nonlinear transients and displays the vast amount of results in an easily understood motion-picture format. A 10-minute, 16-millimeter, color, sound motion-picture supplement is available, on loan, that shows the test data and the computer-made motion picture.

CONCLUSIONS

An implicit method for integrating the equations of motion for a lumped-mass model of a rotor dynamic system was developed. The following conclusions were drawn:

1. The method was numerically stable for any time step.

2. An error estimate was available to control the size of the time step.

3. The computational time was proportional to the number of elements in the rotor dynamics model rather than to the cube of the number.

4. An example problem with 19 mass elements in the rotor dynamics model took 0.7 second of central processing unit time per time step an an IBM 360-67 computer in a time-sharing mode.

For the first time, this code allows the simulation of a complex rotor bearing system experiencing nonlinear transients and displays the vast amount of results in an easily understood motion-picture format.

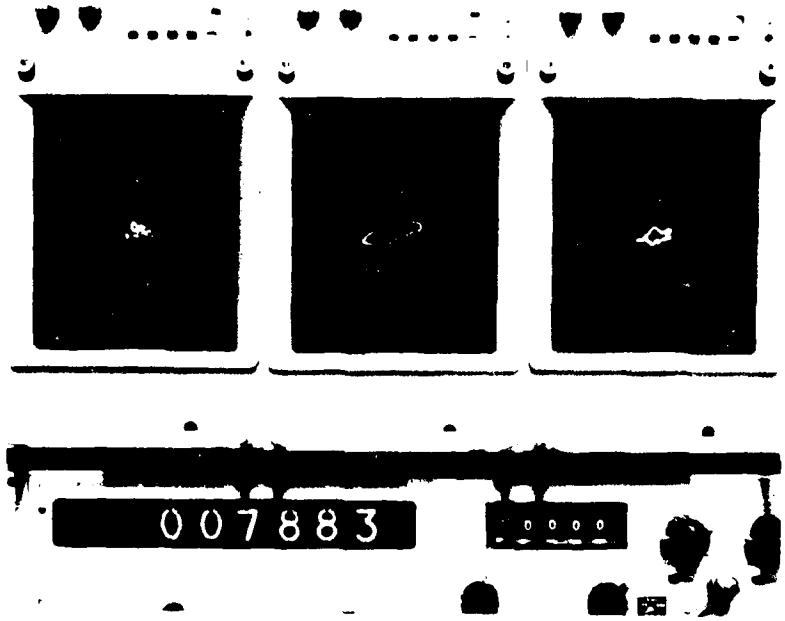
007883

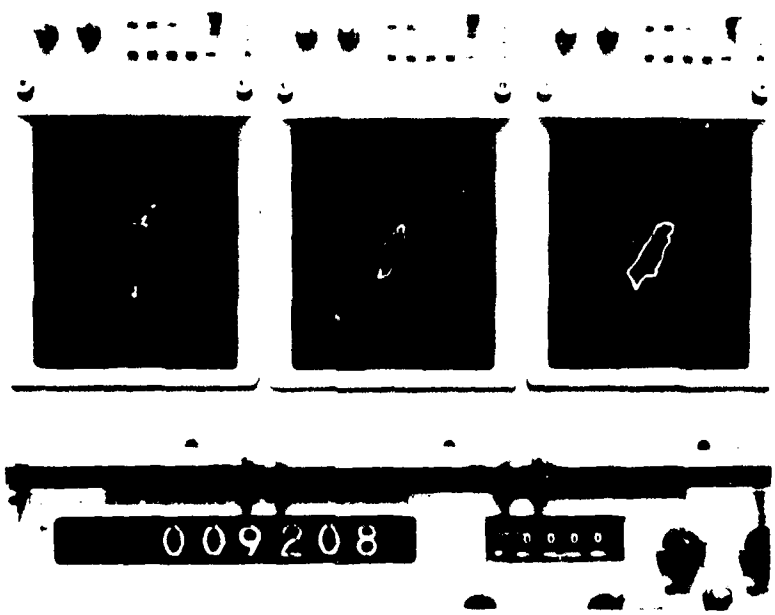
009208

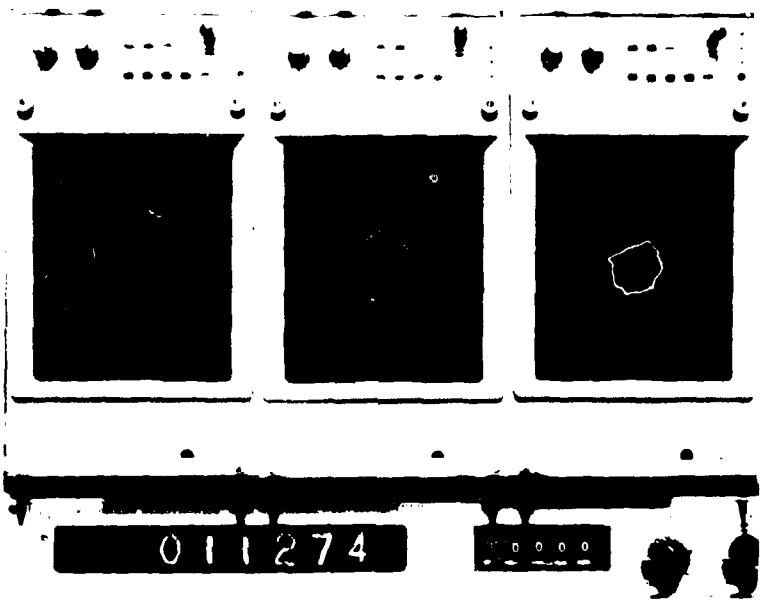

Figure 9. - Rotor passing through third critical speed.

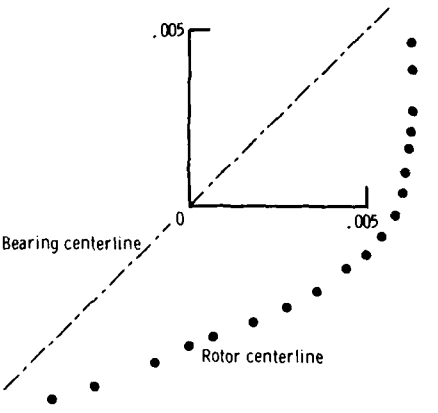

Figure 10. - Oblique view of rotor centerline as rotor passes through first critical speed.

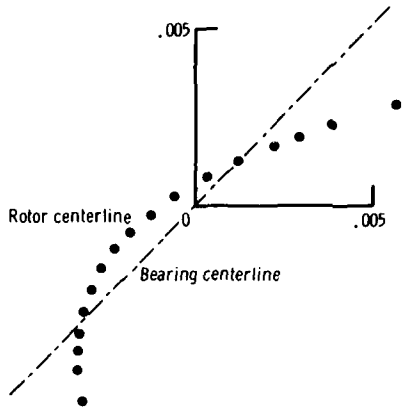

Figure 11. - Oblique view of rotor centerline as rotor passes through third critical speed.

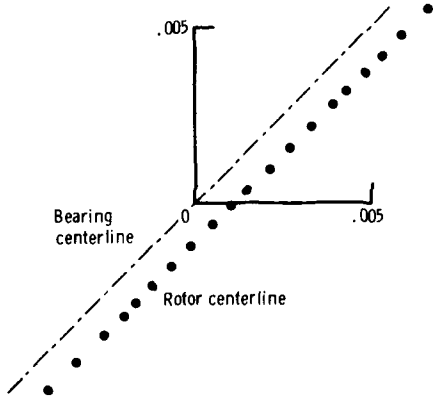

Figure 12. - Oblique view of rotor centerline at rotor speeds much greater than third critical.

REFERENCES

1. Childs, D. W.: A Rotor-Fixed Modal Simulation Model of Flexible Rotating Equipment. J. Eng. Ind., vol. 96, no. 2, May 1974, pp. 659-669.
2. Gunter, E. J.; et al.: Transient and Stability Analysis Using the Modal Method. UVA/528144/ME77/102, University of Virginia, 1977.
3. Shen, F. A.: Flexible Rotor Dynamics Analysis. (R-9252, Rocketdyne; NASA Contract NAS3-14422.) NASA CR-121276, 1973.
4. Kascak, A. F.: Stability of Numerical Integration Techniques for Transient Rotor Dynamics. NASA TP-1092, 1977.
5. Gear, C. W.: Numerical Initial Value Problems in Ordinary Differential Equations. Prentice-Hall, Inc., 1971.
6. Barrett, L. E.; and Gunter, E. J.: Steady-State and Transient Analysis of a Squeeze Film Damper Bearing for Rotor Stability. NASA CR-2548, 1975.
7. Kirk, R. G.; and Gunter, E. J.: Nonlinear Transient Analysis of Multi-Mass Flexible Rotors - Theory and Applications. NASA CR-2300, 1973.
8. Cunningham, R. E.; Fleming, D. P.; and Gunter, E. J.: Design of a Squeeze-Film Damper for a Multi-Mass Flexible Rotor. ASME Trans. J. Eng. Ind., vol. 97, no. 4, Nov. 1975, pp. 1383-1389.

SQUEEZE-FILM DAMPER TECHNOLOGY
AN OVERVIEW OF
SQUEEZE-FILM DAMPERS
APPLICATIONS
AND
TECHNOLOGICAL STATUS

By

Coda H. T. Pan
Technical Director
Shaker Research Corporation
Northway 10 Executive Park
Ballston Lake, New York 12019

ABSTRACT

Trends in the utilization of squeeze-film dampers in rotating machines are reviewed. Design and analysis approaches in current use are outlined. Unresolved technological issues are identified.

TYPICAL APPLICATIONS

Exploitation in earnest of damper technology in the engineering of high speed rotors began about a decade ago. A primary motivation of the use of squeeze-film dampers is the desire to have the choice of operating a rotating machine near or above one or more critical speeds. Some residual imbalance in a rotor assembly is unavoidable in practice. Unless there is adequate damping in the rotor system, resonant excitation of a critical speed at the operating condition or in accelerating through the critical speed can result in rotor vibration amplitudes of traumatic levels.

Gas turbine engines for aircraft propulsion are among the first rotating machine types to benefit from the use of squeeze-film damper to achieve significant improvement in its performance characteristics. A typical aircraft gas turbine rotor is essentially an undamped structure. Its support system traditionally consists of rolling element bearings which are directly attached to the casing. Rolling element bearings behave like very stiff springs (without damping). Thus, in such a rotor system, damping of lateral vibrations is due to Coulomb friction dissipation occurring in the casing assembly which responds sympathetically to vibratory forces transmitted through the support bearings. The inherent damping capacity of this type of rotor system is limited and difficult to predict, therefore, resonant vibrations are potentially very violent. The following design constraints are usually followed:

- Operating speed must be significantly different from all critical speeds.

- Stringent quality control regarding residual mass imbalance must be maintained.

- Critical speeds which fall below the running speed must not display much flexibility of these critical speeds. Therefore, the rotor structure tends to be relatively rugged and thus heavy.

Ever continuing strive for higher thrust-to-weight ratio of aircraft engines has led to more flexible designs of the engine rotor. Most contemporary propulsion engines have damper mounted rotors to allow operation above critical speeds which exhibit considerable rotor flexibility.

Application of dampers in industrial rotating machines is beginning [1]. Because industrial rotating machines are commonly supported by fluid film bearings which are usually effective in the control of imbalance response, the reason for using dampers usually concerns asynchronous vibrations. Of special interest is the "half frequency" variety; this may be either in the form of "oil whip" [2] type instability or due to other types of excitation.

METHODS OF INSTALLATION

Commonly used dampers are of the non-rotating type and are mounted in series with the support bearings. Since a non-rotating fluid film cannot carry a static load, a parallel centering spring is commonly used to insure that a nominal damper clearance is present under the operating static load. (Figure 1).

A series mounted damper can also be used without a parallel centering spring (Figure 2). Such an installation is favored because of simplicity in manufacturing. Strictly speaking, the film of such a damper is nominally bottomed under a static load. If, however, vibrations of moderate magnitude is present, non-linear effects together with film cavitation interact to induce a static lift [3, 4, 5]. Advocates of such a design approach reason that the damper film clearance is not essential except when significant vibrations are present.

Use of fluid film dampers in an intershaft installation for vibration control of multiple spool aircraft gas turbine engines is also under consideration (Figure 3). Because of the rotation speeds of the two shafts, the fluid film will experience the hydrodynamic wedge action and in effect will function as a fluid film journal bearing. The equivalent "half frequency" effect would occur at the algebraic mean of the two shaft speeds, potentially, thus, an instability mechanism exists [6, 7]. In an intershaft installation, alignment of the damper center with the bearing centers should be accurately maintained, lest runout error would cause excitations at rotational frequencies.

The damper can also be installed (through a rolling element bearing) in parallel with the support bearing (Figure 4). The latter may be either a rolling element bearing or a fluid film bearing. The parallel installation complicates the manufacture process somewhat. However, it offers the possibility of an extended linear range which is difficult to realize in a series installation.

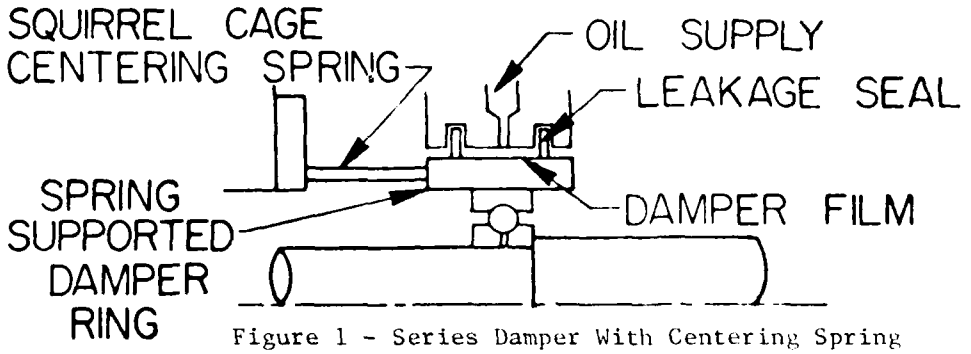

Figure 1 - Series Damper With Centering Spring

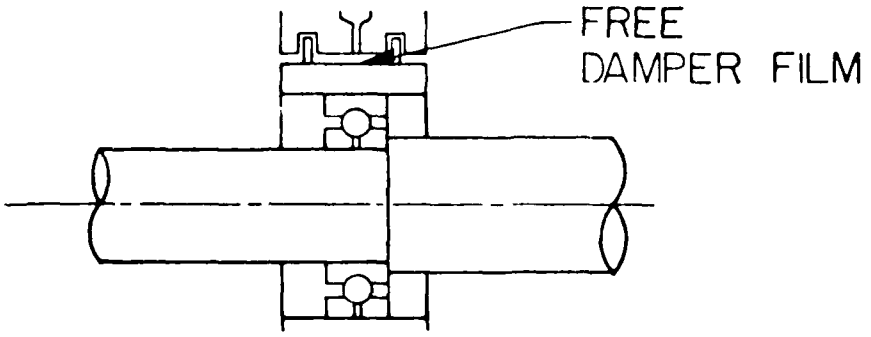

Figure 2 - Series Damper Without Centering Spring

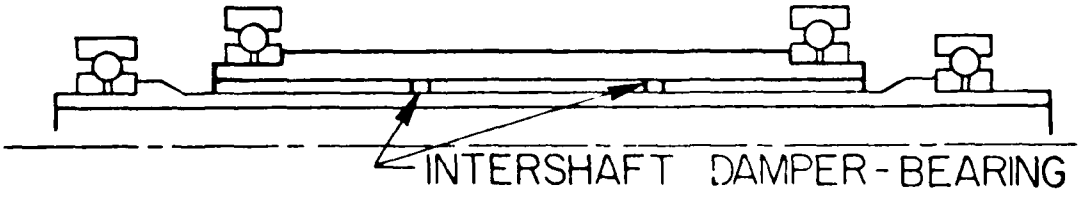

Figure 3 - Intershaft Damper

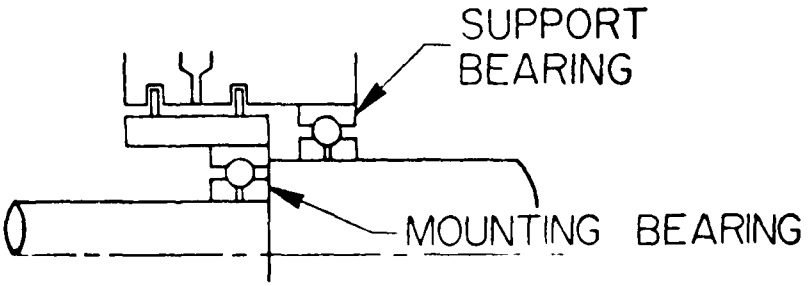

Figure 4 - Parallel Damper

DESIGN PARAMETERS

The component characteristics of the damper should be designed to yield an optimum dynamic characteristics of the rotor system. In a given situation the damper film diameter and the lubricant properties are fixed. However, there are still numerous controllable design parameters. The significance of these design parameters are contained in the scaling law which is derived from the short bearing, π-film approximation; according to which the damping coefficient for a small circular orbit motion is

$$B_{short,\pi} = \frac{\pi\mu}{C}\left(\frac{L}{D}\right)^2 (LD) \qquad (1)$$

It is seen that the most prominent feature in this formula is the factor $(L/C)^3$. This formula is primarily for a damper fed from a circumferential groove at one end and drained through another circumferential groove at the other end. Very often, end-seals are used for such a damper for "housekeeping" purposes. If a damper is used without end-seals, it is most commonly fed through a midplane feed grooves. When this is done, there are effectively two damper films sharing the available length equally. The resulting damping coefficient is 1/4 as large as that of the damper which spans the same axial length without interruption by the axial feed groove (Figure 5). Low leakage end-seals can be used to ameliorate the reduction in the damping capacity. In order to eliminate loss of film pressure due to leakage, axial flow has to be suppressed both globally and locally. Local axial flow is suitably reduced if the hydraulic diameter of any inboard circumferential recirculation passage is of a similar dimension as the damper film thickness as illustrated in Figure 6.

The "end leakage" at the inlet can also be suppressed by supplying lubricant flow through a few discrete small holes in lieu of the circumferential feed groove at midplane (Figure 7). A damper with leakage suppression features at both inlet and exits is more appropriately estimated according to the long bearing, π-film approximation

$$B_{long,\pi} = \frac{3\pi\mu}{C}\left(\frac{R}{C}\right)^2 (LD) \qquad (2)$$

Compared with Eq. (1), it is seen that upon successful suppression of leakage effects, the damping capacity can be increased by the factor $3(D/L)^3$; in typical configurations, this amounts to 12-300.

The above formulae are derived from the π-film approximation, which retains only the portion of film pressure which is above the ambient. With enough pressurization in the supply, it is in principle possible to eliminate cavitation entirely. When this is accomplished, the damping coefficient would then be twice that of the π-film estimate. An additional advantage in the elimination of cavitation is the suppression of the non-linear whirl phenomenon, which can be triggered by an excitation of abusive level, e.g. a blade loss event of a gas turbine and is generally a vibration of intolerable amplitude. A disadvantage upon elimination of cavitation is the concurrent elimination of the static lift capacity.

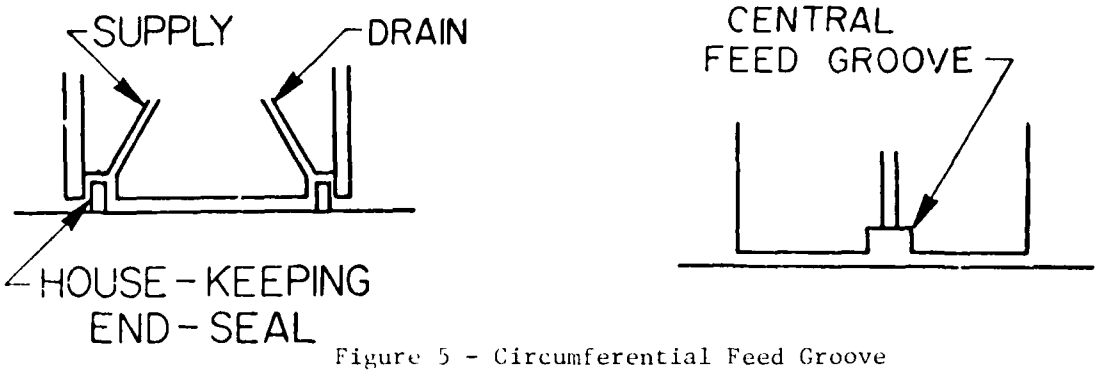

Figure 5 - Circumferential Feed Groove

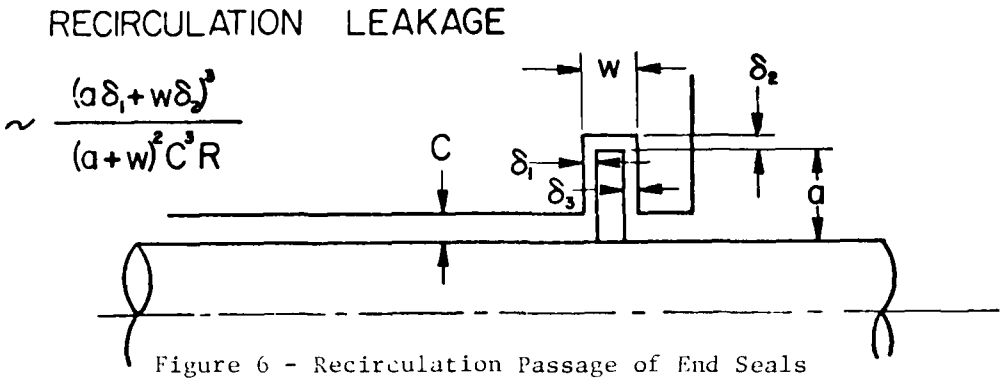

Figure 6 - Recirculation Passage of End Seals

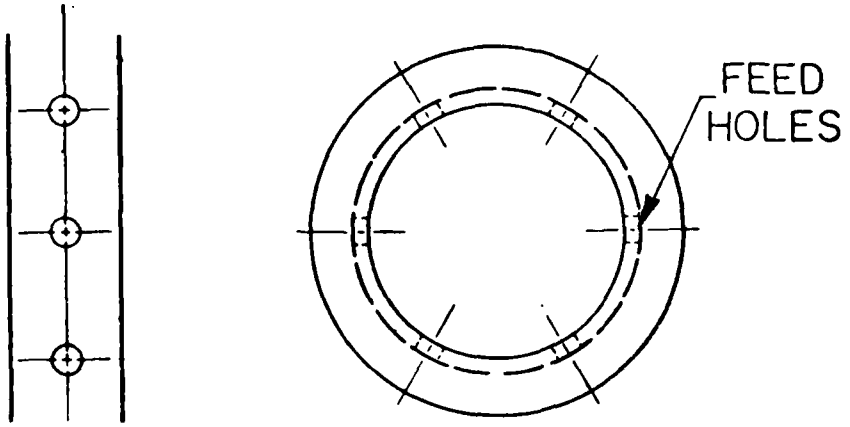

Figure 7 - Discrete Midplane Feed Holes

In summary the typical design parameters include the following:

- Geometry - length
  clearance
  film profile
- Installation - series with centering spring
  without centering spring
  parallel
- Feed - circumferential feed groove
  discrete feedholes
- Drain - flow through
  circumferential collecting groove
  sealed
- Supply Pressure

ANALYTICAL TOOLS

Central in the effective utilization of squeeze-film dampers is the capability of predicting their dynamic characteristics accurately. Simple formulae, similar to Eqs. (1) and (2) and those allowing for orbit amplitude effects [8], give approximate estimates respectively for dampers without and with leakage suppression features. A computer code, which can be used to perform more elaborate computations with allowance for end leakage and cavitation pressure level, is the outcome of a recently concluded program sponsored by the U. S. Army [9]. A simple, weighted average rule between π-film and full-film short bearing formulae was used to study the lift-off process [10], while the weighting factor was empirically determined, a reasonable facsimile of the experimental trajectory was reproduced.

Incorporation of damper effects in the analysis of a flexible rotor is readily accomplished in either the frequency response point of view or in detailed time-domain simulation. In the former case stiffness and damping coefficients are used; whereas in time domain simulation, force components are expressed as functions of the kinematic state variables. In the case of circular orbits non-linear amplitude effects can be included in the frequency response calculation through an iterative process.

APPLICATION PROBLEMS

While the introduction of damper installation invariably would reduce the vibration and noise levels in a rotor system, an optimum damper design requires attention to specific issues which are peculiar to the application in question.

The effectiveness of a damper installation in a highly flexible rotor system is dependent on

- axial location of the damper mount,

- stiffness of the centering spring, and
- the dynamic coefficient of the damper.

Regarding the last factor, one may take note that an oversized damper would inhibit the local motion and thus become self-restrictive in the damping action. Appropriate "tuning" of these factors would reduce the overall vibration levels to a minimum [11]. Particularly if the vibration phenomena are confined to a restricted frequency band, the benefit of the damper installation can be significantly enhanced by optimum tuning.

A damper installed in series with the support bearing without a centering spring behaves unusually as a function of the transmitted vibration force level. At low vibration levels, the damper would be "bottomed" by the static load and motion in the corresponding direction would be selectively restricted, and the local orbit trajectory collapses into a line which is perpendicular to the direction of the static load. Accordingly, the damping action cannot be fully effective. At large vibration levels, fluctuation of pressure in the damper film would result in "cavitation" in the unloaded region. The cavitation pattern is not uniform on account of the asymmetrical geometry. Consequently, a static-lift is induced so that the orbit would open up and motion in all directions induces damping [3, 4]. Controlling the lift-off condition is a unique issue in the design of a series damper without a centering spring.

Dampers can also be beneficially used to suppress instability tendencies in rotor systems. The most common causes for rotor instability are fluid film bearing forces and impeller reaction to tip clearance variation caused by local eccentricity [12]. On the other hand, intershaft installation of a damper can precipitate whirl instability occurring at the average frequency of the two shafts [6, 7]. Use of a "whirl-free" film profile is a crucial consideration in the design of intershaft dampers.

The π-film analysis (for any L/D) shows a strong dependence of the tangential and radial force components on the orbit amplitude. At a small orbit amplitude, the damper force is primarily tangentially oriented. As the orbit increases, both components increases non-linearly. The radial component has a stronger non-linear trend and becomes dominating at large orbit amplitudes. This behavior is illustrated by the eccentricity loci shown in Figure 8. With a series damper installation, if the rotor is required to run past its critical speed, a large response orbit accompanied by excessively large transmitted force can develop. This phenomenon is associated with a bi-stable condition of the rotor-bearing system due to the peculiar non-linear behavior of a cavitated damper [13, 14, 15, 16]. For a rigid rotor, this undesirable behavior would occur if the mass imbalance is equivalent to a mass shift in excess of approximately 1/4 of the damper clearance.

SOME UNRESOLVED ISSUES

Although the squeeze-film dampers is quite effective for the general reduction of vibration and noise levels of rotating machines, the state of technology is still inadequate for its engineering in critical applications.

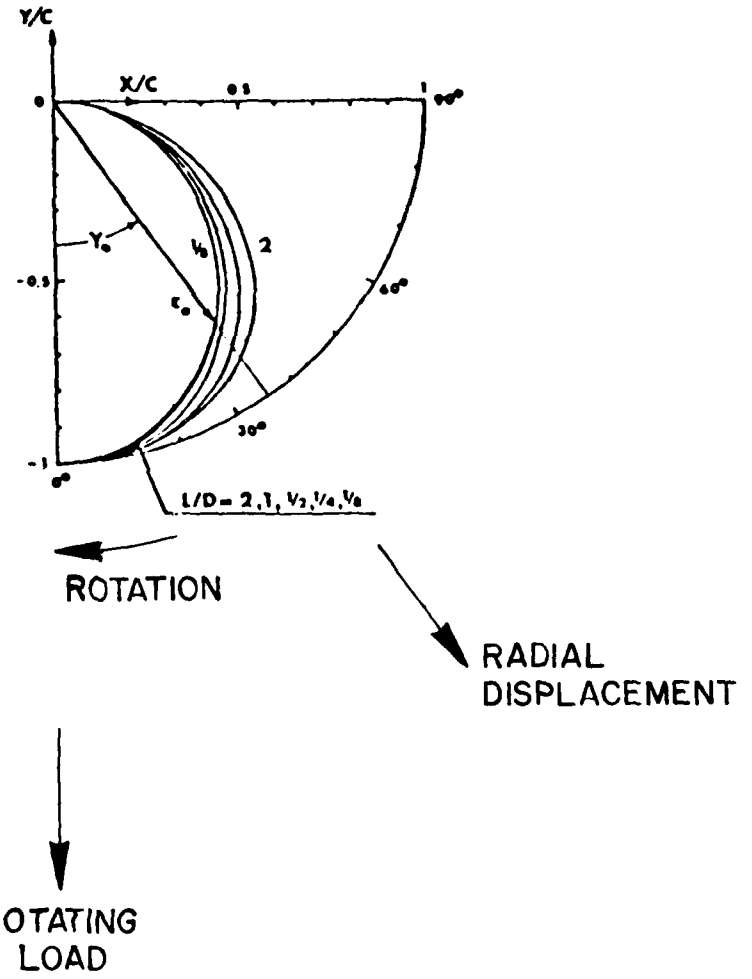

Figure 8 - Eccentricity Loci of Damper for Circular Whirl
(after Childs et al [3])

The importance of the cavitation process in the operation of the damper is revealed by the following observations:

- There is a direct dependence of the damping capacity on the amplitude of the orbit motion which determines if the lubricant film would be cavitated and what is the extent of cavitation.

- The possibility of lift-off in a series installation without a centering spring depends on the occurrence of cavitation.

- The troublesome possibility of bi-stable operation of the damper under high dynamic loading can be eliminated by suppressing the cavitation process.

The common practice of accepting either the π-film or the full-film approximation or of using the Gumbel criterion in a more elaborate computation scheme would not answer the above questions. A more convincing treatment for the circular orbits of short dampers has shed some light on these issues [17]. Representative results are illustrated in Figures 9 and 10.

Use of small clearance end-seals and discrete feedholes are motivated by the desire to realize the largest possible damping capacity. Available treatment of seal effects deals with the overall leakage flow (e.g. [27]) but gives no clue to the appropriate design criteria for the suppression of local recirculation effects. The discrete feeding process is controlled by local flow fields which is characterized by both sharp spatial gradients as well as rapid fluctuations with time. And yet, the coverage of the lubricant film depends on the balance between the net feed flow and end leakage. It is clear that the successful design of high-performance dampers would depend on adequate considerations of detail flow processes in both the feed region and the exit region of the lubricant film.

Non-circular whirl orbits occur when uncompensated static load and the dynamic rotating load are of similar magnitudes. If the dynamic load should be large enough to cause cavitation, such a situation does not admit a steady-state description of the cavitation domain. Consequently, the commonly accepted Swift-Stieber condition for locating the cavitation boundary along with the film re-formation boundary is not applicable. It appears that "history features" should be included in the analysis of cavitated squeeze-films which are associated with non-circular whirl orbits[18].

Discussions on cavitation thus far presumed aggregation of voids primarily in the unloaded film zone. The possibility in the entrainment of finely dispersed bubbles in the entire film has been suggested [19]. Direct evidence of the validity of this hypothesis is yet to be obtained. It is quite possible that the presence of entrained gas is a speed related phenomenon.

Dampers for large propulsion gas turbines operate with moderately large Reynolds numbers. Bernoulli effects which are neglected in the lubrication theory can be prominent. In terms of overall rotor dynamic behaviors, a virtual mass phenomenon is to be expected. This issue is overlooked, most of the time, in prevailing analytical results.

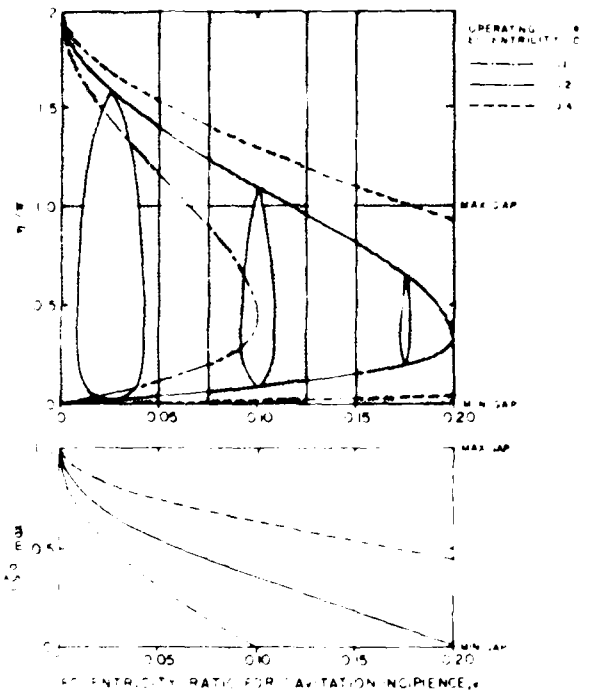

Figure 9 - Cavitation Pattern
(after Pan [17])

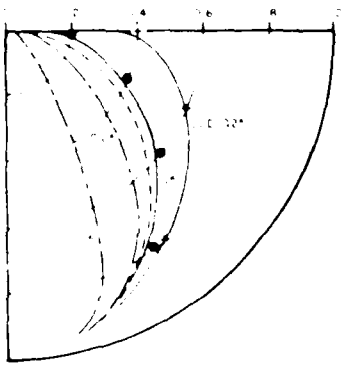

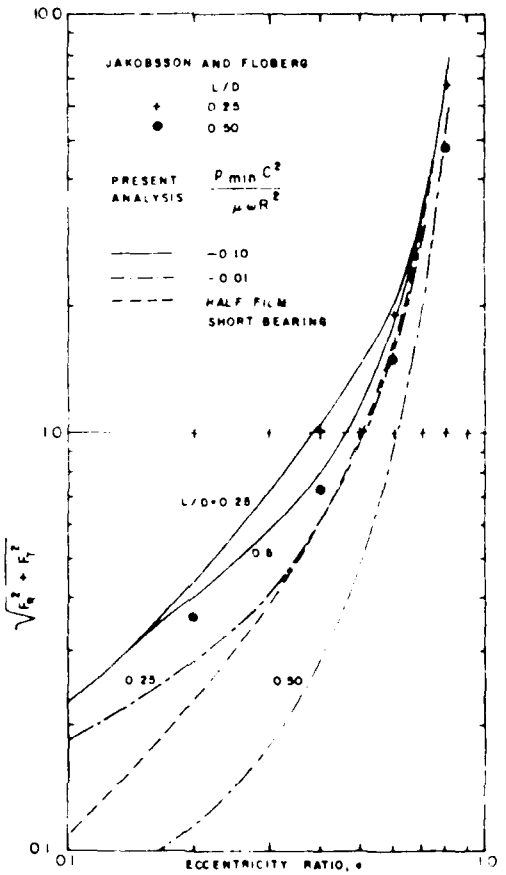

Figure 10 - Eccentricity Loci and
Load Capacity
(after Pan [17])

Interest in the assessment of trans-critical rotor response to mass imbalance at an abusive level has directed attention to the bi-stable, non-linear character of cavitated dampers. For a rotor system with multiple damper installations, time-domain simulation with commeasurate thoroughness in all relevant aspects of the rotor system is potentially capable of yielding accurate and useful results. A convincing demonstration in the efficacy of the simulation method as a tool for rotor engineering remains to be established [20]. Issues requiring careful scrutiny include

- numerical stability of the computation scheme,
- bounds of cumulative error,
- interactions between spatial and temporal resolutions,
- effective display of simulation results,
- computational cost considerations, and
- accurate characterization of the dynamic behavior of critical components.

ACKNOWLEDGMENTS

This work was supported by the U. S. Army Research Office under Contract Number DAAG29-78-C-0027, Project Number P-15657-E.

REFERENCES

1. Malanoski, S. B., "Case Histories in which Subsynchronous or Synchronous Vibration Amplitudes Have Been Minimized After Employing Custom Designed Damper Bearings," Workshop on Stability and Dynamic Response of Rotors with Squeeze-Film Bearings, Charlottesville, VA, May 8-9, 1979.

2. Poritsky, H., "Contribution to the Theory of Oil Whip," Trans. of ASME, Vol. 75, No. 6, 1953.

3. Holmes, R., "The Non-linear Performance of Squeeze-Film Bearings," J. Mech. Engineering Science, Vol. 14, No. 1, 1972.

4. Pan, C. H. T. and Tonnesen, J., "Eccentric Operation of the Squeeze-Film Damper," Journal of Lubrication Technology, Vol. 100, No. 3, July 1978, pp. 369-378.

5. Holmes, R., "The Control of Rotor Vibration Using Squeeze-Film Dampers, "Workshop on Stability and Dynamic Response of Rotors with Squeeze-Film Bearings, Charlottesville, VA, May 8-9, 1979.

6. Hibner, D. H., Kirk, R. G., and Buono, D. F. "Analytical and Experimental Investigation of the Stability of Intershaft Squeeze-Film Dampers--Part 1: Demonstration of Instability," Journal of Engineering for Power, Vol. 99, No. 1, January 1977, pp. 47-52.

7. Hibner, D. H., Bansal, P. N., and Buono, D. F., "Analytical and Experimental Investigation of the Stability of Intershaft Squeeze-Film Dampers--Part 2: Control of Instability," ASME Paper No. 77-DET-26.

8. Childs, D., Moes, H., and Van Leeuwen, H., "Journal Bearing Impedance Descriptions for Rotor Dynamic Applications," Journal of Lubrication Technology, Vol. 99, No. 2, April 1977, pp. 198-214.

9. "User's Manual for Damper Analysis by Numerical Differentiation and Integration," Report No. FR-10732, October 1978, prepared by Pratt and Whitney Aircraft Group, United Technologies, West Palm Beach, Florida, for Applied Technology Laboratory, U. S. Army Research and Development Laboratories, Fort Eastis, under Contract No. DAAJ02-76-C-0011.

10. Humes, B. and Holmes, R., "The Role of Subatmospheric Film Pressures in the Vibration Performance of Squeeze-Film Bearings," Journal of Mech. Engineering Science, Vol. 20, No. 5, 1978, pp. 283-289.

11. Gunter, E. J., Li, D. F., and Barrett, L. E., "Dynamic Characteristics of a Two-Spool Gas Turbine Helicopter Engine," Workshop on Stability and Dynamic Response of Rotors with Squeeze-Film Bearings, Charlottesville, VA, May 8-9, 1979.

12. Alford, J. S., "Protecting Turbomachinery from Self-Excited Rotor Whirl," Journal of Engineering for Power, Vol. 87, No. 4, October 1965, pp. 33-344.

13. Cooper, S. "Preliminary Investigation of Oil Film for the Control of Vibration," Institute of Mechanical Engineers, Lubrication and Wear Convention, Paper 28, 1963, pp. 305-315.

14. White, D. C., "The Dynamics of Rigid Rotor Supported on Squeeze-Film Bearings," Conference of Vibrations in Rotating Systems, Proceedings of the Institute of Mechanical Engineers, 1972, pp. 213-229.

15. Mohan, S., and Hahn, E. J., "Design of Squeeze-Film Damper Supports for Rigid Rotors," Journal of Engineering for Industry, Vol. 46, No. 3, August 1974, pp. 976-982.

16. Hahn, E. J., "Unbalance behavior of Squeeze-Film Supported Rigid Rotors," Workshop on Stability and Dynamic Response of Rotors with Squeeze-Film Bearings, Charlottesville, VA, May 8-9, 1979.

17. Pan, C. H. T., "An Improved Short Bearing Analysis for the Submerged Operation of Plain Journal Bearings and Squeeze-Film Dampers," ASME Paper No. 79-Lub-33, to be published in Journal of Lubrication Technology, Vol. 102, 1980.

18. Olsson, K., "Cavitation in Dynamically Loaded Bearings," Trans. Chalmers Univ. Tech., 1965, 308, Göteburg.

19. Hibner, D. H. and Bansal, P. N. "Effects of Fluid Compressibility on Viscous Damper Characteristics," Workshop on Stability and Dynamic

Response of Rotors with Squeeze-Film Bearings, Charlottesville, VA, May 8-9, 1979.

20. Smalley, A. J., "Transient Dynamics of Squeeze-Film Bearing Systems," Workshop on Stability and Dynamic Response of Rotors with Squeeze-Film Bearings, Charlottesville, VA, May 8-9, 1979.

Communication on Squeeze-Film Damper Workshop, Charlottesville, 8-10 May, 1979

I am sure that I reflect the views of the vast majority of participants when I say that the Workshop was a great success in bringing together engineers of similar interests from around the world. It helped to confirm in my mind that conferences on fairly narrow topics are more successful than ones on wide-ranging topics. The blend of industrial, research and computing experience in the Conference was particularly successful. In the first, Mr. Malcnoski and Mr. Balke illustrated very forcibly their experience in design and development. In the second I thought the paper on the effects of fluid compressibility by Messrs Hibner and Bansal was outstanding and leads the way for more fundamental research on the nature of cavitation. Mr. Simpson's paper is also worthy of publication and I hope will appear in the final volume of Proceedings.

With regard to numerical analyses the papers of Dr. Gunter et al, of Dr. Barrett and of Dr. Stephens contained some very interesting features and results. In particular it would be helpful if Dr. Barrett could elucidate a little on how he included the non-linear squeeze-film effect in his essentially linear program. The inclusion of this paper in the final volume would also be of great value, as would that of Dr. Stephens. In the latter, values of the various integrals that he used would be especially useful.

I thought Dr. Hahn's design charts were very ingenious but in the light of Dr. Hibner's work perhaps a little premature. However, there appears to be no reason why such ingenuity cannot be applied using modified data, when these become available.

In conclusion, I would like to congratulate the organisers, the authors and the U.S. Army Research Office for their organisation with the hope that the Conference might be repeated in a few years' time.

R. Holmes

LIST OF PARTICIPANTS

Dr. Paul E. Allaire
Dept. Mechanical & Aerospace Engr.
University of Virginia
Charlottesville, VA 22901

Mr. Rod Balke
Bell Helicopter
Textron
P.O. Box 482
Ft. Worth, TX 76101

Mr. Prem N. Bansal
Mail Stop EC-353
Commercial Products Div.
Pratt & Whitney Aircraft
400 Main Street
East Hartford, CT 06108

Dr. Lloyd E. Barrett
Dept. Mechanical & Aerospace Engr.
University of Virginia
Charlottesville, VA 22901

Mr. James Blanding
Dept. Mechanical Engineering
Virginia Polytechnic Institute
and State University
Blacksburg, VA 24061

Mr. R. T. Bohm
AVCO-Lycoming
500 Main Street
Stratford, CT 06497

Mr. Matthias Botman
Pratt & Whitney of Canada Ltd.
Lonqueuil, Quebec
Canada

Dr. E. A Bulanowski
Transamerican Delaval Inc.
P. O. Box 8788
Trenton, NJ 08650

Dr. Dara Childs
Dept. Mechanical Engineering
University of Louisville
Louisville, KY 40208

Mr. A. F. Criqui
Solar Turbines International
2200 Pacific Hy.
P. O. Box 80966
San Diego, CA 92138

Mr. Van S. Fehr
Mail Stop R-47
Pratt & Whitney Aircraft Group
West Palm Beach, FL 33401

Dr. R. D. Flack
Dept. Mechanical & Aerospace Engr.
University of Virginia
Charlottesville, VA 22901

Mr. Jack Fleischmann
Box 512
Allis Chalmers Compressor Div.
Milwaukee, WI 53201

Dr. David Fleming MS6-1
NASA Lewis Research Center
21000 Brookpark Road
Cleveland, O 44135

Dr. Leroy Fletcher, Chairman
Dept. Mechanical & Aerospace Engr.
University of Virginia
Charlottesville, VA 22901

Dr. E. J. Gunter
Dept. Mechanical & Aerospace Engr.
University of Virginia
Charlottesville, VA 22901

Mr. Loren A. Gross
NASA - Marshall Space Flight Center
EE 21 (E)
Huntsville, AL 35804

Dr. Eric J. Hahn
School of Mechanical & Industrial
Engr., University of New South Wales
P. O. Box 1
New South Wales
Australia 2033

Mr. Bernard Herbage
Centritech Corporation
9919 Steelman Avenue
Houston, TX 77017

Mr. David Hibner
Pratt & Whitney Aircraft EB 3S3
United Technologies Corporation
400 Main Street
East Hartford, CT 06108

Professor Roy Holmes
Applied Science Laboratory
The University of Sussex
Falmer, Brighton
Sussex BN1 9QT
United Kingdom

Mr. James Johnston
Williams Research
Walled Lake, MI 48088

Mr. Albert Kascak
NASA Lewis Research Center
21000 Brookpark Road
Cleveland, O 44135

Dr. James Kauzlarich
Dept. Mechanical & Aerospace Engr.
University of Virginia
Charlottesville, VA 22901

Dr. David Lewis
Dept. Mechanical & Aerospace Engr.
University of Virginia
Charlottesville, VA 22901

Dr. Clarence J. Mayday
Dept. Mechanical & Aerospace Engr.
North Carolina State University
Raleigh, NC 27607

Dr. E. A. Memmott
Dresser-Clark
Mechanical Analysis Dept.
P. O. Box 560
Olean, NY 14760

Dr. Larry Mitchell
Dept. Mechanical Engineering
Virginia Polytechnic Institute &
State University
Blacksburg, VA 24060

Dr. Harold D. Nelson
Dept. Aerospace Engineering and
Engineering Science
Arizona State University
Tempe, AZ 85281

Dr. C. H. T. Pan
Shaker Research Corp.
Northway 10, Executive Park
Ballston Lake, NY 12019

Mr. William Parker U29 A
Detroit Diesel Allison
P. O. Box 894
Indianapolis, IN 46206

Mr. Ed Parrish
Airesearch Mfg. of Arizona
Box 5217
Phoenix, AZ 85010

Dr. Richard Pendleton
S. Dakota School of Mines and
Technology
CE 103
Rapid City, SD 57701

Dr. W. D. Pilkey
Dept. Mechanical & Aerospace Engr.
University of Virginia
Charlottesville, VA 22901

Mr. T. P. Psichogios
Solar Turbines International
2200 Pacific Hy.
P. O. Box 80966
San Diego, CA 92138

Dr. William Reiter
Dept. Mechanical & Aerospace Engr.
North Carolina State University
Raleigh, NC 27607

Mr. Arnon Rieger
Mechanical Technology, Inc.
968 Shaker Rd.
Latham, NY 12110

Mr. J. B. Roberts
University of Sussex
Falmer, Brighton
Sussex BN1 9QT
United Kingdom

Dr. Keith Rouch
Dept. 3333 CD
Allis Chalmers Corp., Box 512
Milwaukee, WI 53201

Mr. Allen C. Royal
Applied Technology Laboratory
U. S. Army Research & Development Laboratory
Ft. Eustis, VA 23604

Dr. Edward A. Saibel
U. S. Army Research Office
Engineering Section
Research Triangle Park, NC 27709

Mr. Dana Salamone
Centritech Corporation
9919 Steelman Avenue
Houston, TX 77017

Dr. R. K. Sharma
Pratt & Whitney of Canada, Ltd.
Longueuil, Quebec
Canada

Mr. Matthew Simpson
Dept. Mechanical & Aerospace Engr.
University of Virginia
Charlottesville, VA 22901

Dr. A. J. Smalley
Mechanical Technology, Inc.
968 Albany Shaker Road
Latham, NY 12110

Dr. J. B. Stephens
Mail Stop R-47, P. O. Box 2691
Pratt & Whitney Aircraft Co.
West Palm Beach, FL 33401

Mr. Albert Storace
General Electric Company
Aircraft Engine Group
I 75 & Neumann
Cincinnati, O 45215

Dr. Dean Taylor
Dept. Mechanical & Aerospace Engr.
Cornell University
Ithaca, NY 14850

Mr. Joseph A. Tecza
Mechanical Technology Inc.
968 Albany Shaker Road
Latham, NY 12110

Dr. John Tichy
Mechanical Engineering Dept.
Rensselaer Polytechnic Institute
Troy, NY 12181

Professor Jorgen Tonnesen
Dept. of Machine Elements
Technical University of Denmark
Bygning 403
Lyngby, Denmark 2800

Mr. Richard J. Trippett
Mechanical Research
General Motors Research Labs.
Warren, MI 48090

Dr. John M. Vance
Texas A & M University
Dept. Mechanical Engineering
College of Engineering
College Station, TX 77843

Mr. Peter G. Wendt
Solar Turbines International
2200 Pacific Hy., P.O. Box 80966
San Diego, CA 92138